

**UNIVERSITAT POLITÈCNICA DE  
VALÈNCIA**



**Supramolecular and  
heterosupramolecular chemistry in  
controlled release and molecular recognition  
processes**

**PhD. THESIS**

Submitted by  
**Alessandro Agostini**

PhD. Supervisors:  
**Prof. Ramón Martínez Máñez**  
**Dr. Félix Sancenón Galarza**

*Valencia 2013*





Instituto Interuniversitario de Reconocimiento  
Molecular y Desarrollo Tecnológico



RAMÓN MARTÍNEZ MÁÑEZ, PhD in Chemistry and Professor at the *Universitat Politècnica de València*, and FÉLIX SANCECNON GALARZA, PhD in Chemistry and Lecturer at the *Universitat Politècnica de València*.

CERTIFY:

That the work "*Supramolecular and heterosupramolecular chemistry in controlled release and molecular recognition processes*" has been developed by **Alessandro Agostini** under their supervision in the Centro de Reconocimiento Molecular y Desarrollo Tecnológico (IDM) de la *Universitat Politècnica de València*, as a thesis Project in order to obtain the international degree of PhD in Chemistry at the *Universitat Politècnica de València*.

Valencia, \_\_\_\_\_ 2013.

Prof. Ramón Martínez Máñez

Dr. Félix Sancenón Galarza



*Ai miei Genitori...*

*...e a Claudia*



*“Non est quod timeas ne operam perdideris,  
si tibi didicisti”*

**Lucio Anneo Seneca**

but not less important

*“Science is a wonderful thing...  
if one does not have to earn one's living at it”*

**Albert Einstein**



## Acknowledgments

First of all THANK YOU !!!, because if I'm here writing these lines is because I'm finishing my PhD, I wrote a doctoral thesis and I'm very close to be doctor (what an honor !!!).

For all these reasons I'm now here looking at the white and blue screen of my laptop and I'm quite sure that I'm not so good in this kind of things. However I need to put down some confused words to thank you, whoever you are, reading these lines, because I'm sure that you helped me in this great and quite long journey.

En primer lugar me gustaría darles las gracias a mis dos directores de tesis Ramón y Félix. Gracias por haberme dado la posibilidad de empezar y acabar la tesis en vuestro grupo de investigación, gracias por todos vuestros consejos, gracias por haberme explicado y enseñado muchísimas cosas y sobre todo gracias por haberme acogido como un becario cualquiera y por haberme dado muchas responsabilidades a pesar de ser extranjero, en dos palabras gracias por haber confiado en mí. Con te Félix posso anche parlare italiano e preferisco usare la mia lingua per dirti grazie ancora una volta. Sei stato molto più di un capo, sei stato e sarai sempre un vero amico, di quelli che si contano sulle dita di una mano, di quelli che non si dimenticano mai.

Gracias Juan y gracias Luis. Gracias por haberme ayudado con mis miles de dudas de fisicoquímica, de electroquímica y de química de materiales. Sobre todo gracias por las miles de veces que hemos hablado de otras cosas, de temas que no tienen nada a que ver con la química. Gracias por haber hablado de política, de historia y obviamente de fútbol, gracias por estos inolvidables momentos. Por supuesto gracias Loles, gracias por tus miles de consejos y sobre todo gracias por haberme ayudado a gestionar toda la burocracia relacionada con los masters de la ETSID, al final he

conseguido un título inesperado gracias a ti. Obviamente gracias a JN en primer lugar por haberme dado la posibilidad de conseguir la beca que ha financiado mis estudios de doctorado y luego por ayudarme con todos los tramites burocráticos. En pocas palabras gracias por tu gran ayuda.

Certamente devo ringraziare ancora una volta il prof. Mauro Freccero. Ovviamente grazie per avermi accettato ancora nel tuo piccolo grande gruppo di ricerca e per aver creduto nella bontà di quello che è diventato il progetto più importante del mio dottorato, anche se non compare nella tesi. Grazie davvero Mauro è stato e sempre sarà un piacere collaborare con te, per tantissime ragioni. Ovviamente grazie al Dr. Filippo Doria, per me è stato davvero fantastico tornare per qualche mese in lab. G. Ancora una volta ti voglio ringraziare per tutto ciò che mi hai trasmesso e soprattutto per essere un amico prima di un collega. Grazie a Michele anche in questo caso è inutile dire che prima di tutto sei un amico, il resto va da sé. Grazie anche a tutti gli altri membri del lab G. Germa, Riccardone, i due Vincenzi (basta studiare voi due!!!) e Silvia, grazie per gli innumerevoli divertentissimi momenti passati in laboratorio, grazie davvero. Infine un grande in bocca al lupo a Claudia che comincia una nuova avventura in quel di Cambridge, sono più che sicuro che te la caverai benissimo.

Continuando con l'Università di Pavia vorrei ringraziare anche il Prof. Maurizio Lichelli e il Dr. Michele Milani. Grazie per aver collaborato con me, insieme abbiamo iniziato e finito un buon numero di progetti di ricerca di qualità.

Grande Milo !!! sei diventato dottore prima di me... Con te ho passato momenti fantastici a Valencia sia dentro che fuori il lab. È stato un periodo davvero indimenticabile, ancora una volta grande Rambo !!!

Terminando con Pavia un ringraziamento doveroso va al Prof. Paolo Quadrelli: grazie per l'infinita disponibilità dimostratami, per esserti impegnato sia come referee esterno che come membro della commissione, grazie per avermi sopportato. Grazie davvero.

Y ahora debería volver a escribir en Castellano para agradecerlos a todos, amigos académicos, pero no lo haré. La razón es muy sencilla: si ya me cuesta mucho expresar mis sentimientos en mi idioma, os podéis imaginar las dificultades que tendría en hacerlo en Castellano o peor en Inglés. Os pido entonces un pequeño esfuerzo para leer estos agradecimientos y entender cuanto os quiero...

Come detto all'inizio per me questi tre anni sono stati un viaggio affascinante, faticoso e sicuramente indimenticabile. Sono stato lontano dalle persone che amo per molto, probabilmente troppo, tempo. Chi ha reso sopportabile quest'assenza, questa lontananza siete voi. Chi più chi meno, siete stati per me una grande famiglia. Ovviamente non c'è nessun ordine logico in cui vi ringrazierò e sicuramente mi dimenticherò di qualcuno, sono fatto così... Vi prego non arrabbiatevi e perdonate la mia inadeguatezza.

Iniziamo dunque, senza ulteriori indugi... Grazie a Elena e Carmen siete state e sarete sempre le due sorelle maggiori che non ho mai avuto. Mi avete ascoltato, consigliato e ripreso quando me lo meritavo; non ho davvero parole per esprimere la mia gratitudine nei vostri confronti semplicemente grazie di tutto. Vorrei ringraziare Estela e Cris... come se non bastasse sopportarmi in laboratorio, durante questi ultimi mesi mi avete sopportato anche a casa dopo il lavoro... grazie di tutto sorelline è stato davvero bello vivere con voi... Che dire poi di Dani, Almu, Neus, Mar, Lluís (eres y sempre seras el nuevo...), Nùria, Edgar (mauqinaaaaa!!!!!!), Andrea siete

e sempre sarete tutti degli amici fantastici. Vi voglio ringraziare tutti perché con me siete sempre stati voi stessi, abbiamo condiviso gioie, emozioni, momenti belli e meno belli. Ancora una non riesco a esprimere a parole quanto vi voglio bene... semplicemente vi ringrazio per tutto ciò che mi avete dato in questi anni, mille volte grazie !!! Grazie a Raúl, Rafa, Nacho, Sergio, Mireia e David senza la vostra simpatia non sarebbe stato facile passare le giornate in dipartimento. A parte questo grazie per i tanti consigli che mi avete dato. Grazie Inma, grazie per avermi aiutato moltissimo appena arrivato, senza di te non sarei riuscito ad imparare così rapidamente la lingua e sarebbe stato tutto più difficile. Grazie a Luis Enrique e Sameh, anche voi stranieri in Spagna, grazie per i bei momenti passati dentro e fuori il laboratorio. Grazie Yolanda, María e Patri grazie perché senza di voi il gruppo non sarebbe lo stesso. Grazie Inma, ne abbiamo passate tante in questi tre anni e alla fine siamo anche riusciti a condividere l'Odissea burocratica che precede la difesa della tesi. Sei e sarai sempre un'amica... Grazie Román, grazie coglione !!!, ci siamo un po' persi di vista ultimamente ma questo non può cancellare quello che abbiamo vissuto assieme. Grazie dell'aiuto e di essere un amico. Grazie a Pavel e Santi ormai sono passati anni da quando uscivamo assieme a Félix, sono stati davvero dei bei momenti e sarebbe bello riviverli... Ovviamente grazie a Cris (la nueva...) grazie per tutto l'aiuto grazie dentro e fuori l'università e grazie per aver condiviso dubbi e incertezze dei miei bizzarri progetti scientifici. Ad Ana, che ha appena iniziato, faccio i miei più sinceri auguri e spero che i tuoi anni da dottoranda possano essere indimenticabili come lo sono stati per me. Infine grazie a Laura, ma soprattutto spero davvero che la tua esperienza francese possa permetterti di continuare a inseguire i tuoi sogni.

*Rimangono ora i non accademici... Un grazie infinito, nel vero senso della parola, va ai miei genitori. Grazie mamma e grazie papà... Grazie perché siete sempre stati al mio fianco, grazie perché siete sempre presenti e soprattutto grazie perché so che ci sarete sempre. Grazie per avermi sempre spronato a inseguire i miei sogni e infine grazie perché con il vostro esempio ho capito ciò che conta davvero e, so di ripetermi, ma so anche che se mai combinerò qualcosa di buono, lo devo soprattutto a voi. Grazie Paolo e grazie Claudio. Grazie, perché per me ci siete sempre stati e da quando vi conosco siete sempre stati una certezza nella mia vita, grazie di essere dei veri amici...*

*Grazie Sara e Massimo perché siete sempre stati parte della mia famiglia e sempre lo sarete...*

*Grazie a Giorgio, grazie per non avermi mai abbandonato all'aeroporto e, a parte gli scherzi, grazie perché so che su te si può sempre contare grazie perché so che anche tu per me ci sarai sempre.*

*Grazie a Dario perché con il tuo esempio ci hai fatto capire che non basta avere delle idee e semplicemente credere in esse. Ci hai dimostrato che bisogna dare tutti noi stessi e lottare per poter avere anche una sola opportunità di trasformare le nostre idee e i nostri principi in una realtà. Ti faccio i miei più grandi complimenti, perché so che ora darai tutto te stesso per cambiare le cose.*

*Come'è ormai tradizione uso queste ultime righe per ringraziare Claudia ed è davvero difficile esprimere a parole l'immensità della mia gratitudine e del mio amore per te... Grazie perché mi hai capito, tre anni fa, quando ho deciso di partire per un viaggio probabilmente troppo lungo. Grazie perché in quel momento saresti potuta*

essere "normale" invece di straordinaria e non avresti avuto grosse difficoltà a convincermi a restare. Grazie perché mi hai aspettato, credendo nella nostra storia. Grazie perché so che sarebbe stato molto più facile lasciar perdere alle prime difficoltà, ma ancora una volta ti sei dimostrata eccezionale e se sono qui ora a scrivere queste righe lo devo in gran parte a te. Ancora grazie perché ora tu ed io siamo la dimostrazione vivente che credendo nell'amore e nella fiducia reciproca tutto è possibile. Grazie perché soprattutto tu sei una delle poche certezze della mia vita. Infine grazie per essere come sei: eccezionale, straordinaria, incredibile, senza eguali, in poche parole unica. Per tutto questo e per mille altri motivi

*grazie amore mio !!!*

## **Abstract**

This PhD thesis is entitled “*Supramolecular and hetero-supramolecular chemistry in controlled release and molecular recognition processes*” and it is focused on two of the most important and recent subjects of supramolecular chemistry: **molecular recognition** and **controlled delivery processes**.

In particular the first part of this thesis is focused on the design and synthesis of suitable organic compounds as chemosensors for anionic and neutral species. The selected sensing paradigm was the *chemodosimeter* approach. This presents some advantages with respect to the other two paradigms (*displacement* and *binding site-signaling subunit*); among others the possibility of operating in aqueous solution. In particular two selective probes were synthesized one for fluoride anion ( $F^-$ ) and another for glutathione (GSH). The selective chemodosimeter for  $F^-$  is a phenolic azo-dye functionalized, on the phenolic  $-OH$ , with a silylether. This sensor displays an intense absorption band centered at 350 nm and, upon treatment with  $F^-$ , underwent a significant hypochromic and a slight bathochromic shift (of ca. 10 nm), while a new band appeared at ca. 470 nm, resulting in a change from colorless to orange red. In the case of the selective sensing of GSH a pyrylium based chemodosimeter was prepared. This compound was later dissolved in a CTAB/water solution that resulted in an intense blue color. In this case GSH was able to induce a remarkable hypochromic effect in the absorption bands with the subsequent bleaching of the initial blue solution. Moreover, addition of GSH induced the appearance of strong emission band centered at 485 nm (upon irradiation at 350 nm).

The second part of this PhD thesis deals with the design and synthesis of organic-inorganic nanoscopic hybrid systems for controlled delivery of bioactive molecules into intracellular environments. These hybrid materials are composed of two main units: an inorganic silica based mesoporous scaffold, able to store organic molecules (dyes or drugs) and an organic compound anchored on the external surface of the inorganic mesoporous support than acts as *molecular gate*. The application of an external stimulus can modify the steric hindrance of the capping organic compound (molecular gate) enabling or disabling the diffusion of the stored molecules from the inner to the outer of the pores. The first synthesized and studied system was composed of an inorganic mesoporous nanoscopic matrix (MCM-41), loaded with the dye  $\text{Ru}(\text{bipy})_3^{2+}$  and functionalized with an oligoethylene moiety anchored to the silica surface through an ester group. The addition of a esterase enzyme induced the selective hydrolysis of the ester moiety, the subsequent reduction of the steric hindrance of the molecular gate and the release of the entrapped dye. A second delivery system consisted of a MCM-41 matrix and the dye  $\text{Ru}(\text{bipy})_3^{2+}$ , but in this case the outer surface was functionalized with a photocleavable molecule. The irradiation on the molecular gate's absorbance maximum determined the photodegradation of the capping molecule and the consequent delivery of the cargo. A third example contained a gate characterized by the presence of two different enzymatically hydrolyzable groups: urea and amide moieties. The final hybrid material, consisting of a mesoporous MCM-41 characterized inorganic matrix, loaded with  $\text{Ru}(\text{bipy})_3^{2+}$ , was able to specifically release certain amount of dye, depending on the enzyme used. Thus a rapid but less intense delivery or a slower but more intense delivery could be induced, by simply selecting the appropriate enzyme.

Finally a MCM-41 based hybrid material, loaded with rhodamine-B and functionalized with galactooligosaccharides on the outer surface was synthesized. This material was able to deliver the entrapped dye selectively in senescent cells due to the presence in these cells of overexpressed  $\beta$ -galactosidase enzyme, which is able to selectively hydrolyze the galactooligosaccharides groups.



## **Resumen**

La presente tesis doctoral titulada “*Supramolecular and hetero-supramolecular chemistry in controlled release and molecular recognition processes*” está centrada en los dos aspectos principales de la química supramolecular que han experimentado un gran auge en los últimos años: el **reconocimiento molecular** y los **procesos de liberación controlada**.

En particular la primera parte de la tesis se focaliza en el diseño y síntesis de moléculas orgánicas que pueden ser empleados como sensores para especies aniónicas y neutras. El paradigma seleccionado para los procesos de reconocimiento molecular fue la aproximación del *dosímetro químico*. Esta aproximación presenta ventajas con respecto a los otros dos métodos de determinación de aniones (*desplazamiento* y *unidad coordinante-unidad indicadora*), como, por ejemplo, la posibilidad de determinar los analitos en disolución acuosa. Así se sintetizaron dos sensores selectivos, uno para el anión fluoruro (F<sup>-</sup>) y el otro para glutatión (GSH). El sensor selectivo para la determinación de F<sup>-</sup> está basado en un colorante azoico funcionalizado, en su -OH fenólico, como silileter. Esta molécula presenta una banda de absorción muy intensa centrada a 350 nm que, después de la adición de F<sup>-</sup>, sufre un efecto hipocrómico significativo y un desplazamiento batocromico ligero (de ca. 10 nm), mientras aparece una nueva banda a 470 nm, determinando un cambio de incoloro a amarillo-rojo. Para obtener un sensor selectivo para GSH se sintetizó una sonda química basado en una sal de 2,6-difenilpirilio. Sucesivamente se preparó una disolución de este compuesto en agua/CTAB, que se caracterizaba por un intenso color azul. En este caso, la adición de GSH produce una disminución significativa de la banda del visible, acompañada por la consecuente decoloración. Además la adición de GSH induce la aparición de

una intensa banda de emisión centrada a 485 nm (después de la irradiación a 350 nm).

La segunda parte de esta tesis doctoral se basa en el diseño y síntesis de nuevos sistemas híbridos orgánicos-inorgánicos para procesos de liberación controlada en ambiente celular. Estos materiales híbridos se componen en general, de dos unidades: una matriz inorgánica mesoporosa de base silícea, capaz de almacenar moléculas orgánicas (colorantes, farmacos...) y un compuesto orgánico anclado covalentemente a la superficie externa del soporte inorgánico mesoporoso, que actúa como *puerta molecular*. La aplicación de un estímulo externo puede modificar la conformación de la puerta molecular permitiendo o bien impidiendo la difusión de la carga almacenada en los mesoporos hacia el exterior (disolución o citoplasma). El primer sistema sintetizado y estudiado se compone de una matriz inorgánica mesoporosa (MCM-41), cargada con el colorante  $\text{Ru}(\text{bipy})_3^{2+}$  y funcionalizada en la superficie con un oligoetilen glicol mediante un grupo ester. La adición de la enzima esterasa determinaba la hidrólisis del grupo ester y la consecuente reducción del tamaño de la puerta molecular, acompañada por la liberación del colorante previamente cargado. Otro sistema de liberación preparado consiste en el uso de la misma matriz MCM-41 nanoscópica y el mismo colorante  $\text{Ru}(\text{bipy})_3^{2+}$ , pero se funcionalizó la superficie con una puerta molecular fotolabil. La irradiación en el máximo de absorción de la puerta molecular inducía la fotodegradación de la misma y la consecuente liberación del colorante. Un tercer ejemplo de sistema de liberación consiste en una puerta molecular caracterizada por la presencia de dos grupos funcionales hidrolizables con enzimas diferentes: grupos urea y amida.

El material final, caracterizado por la presencia del mismo esqueleto inorgánico, y cargado con  $\text{Ru}(\text{bipy})_3^{2+}$ , era capaz de liberar selectivamente cantidades distintas de colorante, dependiendo del enzima empleado. Así se podían conseguir dos tipos de perfiles de liberación: uno muy rápido y poco intenso y otro más lento pero mucho más intenso. Finalmente se sintetizó un material híbrido siempre basado en la misma matriz de MCM-41, cargado con rodamina-B y funcionalizado en la superficie con galactooligosacáridos. Con este material se podía conseguir una liberación controlada del colorante selectivamente en células senescentes, debido a que estas sobreexpresan el enzima  $\beta$ -galactosidasa que es capaz de hidrolizar los galactooligosacáridos.



## **Resum**

La present tesi doctoral titulada “*Supramolecular and hetero-supramolecular chemistry in controlled release and molecular recognition processes*” està centrada en els dos aspectes fonamentals de la química supramolecular que han experimentat un gran auge en els últims anys: el **reconeixement molecular** y els **processos de lliberació controlada**.

En particular, la primera part de la tesi es focalitza en el disseny i síntesis de molècules orgàniques que poden ser empleades com sensors per a espècies aniòniques i neutres. El paradigma seleccionat per als processos de reconeixement molecular va ser l'aproximació del *dosímetre químic*. Aquesta aproximació presenta avantatges respecte als altres dos mètodes de determinació d'anions (*desplaçament i unitat coordinant-unitat indicadora*), com, per exemple, la possibilitat de determinar els analits en dissolució aquosa. Així, es van sintetitzar dos sensors selectius, un per l'anió fluorur (F<sup>-</sup>) i l'altre per glutatió (GSH). El sensor selectiu per a la determinació de F<sup>-</sup> està basat en un colorant azoic funcionalitzat en el seu -OH fenòlic com silileter. Aquesta molècula presenta una banda de absorció molt intensa centrada a 350 nm que, després de l'addició de F<sup>-</sup>, pateix un efecte hipocròmic significatiu i un desplaçament batocròmic lleuger (de ca. 10 nm), mentre apareix una nova banda a 470 nm, determinant un canvi de incolor a groc-rogenc. Per obtenir un sensor selectiu per GSH es va sintetitzar un dosímetre químic basat en una sal de 2,6-difenilpirili. Seguidament es va preparar una dissolució d'aquest compost en aigua/CTAB, que es caracteritzava per un intens color blau. En aquest cas, l'addició de GSH produeix una disminució significativa de la banda del visible, acompanyat per la conseqüent decoloració. A més, l'addició de GSH

indueix l'aparició d'una banda d'emissió intensa centrada a 485 nm (després de la irradiació a 350 nm).

La segona part d'aquesta tesi doctoral es basa en el disseny i síntesi de nous sistemes híbrids orgànics-inorgànics per a processos d'alliberament controlat en ambient cel·lular. Aquests materials híbrids es componen en general, de dues unitats: una matriu inorgànica mesoporosa de base silícia, capaç d'emmagatzemar molècules orgàniques (colorants, fàrmacs ...) i un compost orgànic ancorat covalentment a la superfície externa del suport inorgànic mesoporós, que actua com a porta molecular. L'aplicació d'un estímul extern pot modificar la conformació de la porta molecular permetent, o bé impedit, la difusió de la càrrega emmagatzemada des dels mesopors cap a l'exterior (dissolució o citoplasma). El primer sistema sintetitzat i estudiat es componia d'una matriu inorgànica mesoporosa (MCM-41), carregada amb el colorant  $\text{Ru}(\text{bipy})_3^{2+}$  i funcionalitzada a la superfície amb un oligoètilen glicol mitjançant un grup ester. L'adició de l'enzim esterasa determinava la hidròlisi del grup ester i la conseqüent reducció de la grandària de la porta molecular, acompanyada per l'alliberament del colorant prèviament carregat. Amb l'objectiu d'obtenir sistemes més selectius, a l'hora d'alliberar controladament fàrmacs en ambient cel·lular, es va sintetitzar un altre material. En aquest cas es van emprar la mateixa matriu MCM-41 nanoscòpica i el mateix colorant  $\text{Ru}(\text{bipy})_3^{2+}$ , però es va funcionalitzar la superfície amb una porta molecular fotolàbil. La irradiació al màxim d'absorció de la porta molecular induïa la fotodegradació de la mateixa i, en conseqüència, l'alliberament del colorant. Amb l'objectiu d'obtenir sistemes cada vegada més selectius a l'hora de la seva aplicació en processos d'alliberament controlat, es va preparar una

porta molecular caracteritzada per la presència de dos grups funcionals hidrolitzables amb enzims diferents: grups urea i amida. El material final, caracteritzat per la presència del mateix esquelet inorgànic, i carregat amb  $\text{Ru}(\text{bipy})_3^{2+}$ , era capaç d'alliberar selectivament quantitats diferents de colorant, depenent de l'enzim emprat. Així, es podien aconseguir dos tipus de perfils d'alliberament: un molt ràpid i poc intens i un altre més lent però molt més intens. Finalment es va sintetitzar un material híbrid basat en la mateixa matriu de MCM-41, carregat amb rodamina-B i funcionalitzat en la superfície amb galactooligosacàrids. Amb aquest material es va aconseguir un alliberament controlat del colorant selectivament en cèl·lules senescentes, pel fet que aquestes sobreexpressen l'enzim  $\beta$ -galactosidasa (capaç d'hidrolitzar els galactooligosacàrids).



## ***Publications***

As a Result of this thesis and other collaboration have resulted in the following scientific publications:

Alessandro Agostini, Laura Mondragón, Carmen Coll, Elena Aznar, Enrique Pérez-Payá, M. Dolores Marcos, Ramón Martínez-Máñez, Félix Sancenón, Juan Soto and Pedro Amorós, *Dual enzyme-triggered controlled release on capped nanometric silica mesoporous supports*, *ChemistryOpen*, **2012**, 1, 17–20.

Alessandro Agostini, Michele Milani, Ramón Martínez-Máñez, Maurizio Licchelli, Juan Soto and Félix Sancenón, *Azo dyes functionalized with alkoxysilyl ethers as chemodosimeters for the chromogenic detection of the fluoride anion*, *Chem. Asian J.* **2012**, 7, 2040 – 2044.

Alessandro Agostini, Félix Sancenón, Ramón Martínez-Máñez, María D. Marcos, Juan Soto and Pedro Amorós, *A photoactivated molecular gate*, *Chem. Eur. J.*, **2012**, 18, 12218 – 12221.

Alessandro Agostini, Laura Mondragón, Andrea Bernardos, Ramón Martínez-Máñez, M. Dolores Marcos, Félix Sancenón, Juan Soto, Ana Costero, Cristina Manguan-García, Rosario Perona, Marta Moreno-Torres, Rafael Aparicio-Sanchis, José Ramón Murguía, *Targeted cargo delivery in senescent cells using capped nanometric silica mesoporous supports*, *Angew. Chem. Int. Ed.*, **2012**, 51, 10556 –10560

Alessandro Agostini, Laura Mondragón, Lluís Pascual, Elena Aznar, Carmen Coll, Ramón Martínez-Máñez, Félix Sancenón, Juan Soto, M. Dolores Marcos, Pedro Amorós, Ana M. Costero, Margarita Parra and

## Publications

Salvador Gil, *Design of enzyme-mediated controlled release systems based on silica mesoporous supports capped with ester-glycol groups*, *Langmuir*, **2012**, *28*, 14766–14776.

Núria Mas, Alessandro Agostini, Laura Mondragón, Andrea Bernardos, Félix Sancenón, M. Dolores Marcos, Ramón Martínez-Mañez, Ana M. Costero, Salvador Gil, Matilde Merino-Sanjuán, Pedro Amorós, Mar Orzáez, and Enrique Pérez-Payá, *Enzyme-Responsive Silica Mesoporous Supports Capped with Azopyridinium Salts for Controlled Delivery Applications*, *Chem. Eur. J.*, **2013**, *19*, 1346 – 1356.

Luis E. Santos Figureoa, María E. Moragues, Estela Climent, Alessandro Agostini, Ramón Martínez-Mañez, Félix Sancenón, *Chromogenic and fluorogenic chemosensors and reagents for anions. A comprehensive review of the years 2010-2011*, *Chem. Soc. Rev.*, **2013**, *42*, 3489-3613.

Yolanda Salinas, Alessandro Agostini, Edgar Pérez-Esteve, Ramón Martínez-Mañez, Félix Sancenón, M. Dolores Marcos, Juan Soto, Ana M. Costero, Salvador Gil, Margarita Parra, Pedro Amorós, *Fluorogenic detection of Tetryl and TNT explosives using nanoscopic-capped mesoporous hybrid materials*, *J. Mater. Chem. A*, **2013**, *1*, 3561–3564.

Ramón Martínez-Mañez, Alessandro Agostini, María Dolores Marcos, Juan Soto, Félix Sancenón, Laura Mondragón, José Ramón Murguía, Marta Moreno-Torres, Rosario Perona, Cristina Manguan-García, “Liberación de sustancias en células senescentes”, Patent application P201231370. Date: 4th September 2012.

## ***Abbreviations and Acronyms***

<b><i>AIDS</i></b>	Acquired Immunodeficiency Syndrome
<b><i>BET</i></b>	Brunauer-Emmett-Teller model
<b><i><math>\beta</math>-gal</i></b>	$\beta$ -galactosidase
<b><i><math>\beta</math>-gal<sup>OE</sup></i></b>	Over Expressed $\beta$ -galactosidase
<b><i>BJH</i></b>	Barrett-Joyner-Halenda model
<b><i>BODIPY</i></b>	Boron-dipyrromethene
<b><i>CBOQT<sup>4+</sup></i></b>	Cyclobis-(paraquat- <i>p</i> -phenylene)
<b><i>CD</i></b>	Cyclodextrin
<b><i>CMC</i></b>	Critical Micelle Concentration
<b><i>COSY</i></b>	Correlation Spectroscopy (NMR)
<b><i>CPT</i></b>	Camptothecin
<b><i>CTAB</i></b>	Cetyltrimethylammonium bromide
<b><i>Cys</i></b>	Cysteine
<b><i>DB24C8</i></b>	Dibenzo[24]crown-8
<b><i>DBU</i></b>	1,8-Diazabicyclo-undec-7-ene
<b><i>DEPT</i></b>	Distortionless Enhancement by Polarization Transfer (NMR)
<b><i>DET</i></b>	Diethyl tartrate
<b><i>DMSO</i></b>	Dimethyl Sulfoxide
<b><i>DNA</i></b>	Deoxyribonucleic acid
<b><i>DNPD</i></b>	Dioxynaphtalene Derivative
<b><i>DTT</i></b>	Dithiothreitol
<b><i>EA</i></b>	Elemental Analysis
<b><i>GOS</i></b>	Galactooligosaccharide
<b><i>GSH</i></b>	Glutathione
<b><i>Hcy</i></b>	Homocysteine
<b><i>HeLa</i></b>	Henrietta Lacks cells
<b><i>HPLC</i></b>	High Performance Liquid Chromatography
<b><i>HSQC</i></b>	Heteronuclear Single Quantum Coherence (NMR)
<b><i>LCST</i></b>	Lower Critical Solution Temperature
<b><i>LLC-PK1</i></b>	Pig Kidney Epithelial Cells
<b><i>MCF-7</i></b>	Michigan Cancer Foundation - 7 cells
<b><i>MCM</i></b>	Mobile Crystalline Material

## Abbreviations and Acronyms

<b>ME</b>	Mercaptoethanol
<b>MO</b>	Methyl Orange
<b>MS-EI</b>	Mass Spectrometry Electron Impact Ionization
<b>MSNs</b>	Mesoporous Silica Nanospheres
<b>NAIDs</b>	Non Steroidal Anti Inflammatory Drug
<b>NMR</b>	Nuclear Magnetic Resonance
<b>NPs</b>	Nanoparticles
<b>PAMAM</b>	Poly(amido amine)
<b>PDDA</b>	Poly-(dimethyldiallylammonium chloride)
<b>PEI</b>	Polyethyleniminc
<b>PI</b>	Propidium Iodide
<b>PMMA</b>	Poly(methyl methacrylate)
<b>PNAS-MS</b>	Poly( <i>N</i> -acryloxysuccinimide)-grafted mesoporous silica
<b>PNIPAAm</b>	<i>N</i> -isopropylacrylamide
<b>PXRD</b>	Powder x-Ray Diffraction
<b>R&amp;D</b>	Research and Development
<b>RGB</b>	Red-Green_Blue
<b><i>Ru(bipy)</i><sub>3</sub><sup>3+</sup></b>	Tris(bipyridine)ruthenium(II)
<b><i>SA-b-gal</i></b>	Senescence associated b-galactosidase
<b>SBA</b>	Santa Barbara Amorphous
<b>SDTA</b>	Simultaneous Differential Thermal Analysis
<b><i>sel-TOCSY</i></b>	Selective Total Correlation Spectroscopy
<b>SEM</b>	Scanning Electron Microscopy
<b>TBDMS</b>	t-Butyldimethylsilyl
<b><i>t-butOOH</i></b>	t-Butyl hydroperoxide
<b>TEM</b>	Transision Electron Microscopy
<b>TEOS</b>	Tetraethyl Orthosilicate
<b>TGA</b>	Thermogravimetric Analysis
<b>TIPS</b>	Triisopropyl Silane
<b>TLC</b>	Thin Layer Chromatography
<b>TLTC</b>	True Liquid Crystal Templating
<b>TMOS</b>	Tetramethyl Orthosilicate
<b>TSUA</b>	4-(3-Triethoxysilylpropylureido)azobenzene

<b><i>TTF</i></b>	Tetramethyltetrathiafulvalene
<b><i>UVM</i></b>	Universitat de València Material
<b><i>UV-vis</i></b>	Ultra Violet-visible



# Table of Contents

<b>Chapter 1: General Introduction</b> .....	1
1.1 Introduction .....	3
1.2 Supramolecular Chemistry .....	3
1.3 Molecular Recognition Chemistry .....	5
1.4 Molecular Self-Assembly Chemistry .....	11
<b>Chapter 2: Chemosensors</b> .....	19
2.1 Introduction .....	21
2.2 Objectives .....	31
2.3 Chemodosimeters Design.....	32
2.3.1 Design of a reactive subunit, how to achieve selectivity .....	32
2.3.2 Design of a signaling subunit.....	37
<b>Chapter 3: Azo dyes functionalized with alkoxysilyl ethers as chemodosimeters for the chromogenic detection of the fluoride anion</b> ..	41
3.1 Abstract.....	42
3.2 Introduction .....	42
3.3 Results and Discussion.....	44
3.4 Conclusions.....	52
3.5 Experimental Section.....	53
3.6 Acknowledgments.....	55
3.7 Bibliography.....	55
<b>Chapter 4: A surfactant-assisted probe for the chromo-fluorogenic recognition of GSH over cysteine in water</b> .....	61

Table of Contents

4.1 Acknowledgments .....	70
4.2 Bibliography.....	70
<b>Chapter 5: Controlled Delivery Systems.....</b>	<b>109</b>
5.1 Introduction .....	111
5.1.1 Organic-Inorganic-Hybrid Materials .....	112
5.1.2 Mesoporous Materials .....	113
5.1.3 Synthesis of Mesoporous Materials.....	115
5.1.4 Functionalization of Mesoporous-Silica-Scaffolds: How to Obtain Organic-Inorganic Hybrid Materials .....	118
5.1.5 Characterization of the Organic-Inorganic-Mesoporous Hybrid materials .....	122
5.1.6 Application of Organic-Inorganic Hybrid Materials: Molecular Gates .....	125
5.2 Objectives .....	149
<b>Chapter 6: Design of enzyme-mediated controlled release systems based on silica mesoporous supports capped with ester-glycol groups.....</b>	<b>153</b>
6.1 Abstract.....	154
6.2 Introduction .....	155
6.3 Experimental Section .....	157
6.4 Results and discussion.....	162
6.5 Conclusions.....	179

6.6 Bibliography.....	179
<b>Chapter 7: Dual enzyme-triggered controlled release on capped nanometric silica mesoporous supports.....</b>	<b>189</b>
7.1 Introduction .....	190
7.2 Results and Discussion.....	191
7.3 Conclusions.....	198
7.4 Bibliography.....	199
<b>Chapter 8: Targeted cargo delivery in senescent cells using capped nanometric silica mesoporous supports.....</b>	<b>221</b>
8.1 Introduction .....	222
8.2 Results and Discussion.....	224
8.3 Conclusions.....	230
8.4 Acknowledgments.....	231
8.5 Bibliography.....	231
<b>Chapter 9: A photoactivated molecular gate.....</b>	<b>249</b>
9.1 Introduction .....	250
9.2 Results and discussion.....	251
9.3 Conclusions.....	257
9.4 Acknowledgements.....	258
9.5 Bibliography.....	258
<b>Chapter 10: Conclusions and Future Perspectives.....</b>	<b>275</b>



***Chapter 1:***  
***General Introduction***



## ***1.1 Introduction***

All the contents of this PhD thesis, from the simplest sensors to the more complex nanoscopic organic-inorganic hybrid materials, is based on supramolecular chemistry. Thus in this first general introduction the fundamentals of supramolecular chemistry will be furnished.

## ***1.2 Supramolecular Chemistry***

A vast number of molecules of different sizes and structure are known, ranging from the simple hydrogen molecule ( $\text{H}_2$ ) to the infinitely more

## 1.2 Supramolecular Chemistry

complex biological protein and nucleic acid or the high-molecular-weight man-made polymers. We may therefore be tempted to believe that the structures and properties of these materials and compounds can be directly related to those of the individual molecules that comprise them in a straightforward way. Unfortunately, this notion is not correct. However deeply we understand the nature of individual molecules, this knowledge is not enough to explain the structures, functions and micro-macroscopic properties of materials and molecular assemblies, that are derived as a result of organizing individual molecules. The discipline that provides us the tools to understand how simple molecules organize themselves to build-up more complex units is *Supramolecular Chemistry*.

Supramolecular Chemistry is often defined as “*chemistry beyond the molecules*” intended as chemistry beyond the covalent bond. Thus this new branch of chemistry deals mainly with how discrete molecules can cooperate through non-covalent interactions as hydrogen bonding, metal coordination, hydrophobic forces, van der Waals forces,  $\pi$ - $\pi$  interactions and electrostatic effects, to easily generate unique nanostructured supermolecules that present different properties (often better) than the sum of the properties of each individual component.<sup>1</sup>

It can be said that J. M. Lehn, D. J. Cram and C. J. Pedersen are the founding fathers of supramolecular chemistry and the great importance of their job was universally recognized in 1987 when they received the Nobel Prize for their fundamental contributions to the development of this new area inside chemistry. According to Dr. Lehn, who introduced the term, a *supermolecule* is an organized complex entity that is created from the association of two or more chemical species held together by

---

<sup>1</sup> K. Ariga, T. Kunitake, *Supramolecular Chemistry-Fundamentals and application*, © Springer-Verlag Berlin Heidelberg edition 2006.

intermolecular forces, whereas the term *Supramolecular Chemistry* may be defined as “*chemistry beyond the molecule*”, focusing on the organized entities of higher complexity that result from the association of two or more chemical species held together by intermolecular forces.<sup>2</sup>

Bearing in mind the infinite number of possibilities given by the non-covalent bond chemistry an organization of this new discipline should be useful; thus supramolecular chemistry can be divided in two main areas:

- i. molecular recognition chemistry*, chemistry associated with a molecule recognizing a partner molecule, also defined as *Host-Guest chemistry*
- ii. self-assembly chemistry*, chemistry of molecular assembly of many molecules.

This doctoral thesis embraces both of these two areas; in fact dealing with molecular recognition two chemosensing ensemble were prepared for the selective detection of fluoride anion and for glutathione whereas the synthesis of the nanoscopic silica based mesoporous materials and their superficial functionalization with organic molecules to obtain triggerable gated systems for drug delivery processes is somehow related with self assembly supramolecular chemistry.

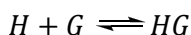
### ***1.3 Molecular Recognition Chemistry***

Molecular recognition is the base of all the supramolecular chemistry because the construction of any supramolecular aggregate involves selective molecular combination. In particular a molecular recognition event can take place only if a host molecule or (*receptor*) selectively interacts with a guest molecule (*substrate*) usually through *non-covalent bonds*.

---

<sup>2</sup>J. -M. Lehn, *Supramolecular Chemistry*, Ed. VCH, 1995; J.-M. Lehn, Nobel lecture, 1987.

To produce this recognition event, specific conditions of spatial and electronic compatibility between the host and guest binding sites must be satisfied. In particular we have to consider that the recognizing event is an equilibrium between the unbound state, in which the host and the guest are separate from each other, and the bound state, in which there is a structurally defined host-guest complex:



*H*: Host molecule, *G*: Guest molecule, *HG*: Host-Guest complex

This chemical equilibrium is displaced to the right, because there are several thermodynamic benefits deriving from the host guest co-operative non-covalent chemistry interaction that determine the reduction of the overall Gibbs free energy.

The first example of supramolecular recognition chemistry was reported by H. E. Fischer in 1890 when he suggested that the enzyme-substrate interactions take the form of a "lock and key" in which the guest has a geometric size or shape complementary to the receptor or host. This concept laid the basis for *molecular recognition*; i.e. the discrimination by a host between a number of different guests (see figure 1).

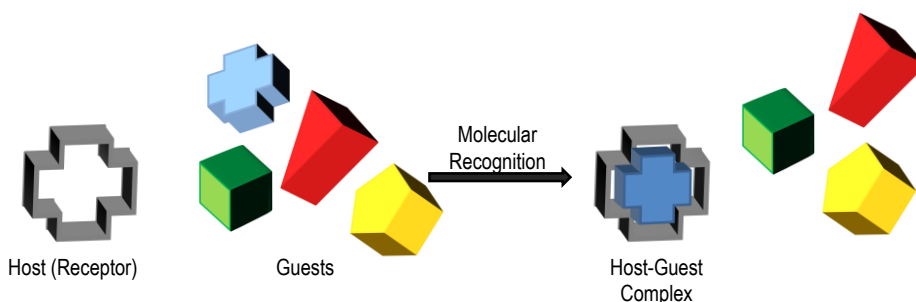


**Figure 1.** Schematic representation of a molecular recognition event: the host is able to discriminate between different guests

The receptor ability to selectively react with only one specific substrate is given by the above mentioned electronic and spatial complementarities which reflect in a major kinetic/thermodynamic stabilization of the complex. In particular if the equilibrium association constant  $K_a$  is:

$$K_a = \frac{[HG]_{eq}}{[H]_{eq}[G]_{eq}}$$

and the reaction Gibbs free energy at the equilibrium  $\Delta G_r^0$  is expressed as:

$$\Delta G_r^0 = -RT \ln K_a$$

it can be stated that the higher  $K_a$  the lower  $\Delta G_r^0$  at constant pressure and temperature, thus the selective interaction between H and a particular G is given by the ensemble of the non covalent interaction that determine the greater value of  $K_a$  and the lowest value of  $\Delta G_r^0$  among the possible products, yielding the most stable complex. From a simplistic point of view: H reacts with a particular G because the reaction is kinetically and thermodynamically favoured and the stabilization  $\Delta E$  is major (see figure 2).<sup>3</sup>

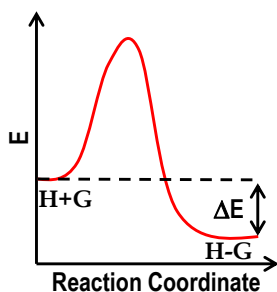


**Figure 2.** Free energy diagram of Host-Guest complex formation. X axis = Reaction Coordinate. Y axis = Free Energy. One can see that the host-guest complex is at a lower overall energy that the individual molecules

<sup>3</sup>P. W. Atkins, L. L. Jones, *Chemistry: Molecules, Matter, and Change. Third Edition.* © 1997 W H Freeman & Co (Sd).

The chemistry of specific non-covalent interaction between host and guest molecule has resulted in a number of applications and among others has allowed the development of new molecular devices for *nano-medicine*, *catalysis* and *sensing* with different applications. For example the use of dendrimers in medicine has shown to improve drug delivery by increasing the solubility and bioavailability of the drug.

In conjunctions, dendrimers can increase both cellular uptake and targeting ability, and decrease drug resistance. In this case the dendrimer present several receptor units (hosts) able to bind the drug (the guest) usually through hydrophobic interaction. The new complex form is usually able to better permeate the cell membrane without altering the physiological properties of the drug.<sup>4</sup>

A particular example is the case of poor water soluble non-steroidal anti-inflammatory drugs (NSAIDs) whose solubility increases when are encapsulated in PAMAM dendrimers.<sup>5</sup> The enhancement of NSAID solubility is due to the electrostatic interactions between the surface amine groups in PAMAM and the carboxyl groups found in NSAIDs. Contributing to the increase in solubility are the hydrophobic interactions between the aromatic groups in the drugs and the inner cavities of the dendrimer. When a drug is encapsulated within a dendrimer, its physical and physiological properties remains unaltered, including non-specificity and toxicity. This principle is also being studied for cancer treatment application. Several groups have encapsulated anti-cancer drugs such as: camptothecin, methotrexate, and doxorubicin. Results from these research has shown that dendrimers have increased aqueous solubility, slowed release rate, and drug cytotoxicity control by the direction of the molecule

---

<sup>4</sup> Y. Cheng, J. Wang, T. Rao, X. He, T. Xu, *Frontiers in Bioscience* **2008**, 1447-1471.

<sup>5</sup> Y. Cheng, T. Xu, *Eur. J. Med. Chem.* **2005**, 1188-1192.

to target cells. For example cisplatin has been conjugated to PAMAM dendrimers that resulted in the same pharmacological results listed above, but the conjugation also helped in accumulating cisplatin in solid tumors in intravenous administration. <sup>6</sup> In the case of asymmetric and/or chemoselective catalysis it can be stated that just a portion of the first reactant is able to recognize and react with other reactants thanks to the formation of an activated complex with the catalyst yielding products with a high chemo and enantio-purity ratio. One of the most famous examples of this chemistry is the Sharpless' asymmetric epoxidation reaction. <sup>7</sup>

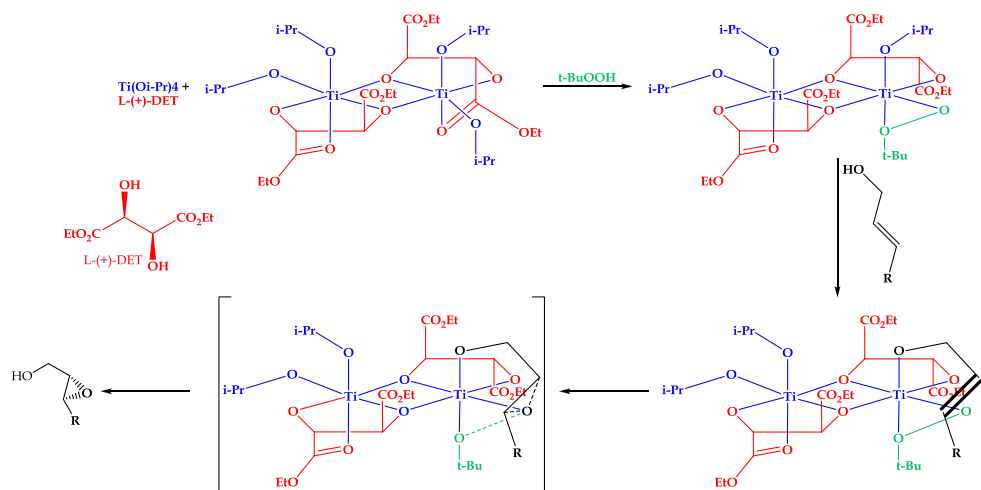


Figure 3. Sharpless epoxidation reaction

In particular the first step is the preparation of the catalyst formed by an enantiopure diethyl tartrate (D(-)-DET or L(+)-DET) (showed in red), and titanium isopropoxyde (showed in blue) followed by the addition of the oxidant tertbutylhydroperoxyde ( $t\text{-BuOOH}$ ). When the oxidizing agent ( $t\text{-BuOOH}$ , shown in green) is added to the mixture, it displaces one of the remaining isopropoxide ligands and one of the tartrate carbonyl groups

<sup>6</sup> N. Malik, E. Evagorou, R. Duncan, *Anti-cancer Drugs* **2005**, 767-776.

<sup>7</sup> T. Katsuki, K. B. Sharpless, *J. Am. Chem. Soc.* **1980**, 5974-5976

(see figure 3). Now, for this oxidizing complex to react with an allylic alcohol, the alcohol must become coordinated also with the titanium, displacing a further isopropoxide ligand.

Because of the shape of the complex the reactive oxygen atom of the bound hydroperoxide has to be delivered to the lower face of the alkene (as drawn), and the epoxide is formed in high enantiomeric excess.<sup>8</sup> Thus it can be stated that the allylic alcohol is recognized and pre-oriented by the binding site of the catalyst to suffer an enantioselective epoxidation on its double bond moiety, as showed in figure 4.

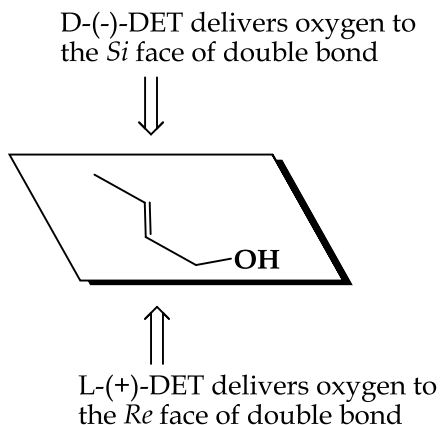


**Figure 4.** Enantioselectivity in the Sharpless asymmetric epoxidation reaction

Another example of the application of molecular recognition chemistry is related with the concept of chemical sensing. In the last decades this field has been extensively studied and strong efforts for the design of selective **molecular probes** have been carried out.<sup>9</sup>

<sup>8</sup> J. Clayden, N. Greeves, S. Warren, *Organic Chemistry second edition*, **2012**, © Oxford University Press.

<sup>9</sup> (a) R. Martínez-Mañez, F. Sancenón, *Chem. Rev.*, **2003**, *103*, 4419-4476. (b) P. D. Beer, P. A. Gale, *Angew. Chem.* **2001**, *113*, 502-532. (c) C. R. Bondy, S. J. Loeb, *Coord. Chem. Rev.*, **2003**, *240*, 77-99. (d) J. L. Sessler, S. Camiolo, P. A. Gale, *Coord. Chem. Rev.* **2003**, *240*, 17-55. (e) R.

A *molecular probe* or *chemosensor* is a molecule that specifically interacts with an analyte producing a detectable signal. Thus chemosensors combine selective molecular recognition events with the generation of a macroscopic signal.<sup>10</sup> A molecular chemosensor is usually composed of two main units: a *receptor subunit* and a *signaling subunit*. In particular the receptor subunit, which is the responsible of the recognition event and grants the host ability to discriminate a guest between many, must present a high grade of selectivity and complementarity with the guest in terms of size, shape, charge, etc. The second fundamental moiety of a chemosensor is the *signaling subunit*, which acts as a signal transducer, and informs that the recognition event takes place at molecular level, through a macroscopic measurable signal (for a detailed description see chapter 1, page 24). Traditionally, changes in color, fluorescence or redox potential have been used as signal outputs.

## **1.4 Molecular Self-Assembly Chemistry**

Molecular self-assembly is the spontaneous organization of molecules under thermodynamic equilibrium conditions into a structurally well-defined and rather stable arrangement through a number of non-covalent interactions.<sup>11</sup> Even if a supramolecular assembly can be simply composed of two molecules (e.g., a DNA double helix or an inclusion compound), it is more often used to denote larger complexes of molecules that form sphere-,

---

Martínez-Máñez, F. Sancenón, *J. Fluoresc.* **2005**, *15*, 267-285. (f) S. Royo, R. Martínez-Máñez, F. Sancenón, A. M. Costero, M. Parra, S. Gil, *Chem. Commun.*, **2007**, 4839-4847. (g) E. Climent, M.D. Marcos, R. Martínez-Máñez, F. Sancenón, J. Soto, K. Rurack, P. Amorós, *Angew. Chem. Int. Ed.*, **2009**, *48*, 8519-8522.

<sup>10</sup> W. C. Rogers, M. O. Wolf, *Coord. Chem. Rev.*, **2002**, 341-350.

<sup>11</sup> J. M. Lehn. *Supramolecular Chemistry*, *Science*, **1993**, *260*, 1762-1763

rod-, or sheet-like species. The dimensions of supramolecular assemblies can range from nanometers to micrometers allowing access to nano-scale objects using a bottom-up approach in far fewer steps than a single molecule of similar dimensions. The driving forces for these self-assembling processes have classified into two categories: *precisely defined recognition* and *fuzzy molecular interaction*.

In the first part of this introduction, dealing with molecular recognition chemistry, it has been commented how certain interactions (such as hydrogen bonding and coordination) allow a host molecule to bond precisely with a guest molecule to form a relatively small supermolecule. The geometry of the host-guest complex is dictated by the relative positions of the interacting functional groups, and applying many of these recognition interactions leads to the construction of assemblies with well defined shapes. One way of looking at self-assembly processes is that the structure of the supramolecular assembly is programmed in the molecular units that it is constructed from. Interestingly, this concept is widely seen in nature. For example, the three-dimensional structures of proteins are defined by their amino acid sequences; in other words, the structure of a protein is programmed in its amino acid sequence. An abiotic example is the  $\text{Cu}^+$  directed formation of artificial helicates from single poly-bipyridine strands (see figure 5).

In this case each  $\text{Cu}^+$  ion coordinates with two pyridine units, inducing a helical complex that is called a helicate. When  $\text{Cu}^+$  ions are added to a mixture of the ligands, complexes with random ligand combinations are initially formed, but then spontaneous ligand exchange occurs, forming size-matched helicates. The size-matched helicates use all of the binding

sites and should therefore be more stable. Therefore, less stable hetero-ligand complexes are gradually weeded out.<sup>12</sup>

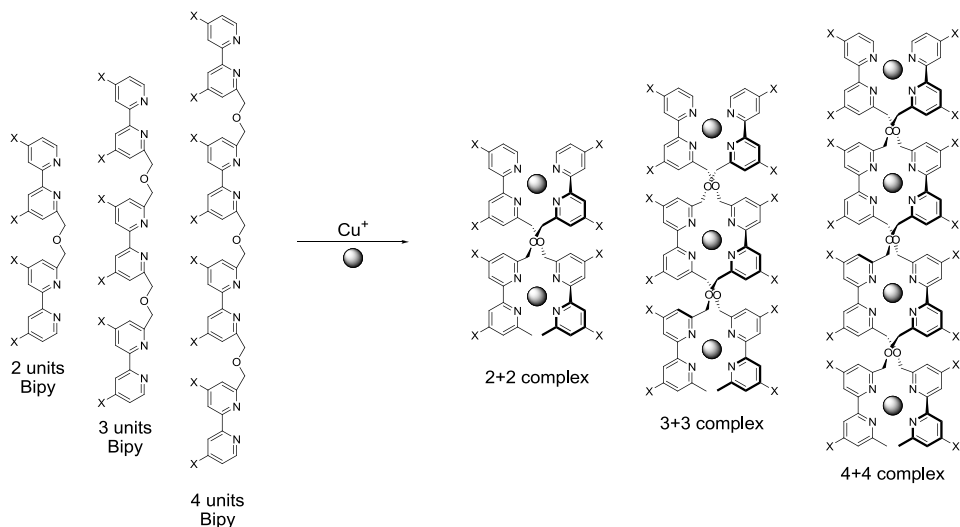


**Figure 5.** Schematic representation of  $\text{Cu}^+$  induced formation of helicate from polymeric bipyridines

The other important category of driving forces to build-up supramolecular assemblies relies on *fuzzy* non covalent interactions. In this case supramolecular assemblies characterized by more flexible, sensitive and adaptable functionality can be obtained. Living creatures can be regarded as ultimate examples of supermolecules, because they are formed from a huge number and variety of molecules through supramolecular interactions. However, the functionalities observed in living creatures, including those used in our daily life, are not always based on precise recognition and combinations of ambiguous recognition and control processes result in highly sophisticated overall functionality.

The most exemplificative and simple system obtained by fuzzy intermolecular interaction is the *micelle*. A micelle is formed when the

<sup>12</sup> B. Linton, A.D. Hamilton, *Chem. Rev.*, **1997**, 1669-1680

## 1.4 Molecular Self-Assembly

aqueous concentration of amphiphilic molecules (also called surfactant) overtakes a precise value named *critical micelle concentration* (CMC). The formation of micelles is thermodynamically favored because these amphiphilic species self-organize in order to minimize their hydrophobicity by aggregating their non-polar cues. The micelle structure depicted in figure 6 is just a cross section because the actual structure is tridimensional.

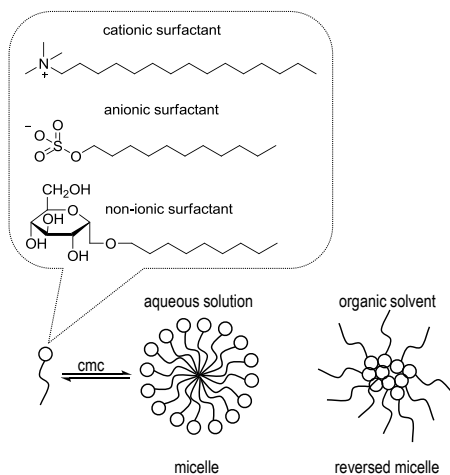


**Figure 6.** Schematic representation of micelle and reverse micelle formation

The assembled structure is completely nonregular, in fact rapid exchange between micelle molecules and monomeric soluble molecules occurs. Therefore, a micelle can be regarded as a disordered dynamic supramolecular assembly (a *fuzzy supermolecule*).

A similar structure, but with the roles of the hydrophilic part and the hydrophobic part exchanged, can occur in nonpolar media, such as organic solvents. This structure is called a *reversed micelle*. In this case the hydrophobic part of the amphiphile is exposed to the outer medium, shielding the polar head inside the assembly. Under appropriate conditions of surfactant concentration, micelles can “over-organize” into various

definite shaped aggregates such as lamellar, cubic and hexagonal (see figure 7). Those supramolecular aggregates are usually employed as templates for the preparation of different kind of silica based materials featured by different porous phases.

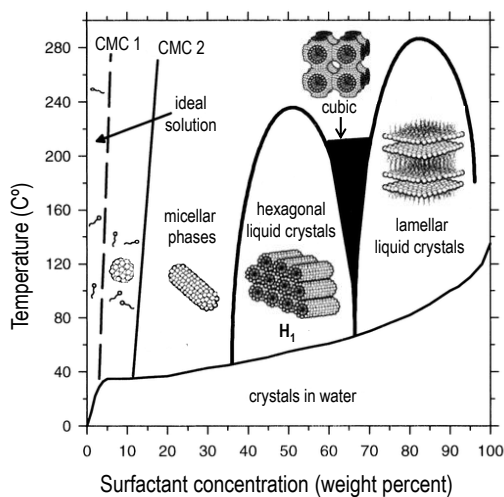


**Figure 7.** Schematic phase diagram for the surfactant cetyltrimethylammonium bromide (CTAB) in water. Adapted from Raman et al.<sup>13</sup>

In particular solidifying the surroundings of the supramolecular shaped aggregate using a sol-gel reaction with an appropriate silica precursor results in the formation of porous materials whose porosity present a well defined phase. For example the hexagonal supermolecular aggregates obtained from the micellar packaging is generally used for the preparation of the mesoporous silica nano and micro-particles (see chapter 2).

It has just been showed how modifying surfactant concentration and temperature different supramolecular aggregates featured by specific phases can be obtained. Moreover the use of a double tailed surfactant led to the formation of lipidic double layers. In this case these lipid structures present ratios between the sizes of the hydrophilic heads and the

<sup>13</sup> N. Raman, M. Anderson, C. Brinker, *Chem. Mater.*, **1996**, 1682-1701

## 1.4 Molecular Self-Assembly

hydrophobic tails different to those for micelle-forming surfactants. Amphiphiles that are able to form bilayer structures tend to have larger tails than heads (see figure 8).

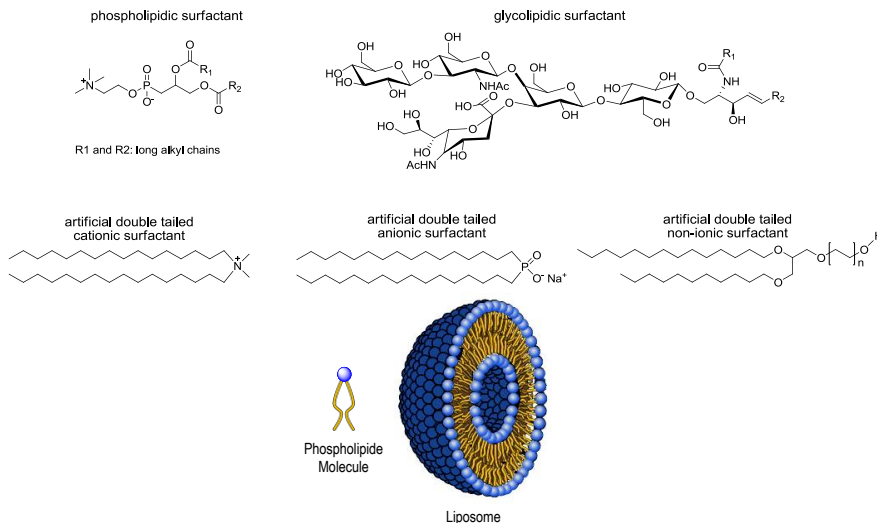


**Figure 8.** Schematic representation of the chemical structure of the most common bi-tailed amphiphilic natural (upper part of the scheme) and artificial (lower part) molecules, used for the preparation of liposome and vesicles respectively.

When these amphiphiles are dispersed in water, they assemble in order to avoid unfavorable contact of the hydrophobic parts with the water and thus the overall system Gibbs free energy is lowered. However, in these particular conditions, they cannot form micelle like small assemblies because of their large and bulky hydrophobic tails. Therefore, the phospholipid-like amphiphiles form double-layer structures (lipid bilayers) by contacting the hydrophobic faces of two leaf-like monolayer amphiphile assemblies.

This lipid bilayer structure extends two-dimensionally and forms the “skin” of a closed sphere that has a water pool inside. Depending on the kind of the double tailed amphiphilic molecule used this capsule-like

structure is called *liposome* (when the double tailed surfactant is a phosphor or glycolipid) or *vesicle* (when the double tailed surfactant is synthetic).



***Chapter 2:***  
***Chemosensors***



## 2.1 Introduction

This chapter focuses on the development of chemical sensors based on specific interaction between a particular analyte and usually a hetero-aromatic system. To fulfill this aim it is necessary to define what is intended for *chemical sensor*. The IUPAC Commission on General Aspects of Analytical Chemistry defined chemical sensors as follow:

*“A chemical sensor is a device that transforms chemical information, ranging from the concentration of a specific sample component to a total composition analysis, into a useful analytical signal”.*<sup>14</sup>

---

<sup>14</sup> a) A. Hulanicki, S. Glab, F. Ingman, *IUPAC Discussion Paper*, Commission V. 1., July, **1989**.  
b) A Hulanicki, S. Glab, F. Ingman, *Pure & Appl. Chem.* **1991**, 63, 1247–1250. c) U. E. Spichiger-Keller, *“Chemical Sensors for Medical and Biological Application”*, Wiley-VCH, **1998**.

## 2.1 Introduction

In this sense chemosensors combine molecular recognition events with the generation of a macroscopic signal (by a reporter molecule) that revealed the presence of the guest, as depicted in figure 9.<sup>10</sup>

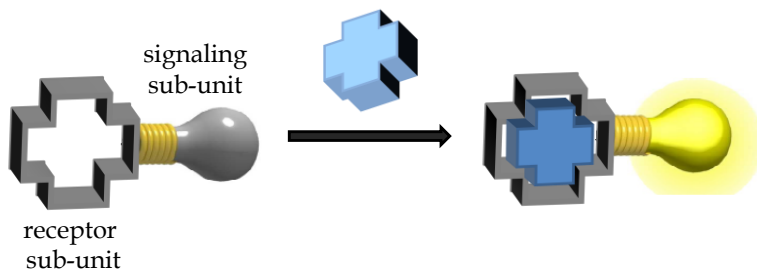


Figure 9. Schematic representation of the operation mechanism of a chemosensor

This phenomenon should be selective ideally, reversible and fast, in order to be applicable. Whereas chemical sensors or chemosensors usually refer to systems that typically used coordinative forces for guest binding the term reagents or *chemodosimeter* is related with the use of specific *irreversible* reactions involving guests.<sup>15</sup> Thus it can be deduced that a chemical sensor must be featured by the presence of two fundamental subunits: a *receptor* that grants the specificity of the interaction with a particular analyte and allows the sensor to discriminate between a number of different substrates, and a *signaling subunit* whose function is to transduce the recognition event into a measurable signal related to the concentration of the analyte.

Depending on the type of the signal transduced, chromo-fluorogenic changes and/or redox potential variations, different kind of chemosensors can be distinguished. The important advantages, with respect to other analytical methods, offered by a chromo-fluorogenic chemosensor are related to the possibility of use cheap and simple instrumentation, the need

<sup>15</sup> M. Moragues, R. Martínez-Mañez, F. Sancenón, *Chem. Soc. Rev.*, **2011**, *40*, 2593-2643.

of very small quantity of sample and, in some cases, the possibility of in situ and on-time measurements. Moreover colorimetric sensors induced noticeable color changes, observable to the naked eye, and can be used for rapid qualitative determinations. On the other hand, fluorogenic sensors have a high degree of sensitivity and specificity due to the possibility of specifying excitation and emission wavelengths, and normally allow the achievement of lower detection limits when compared with colorimetric techniques. In this field the development of molecular sensors for cations, anions and neutral species has been reported. Among them perhaps the most studied in the last ten years are anions sensors due to their applicability for detection of environmental contaminants and monitorizaion of anion driven biological processes. By now, still most of the reported examples of chemosensors or reagents for anions use one of the following tree main approaches; namely (i) the “binding site-signaling subunit” protocol, (ii) the “displacement” approach and (iii) the “chemodosimeter” paradigm. In the first approach (i) “binding sites” and optical “signalling subunit” are covalently bonded in such a way that the interaction of the anion with the binding site induces electronic modulations in the signalling subunit which result in colour or emission changes (see figure 10).<sup>16</sup> In the case of the “binding site-signaling subunit” approach in general a sort of active site for recognition is coupled to a chromophore or to a fluorophore. Then a non-covalent interaction between the anionic analyte and the binding site induces measurable chromo-fluorogenic changes. The most common drawback of this approach is that

---

<sup>16</sup> a) T. Gunnlaugsson, M. Glynn, G. M. Tocci, P. E. Kruger, F. M. Pfeffer, *Coord. Chem. Rev.*, 2005, **250**, 3094-3117. b) V. Amendola, D. Esteban-Gómez, L. Fabbrizzi, M. Licchelli, *Acc. Chem. Res.*, 2006, **39**, 343-353. c) T. Gunnlaugsson, H. P. D. Ali, M. Glynn, P. E. Kruger, G. M. Hussey, F. M. Pfeffer, C. M. G. dos Santos, J. Tierney, *J. Fluoresc.*, 2005, **15**, 287-299.

## 2.1 Introduction

the interaction of the anion with the binding sites usually relies on relatively weak hydrogen bonding interactions or anion-induced deprotonation, and in most cases, optical modulations are only observed in organic solvents. A classic binding site-signaling subunit paradigm probe is usually formed by a macrocycle (e.g. crownether) conjugated to an aromatic chromo-fluorophore, through urea moieties. Consequently anions coordination to urea groups via hydrogen bond induces the chromo-fluorogenic change.

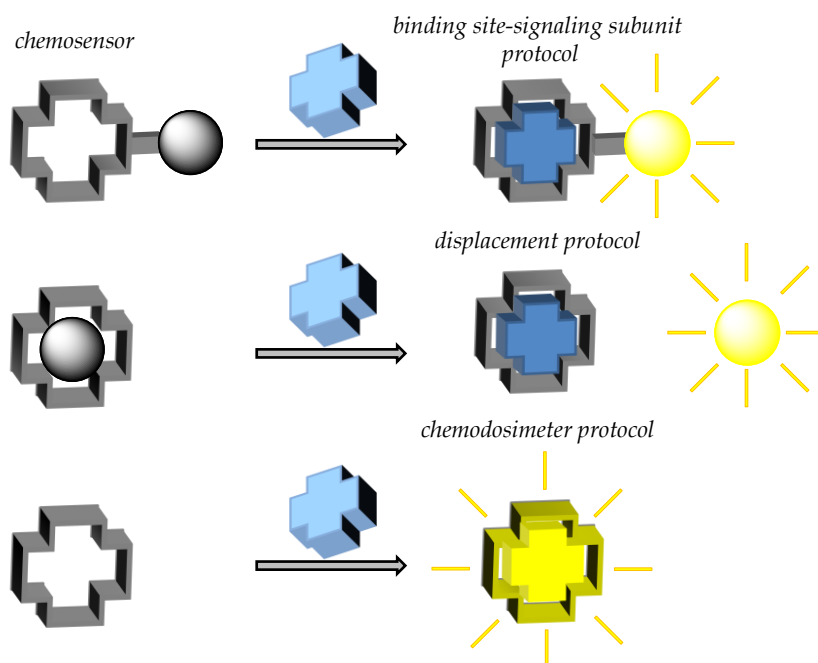


**Figure 10.** Schematic representation of the three different possible paradigms for the operation of a chemosensor

Particular examples of binding site-signaling subunit chemosensors were reported in 2010 by A. Aldrey and co-workers.<sup>17</sup> In this case ligands **1** and **2** (see figure 11) containing macrocyclic structures linked to three

<sup>17</sup> A. Aldrey, C- Núñez, V. García, R. Bastida, C. Lodeiro, A. Macías, *Tetrahedron Letters*, **2010**, 66,9223-9230.

nitrophenylurea groups were proved to show changes in colour in the presence of  $F^-$ ,  $OH^-$ ,  $CN^-$  and  $H_2PO_4^-$  in DMSO. The interaction of the urea H atoms with these anions enhanced  $\pi$  delocalization and red shifted the  $\pi-\pi^*$  transition (decreasing the band centred at 348 nm) therefore inducing the formation of a charge transfer band in the visible region (at ca. 480 nm). This resulted in the generation of orange or intense yellow solutions depending on the anion.

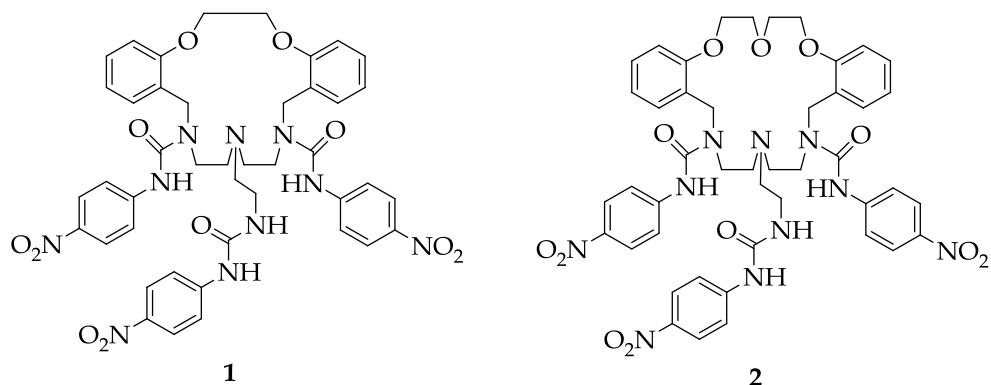


**Figure 11.** Structures of binding site receptors **1** and **2**.

No colour change occurred upon addition of the less basic  $NO_3^-$ ,  $ClO_4^-$ ,  $Cl^-$ ,  $Br^-$  and  $I^-$  anions. Addition of 1 equiv. of  $F^-$  to the solutions of receptors **1** and **2** was enough to promote the complete deprotonation of NH protons as proved by  $^1H$ -NMR studies. The authors suggested that the larger stability constants calculated for chemosensor **2** ( $F^- > OH^- > CN^- > H_2PO_4^-$ ) were in agreement with the strongest interaction expected for **2** which contains a bigger and more flexible cavity.

Another approach to binding site-signaling subunit receptors is the combination of the recognition active site with a metallic centre in order to discriminate the anions through their affinity for the binding site and the

## 2.1 Introduction

metal. A recent example of this paradigm was reported in 2011 by X. Lou and collaborators.<sup>18</sup> In this case rhodamine-based colorimetric probe **3** was reported to be selective to  $\text{ClO}^-$  with a remarkable detection limit as low as  $8.1 \times 10^{-7} \text{ mol L}^{-1}$  in aqueous solution. Compound **3** (existing in the spirolactam form predominantly) formed a colourless solution in  $\text{H}_2\text{O}:\text{CH}_3\text{CN}$  1:1 v/v (Tris buffer at pH 7). Upon addition of increasing amount of  $\text{ClO}^-$  to solutions of **3** in the presence of  $\text{Cu}^+$ , the spectrum changed dramatically; i.e a new absorption band at 555 nm appeared and increased gradually (with an enhancement as high as 198-fold at 30 min), with a color change from colourless to magenta, suggesting the formation of the  $\text{Cu}^{2+}$ -induced ring opening of the spirolactam form (see figure 12). When probe **3** was treated with various anions and oxidants such as  $\text{CO}_3^{2-}$ ,  $\text{SO}_4^{2-}$ ,  $\text{ClO}_4^-$ ,  $\text{ClO}_3^-$ ,  $\text{NO}_2^-$ ,  $\text{AcO}^-$  and  $\text{P}_2\text{O}_7^{4-}$  nearly no changes were observed. **3** was sensitive toward  $\text{ClO}^-$  even in real tap water samples.

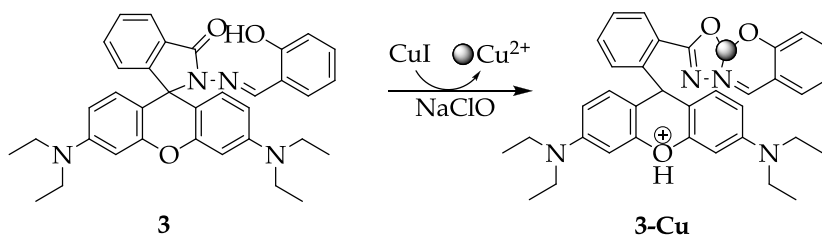


**Figure 12.** Binding mode of receptor **3** with  $\text{Cu}^{2+}$ .

A second important chemosensing protocol is the displacement approach. In this modus operandi “binding sites” and “signalling subunits” are not covalently bonded but from a molecular ensemble.<sup>19,20</sup> In this case, the coordination of a certain anion to the binding site results in

<sup>18</sup> X. Lou, Y. Zhang, Q. Li, J. Qin, Z. Li, *Chem. Commun.*, 2011, **47**, 3189-3191.

<sup>19</sup> S. L. Wiskur, H. Ait-Haddou, J. J. Lavigne, E. V. Anslyn, *Acc. Chem. Res.*, 2001, **34**, 963-972.

<sup>20</sup> B. T. Nguyen, E. V. Anslyn, *Coord. Chem. Rev.*, 2006, **250**, 3118-3127.

the displacement of the signalling subunit which is usually reflected in optical changes. Among the recent examples of anion chemosensors based on the displacement approach the work of Saeed's et al. can be cited. In this case the authors described a displacement assay for anions using the dinuclear ligand **4** (figure 13) and Eosine Y (**EY**) as fluorescent dye.<sup>21</sup> Upon increasing addition of **4** to a solution of **EY** (HEPES at pH 7.0), the fluorescence intensity of **EY** gradually decreased finally resulting in an almost complete quenching due to the formation of the corresponding complex between **4** and the anionic dye.

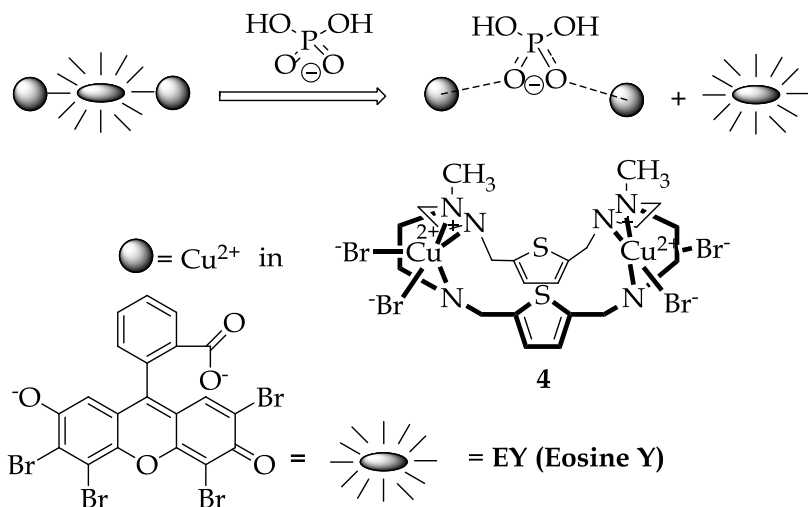


**Figure 13.** Schematic representation of a displacement assay using the dinuclear complex **4**

The change in the fluorescence intensity gave the best fit for a 1:1 binding model. Upon the addition of  $\text{H}_2\text{PO}_4^-$  to a **4**-**EY** solution a fluorescence increase was observed, due to the displacement of the dye (**EY**). Under identical conditions, addition of others anions including  $\text{F}^-$ ,  $\text{Cl}^-$ ,  $\text{Br}^-$ ,  $\text{I}^-$ ,  $\text{SO}_4^{2-}$ ,  $\text{NO}_3^-$  and  $\text{ClO}_4^-$  did not result in any enhancement in the

<sup>21</sup> M. A. Saeed, D. R. Powell, M. A. Hossain, *Tetrahedron Lett.*, 2010, **51**, 4904-4907.

## 2.1 Introduction

fluorescence. Another example of the use of the displacement approach was reported by Chen et al. In particular the authors described a NIR fluorescent probe able to selectively sense  $\text{CN}^-$  in aqueous solution.<sup>22</sup> Ligand **5** (figure 14) comprises a  $\text{N}_5$ -donor coordination sphere showing a strong affinity for  $\text{Cu}^{2+}$ . In the presence of copper the fluorescence of **5** (centered at 748 nm) was quenched due to the short distance between the fluorophore moiety and the metal. Other metal centers were tested by the authors to determine possible interference, however negligible effects were observed with cations different from  $\text{Cu}^{2+}$ .

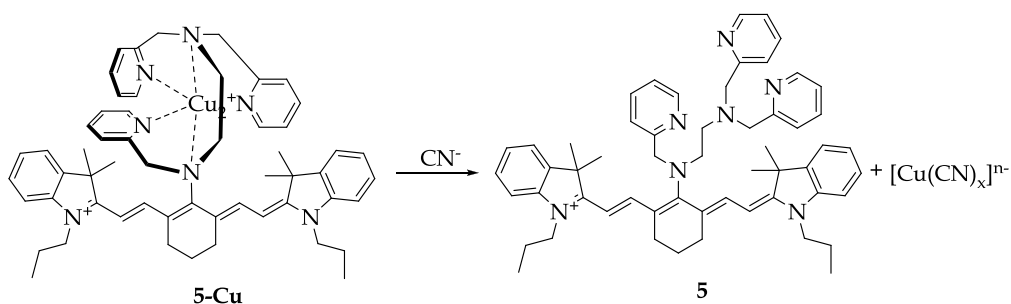


Figure 14. Reaction of receptor **5**- $\text{Cu}^{2+}$  with  $\text{CN}^-$

When  $\text{CN}^-$  was added to the solution containing the **5**- $\text{Cu}^{2+}$  complex, the 748 nm emission peak increased, as a consequence of the removal of the copper ion due to the formation of  $[\text{Cu}(\text{CN})_x]^{n-}$  complexes. The authors used the nematode *C. elegans* (a three blast microorganism) to test the probe and demonstrated the possibility to sense  $\text{CN}^-$  in these microorganisms when infected with *Pseudomonas aeruginosa* (responsible of the infection of  $\text{CN}^-$  in living organisms) and when contaminated with exogenous  $\text{CN}^-$ .

Finally the “chemodosimeter” approach takes advantage of anion-induced chemical reactions, usually irreversible, that results in changes in

<sup>22</sup> X. Chen, S. W. Nam, G. H. Kim, N. Song, Y. Jeong, I. Shin, S. K. Kim, J. Kim, S. Park, J. Yoon, *Chem. Commun.*, 2010, **46**, 8953-8955.

fluorescence or in colour.<sup>23,24</sup> Although this approach was minimal some years ago, today is a well established procedure for the design of anion probes. In this paradigm specific anion-induced reactions commonly involving the rupture or formation of several covalent bonds occur. This generally results in large chemical changes in the probe and remarkable spectroscopic modulations. The key issue in this paradigm consists in finding rather quick selective anion-induced reactions that work preferably in water or mixed organic-aqueous solutions. As we will see below, in most cases, chemodosimeters take advantage of the nucleophilic attack of target species to electron deficient functional groups that results in a re-organization of the electron density in the whole molecule and color/fluorescence modulation. Based on this paradigm S. Park and co-workers developed a new chemodosimeter for cyanide anion based on the turn-on of the fluorescence upon a Michael addition reaction.<sup>25</sup> In particular, acetonitrile solutions of **6** (see figure 15) showed an absorption band at 430 nm that, upon addition of increasing amounts of CN<sup>-</sup> anion, decreased with the concomitant appearance of a new band at 260 nm (the colour of the solution changed from yellow to colourless). Acetonitrile solutions of **6** were non-fluorescent (excitation at 272 nm). However, addition of CN<sup>-</sup> anion induced the grown of an emission at 469 nm. The presence of other selected anions (i.e. F<sup>-</sup>, Cl<sup>-</sup>, Br<sup>-</sup>, I<sup>-</sup>, N<sub>3</sub><sup>-</sup>, HPO<sub>4</sub><sup>-</sup>, HSO<sub>4</sub><sup>-</sup> and AcO<sup>-</sup>) induced negligible optical changes. The  $\alpha,\beta$ -unsaturated carbonyl group (activated by an intramolecular hydrogen bond with the *o*-hydroxyl moiety) plays a crucial role as Michael acceptor and reacts fast with CN<sup>-</sup>

---

<sup>23</sup> Z. Xu, X. Chen, H. N. Kim, J. Yoon, *Chem. Soc. Rev.*, 2010, **39**, 127-137.

<sup>24</sup> K. Kaur, R. Saini, A. Kumar, V. Luxami, N. Kaur, P. Singh, S. Kumar, *Coord. Chem. Rev.*, 2012, **256**, 1992-2028.

<sup>25</sup> S. Park, H. J. Kim, *Chem. Commun.*, 2010, **46**, 9197-9199.

## 2.1 Introduction

anion to afford an intermediate enol, which tautomerize to yield the highly fluorescent compound **8**. In contrast compound **7**, which was not bearing the -OH moiety, was not able to react with cyanide.

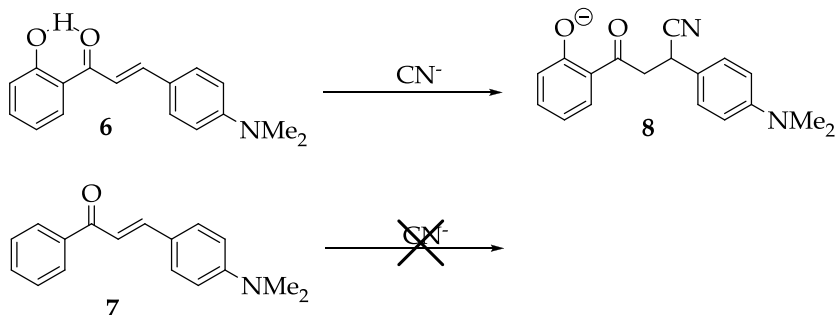


**Figure 15.** Chemical structures of receptors **6-7** and the reaction product (**8**) upon reaction of **7** of **6** with  $\text{CN}^-$  anion.

Moreover a new method for the detection of  $\text{NO}_2^-$  anion by using a family of 2-arylethynyl aniline derivatives (**9**) was reported.<sup>26</sup> The authors exploited the ability of  $\text{NO}_2^-$  anion to form diazonium salts in acidic ambient which in this case was additionally coupled with the subsequent intramolecular annulation reaction to give the final 4(1H)-cinnolone derivatives **10** (see figure 16).

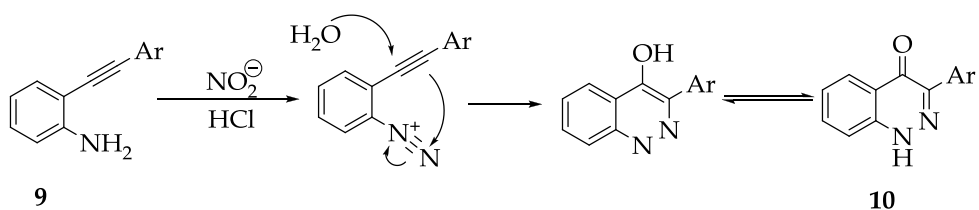


**Figure 16.** Chemical reaction of 2-arylethynyl aniline derivative **9** with  $\text{NO}_2^-$  anion.

In order to produce these reactions an acidic solution and low temperatures were required. In a typical experiment a water solution of **9** was first treated with HCl 2N (temperature in the 0- 5 °C range) and then

<sup>26</sup> R. Dey, T. Chatterjee, B. C. Ranu, *Tetrahedron Lett.*, 2011, **52**, 461-464.

the  $\text{NO}_2^-$  anion was added to observe a colour change from colourless to yellow due to the formation of **10**. Other anions tested (i.e.  $\text{F}^-$ ,  $\text{Cl}^-$ ,  $\text{Br}^-$ ,  $\text{I}^-$ ,  $\text{NO}_3^-$ ,  $\text{AcO}^-$ ,  $\text{N}_3^-$ ,  $\text{SCN}^-$ ,  $\text{SO}_4^{2-}$  and  $\text{PO}_4^{3-}$ ) induced no colour changes. Moreover, if the aryl group in **9** was a methoxynaphthyl moiety the starting aryl ethynyl aniline showed a strong fluorescence emission at 401 nm (excitation at 315 nm) which was selectively quenched by  $\text{NO}_2^-$  anion. A limit of detection of less than 1 ppm was calculated.

## **2.2 Objectives**

Taking into account the growing and always current interest in chemosensors, demonstrated by the great number of yearly related publications, we decided to design new porbes for the detection of chemical species of interest. In particular in the following section we report the synthesis, characterization and sensing properties of a chemodosimeter for the selective detection of fluoride anion ( $\text{F}^-$ ) and a chemosensing ensemble for selective detection of glutathione (GSH) in water.

Our choice to develop a chemodosimeter for selective recognition of fluoride anion rose from the extremely poor quantity of described probes for detection of fluoride in aqueous environment. In the same manner when we designed and developed the probe for GSH there were no described chemosensors able to discriminate between biological thiols such as GSH and cysteine in an aqueous environment.

Specifically our aims were:

- ✓ Design and synthesis of chemodosimeters featured by two main conjugated parts: a reactive sub-unit whose function is to react only with the targeted analyte and a dye with tunable chromo-fluorogenic properties.

## 2.2 Objectives

- ✓ Purification and characterization of the new molecules with standard techniques (Nuclear Magnetic Resonance, High Resolution Mass Spectrometry, HPLC, LC...) before and after the reaction with the analyte.
- ✓ Evaluation of the reactivity of the synthesized probes in the presence of different species, to state their applicability as selective chemodosimeter for the selected analytes in water solution.

## **2.3 Chemodosimeters Design**

The design of new chemosensors for the detection of F<sup>-</sup> and GSH was based on three main aspects: the selection of a *binding* or *reactive unit*, the presence of a suitable *signaling subunit*, and the possibility of use the probe in *water*. The latter is of importance as many analytes of interest are usually soluble, and thus located, in aqueous solution. In our case the chemodosimeter paradigm was selected, because it is a suitable approach for the detection of analytes in aqueous environment. In fact the chemodosimeters are usually poorly influenced by the problems of analyte and receptor solvation that frequently determine slow response or no response at all as in the case of the other detection methods (displacement and binding site-signaling subunit approaches, see 1.1).

### **2.3.1 Design of a reactive subunit, how to achieve selectivity**

The choice of the reactive subunit for a chemodosimeter is based on the reactive nature of the analyte, because in this paradigm the analyte has to induce a “covalent modification” of the probe. In particular the selected reactive unit determines the selectivity of the sensor and thus the ability to discriminate between different analytes.

In the case of the probe for the detection of fluoride anion, a *t*-butyldimethylsilyl (TBDMS) functionalized phenol was selected as reactive subunit. In fact the reactivity of F<sup>-</sup> toward the hydrolysis of R<sub>3</sub>-Si-O moieties is well known.<sup>27</sup> In particular F<sup>-</sup> is specifically used for orthogonal deprotection reactions of the protected R<sub>3</sub>Si-X alcohols and phenols, thanks to its specific ability to form Si-F bond and induce the hydrolysis of the silylether moiety, with the subsequent formation of the deprotected free R-OH and the corresponding F-Si-R'<sub>3</sub> silane. Moreover F<sup>-</sup> anion presents the same reactivity towards alkynylsilane moieties. This well established orthogonality of F<sup>-</sup> toward R<sub>3</sub>Si-O and alkynylsilanes moieties resulted in the development of a variety of chemodosimeters for the sensing of F<sup>-</sup> in the last ten years. For example probes **11** and **12** (figure 17) for the selective sensing of F<sup>-</sup> anion in CH<sub>3</sub>CN were described.<sup>28</sup> In this case the reactive site was a phenolic -OH protected with a triisopropylsilyl (TIPS) group which was conjugated with a fluorophore (BODIPY). Both compounds were highly emissive in CH<sub>3</sub>CN solutions showing bands at 507 (excitation at 480 nm) and 580 nm (excitation at 550 nm) for **11** and **12**, respectively. Addition of F<sup>-</sup> anion to solutions of both receptors induced a dramatic emission quenching due to the deprotection of the silyl ether moiety that generated a phenolate anion.

This phenolate anion quenched the emission of the BODIPY dye through a PET process. In the case of **12** the reaction with F<sup>-</sup> was additionally accompanied by a strong bathochromic shift of the absorption band (from 560 to 682 nm) that results in a purple to green colour change.

---

<sup>27</sup> P. G. M. Wuts, T. Greene, *Protective Groups in Organic Synthesis (fourth edition)*, 2007, © a John Wiley and Sons publication

<sup>28</sup> O. A. Bozdemir, F. Sozmen, O. Buyukcakil, R. Gulyev, Y. Cakmak, E. U. Akkaya, *Org. Lett.*, 2010, **12**, 1400-1403.

### 2.3 Chemodosimeter Design

Addition of  $\text{AcO}^-$ ,  $\text{Br}^-$ ,  $\text{Cl}^-$ ,  $\text{CN}^-$ ,  $\text{H}_2\text{PO}_4^-$ ,  $\text{HSO}_4^-$ ,  $\text{I}^-$  and  $\text{NO}_3^-$  induced negligible changes in the absorption and emission profiles. To complete their work the authors prepared poly(methyl methacrylate) (PMMA) films impregnated with the probes **11** and **12** that were able to respond to  $\text{F}^-$  in  $\text{CH}_3\text{CN-H}_2\text{O}$  4:1 solutions.

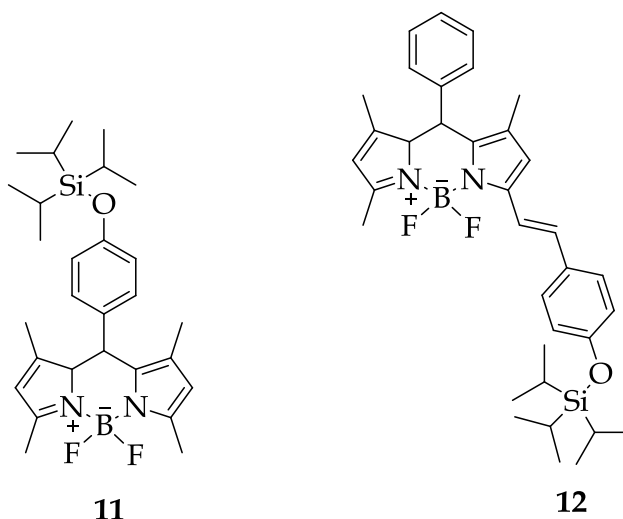
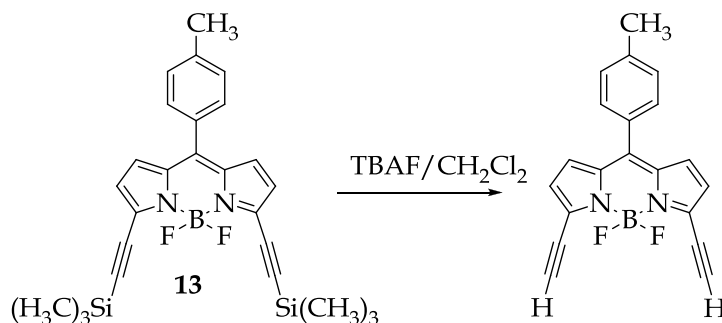


Figure 17. Chemical structure of probes 10 and 11

Another example based on a fluoride-induced bond rupture was reported by M. R. Rao et al.<sup>29</sup> In this case  $\text{CH}_2\text{Cl}_2$  solutions of chemodosimeter **13** presented an absorption band at 571 nm adscribable to the BODIPY subunit. Moreover, solutions of **13** were highly fluorescent with an emission band centred at 584 nm upon excitation at 425 nm. Of all the anions tested (i.e.  $\text{F}^-$ ,  $\text{Cl}^-$ ,  $\text{Br}^-$ ,  $\text{I}^-$ ,  $\text{HPO}_4^{2-}$  and  $\text{ClO}_4^-$ ) only  $\text{F}^-$  was able to induce a chromo-fluorogenic response. Addition of  $\text{F}^-$  anion induced a decrease in the intensity at 571 nm together with the appearance of a new

<sup>29</sup> M. R. Rao, S. M. Mobin, M. Ravikanth, *Tetrahedron*, 2010, **66**, 1728-1734.

band at 551 nm, whereas the emission at 584 nm diminished with the simultaneous grown of a new fluorescence at 564 nm.



**Figure 18.** Chemical reaction of **13** with F<sup>-</sup> anion

These changes were attributed to the removal of the electron-rich trimethylsilyl protective groups induced by F<sup>-</sup> that yielded the corresponding electron-deficient ethyne groups, as shown in figure 18.

On the other hand the design selected to prepare a probe for GSH relayed in the choice of a soft electrophile, as a Michael acceptor, as reactive subunit able to suffer nucleophilic attack from the biological thiol.

In fact, there are several examples reported for the detection of biological thiols, such as GSH but also for cysteine (Cys) and homocysteine (Hcy), based on this approach. Among them there is the recent work reported by H. S. Jung and coworkers.<sup>30</sup> In this case addition of Cys to **14** (figure 19) in H<sub>2</sub>O:DMSO 9:1 v/v (buffered at pH 7.4) induced a 62 nm hypsochromic shift of the absorption maximum at 426 nm, resulting in a color change from dark orange to green, while the fluorescence maximum at 502 nm ( $\lambda_{\text{exc}} = 440 \text{ nm}$ ) was enhanced by ca. 107-fold. A comparison of

<sup>30</sup> H. S. Jung, K. C. Ko, G.-H. Kim, A.-R. Lee, Y.C. Na, C. Kang, J. Y. Lee, J. S. Kim, *Org. Lett.*, 2011, **13**, 1498-1501.

### 2.3 Chemodosimeter Design

the reactivity of **14** toward Cys, Hcy and GSH showed that **14** had preference for Cys over the other biological thiols. This selectivity arises from the lower  $pK_a$  value and lower steric hindrance of Cys, when compared with Hcy and GSH. Finally, probe **14** was tested to detect intracellular thiols by confocal microscopy.

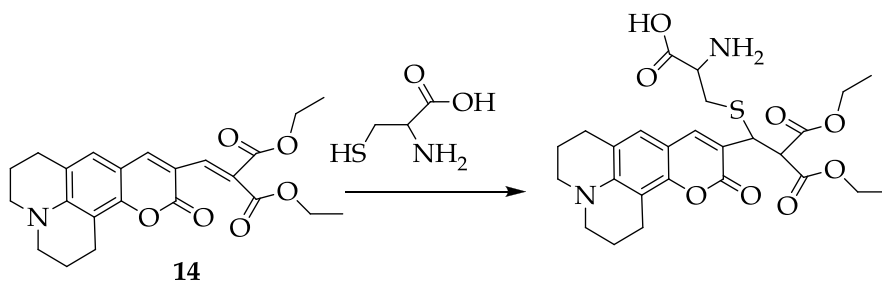


**Figure 19.** Schematic representation of the Michael addition reaction for the detection of Cys using **14**

Following a similar procedure, the coumarin derivative **15** (figure 20) was designed for the detection of bio-thiols using the Michael addition reaction to a nitroolefin.<sup>31</sup> In this case a blue shift in the absorption of **15** from 483 nm to 400 nm was observed in  $\text{CH}_3\text{CN}:\text{H}_2\text{O}$  1:1 v/v, (buffered at pH 7.4) upon addition of Cys. Moreover, an enhancement in the emission intensity at 480 nm was also observed ( $\lambda_{\text{exc}} = 365$  nm).

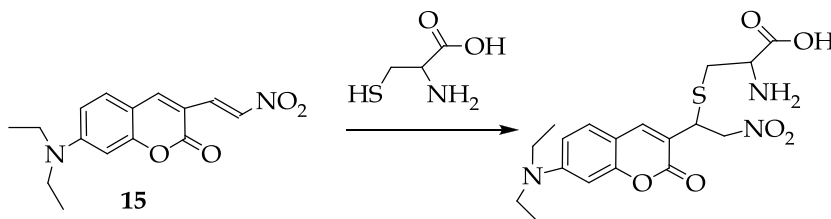


**Figure 20.** Representation of the Michael addition reaction for the detection of Cys using **15**

<sup>31</sup> Y.-Q. Sun, M. Chen, J. Liu, X. Lv, J.-F. Li, W. Guo, *Chem. Commun.*, 2011, **47**, 11029-11031.

A limit of detection for Cys of  $8.6 \times 10^{-7}$  mol L<sup>-1</sup> was determined. The probe also exhibited fast response and high selectivity toward bio-thiols over other natural amino acids (i.e. Ala, Arg, Asn, Glu, Gln, Gly, His, Ile, Leu, Lys, Met, Phe, Pro, Ser, Thr, Trp, Tyr and Val). This probe was also used to image thiols in living cells.

### ***2.3.2 Design of the signaling subunit***

The presence of a signaling subunit in the chemodosimeter is necessary to transduce the analyte-induced molecular event into a measurable signal. In our two particular cases we selected chromo-fluorogenic moieties able to modify their optical properties upon the changes in the reactive subunit.

In particular in the case of the fluoride probe a silylether moiety was conjugated to an azoic dye. Consequently the fluoride-induced specific silylether hydrolysis determined a change in the electronic properties of the aromatic core, which was transduced into a measurable chromogenic change. Moreover the probe was also functionalized with a trialkoxysilane moiety in order to covalently anchor the chemosensor to a silica thin layer surface to obtain reactive dip-sticks for the chromogenic detection of fluoride, in aqueous solution.

For glutathione the selected signaling subunit was a 2,6-diphenyl pyrylium salt conjugated through a carbon-carbon (E)-stilbene double bond to a phenol. This molecule was poorly soluble in water therefore it was internalized into micelles. This internalization determined the deprotonation of the phenol and the consequent isomerization of the pyrylium salt to its quinonic form. The treatment with biological thiols yielded a 1,6 Michael addition to the double bond conjugated to the

### 2.3 Chemodosimeter Design

benzoquinone moiety, inducing naked eye detectable chromo/fluorogenic changes.

***Chapter 3:  
Azo dyes functionalized with alkoxysilyl ethers as  
chemodosimeters for the chromogenic  
detection of the fluoride anion***



***Azo dyes functionalized with alkoxy silyl ethers as chemodosimeters for the chromogenic detection of the fluoride anion***

Alessandro Agostini,<sup>[a]</sup> Michele Milani,<sup>[b]</sup> Ramón Martínez-Mañez,<sup>\*[a]</sup> Maurizio Licchelli,<sup>\*[b]</sup> Juan Soto<sup>[a]</sup> and Félix Sancenón<sup>[a]</sup>

<sup>[a]</sup>*Centro de Reconocimiento Molecular y Desarrollo Tecnológico (IDM), Unidad Mixta Universidad Politécnica de Valencia-Universidad de Valencia, Departamento de Química, Universidad Politécnica de Valencia, Camino de Vera s/n, 46022, Valencia, Spain. CIBER de Bioingeniería, Biomateriales y Nanotecnología (CIBER-BNN).*

<sup>[b]</sup>*Dipartimento di Chimica, Università di Pavia, via Taramelli 12, 27100, Pavia, Italy.*

***Received: April 11, 2012***

***Published online: June 11, 2012***

### **3.1 Abstract**

An azo dye functionalized with *tert*-butyldimethylsilyl ether has been synthesized and used as a selective chromogenic fluoride sensor in the acetonitrile/water mixtures. The chromogenic response arises from the fluoride-induced hydrolysis of the silyl ether moiety, which yields a highly colored phenolate anion. The sensor molecule can be grafted to silica to make dip-sticks for fluoride sensing.

### **3.2 Introduction**

Selective recognition of anions is a very active field in supramolecular chemistry. In particular, the development of fluorogenic and chromogenic chemosensors and reagents for anions has been extensively explored in the last few years given the important roles played by anionic species in biological processes, in deleterious effects such as environmental pollutants, or as toxic compounds or carcinogenic species.<sup>1</sup>

Among inorganic anions, fluoride is routinely used for the prevention of dental caries<sup>2</sup> and for the treatment of osteoporosis.<sup>3</sup> However, acute fluoride exposure can cause various diseases: nausea, abdominal pain, coma, cardiac arrest determined by hypocalcemia. Moreover, epidemiological studies have demonstrated that chronic fluoride exposure can determine skeletal fluorosis and osteomalacia. Furthermore, there are other studies on the possible carcinogenic effects of fluoride anion in humans.<sup>4</sup> For all these reasons, it is not surprising that the development of chromogenic and fluorogenic chemosensors and reagents for the selective detection of fluoride has increased in recent years. Some of these probes have been prepared after considering the "binding site-signaling subunit" approach in which an optical signaling unit is covalently linked to the

binding sites containing one or several H-bond donor moieties, such as urea and thiourea groups.<sup>5</sup> In some of these systems, dual processes involving coordination and deprotonation have been reported.<sup>6</sup> However, most of these receptors, which are based on the coordination and/or basicity properties of fluoride, have shown certain limitations as practical sensors typically involving poor selectivity versus other basic anions such as cyanide, acetate and dihydrogen phosphate, and being unable to display sensing features in water or in mixed water-organic solvent mixtures, even with a very small amount of water.<sup>7</sup> In order to overcome these major drawbacks, the use of chemodosimeters for the chromo-fluorogenic detection of fluoride anions has been recently explored. These chemodosimeters employ selective reactions induced by the target anion coupled with a chromo or fluorogenic event. In this area, the well-known fluoride-induced hydrolysis of silyl ethers has been used to develop probes for the optical recognition of this anion.<sup>8</sup>

One recent example has been published by Akkaya et al. in 2010, who prepared two bodipy derivatives with silyl-protected phenolic moieties.<sup>9</sup> The emission intensity of both chemodosimeters was quenched upon fluoride anion addition due to the formation of phenolate anions. Bodipy derivatives functionalized with silylacetylenes have also been prepared and used for the fluorogenic detection of fluoride.<sup>10</sup> In another recent work, Bhalla and coworkers prepared terphenyl derivatives functionalized with *t*-butyldimethylsilyl groups.<sup>11</sup> Upon the addition of the fluoride anion to the THF solutions of the chemodosimeters, a change in color from colorless to violet was observed due to the cleavage of the O-Si bond with the concomitant formation of the corresponding triphenylene derivatives. Despite following a chemodosimeter approach, the above fluoride probes

only displayed sensing features in organic solvents. In fact there are very few examples of fluoride optical probes that are able to detect this anion in water or in water-organic solvent mixtures. One recent example is the work of Zhang et al., which prepared a benzothiazolium hemicyanine dye functionalized with a *t*-butyldimethylsilyl moiety as a specific reaction site for fluoride.<sup>12</sup> The ethanol-water 3:7 v/v mixtures of this chemodosimeter showed an emission band at 500 nm, which shifted to 558 nm upon fluoride addition. However, emission changes were achieved after 50 minutes.

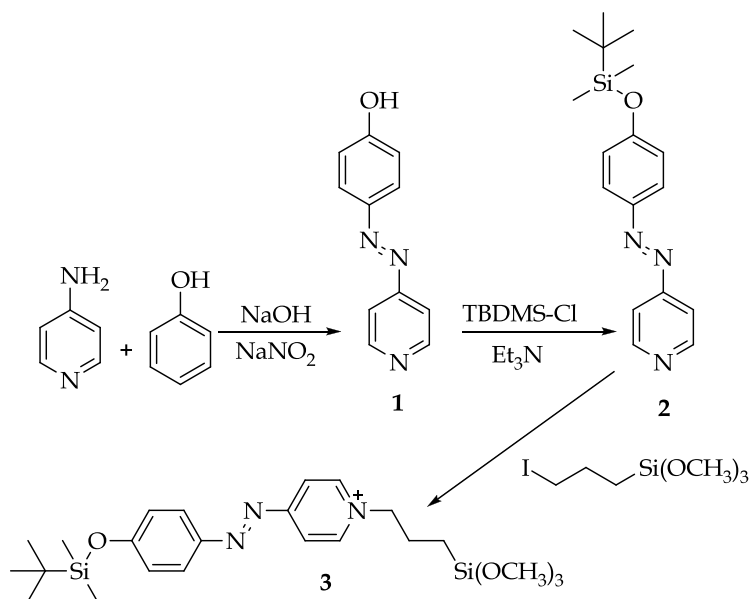
A colorimetric sensory material for fluoride detection, based on the use of an MCM-41 solid functionalized with different dyes, has also been reported.<sup>13</sup> In this case, the addition of fluoride to the acidic acetonitrile-water 7:3 v/v mixtures of the functionalized solid resulted in the hydrolysis of the solid support, with a subsequent dye release and chromogenic response.

Given our interest in the development of chromo-fluorogenic chemosensors for anions<sup>14</sup> and the very few examples described that are able to signal fluoride in the presence of water, we report herein the synthesis, characterization and sensing studies of a new fluoride-selective chemodosimeter based on a pyridine azo dye functionalized with a *t*-butyldimethylsilyl moiety which displays a selective chromogenic response to fluoride anion in mixed acetonitrile-water mixtures.

### **3.3 Results and Discussion**

The synthesis of chemodosimeter **2** was achieved by a two-step procedure (see Scheme 1 and the Experimental section for details). In a first step, the phenolic-pyridine azo dye (**1**) was prepared following a well-

known diazotation procedure.<sup>15</sup> In a second step, the phenolic hydroxyl was protected as TBDMS ether using TBDMS-Cl and triethylamine. Scheme 1 also shows the synthesis of trialkoxysilane derivative **3** by a nucleophilic substitution reaction between **2** and (3-iodopropyl)trimethoxysilane. **3** was used to anchor the chemodosimeter in a silica matrix (*vide infra*).



**Scheme 1.** Synthesis of chemodosimeter **2** and trialkoxysilane derivative **3**.

The <sup>1</sup>H-NMR spectrum of **2** showed two singlets at 0.29 ppm and 1.03 ppm ascribed to the methyl moieties linked directly to the Si atom and to the *t*-butyl group, respectively. In the downfield zone, two pairs of doublets centered at 7.00 ppm and 7.92 ppm and at 7.68 ppm and 8.80 ppm were found and attributed to the 1,4-disubstituted benzene and to the pyridine moieties, respectively. Acetonitrile-water 9:1 v/v solutions of **2** at pH 8.0 exhibited an absorption band at 350 nm ( $\epsilon = 19000 \text{ M}^{-1} \text{ cm}^{-1}$ ). The chromogenic behavior of **2** was studied upon the addition of 10 equivalents of selected anions: acetate, benzoate, hydrogen sulfate, dihydrogen

phosphate, fluoride, chloride, cyanide, nitrate and carbonate (such as tetrabutylammonium salts). The obtained results are shown in Figure 1.

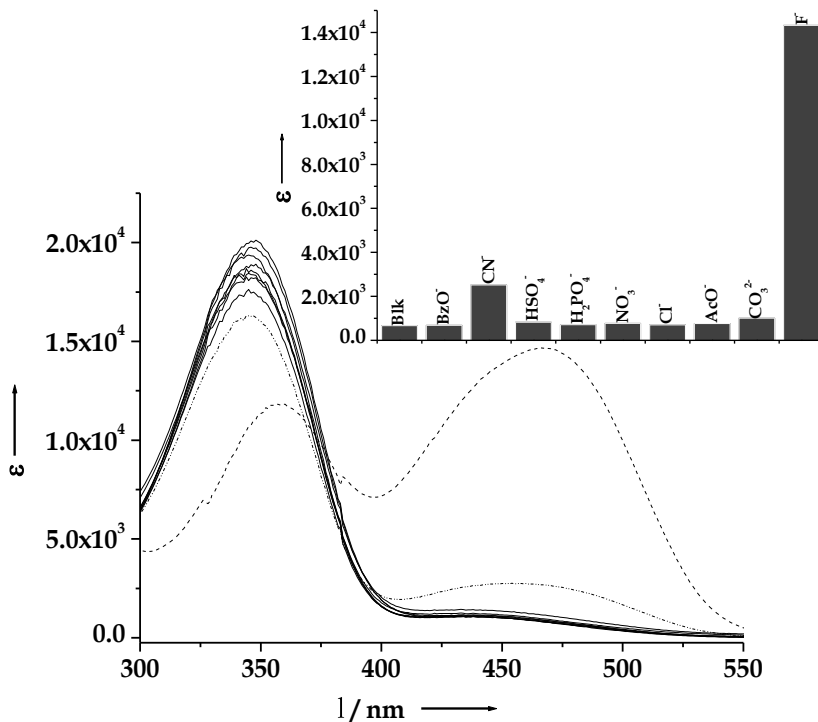


**Figure 1.** The UV-vis spectra of the acetonitrile-water 9:1 v/v solutions of probe 2 ( $3.0 \times 10^{-5}$  mol dm<sup>-3</sup>) at pH 8.0 in the presence of 10 equivalents of selected anions (added as tetrabutylammonium salts). The inset shows the  $\epsilon$  of the 470 nm band in the presence of the selected anions.

As Figure 1 illustrates, the most remarkable feature was observed in the presence of fluoride. In this case, the band at 350 nm underwent a significant hypochromic and a slight bathochromic shift (of ca. 10 nm), while a new band appeared at ca. 470 nm. Due to these changes, the solutions of receptor 2 changed in color from colorless to orange-red upon fluoride addition. A similar, but much less pronounced, effect was noted in the presence of cyanide, whereas acetate, benzoate, hydrogen sulfate,

dihydrogen phosphate, chloride, nitrate and carbonate anions induced negligible changes in the UV-vis profile of **2**.

To further characterize the chromogenic behavior of probe **2**, changes in the band intensity at 470 nm were studied in the presence of increasing amounts of fluoride. Figure 2 shows a typical titration profile. From this calibration curve, a remarkable detection limit of 0.04 ppm was calculated using conventional UV-vis equipment.

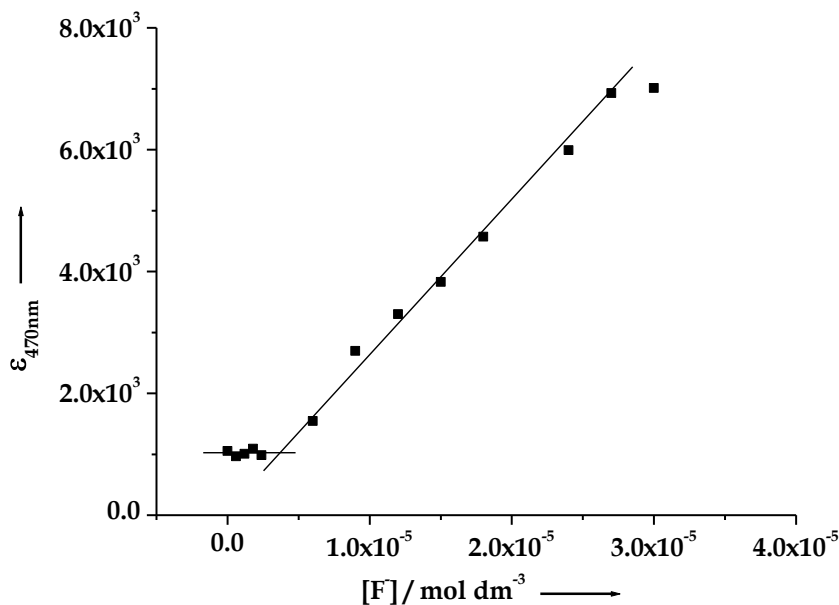
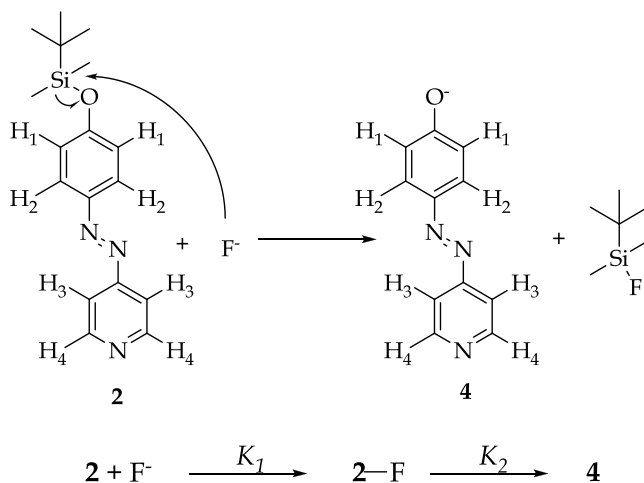


Figure 2. Calibration curve for fluoride using probe **2** ( $3.0 \times 10^{-5}$  mol dm<sup>-3</sup>) in acetonitrile-water 9:1 v/v at pH 8.0.

The fluoride selective chromogenic response arose from the hydrolysis reaction of the silyl ether moiety induced by this anion, which resulted in the formation of the corresponding phenolate anion **4** (see Scheme 2). This phenolate anion has a strong donor negatively charged oxygen atom, which was responsible for the appearance of the red shifted band at 470 nm and the concomitant color modulation observed. The results are in agreement with the assumed case that the increased donor

ability of a donor group in a push-pull system would induce a bathochromic shift.<sup>16</sup> As the above figure illustrates, the most remarkable feature was observed in the presence of fluoride. In this case, the band at 350 nm underwent a significant hypochromic and a slight bathochromic shift (of ca. 10 nm), while a new band appeared at ca. 470 nm.



**Scheme 2.** Mechanism of the chromogenic response of **2** in the presence of the fluoride anion.

The <sup>1</sup>H-NMR studies were also in agreement with this proposed response mechanism. Figure 3 shows <sup>1</sup>H-NMR peaks due to the aromatic protons of receptor **2** alone and in the presence of 10 equivalents of the fluoride anion in CDCl<sub>3</sub>. As shown, all the aromatic protons in **2** underwent significant upfield shifts upon fluoride addition. This effect was in agreement with the formation of the phenolate anion **4** upon the fluoride-induced hydrolysis of the silyl ether moiety.

In order to further assess the potential applicability of **2** for the detection of the fluoride anion in the presence of the water UV-vis

measurements at a certain concentration of fluoride ( $0.01 \text{ mol dm}^{-3}$ ) in the presence of different water contents, were carried out. When using acetonitrile-water 9:1 v/v solutions, fluoride-induced silyl ether hydrolysis was relatively fast, whereas upon increasing the water content, the reaction became slower. By way of example, Figure 4 shows the time-dependent disappearance of the band centered at 350 nm for the acetonitrile mixtures containing 10%, 25% and 50% of water. It can be seen that the chromogenic response is clearly related with the water content in the solvent; i.e., the greater the water contents, the lower the silyl ether hydrolysis rate.

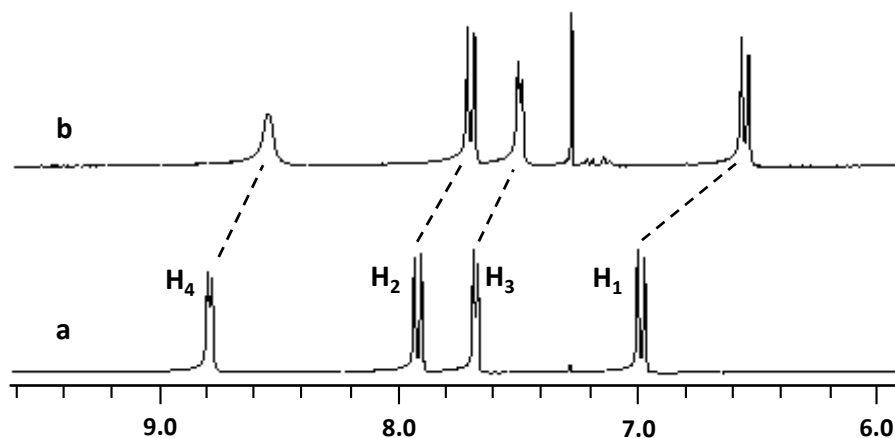


**Figure 3.** Aromatic zone of the  $^1\text{H}$ -NMR spectra of probe **2** alone (a) and in the presence of 10 equivalents of the fluoride anion (b) in  $\text{CDCl}_3$ . For the assignation of the aromatic protons of probe **2**, see scheme 2.

This was an expected result which is related with the larger solvation of the fluoride anion and with the concomitant reduction of its nucleophilicity when the amount of water increases. Figure 4 shows that the reaction was completed in ca. 15 min when using 10% water, whereas a higher percentage of water showed a partial inhibition of the reaction. For

instance, reaction times of ca. 40 min. and 60 min. were necessary to reach a plateau when using the 75:25 or the 50:50 v/v acetonitrile-water mixtures. However, it should be noted that although the reaction was slower as the amount of water increased, the method using probe 2 allowed to sense fluoride, even though a percentage of 50% water was used. Indeed, to complete the characterization of the systems using different amounts of water, the sensing behavior of 2 was studied (via the changes noted in the 470 nm band) in the presence of increasing amounts of fluoride when using the 75:25 or the 50:50 v/v acetonitrile-water mixtures; under these conditions, the detection limits of 0.09 ppm and 0.14 ppm for fluoride were calculated, respectively.

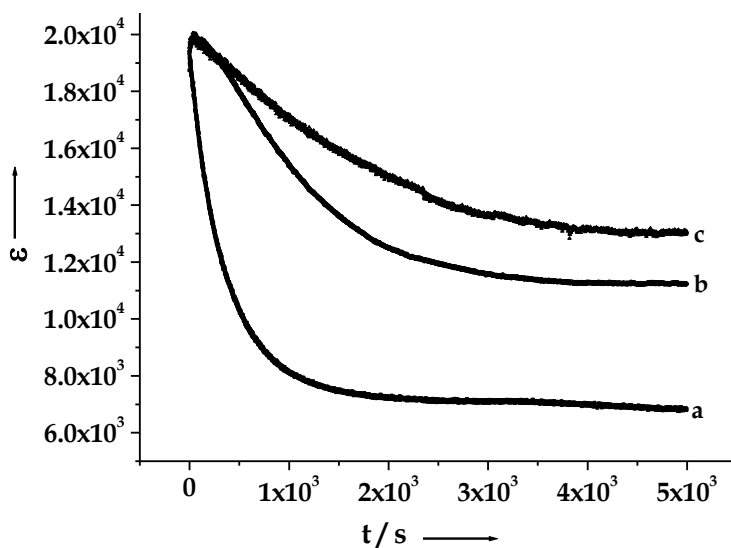


**Figure 4.** Time-dependent decrease of  $\epsilon$  at 350 nm upon the addition of the fluoride anion (final concentration of  $0.01 \text{ mol dm}^{-3}$ ) to the solutions of receptor 2 ( $6 \times 10^{-5} \text{ mol dm}^{-3}$ ) in: a) acetonitrile-water 90:10 v/v, b) acetonitrile-water 75:25 v/v, c) acetonitrile-water 50:50 v/v mixtures.

As suggested for similar systems, the sensing response comprises two steps: (i) the nucleophilic attack of the fluoride anion to the silyl ether moiety, which would yield an intermediate product; (ii) the subsequent release of *t*-butyldimethylsilyl fluoride with the generation of phenolate 4 (see Scheme 2). Processing the kinetic data shown in Figure 4 allowed us to obtain the rate constants ( $k_1$  and  $k_2$ ) for these two steps in the presence of certain water contents. These data are provided in Table 1. As seen, the rate determining step was the release of *t*-butyldimethylsilyl fluoride. Moreover, the rate constants became lower as the amount of water increased.

**Table 1.** The rate constants for the reaction of 2 and fluoride using the acetonitrile-water mixtures containing different water contents.

water content (%)	$k_1$	$k_2$
10	2.016	$47.7 \times 10^{-4}$
25	1.086	$17.3 \times 10^{-4}$
50	0.450	$9.2 \times 10^{-4}$

Encouraged by the sensing properties of probe 2, we took one step further and studied the possible use of 2 to design dip-sticks for fluoride detection. For this purpose, chemodosimeter 2 was reacted with (3-iodopropyl)trimethoxysilane in order to obtain the corresponding pyridinium cation 3 (see Scheme 1). Compound 3 contains a trialkoxysilane moiety and was easily anchored onto a silica support. Specifically, we used silica TLC foils (1 x 3 cm) as the inorganic material. These dip-sticks were used for the semiquantitative chromogenic detection of the fluoride anion in the acetonitrile-water mixtures. In this case, probe 3, which was red, changed color and became violet in the presence of fluoride. Photographs of the dip-sticks after their immersion in solutions containing fluoride at

concentrations of  $1.0 \times 10^{-4}$ ,  $1.0 \times 10^{-3}$  and  $1.0 \times 10^{-2}$  mol dm<sup>-3</sup> were taken. The red, green and blue values of each photograph were measured and color difference maps were generated (see Figure 5).<sup>17</sup> A gradual color change from blue to light green was observed as the fluoride concentration increased. Following this simple procedure, fluoride concentrations of  $10^{-4}$  mol dm<sup>-3</sup> could be detected.

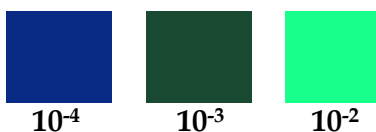


**Figure 5.** The color difference maps of fluoride at the specified concentrations (in mol dm<sup>-3</sup>) after the immersion of the dip-sticks functionalized with 3 in the acetonitrile-water 9:1 v/v solutions (pH 8.0) containing the anion. For display purposes, the color range of the difference maps was expanded from 4 bits to 8 bits per color (RGB range of 3-16 expanded to 0-225).

### 3.4 Conclusions

In summary, we prepared and studied a novel azoic-based colorimetric chemodosimeter (2) which can selectively sense fluoride in acetonitrile-water mixtures over several other anions by a visible color change. The chromogenic response mechanism arises from a fluoride-hydrolysis of a silyl ether moiety embedded in the chemical structure of the chemodosimeter. Studies into different acetonitrile-water mixtures have shown that the fluoride signaling reaction slowed down as the amount of water increased. Typical detection times of 15 min, 40 min and 60 min when using the 90:10, 75:25 and 50:50 v/v acetonitrile-water mixtures were found. Moreover although the reaction was slower as the amount of water increased, the method using probe 2 allowed to sense fluoride at low concentrations, with detection limits of 0.04, 0.09 and 0.14 ppm in the 90:10,

75:25 and 50:50 v/v acetonitrile-water mixtures, respectively. This simple molecule is one of the few probes capable of displaying selective chromogenic sensing features for fluoride in mixed aqueous solutions. Furthermore, we designed and prepared TLC silica foils functionalized by the reaction with **3**, and we used them to detect the fluoride anion in solution.

### 3.5 Experimental Section

**Methods:**  $^1\text{H}$  and  $^{13}\text{C}$  nuclear magnetic resonances (NMR) were acquired using a Varian 300 spectrometer (Sunnyvale, CA, USA). UV-visible spectroscopy was carried out with a Lambda 35 UV/Vis Spectrometer (Perkin Elmer Instruments).

**Reagents:** All the reagents and anhydrous acetonitrile were purchased from Sigma-Aldrich. Analytical-grade solvents were acquired from Sharlab (Barcelona, Spain).

**Synthesis of (E)-4-(pyridin-4-yl diazenyl)phenol (1):** Azoic dye **1** was obtained through a well-known procedure.<sup>15</sup> 4-aminopyridine (3g, 0.0318 mol) was dissolved with 7.5 M hydrochloric acid (25 mL). Then, a mixture containing 10% NaOH (20 ml), phenol (2.5 g, 0.0265 mol) and  $\text{NaNO}_2$  (2 g, 0.028 mol) was prepared and added dropwise at  $0^\circ\text{C}$  to the 4-aminopyridine solution. The crude product was isolated by filtration and purified by crystallization from acetone/ethanol to give an orange powder.  $^1\text{H}$  NMR and  $^{13}\text{C}$  NMR agree with those reported by Cui et al.

**Synthesis of (E)-4-(4-(tert-butyltrimethylsilyloxy)styryl)pyridine (2):** *t*-butylchlorodimethylsilane (125 mg, 0.833 mmol) was added to a triethylamine solution (0.180 ml, 1.25 mmol) in anhydrous acetonitrile (15 ml). The appearance of a white precipitate was observed. Then, the mixture was added to an acetonitrile (50 ml) suspension of **1** (163 mg, 1.22 mmol). The mixture was stirred overnight in an argon atmosphere. The final crude was purified by column chromatography using Al<sub>2</sub>O<sub>3</sub> as the stationary phase and ethyl acetate-hexane 1:9 v/v as the eluent. The final dosimeter **2** was isolated as yellow crystals.

<sup>1</sup>H NMR (300Mhz, CDCl<sub>3</sub>): δ 0.24 (s, 6H), 0.98 (s, 9H), 6.94 (d, 2H, J = 9 Hz), 7.64 (d, 2H, J = 6 Hz), 7.87 (d, 2H, J = 9 Hz), 8.74 (d, 2H, J = 6 Hz).

<sup>13</sup>C NMR (300Mhz, CDCl<sub>3</sub>): δ -4.05, 18.57, 25.89, 116.44, 120.91, 125.71, 147.48, 151.48, 157.69, 160.27.

**Synthesis of pyridinium salt (3):** **2** (100 mg, 0.32 mmol) and (3-iodopropyl)trimethoxysilane (0.093 mL, 0.32 mmol) were dissolved in anhydrous acetonitrile (25 mL). To this solution, excess sodium carbonate was added and the resulting suspension was refluxed for 72 hours in an argon atmosphere. The crude reaction was filtered to eliminate sodium carbonate, dissolved in dichloromethane, filtered again and evaporated to give the title product **3** with no need for further purification.

<sup>1</sup>H NMR (300Mhz, CDCl<sub>3</sub>): δ 0.29 (s, 6H), 0.79 (m, 2H), 1.03 (s, 9H), 1.94 (m, 2H) 3.24 (m, 2H), 3.59 (s, 9H), 7.01 (d, 2H, J = 9 Hz), 7.72 (d, 2H, J = 6 Hz), 7.94 (d, 2H, J = 9 Hz), 8.79 (d, 2H, J = 6 Hz).

<sup>13</sup>C NMR (300Mhz, CDCl<sub>3</sub>): δ -4.05, 10.72, 11.21, 18.57, 25.87, 27.54, 50.88, 51.01, 116.79, 120.96, 125.89, 147.50, 150.69, 157.69, 160.27.

**Preparation of the TLC foils functionalized with 3:** 1 x 3 cm silica TLC foils were immersed in an acetone solution of chemodosimeter **3** ( $3.0 \times 10^{-4}$  mol dm<sup>-3</sup>) for 10 minutes. By this simple procedure, the alkoxy silane moieties of **3** reacted with the silanols of the surface leading to a covalent grafting of the chemodosimeter.

**Anion sensing studies:** A stock solution of **2** ( $3.0 \times 10^{-4}$  mol dm<sup>-3</sup>) in acetonitrile was obtained and used to prepare an acetonitrile-water 9:1 v/v solution of **2** ( $3.0 \times 10^{-5}$  mol dm<sup>-3</sup>), which was used directly for the UV-visible measurements in the presence of the selected anions. In a typical assay, 2.5 ml of the final solution of **2** were placed in a 3 ml glass cuvette and the necessary amounts of the selected anions (acetonitrile solutions) were added. Finally, the UV-visible spectrum was measured.

### 3.6 Acknowledgments

The authors thank the Spanish Government (project MAT2009-14564-C04), the Generalitat Valenciana (project PROMETEO/2009/016) and the CIBER-BBN for their support. AA also thanks the Generalitat Valenciana for his Santiago Grisolia fellowship.

### 3.7 Bibliography

- 1 (a) J. L. Sessler, P. A. Gale, W.-S. Cho, *Anion Receptor Chemistry*, Royal Society of Chemistry, Cambridge, **2006**. (b) A. Bianchi, K. Bowman, E. Garcia-España *Supramolecular Chemistry of Anions*, Wiley-VCH, New York, **1997**. (c) P. D. Beer, P. A. Gale, *Angew. Chem., Int. Ed.*, **2001**, *40*, 486-516.
- 2 M. Kleerekoper, *Endocrinol. Metab. Clin. North. Am.*, **1998**, *27*, 441-452.

- 3 R. H. Dreisbuch, *Handbook of Poisoning*, Lange Medical Publishers, Los Altos, CA, 1980.
- 4 WHO (World Health Organization), Geneva, **2002**
- 5 (a) P. A. Gale, S. E. Garcia Garrido, J. Garric, *J. Chem. Soc. Rev.* **2008**, *37*, 151-190. (b) R. Martínez-Máñez, F. Sancenón, *Chem. Rev.*, **2003**, *103*, 4419-4476. (c) M. E. Moragues, R. Martínez-Máñez, F. Sancenón, *Chem. Soc. Rev.*, **2011**, *40*, 2593-2643. (d) J. Yoon, S. K. Kim, N. J. Singh, K. S. Kim, *Chem. Soc. Rev.*, **2006**, *35*, 355-360. (e) J. W. Steed, *Chem. Soc. Rev.*, **2009**, *38*, 506-519. (f) C. Caltagirone, P. A. Gale, *Chem. Soc. Rev.*, **2009**, *38*, 520-563. (g) R. Quesada, P. A. Gale, *Coord. Chem. Rev.*, **2006**, *250*, 3219-3244. (h) V. Amendola, M. Bonizzoni, D. Estebán-Gómez, L. Fabbrizzi, M. Lichelli, F. Sancenón, A. Taglietti, *Coord. Chem. Rev.*, **2006**, *250*, 1451-1470.
- 6 See for example: (a) J. Y. Lee, E. J. Chao, S. Mukamel, K. C. Nam, *J. Org. Chem.*, **2004**, *69*, 943-950. (b) C. H. Zhao, E. Sakuda, A. Wakamiya, S. Yamaguchi, *Chem. Eur. J.*, **2009**, *15*, 10603-10612. (c) Q.-S. Lu, L. Dong, J. Zhang, J. Li, L. Jiang, Y. Huang, S. Qin, C.-W. Hu, X.-Q. Yu, *Org. Lett.*, **2009**, *11*, 669-672. (d) T. Mizuno, W. H. Wei, L. R. Eller, J. L. Sessler, *J. Am. Chem. Soc.*, **2002**, *124*, 1134-1135. (e) T. W. Hudnall, C. -W. Chiu, F. P. Gabbai, *Acc. Chem. Res.*, **2009**, *42*, 388-397 (f) S. Rochat, K. Severin, *Chem. Commun.*, **2011**, *47*, 4391-4393. (g) P. Rajamalli, E. Prasad, *Org. Lett.*, **2011**, *13*, 3714-3717.
- 7 (a) V. Amendola, D. Estebán-Gómez, L. Fabbrizzi, M. Licchelli, *Acc. Chem. Res.*, **2006**, *39*, 343-353. (b) M. Boiocchi, L. Del Boca, D. Estebán-Gómez, L. Fabbrizzi, M. Licchelli, E. Monzani, *J. Am. Chem. Soc.*, **2004**, *126*, 16507-16514. (c) D. Estebán-Gómez, L. Fabbrizzi, M. Licchelli, *J. Org. Chem.*, **2005**, *70*, 5717-5720.
- 8 (a) S. K. Kim, J. -I. Hong, *Org. Lett.*, **2007**, *9*, 3109-3112. (b) T. -H. Kim, T. M. Swager, *Angew. Chem. Int. Ed.*, **2003**, *42*, 4803-4806. (c) X. Jiang, M. C. Vieweger, J. C. Bollinger, B. Dragnea, D. Lee, *Org. Lett.*, **2007**, *9*, 3579-3582. (d) X. F. Yang, *Spectrochim. Acta, Part A*, **2007**, *67*, 321-326. (e) X. F. Yang, S. J. Ye, Q. Bai, X. -Q. Wang, *J. Fluoresc.*, **2007**, *17*, 81-87. (f) C. -Q. Zhu, J. -L. Chen, H. Zheng, Y. -Q. Wu, J. -G. Xu, *Anal. Chim. Acta*, **2005**, *539*, 311-316. (g) S. Y. Kim, J. Park, M. Koh, S. B. Park, J. -I. Hong, *Chem. Commun.*, **2009**, 4735-4737. (h) P. Sockalingam, C. -H. Lee, *J. Org. Chem.*, **2011**, *76*, 3820-3828. (i) X. Cao, W. Lin, Q. Yu, J. Wang, *Org. Lett.*, **2011**, *13*, 6098-6101.
- 9 A. O. Bozdemir, F. Sozmen, O. Buyucakir, R. Guliyev, Y. Cakmak, E. U. Akkaya, *Org. Lett.*, **2010**, *12*, 1400-1403.

- 10 L. Fu, F.-L. Jiang, D. Fortin, P. D. Harvey, Y. Liu, *Chem. Commun.*, **2011**, 47, 5503-5505.
- 11 V. Bhalla, H. Singh, M. Kumar, *Org. Lett.*, **2010**, 12, 628-631.
- 12 B. Zhu, F. Yuan, R. Li, Y. Li, Q. Wei, Z. Ma, B. Du, X. Zhang, *Chem. Commun.*, **2011**, 47, 7098-7100.
- 13 A. B. Descalzo, D. Jiménez, J. El Haskouri, D. Beltrán, P. Amorós, M. D. Marcos, R. Martínez-Máñez, J. Soto, *Chem. Commun.*, **2002**, 562-563.
- 14 See for example: (a) F. Sancenón, R. Martínez-Máñez, M. A. Miranda, M. J. Seguí, J. Soto, *Angew. Chem. Int. Ed.*, **2003**, 42, 647-650. (b) M. Comes, G. Rodríguez-López, M. D. Marcos, R. Martínez-Máñez, F. Sancenón, J. Soto, L. A. Villaescusa, P. Amorós, D. Beltrán, *Angew. Chem. Int. Ed.*, **2005**, 44, 2918-2922. (c) R. Casasús, E. Aznar, M. D. Marcos, R. Martínez-Máñez, F. Sancenón, J. Soto, P. Amorós, *Angew. Chem. Int. Ed.*, **2006**, 45, 6661-6664. (d) E. Climent, R. Casasús, M. D. Marcos, R. Martínez-Máñez, F. Sancenón, J. Soto, *Chem. Commun.*, **2008**, 6531-6533. (e) E. Climent, P. Calero, M. D. Marcos, R. Martínez-Máñez, F. Sancenón, J. Soto, *Chem. Eur. J.*, **2009**, 15, 1816-1820. (f) T. Ábalos, S. Royo, R. Martínez-Máñez, F. Sancenón, J. Soto, A. M. Costero, S. Gil, M. Parra, *New J. Chem.*, **2009**, 33, 1641-1645. (g) P. Calero, M. Hecht, R. Martínez-Máñez, F. Sancenón, J. Soto, J. L. Vivancos, K. Rurack, *Chem. Commun.*, **2011**, 47, 10599-10601.
- 15 L. Cui, Y. Zhao, *Chem. Mater.*, **2004**, 16, 2076-2082.
- 16 (a) B. Valeur, I. Leray, *Coord. Chem. Rev.*, **2000**, 205, 3-40. (b) L. Fabbrizzi, M. Licchelli, G. Rabaioli, A. Taglietti, *Coord. Chem. Rev.*, **2000**, 205, 85-108. (c) K. Rurack, *Spectrochim. Acta, Part A*, **2001**, 57, 2161-2195.
- 17 H. Lin, K. S. Suslick, *J. Am. Chem. Soc.*, **2010**, 132, 15519-15521.



***Chapter 4:***  
***A surfactant-assisted probe for the***  
***chromo-fluorogenic recognition***  
***of GSH over cysteine in water***



***A surfactant-assisted probe for the chromo-  
fluorogenic recognition of GSH over cysteine in  
water***

Alessandro Agostini,<sup>[a]</sup> Inmaculada Campos,<sup>[a]</sup> Michele  
Milani,<sup>[b]</sup> Ramón Martínez-Máñez,<sup>\*[a]</sup> Maurizio Licchelli,<sup>\*[b]</sup>  
and Félix Sancenón<sup>[a]</sup>

<sup>[a]</sup>*Centro de Reconocimiento Molecular y Desarrollo Tecnológico (IDM),  
Unidad Mixta Universidad Politécnica de Valencia-Universidad de Valencia.*

*Departamento de Química, Universidad Politécnica de Valencia,*

*Camino de Vera s/n, 46022, Valencia, Spain.*

*CIBER de Bioingeniería, Biomateriales y Nanotecnología (CIBER-BNN).*

<sup>[b]</sup>*Dipartimento di Chimica, Università di Pavia,*

*via Taramelli 12, 27100, Pavia, Italy.*

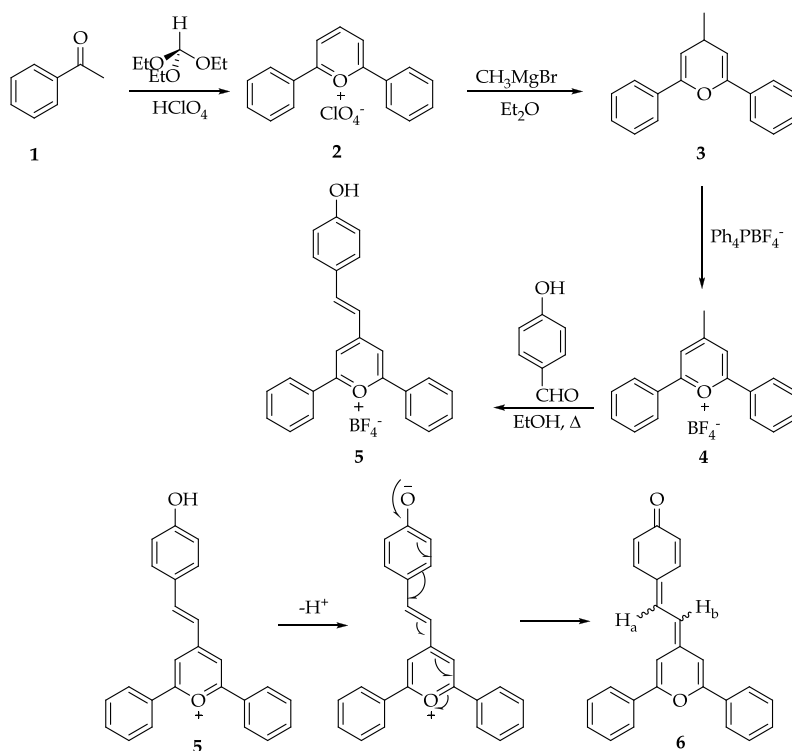
***Submitted on 8-02-2013***

**A chromo-fluorogenic probe for the detection of GSH versus cysteine in water was accomplished using a pyrylium-stilbene derivative and CTAB micelles.**

Biothiols, such as cysteine (Cys) and glutathione (GSH) are molecules which play crucial roles in several biological processes. In particular, GSH is a fundamental small peptide having many biological functions such as maintenance of intra-cellular redox activity, xenobiotic metabolism, intra-cellular signal transduction and gene regulation.<sup>1</sup> Besides, low levels of GSH are involved in several human diseases such as leucocyte loss, psoriasis, liver damage, cancer and AIDS.<sup>2</sup> For all these reasons, the development of novel and simple chromo-fluorogenic probes for the selective and sensitive detection of GSH is of marked interest.<sup>3</sup> In this context, a number of work has been devoted to the preparation of probes for thiol-containing biomolecules.<sup>4</sup> In most cases these chemosensors are designed following the chemodosimeter paradigm, which makes use of the high nucleophilic reactivity of the thiol group. Among several reactions, Michael type additions have been the most commonly employed.<sup>5</sup> However, many of these thiol chemodosimeters display sensing features in organic or water-organic solvent mixtures and a similar response is usually observed for related thiols such as Cys, Hcy and GSH.<sup>6</sup> Although recently some nano-sensing systems based in gold nanoparticles,<sup>7</sup> gold nanoclusters<sup>8</sup> quantum-dots<sup>9</sup> have been described for the optical detection of GSH, the number of simple molecular-based probes for the selective sensing of GSH are scarce. In this area, Yao and co-workers used a charged polythiophene and *o*-phthalaldehyde for the chromo-fluorogenic selective recognition of GSH.<sup>10</sup> In particular the authors found that, only addition of GSH induced the aggregation of the polymer and the generation of a highly colored and non-fluorecent isoindole derivative. Yang and co-workers

prepared a bis-spiropyran receptor able to recognize selectively GSH.<sup>11</sup> Addition of GSH induced the isomerization of the receptor to the merocyanine form upon coordination with a clear color change and emission enhancement. In other recent example a BODIPY derivative for the ratiometric fluorescent selective sensing of GSH was prepared.<sup>12</sup> Finally, Strongin et al recently reported a resorufin-based probe for GSH detection.<sup>13</sup>

Bearing the above-mentioned circumstances, it is apparent that the development of probes able to display colour and/or fluorescence changes in pure water in the presence of target biorelevant thiols is a timely research area.



**Scheme 1.** Synthesis of 5 and the deprotonation-induced formation of the quinone derivative 6.

Given our interest in the design of chromo-fluorogenic chemosensors,<sup>14</sup> we report herein the synthesis, characterization and sensing features of a new probe based on a pyrylium-stilbene derivative which displays an excellent specific surfactant-assisted selective chromo-fluorogenic response to GSH over Cys in water.

The synthesis of pyrylium-stilbene derivative **5** is shown in Scheme 1 and began with a condensation reaction in acid media between acetophenone (**1**) and triethylorthoformate that yielded 2,6-diphenylpyrylium perchlorate (**2**). Addition of methylmagnesium bromide to diethylether solutions of **2** afforded 4-methyl-2,6-diphenyl-4H-pyran (**3**) that was aromatized to 4-methyl-2,6-diphenylpyrylium tetrafluoroborate (**4**) upon addition of tetraphenylphosphonium tetrafluoroborate. Condensation of **4** with *p*-hydroxybenzaldehyde yielded the final derivative **5** as a red powder. The most characteristic signals of the <sup>1</sup>H-NMR spectra of **5** are two doublets centered at ca. 7.4 (see Scheme 1 and Figure 1, proton H<sub>a</sub>) and 8.7 ppm (proton H<sub>b</sub>), with a 16 Hz coupling constant, ascribed to the protons of the stilbene double bond. Also significant are the singlets at 10.8 and 8.8 ppm attributed to the phenol and pyrylium ring protons, respectively.

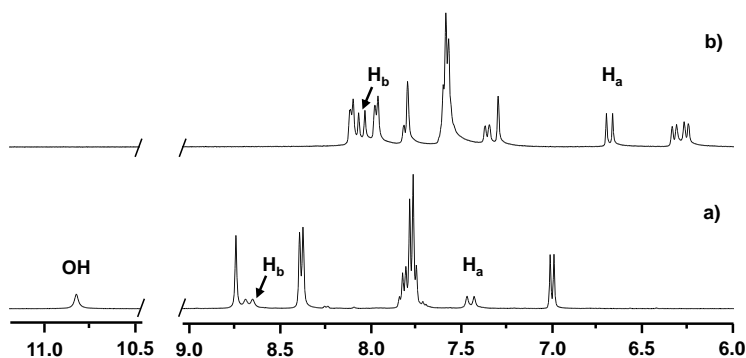


**Figure 1.** <sup>1</sup>H-NMR spectra of **5** alone (a) and after addition of DBU (b) both in deuterated acetonitrile.

$^{13}\text{C}$ -NMR and HRMS studied were also in agreement with the proposed formulation (see Supporting Information). Moreover **5** was characterized using single crystal X-ray diffraction techniques (see Supporting Information for the structure of **5** isolated as nitrate or tetrafluoroborate salts). Acetonitrile solutions of **5** showed two absorption bands centered at 410 and 500 nm that are the responsible of the red-orange colour observed. Moreover, **5** is weakly soluble in pure water but readily solubilize in HEPES (30 mM, pH 7.5)-CTAB (20 mM) solutions. HEPES-CTAB solutions of **5** are blue due to the presence of a resolved absorption band in the 500-700 nm region. The bathochromic shift of the absorption band of **5** when changed from acetonitrile to HEPES-CTAB solutions, was ascribed to the inclusion of **5** into the hydrophobic environment of the CTAB micelles and its deprotonation which results in the less polar hydrophobic quinone **6** (see Scheme 1).

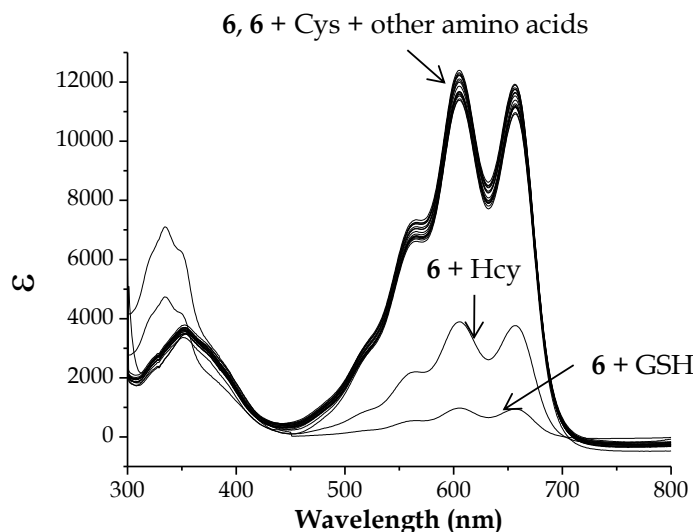


**Figure 2.** UV-visible spectra of **6** ( $2.5 \times 10^{-5}$  M) in HEPES (30 mM, pH 7.5)-CTAB (20 mM) solutions in the presence of 2 equiv. of amino acids (i.e, Cys, Hcy, Ala, Arg, Asn, Asp, Glu, Gln, Gly, His, Ilc, Leu, Lys, Met, Phe, Pro, Ser, Thr, Trp, Tyr, Val and GSH). Spectra were taken immediately upon addition of thiols and amino acids.

The occurrence of this deprotonation is in agreement with the  $pK_a$  of the phenolic hydroxyl of **5** in acetonitrile which was determined to be 7.10 (see Supporting Information) indicating a relatively high acidity of the phenolic proton favoured by the electronic conjugation with the electron withdrawing pyrylium ring. Moreover, the formation of **6** inside the CTAB micelles was proved from additional experiments. For instance, addition of DBU (a non-nucleophilic strong organic base) to acetonitrile solutions of **5** induced an immediate colour modulation from red-orange to blue with the appearance of intense absorptions in the 500-700 nm interval (peaks at 547, 583 and 640 nm) which were very similar to those found in HEPES-CTAB solutions of **5** (see Supporting Information). These colour changes in acetonitrile went also along with a remarkable modulation in the  $^1\text{H-NMR}$  spectrum (see Figure 1).

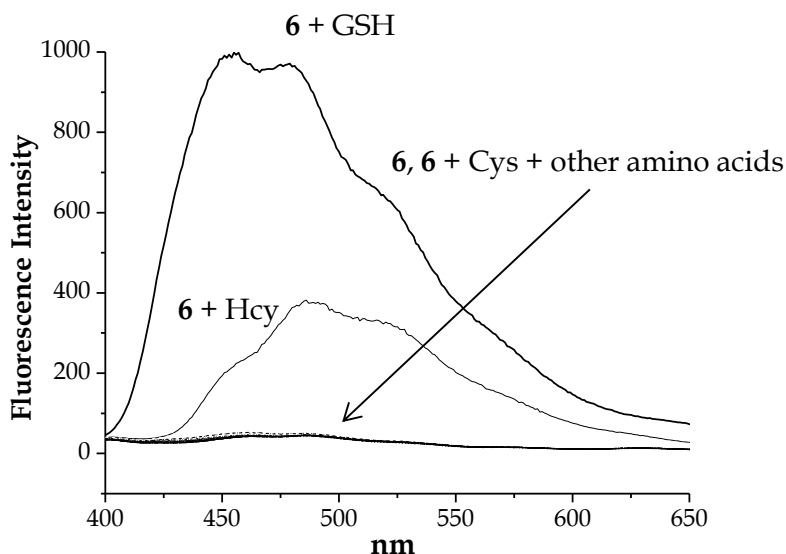
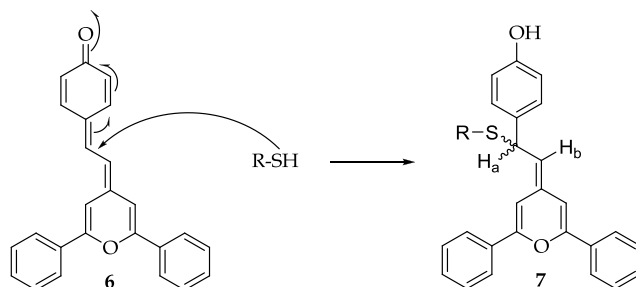


**Figure 3.** Emission spectra (excitation at 350 nm) of HEPES (30 mM, pH 7.5)-CTAB (20 mM) solutions of **6** ( $2.5 \times 10^{-5}$  M) in the presence of 2 equiv. of GSH and other amino acids (i.e., Cys, Hcy, Ala, Arg, Asn, Asp, Glu, Gln, Gly, His, Ile, Leu, Lys, Met, Phe, Pro, Ser, Thr, Trp, Tyr and Val). Spectra were taken immediately upon addition of thiols and amino acids.

As could be seen in the figure the signals of the double bond protons ( $H_a$  and  $H_b$ ) of **5** suffered a significant upfield shifts with a reduction of the coupling constant (from 16 to 12 Hz) upon addition of DBU. Also, the hydroxyl proton signal centred at 10.8 ppm disappeared upon addition of base. All these data point towards the phenol deprotonation of **5** inside the micelles to give **6**. Moreover, the sensing behaviour on HEPES-CTAB solutions of **6** in the presence of GSH, Cys, Hcy, Ala, Arg, Asn, Asp, Glu, Gln, Gly, His, Ilc, Leu, Lys, Met, Phe, Pro, Ser, Thr, Trp, Tyr and Val was studied and the results are shown in Figures 2 and 3. Of all the species tested only GSH was able to induce a remarkable, instantaneous, hypochromic effect in the absorption bands with the subsequent bleaching of the initial blue solution (see Figure 2), whereas Hcy induced a moderate bleaching. Besides, HEPES-CTAB solutions of **6** showed a very weak emission centered at 481 nm upon excitation at 350 nm (see Figure 3). Moreover, a remarkable selective grown of a red-shifted emission band at 485 nm was observed in the presence of GSH (25-fold enhancement upon addition of 2 equivalents). The presence of Hcy also induced a moderate (8-fold upon addition of 2 equiv) emission enhancement of the emission at 485 nm.



**Scheme 2.** Proposed mechanism of the 1,6-conjugated addition of thiol-containing biomolecules to probe **6**.

The change in colour and in emission of **6** upon addition of GSH and Hcy is ascribed to a 1,6-conjugated thiol addition reaction (see Scheme 2) that yielded the phenol **7**. This addition was confirmed by NMR experiments. In particular, the model reaction between **6** and 2-mercaptoethanol was studied in detail by  $^1\text{H}$ ,  $^{13}\text{C}$ , COSY, HSQC and sel-TOCSY NMR in DMSO- $\text{D}_6$  (see Supporting Information). HSQC spectra of the reaction product clearly indicated the existence of a correlation between the  $\text{H}_b$  proton (see Scheme 2) and a benzylic carbon (at ca. 45 ppm) and between the  $\text{H}_a$  proton and an olefinic carbon (at ca. 116 ppm) strongly suggesting the presence of **7**.

At this point it is important to note that the concept of using a surfactant in order to solubilize the probe for GSH has also been recently reported by Strongin et al.<sup>13</sup>

Apart of the sensing *turn-on* emission features displayed in water, one additional remarkable characteristic of **6** is the selective response to GSH versus similar biologically relevant thiol derivatives such as Cys. Although Hcy also induces some response, it has to be taken into account that the amount of Hcy in real samples such as plasma is low when compared with GSH and Cys, suggesting that probe **6** can be suitable for the quantification of GSH without Cys interference.<sup>16</sup> In order to study more in detail the selective response of **6** further studies dealing with the response of HEPES-CTAB solution of **6** in the presence of GSH and Cys were carried out (see Figure 4). As it can be seen, the progressive addition of GSH induced a marked enhancement in the emission band whereas in the presence of Cys negligible changes were obtained even at relatively high concentrations. Moreover no optical changes were observed in the presence of Cys even after several hours. The selective reaction of **6** with GSH is attributed to the more hydrophobic character of GSH and its preferential internalization into

the micellar core when compared with Cys which is much more hydrophilic. Using this simple procedure a selective detection for GSH as low as  $1.0 \times 10^{-6}$  mol  $\text{dm}^{-3}$  in HEPES-CTAB solution was determined.

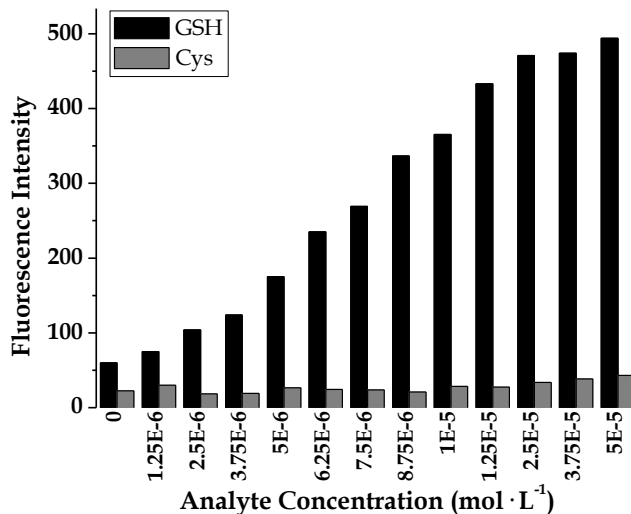


**Figure 4.** Emission intensity at 483 nm (excitation at 350 nm) of HEPES (30 mM, pH 7.5)-CTAB (20 mM) solutions of **6** ( $2.5 \times 10^{-5}$  M) upon addition of increasing quantities of Cys and GSH. Emission intensity was measured immediately upon addition of GSH and Cys.

Finally, the possible application of probe **6** for the determination of GSH in more competitive and complex samples was tested. In particular, GSH was determined in artificial human plasma from the regression equation of a standard calibration curve. The artificial plasma was prepared according to a well established protocol<sup>17</sup> and it was spiked with conventional quantities of biothiols (Cys: 178.4  $\mu\text{M}$ ; Hcy: 5.9  $\mu\text{M}$  and GSH: 6.3  $\mu\text{M}$ ).<sup>18</sup> Following this procedure the GSH content in the sample was determined to be 5.92  $\mu\text{M}$  (recovery of 94%, see supporting information for details). In summary, we have reported the synthesis of a pyrylium-based probe (**6**) able to give a selective chromo-fluorogenic response in the presence of GSH in water. The observed optical change is ascribed to a 1,6-conjugated addition of the thiol moiety of GSH to **6** which yielded the

corresponding phenol **7**. As remarkable results the probe allows a *turn-on* emission detection of GSH in pure water (containing CTAB micelles) at concentration as low as 1  $\mu$ M. Besides the probe is able to display selective sensing features and it is one of the few reported examples able to give an optical response to GSH but not to the similar thiol derivative Cys.

#### 4.1 Acknowledgments

The authors thank the Spanish Government (project MAT2012-38429-C04-01), the Generalitat Valenciana (project PROMETEO/2009/016) and the CIBER-BBN for their support. AA also thanks the Generalitat Valenciana for his Santiago Grisolia fellowship. Thanks are due to Dr. Massimo Boiocchi (Centro Grandi Strumenti, Università di Pavia) for the X-ray data collection.

#### 4.2 Bibliography

- 1 (a) A. Meister, *J. Biol. Chem.*, 1988, **263**, 17205. (b) M. E. Anderson, *Chem. Biol. Interact.*, 1998, **112**, 1.
- 2 (2) (a) Lu, S. C. *Mol. Aspects Med.* **2009**, *30*, 42. (b) Smith, C. V.; Jones, D. P.; Guenther, T. M.; Lash, L. H.; Lauterburg, B. H. *Toxicol. Appl. Pharmacol.* **1996**, *140*, 1.
- 3 (a) Chen, X.; Zhou, Y.; Peng, X.; Yoon, J. *Chem. Soc. Rev.* **2010**, *39*, 2120. (b) Moragues, M. E.; Martínez-Máñez, R.; Sancenón, F. *Chem. Soc. Rev.* **2011**, *40*, 2593. (c) Santos-Figueroa, L. E.; Moragues, M. E.; Climent, E.; Agostini, A.; Martínez-Máñez, R.; Sancenón, F. *Chem. Soc. Rev.* **2013**, *42*, 3489. (d) Zhou, Y.; Yoon, J. *Chem. Soc. Rev.* **2012**, *41*, 52.
- 4 See for example: (a) Kaur, K.; Saini, R.; Kumar, A.; Luxami, V.; Kaur, N.; Singh, P.; Kumar S. *Coord. Chem. Rev.* **2012**, *256*, 1992. (b) Long, L.; Lin, W.; Chen, B.; Gao, W.; Yuan, L. *Chem. Commun.* **2011**, *47*, 893. (c) Deng, L.; Wu, W.; Guo, H.; Zhao, J.; Ji, S.; Zhang, X.; Yuan, X.; Zhang, C. *J. Org. Chem.* **2011**, *76*, 9294.

- 5 (a) Jung, H. S.; Ko, K. C.; Kim, G. -H.; Lee, A. -R.; Na, Y. C.; Kang, C.; Lee, J. Y.; Kim, J. S. *Org. Lett.* **2011**, *13*, 1498. (b) Kwon, H.; Lee, K.; Kim, H. J. *Chem. Commun.* **2011**, *47*, 1773. (c) Huo, F. -J.; Sun, Y. -Q.; Su, J.; Chao, J. -B.; Zhi, H. -J.; Yin, C. -X. *Org. Lett.* **2009**, *11*, 4918. (d) Lin, W.; Yuan, L.; Cao, Z.; Feng, Y.; Long, L. *Chem. Eur. J.* **2009**, *15*, 5096. (e) Tang, X.; Liu, W.; Wu, J.; Zhao, W.; Zhang, H.; Wang, P. *Tetrahedron Lett.* **2011**, *52*, 5136. (f) Lim, S. -Y.; Lee, S.; Park, S. B.; Kim, H. -J. *Tetrahedron Lett.* **2011**, *52*, 3902. (g) García-Beltrán, O.; Mena, N.; Pérez, E. G.; Cassels B. K.; Muñoz, M. T.; Werlinger, F.; Zavala, D.; Aliaga, M. E.; Pavez, P. *Tetrahedron Lett.* **2011**, *52*, 6606. (h) Ha H. -J.; Yoon, D. -H.; Park, S.; Kim, H. -J. *Tetrahedron* **2011**, *67*, 7759. (i) Chen, X.; Ko, S. -K.; Kim, M. J.; Shin, I.; Yoon J. *Chem. Commun.* **2010**, *46*, 2751. (j) Huo, F. -J.; Sun, Y. -Q.; Su, J.; Yang, Y. -T.; Yin, C. -X.; Chao, J. -B. *Org. Lett.* **2010**, *12*, 4756. (k) Zhao, N.; Wu, Y. -H.; Shi, L. -X.; Lin, Q. -P.; Chen, Z. -N. *Dalton Trans.* **2010**, *39*, 8288. (l) Kand, D.; Kalle, A. M.; Varma, S. J.; Talukdar, P. *Chem. Commun.* **2012**, *48*, 2722.
- 6 (a) Chen, X.; Ko, S. K.; Kim, J.; Yoon, J. *Chem. Commun.* **2010**, *46*, 2751. (b) Li, X.; Quian, S.; He, Q.; Yang, B.; Li, J.; Hu, Y. *Org. Biomol. Chem.* **2010**, *8*, 3627. (c) Cao, X.; Lin, W.; Yu, Q. *J. Org. Chem.* **2011**, *76*, 7423. (d) Wang, S. -P.; Deng, W. -J.; Sun, D.; Yan, M.; Zheng, H.; Xu, J. -G. *Org. Biomol. Chem.* **2009**, *7*, 4017. (e) Hong, V.; Kislukhin, A. A.; Finn, M. G. *J. Am. Chem. Soc.* **2009**, *131*, 9986. (f) Ruan, Y. -B.; Li, A. -F.; Zhao, J. -S.; Shen, J. -S.; Jiang, Y. -B. *Chem. Commun.* **2010**, *46*, 4938. (g) Wu, J.; Sheng, R.; Liu, W.; Wang, P.; Ma, J.; Zhang, H.; Zhuang, X. *Inorg. Chem.* **2011**, *50*, 6543. (h) Yue, Y.; Guo, Y.; Xu, J.; Shao, S. *New J. Chem.* **2011**, *35*, 61. (i) Zhu, B.; Zhang, X.; Li, Y.; Wang, P.; Zhang, H.; Zhuang, X. *Chem. Commun.* **2010**, *46*, 5710. (j) Lee, J. H.; Lim, C. S.; Tian, Y. S.; Han, J. H.; Cho, B. R. *J. Am. Chem. Soc.* **2010**, *132*, 1216. (k) Lan, M.; Wu, J.; Liu, W.; Zhang, H.; Zhang, W.; Zhuang, X.; Wang, P. *Sensors Act. B* **2011**, *156*, 332. (l) Huang, Z.; Pu, F.; Lin, Y.; Ren, J.; Qu, X. *Chem. Commun.* **2011**, *47*, 3487. (m) Xie, W. Y.; Huang, W. T.; Li, N. B.; Luo, H. Q. *Chem. Commun.* **2012**, *48*, 82. (n) Duan, Y. L.; Shi, Y. G.; Chen, J. H.; Wu, X. H.; Wang, G. K.; Zhou, Y.; Zhang, J. F. *Tetrahedron Lett.* **2012**, *53*, 6544. (o) Zhou, L.; Lin, Y.; Huang, Z.; Ren, J.; Qu, X. *Chem. Commun.* **2012**, *48*, 1147. (p) Ma, B.; Zeng, F.; Li, X.; Wu, S. *Chem. Commun.* **2012**, *48*, 6007. (q) Chen, Z.; Lin, Y.; Zhao, C.; Ren, J.; Qu, X. *Chem. Commun.* **2012**, *48*, 11428. (r) Lou, Z.; Li, P.; Sun, X.; Yang, S.; Wang, B.; Han, K. *Chem. Commun.* **2013**, *49*, 391. (s) Leung, K. -H.; He, H. -Z.; Ma, V. P. -Y.; Chan, D. S. -H.; Leung, C. -H.; Ma, D. -L. *Chem. Commun.* **2013**, *49*, 771. (t) Li, G.; Chen, Y.; Wu, J.; Ji, L.; Chao, H. *Chem. Commun.* **2013**, *49*, 2040. (u) Yang, P.; Xu, Q. -Z.; Jin, S. -Y.; Zhao, Y.; Lu, Y.; Xu, X. -W.; Yu, S. -H. *Chem. Eur. J.* **2012**, *18*, 1154. (v) Wang, R.; Chen, L.; Liu, P.; Zhang, Q.; Wang, Y. *Chem. Eur. J.* **2012**, *18*, 11343. (x) Jia, X.;

- Li, J.; Wang, E. *Chem. Eur. J.* **2012**, *18*, 13494. (y) Sun, W.; Li, W.; Li, J.; Zhang, J.; Du, L.; Li, M. *Tetrahedron* **2012**, *68*, 5363. (z) Sun, W.; Li, W.; Li, J.; Zhang, J.; Du, L.; Li, M. *Tetrahedron Lett.* **2012**, *53*, 2332.
- 7 (a) Li, Y.; Wu, P.; Xu, H.; Zhang, H.; Zhong, X. *Analyst* **2011**, *136*, 196. (b) Chen, Z.; Wang, Z.; Chen, J.; Wang, S.; Huang, X. *Analyst* **2012**, *137*, 3132.
- 8 Tian, D.; Qian, Z.; Xia, Y.; Zhu, C. *Langmuir* **2012**, *28*, 3945.
- 9 Liu, J.; Bao, C.; Zhong, X.; Zhao, C.; Zhu, L. *Chem. Commun.* **2010**, *46*, 2971.
- 10 Yao, Z.; Feng, X.; Li, C.; Shi, G. *Chem. Commun.* **2009**, 5886.
- 11 Shao, N.; Jin, J.; Wang, H.; Zheng, J.; Yang, R.; Chan, W.; Abliz, Z. *J. Am. Chem. Soc.* **2010**, *132*, 725.
- 12 Niu, L. -Y.; Guan, Y. -S.; Chen, Y. -Z.; Wu, L. -Z.; Tung, C. -H.; Yang, Q. -Z. *J. Am. Chem. Soc.* **2012**, *134*, 18928.
- 13 Guo, Y.; Yang, X.; Hakuna, L.; Barve, A.; Escobedo, J. O.; Lowry, M.; Strongin, R. M. *Sensors* **2012**, *12*, 5940.
- 14 (a) Agostini, A.; Milani, M.; Martínez-Máñez, R.; Licchelli, M.; Soto, J.; Sancenón, F. *Chem. As. J.* **2012**, *7*, 2040. (b) Moragues, M. E.; Esteban, J.; Ros-Lis, J. V.; Martínez-Máñez, R.; Marcos, M. D.; Martínez, M.; Soto, J.; Sancenón, F. *J. Am. Chem. Soc.* **2011**, *133*, 15762.
- 15 For examples on micelle-based chemosensors see: (a) Hu, X. -J.; Li, C. -M.; Song, W. -Y.; Zhang, D.; Li, Y. -S. *Inorg. Chem. Commun.* **2011**, *14*, 1632. (b) Riis-Johannessen, T.; Severin, K. *Chem. Eur. J.* **2010**, *16*, 8291. (c) Grandini, P.; Mancin, F.; Tecilla, P.; Scrimin, P.; Tonellato, U. *Angew. Chem. Int. Ed.* **1999**, *38*, 3061. (d) Cavallaro, G.; Giammona, G.; Pasotti, L.; Pallavicini, P. *Chem. Eur. J.* **2011**, *17*, 10574. (e) Pallavicini, P.; Díaz-Fernández, Y. A.; Foti, F.; Mangano, C.; Patroni, S. *Chem. Eur. J.* **2007**, *13*, 178.
- 16 Andersson, A.; Lindgren, A.; Arnadottir, M.; Prytz, H.; Hultberg, B. *Clin. Chem.* **1999**, *45*, 1084.
- 17 for plasma preparation see: Marques, R. C.; Loebenberg, R.; Almukainzi, M. *Dissolut. Technol.* **2011**, *18*, 15-28.

- 18 For typical biothiols plasma concentration see: Salazar, F.; Schorr, H.; Herrmann, W.; Herbeth, B.; Siest, G.; Leroy, P. *J. of Chromatogr. Sci.* **1999**, *37*, 469-476.



***A surfactant-assisted probe for the chromo-  
fluorogenic recognition of GSH over cysteine in  
water***

Alessandro Agostini,<sup>[a]</sup> Inmaculada Campos,<sup>[a]</sup> Michele  
Milani,<sup>[b]</sup> Ramón Martínez-Mañez,<sup>\*[a]</sup> Maurizio Licchelli,<sup>\*[b]</sup>  
and Félix Sancenón<sup>[a]</sup>

<sup>[a]</sup>*Centro de Reconocimiento Molecular y Desarrollo Tecnológico (IDM),  
Unidad Mixta Universidad Politécnica de Valencia-Universidad de Valencia.*

*Departamento de Química, Universidad Politécnica de Valencia,  
Camino de Vera s/n, 46022, Valencia, Spain.*

*CIBER de Bioingeniería, Biomateriales y Nanotecnología (CIBER-BNN).*

<sup>[b]</sup>*Dipartimento di Chimica, Università di Pavia,  
via Taramelli 12, 27100, Pavia, Italy.*

***Supporting Information***

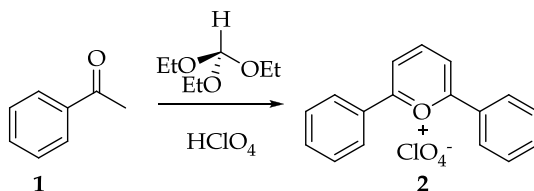
### **Chemicals**

The chemicals cetyltrimethylammonium bromide (CTAB), 4-(2-hydroxyethyl)-1-piperazineethanesulfonic acid (HEPES), acetophenone, triethylorthoformate, methyl iodide, magnesium, perchloric acid, tetraphenylphosphonium tetrafluoroborate, 4-hydroxybenzaldehyde, GSH and selected amino-acids (Cys, Hcy, Ala, Arg, Asn, Asp, Glu, Gln, Gly, His, Ile, Leu, Lys, Met, Phe, Pro, Ser, Thr, Trp, Tyr, Val) were provided by Sigma-Aldrich. Analytical-grade solvents were from Scharlab (Barcelona, Spain). All reagents were used as received.

### **General Techniques**

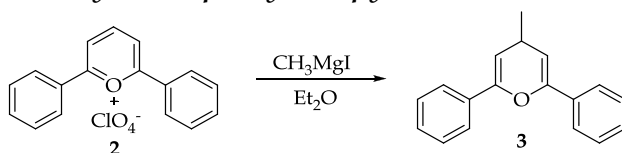
Fluorescence spectroscopy was carried out with a Jasco Spectrofluorometer FP-8500. 1D and 2D NMR spectra were recorded on a Bruker AVANCE III 400 MHz Spectrometer, where  $^1\text{H}$  NMR spectra were recorded at 400 MHz at 298 K, while  $^{13}\text{C}$  NMR spectra were recorded at 100 MHz at 298 K. The NMR samples were dissolved in deuterated solvents purchased from Cambridge Isotope Labs or Sigma-Aldrich, and TMS or the residual solvent were used as internal standard. Electron impact ionization mass spectrometry (MS-EI) was performed on a Thermo Finnigan MAT SSQ710 single stage quadrupole instrument. Matrix-assisted laser-desorption/ionization mass spectrometry was performed on a Bruker Autoflex III Smartbeam mass spectrometer, utilizing a 2,5-dihydroxybenzoic acid (DHB) matrix.

### **Synthesis of 2,6-diphenylpyrylium perchlorate (2)**



Acetophenone (4 mL, 34.3 mmol) and triethylorthoformiate (10 mL) were placed in a round bottomed flask (250 mL) under Ar atmosphere and at 0 °C. After 15 minutes perchloric acid (7.4 mL, 86.5 mmol) was added dropwise during 30 minutes. Then, the crude reaction was allowed to react at room temperature for 60 minutes. The final 2,6-diphenylpyrylium perchlorate (**2**, 10.1 g, 30.4 mmol, 88.6% yield) was isolated as a yellow solid by addition of diethylether. <sup>1</sup>H- and <sup>13</sup>C-NMR data and mass spectra are coincident with the reported in the literature. <sup>1</sup>

### Synthesis of 4-methyl-2,6-diphenyl-4H-pyran (**3**)



a) *Preparation of the Grignard reagent.* Magnesium (1 g, 0.042 mol) was placed in a round bottomed flask with refrigerant, septum and connected to a vacuum line. Firstly, the air was removed by vacuum and replaced by Argon. In a second step, a solution of methyl iodide (2.58 ml, 0.042 mol) in diethyl ether (30 ml) was added through the septum in total absence of air to avoid the degradation of the just formed Grignard reagent. The mixture was stirred at room temperature during 1 hour.

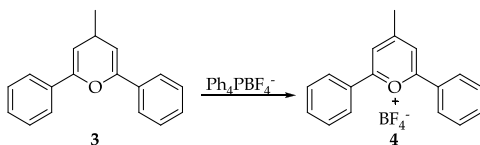
b) *Nucleophilic addition of methylmagnesiumiodide to 2,6-diphenylpyrylium perchlorate.* The as made Grignard reagent in diethyl ether was added, under inert Ar atmosphere, to a diethyl ether (10 ml) solution of 2,6-diphenylpyrylium perchlorate (790 mg, 2.37 mmol). The reaction mixture was stirred at room temperature overnight. Subsequently the reaction mixture was washed twice with saturated aqueous NH<sub>4</sub>Cl (2 x 30 ml), water (3 x 20 ml) and finally dried over sodium sulfate. The elimination of

the diethyl ether gave the title product **3** (581 mg, 2.37 mmol) in nearly quantitative yield.

$^1\text{H-NMR}$  ( $\text{CDCl}_3$ , 400 Mhz):  $\delta$ : 1.43-1.51 (dd, 3H,  $J = 3$  Hz,  $J = 6$  Hz), 3.47 (m, 1H), 5.59-5.61 (dd, 2H,  $J = 3$  Hz,  $J = 6$  Hz), 7.61 (m, 6H), 7.97 (m, 4H).

$^{13}\text{C-NMR}$  ( $\text{CDCl}_3$ , 100 Mhz):  $\delta$ : 21.1, 31.5, 107.3, 126.5, 128.3, 130.5, 133.5, 159.3.

### Synthesis of 4-methyl-2,6-diphenylpyrylium tetrafluoroborate (**4**)



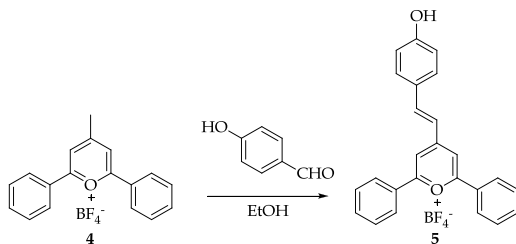
A solution of **3** (520 mg, 2.1 mmol) in anhydrous  $\text{CH}_3\text{CN}$  (30 ml) was treated with tetraphenylphosphonium tetrafluoroborate (629 mg, 2.53 mmol) at room temperature overnight. After this, the acetonitrile was eliminated by rotary evaporation and the dark-brown residue dissolved in the minimum amount of acetone (1 ml). Finally product **4** was isolated as a brown powder (580 mg, 1.7 mmol, 82% yield) through precipitation with diethylether. <sup>2</sup>

$^1\text{H-NMR}$  ( $\text{CDCl}_3$ , 400 Mhz):  $\delta$ : 2.84 (s, 3H), 7.82 (m, 6H), 8.42-8.45 (d, 4H,  $J = 9$  Hz), 8.85 (s, 9H).

$^{13}\text{C-NMR}$  ( $\text{CDCl}_3$ , 100 Mhz):  $\delta$ : 24.1, 120.1, 127.8, 128.4, 130.7, 136.0, 170.9, 180.2.

M.p. 233.5–234.1 °C

### Synthesis of chemodosimeter **5**



A solution of 4-methyl-2,6-diphenylpyrylium tetrafluoroborate (**4**, 3.033 g, 9.1 mmol) and 4-hydroxybenzaldehyde (1.108 g, 9.1 mmol) in absolute ethanol (150 ml) was refluxed overnight under argon atmosphere. Then ethanol was removed by rotary evaporation and the dark-red residue taken up with the minimum amount of acetone. This solution was treated with diethyl ether (500 mL) to precipitate the final product **5** (3.585 mg, 8.2 mmol, 89.8% yield) as a dark-red crystalline powder. The reported NMR (figure SI-1 - SI-4 ) confirmed the obtention of the titled product.

$^1\text{H-NMR}$  ( $\text{CDCl}_3$ , 400 Mhz):  $\delta$ : 7.00 (d, 2H,  $J = 6.5$  Hz), 7.45 (d, 1H,  $J = 14$  Hz), 7.76 (m, 6H), 7.83 (d, 2H,  $J = 6.5$  Hz), 8.38 (d, 4H,  $J = 6.7$  Hz), 8.67 (d, 1H,  $J = 14$  Hz), 8.74 (s, 2H), 10.82 (s, 1H).

$^{13}\text{C-NMR}$  ( $\text{CDCl}_3$ , 100 Mhz):  $\delta$ : 113.8, 117.2, 120.3, 125.5, 128.2, 129.5, 130.1, 133.0, 134.6, 150.8, 163.3, 167.6.

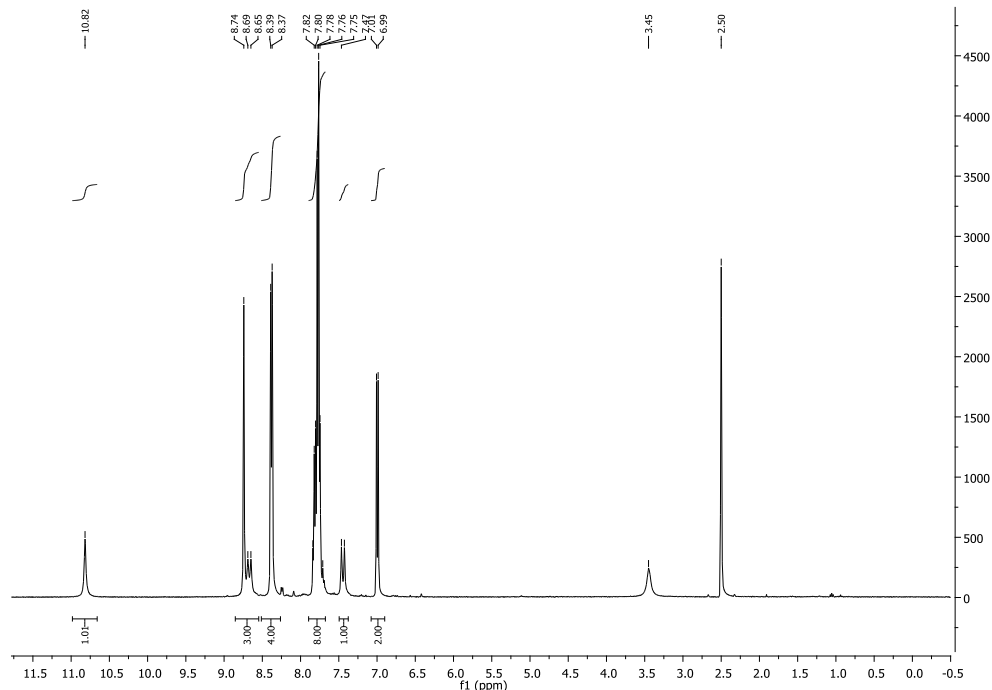


Figure SI-1  $^1\text{H-NMR-5}$

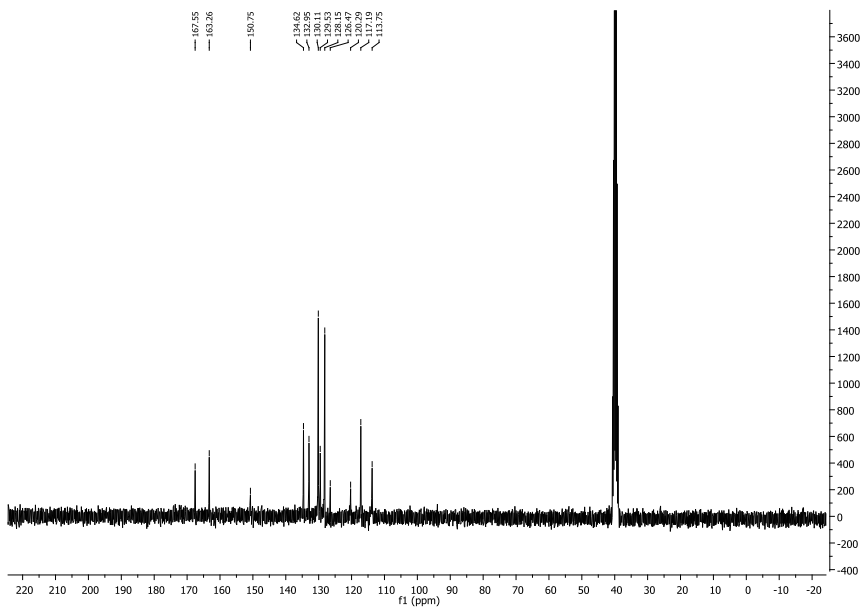


Figure SI-2  $^{13}\text{C}$ -NMR-5

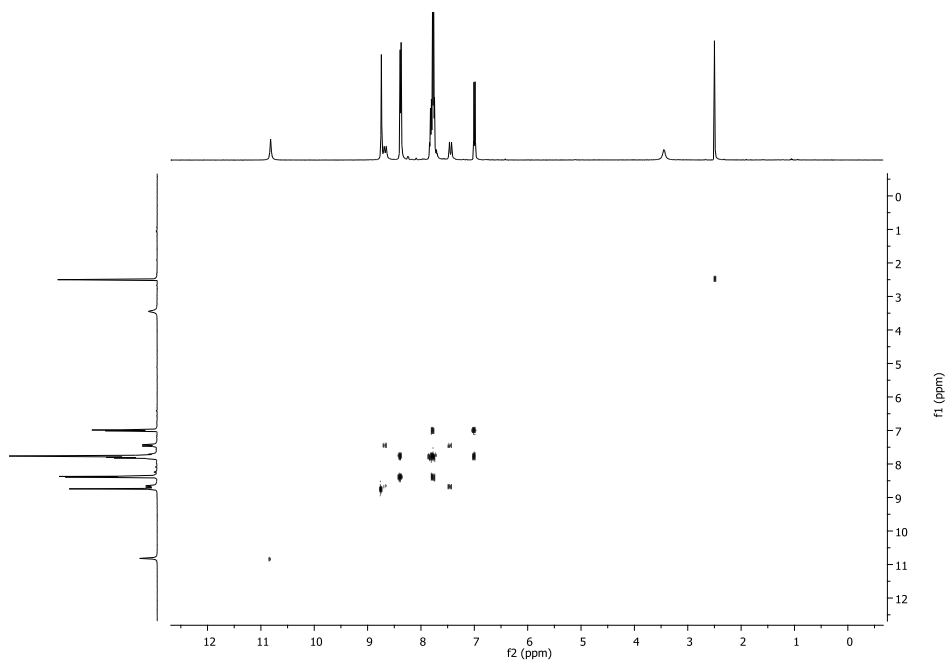


Figure SI-3 COSY-5

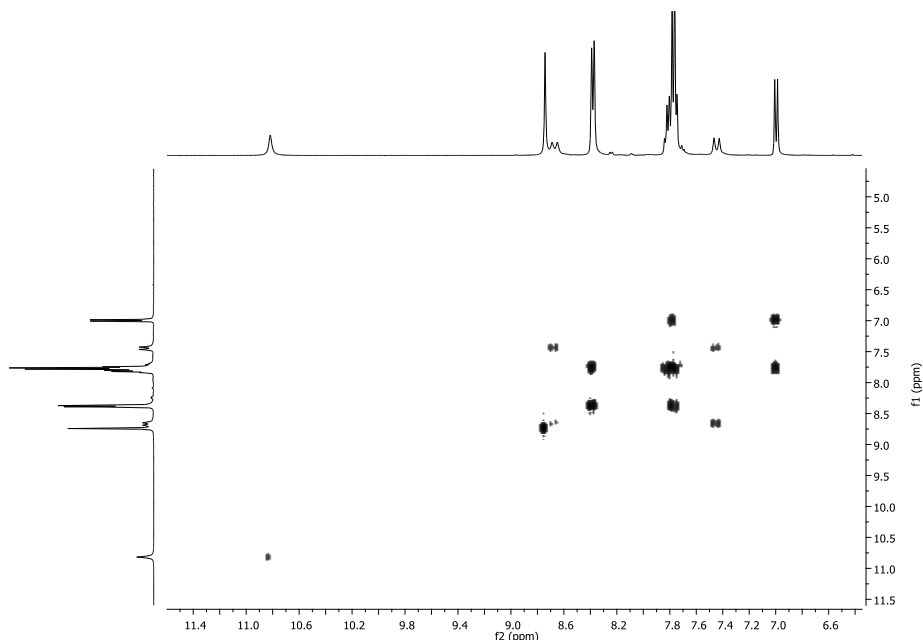


Figure SI-4 Aromatic zone COSY -5

**HRMS-EI**  $m/z$ : calcd for  $C_{25}H_{19}O_2^+$  351.1385; found: 351.1364.

#### *Deprotonation of 5 in non aqueous solvents*

An acetonitrile solution of **5** ( $2.5 \times 10^{-5}$  mol  $dm^{-3}$ ) was titrated with *N,N,N',N'*-tetramethyl-1,8-diaminonaphthalene (*proton sponge*, strong non-nucleophilic base), and the chromogenic changes were monitored. Spectra taken during the titration experiment and the corresponding titration profile are reported in figure SI-5. Chemodosimeter **5** displays a strong absorption in the 350-700 nm range of the electronic spectrum (maxima at 410 and 500 nm) that is responsible for the observed red-orange colour. Addition of increasing quantities of the non-nucleophilic base induced a progressive red-shift of the absorption bands with an intensity increase in the 500-700 nm interval (maximum at 549 nm). The titration profile determined by plotting molar absorbance at 550 nm vs equivalent ratio

(mol of *proton sponge*/mol of **5**) suggest an 1:1 stoichiometry for the process involving **5** and the base. The spectral changes were ascribed to the deprotonation of phenol moiety of **5** that yielded the quinone derivative **6** (see Scheme 1 in the manuscript). The presence of an isosbestic point (508 nm) supports the coexistence of only two species (i.e. chemodosimeter **5** and quinone **6**) at the equilibrium. Non-linear least-square treatment of spectral data by Hyperquad software package <sup>3</sup> provided a  $\log K = 7.10 \pm 0.06$  for the deprotonation equilibrium.

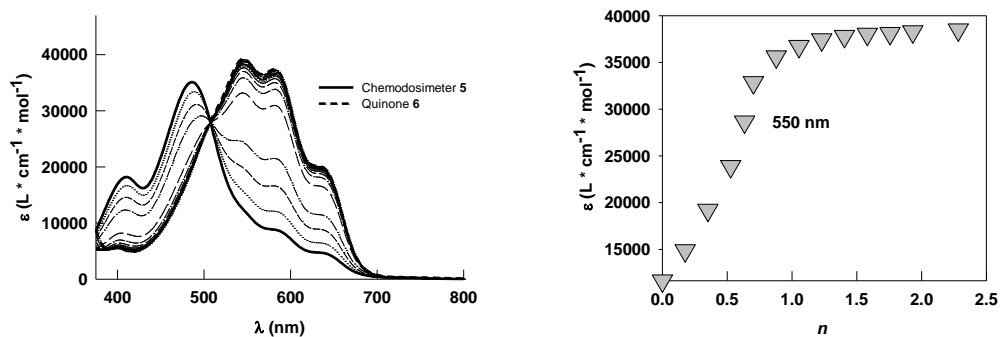


**Figure SI-5.** Family of spectra taken in the course of the titration of an acetonitrile solution of **5** ( $2.5 \times 10^{-5}$  mol dm<sup>-3</sup>) with a standard solution of proton sponge (left) and the corresponding titration profile ( $n = \text{equiv } \textit{proton\ sponge} / \text{equiv } \textbf{5}$ ) determined at 550 nm (right).

The formation of the quinone form **6**, upon deprotonation of chemodosimeter **5** with 1,8-diazabicyclo[5.4.0]undec-7-ene (DBU, non-nucleophilic base) was also assessed by <sup>1</sup>H- and <sup>13</sup>C-NMR measurements in DMSO-D<sub>6</sub> (see figure SI-6 - SI-9). <sup>1</sup>H-NMR spectrum of the product obtained upon DBU-induced deprotonation of chemodosimeter **5** is reported in figure SI-6, whereas the <sup>13</sup>C-NMR spectrum is depicted in figure SI-7.

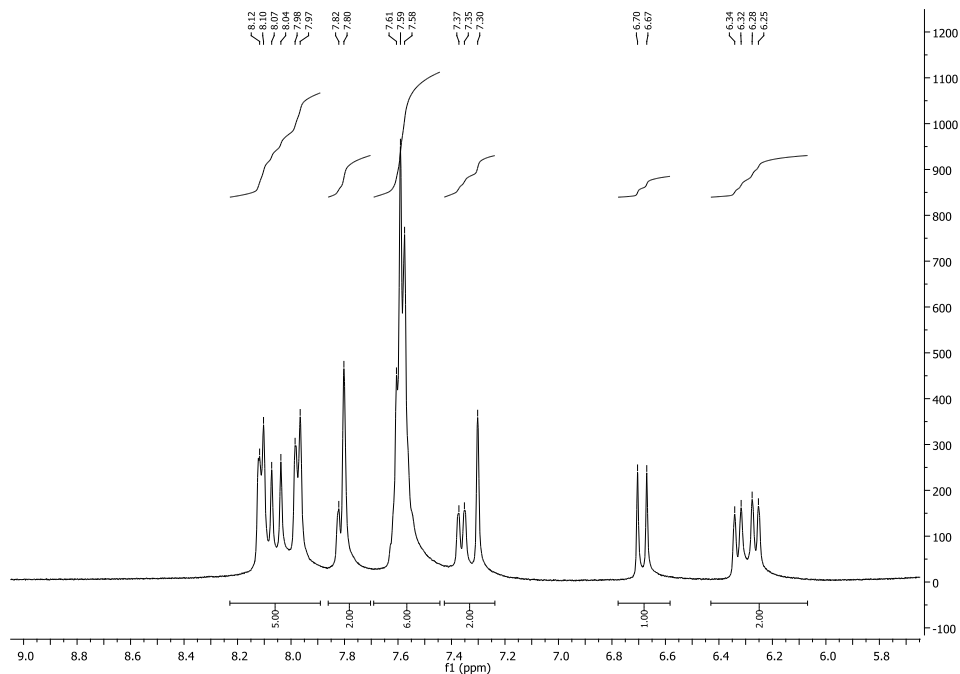


**Figure SI-6.**  $^1\text{H}$ -NMR spectra of **6** (obtained upon addition of DBU to chemodosimeter **5**) in DMSO- $\text{D}_6$ .

As could be seen in figure SI-6, the most remarkable features of the  $^1\text{H}$ -NMR spectra of quinone **6**, when compared with the spectra of chemodosimeter **5** (see figure 1 in the manuscript), are the significant upfield shifts (from 8.7 and 7.4 ppm in **5** to 8.1 and 6.7 ppm in **6**) of the signals of the double bond protons ( $\text{H}_a$  and  $\text{H}_b$ , see scheme 1 in the manuscript) together with a reduction of the coupling constant (from 16 to 12 Hz). Also, the hydroxyl proton signal centred at 10.8 ppm (see also figure 1 in the manuscript) disappeared upon addition of base.

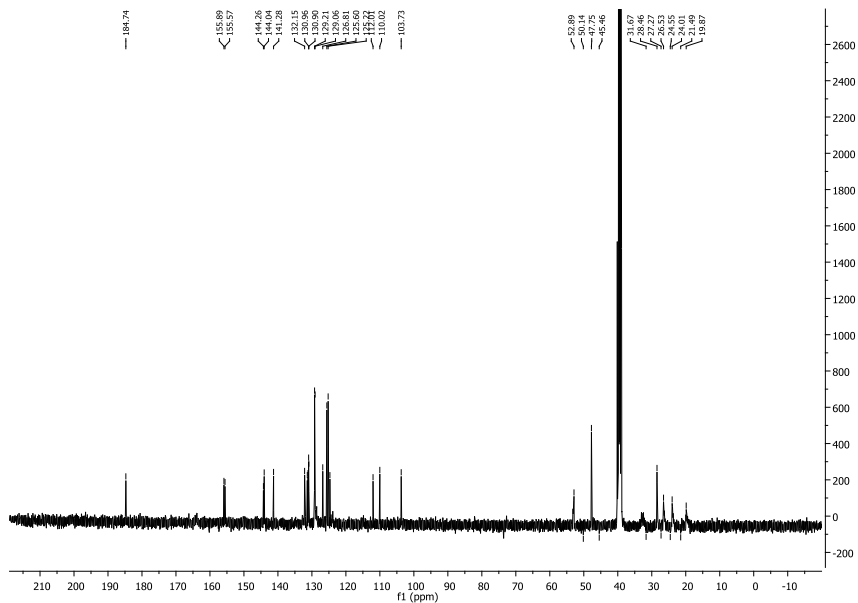


Figure SI-7.  $^{13}\text{C}$ -NMR spectra of **6** (obtained upon addition of DBU to chemodosimeter **5**) in DMSO- $\text{D}_6$ .

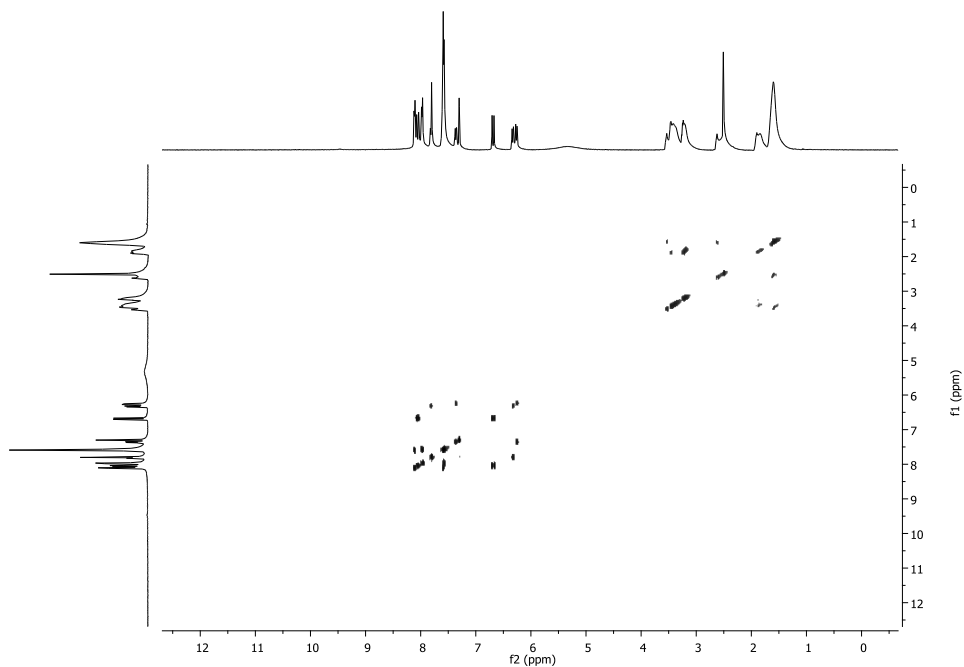
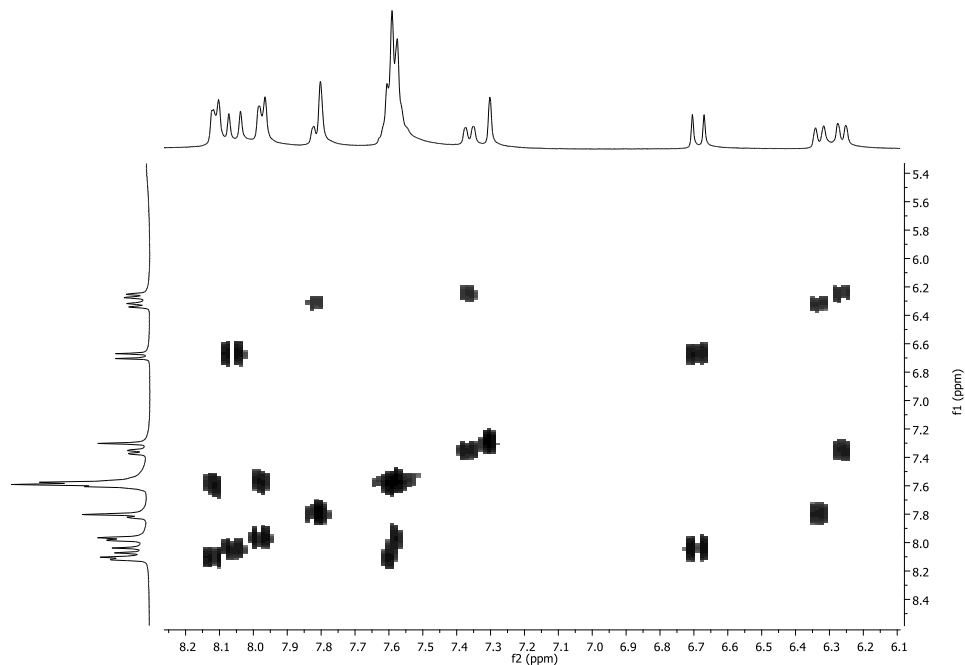


Figure SI-8. COSY-NMR spectra of **6** (obtained upon addition of DBU to chemodosimeter **5**) in DMSO- $\text{D}_6$ .



**Figure SI-9.** Aromatic zone of COSY-NMR spectra of **6** (obtained upon addition of DBU to chemodosimeter **5**) in DMSO-D<sub>6</sub>.

### *Formation of 6 in micelles proved by UV-vis measurements*

In order to assess the formation of the quinone form **6** (see Scheme 1 in the manuscript) when chemodosimeter **5** was dissolved in HEPES (30 mM, pH 7.5)-CTAB (20 mM) solutions further UV-visible measurements were carried out. As described above, addition of one equivalent of proton sponge (as well as DBU) to acetonitrile solutions of **5** ( $1.0 \times 10^{-5}$  mol dm<sup>-3</sup>) induced a change in color from orange-red to blue due to the appearance of intense absorption bands in the 500-700 nm range. The change in color and the new bands were ascribed to the quinone **6** generated by the deprotonation reaction of the phenol moiety of chemodosimeter **5** (see figure SI-10).

Figure SI-10 also shows the UV-visible spectrum of chemodosimeter **5** ( $2.5 \times 10^{-5} \text{ mol dm}^{-3}$ ) in HEPES (30 mM, pH 7.5)-CTAB (20 mM) solution. The same intense absorption bands (in the 500-700 nm interval) obtained upon treatment of acetonitrile solutions of **5** with DBU were observed in aqueous environment.

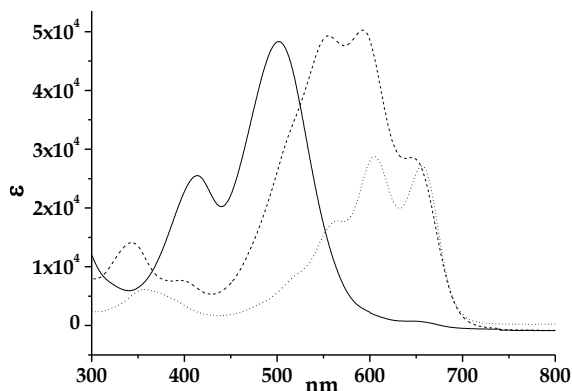


**Figure SI-10.** UV-visible spectra of chemodosimeter **5** ( $1.0 \times 10^{-5} \text{ mol dm}^{-3}$ ) in acetonitrile (filled line), **5** upon addition of one equivalent of DBU (dashed line) and **5** ( $2.5 \times 10^{-5} \text{ mol dm}^{-3}$ ) dissolved in HEPES-CTAB solution (dotted line).

This suggests that inclusion of chemodosimeter **5** into the hydrophobic environment in the inner of the CTAB micelles induced the deprotonation of the phenol moiety with the subsequent stabilization of the less polar quinone **6**.

### ***Mechanism of the chromo-fluorogenic response in the presence of GSH***

The mechanism of the chromo-fluorogenic response was studied by means of NMR measurements with quinone **6** (generated upon addition of DBU or *proton sponge* to chemodosimeter **5**) and GSH in DMSO-D<sub>6</sub>. The high complexity of the spectra obtained upon reaction of GSH with quinone **6** suggested us the use of a simple thiol derivative (such as 2-mercaptoethanol) in order to determine the mechanism of the observed

response.  $^1\text{H}$  (figure SI-11), COSY (figure SI-12), DEPT (figure SI-13), sel-TOCSY (figure SI-14) and HSQC (figure SI-15) NMR measurements were carried out, in order to characterize the addition product of 2-mercaptoethanol to **6**.

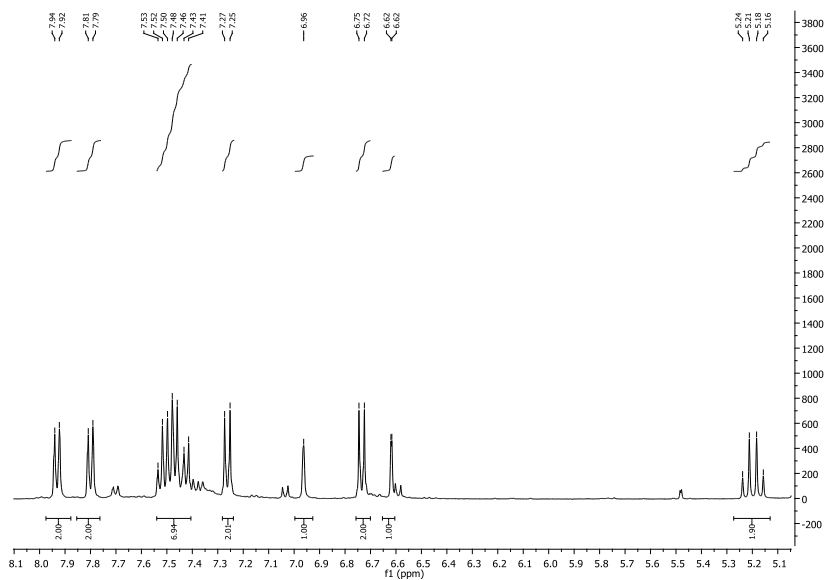


**Figure SI-11.** Aromatic part of the  $^1\text{H}$ -NMR spectra of the addition product of 2-mercaptoethanol to **6** in DMSO- $D_6$ .

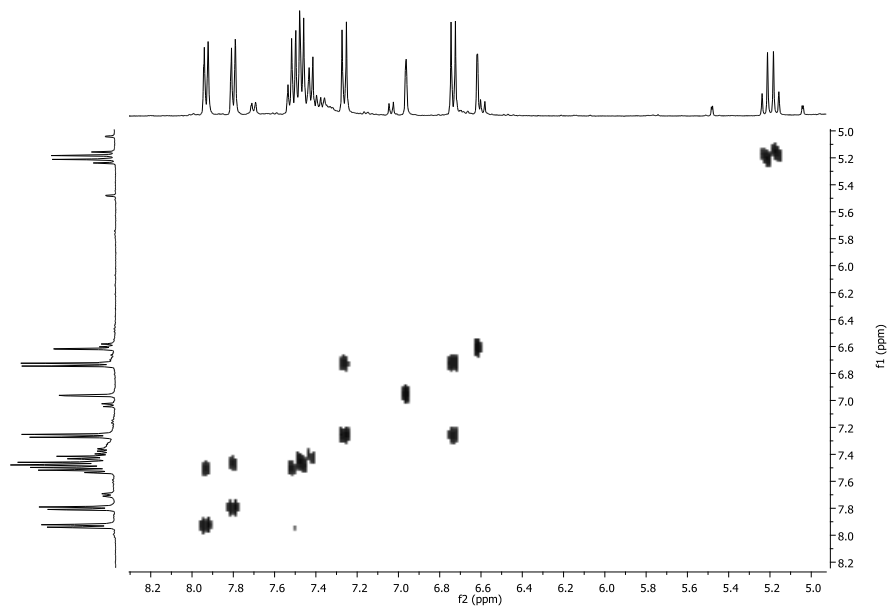


Figure SI-12. COSY spectra of the addition product of 2-mercaptoethanol to **6** in DMSO-D<sub>6</sub>.

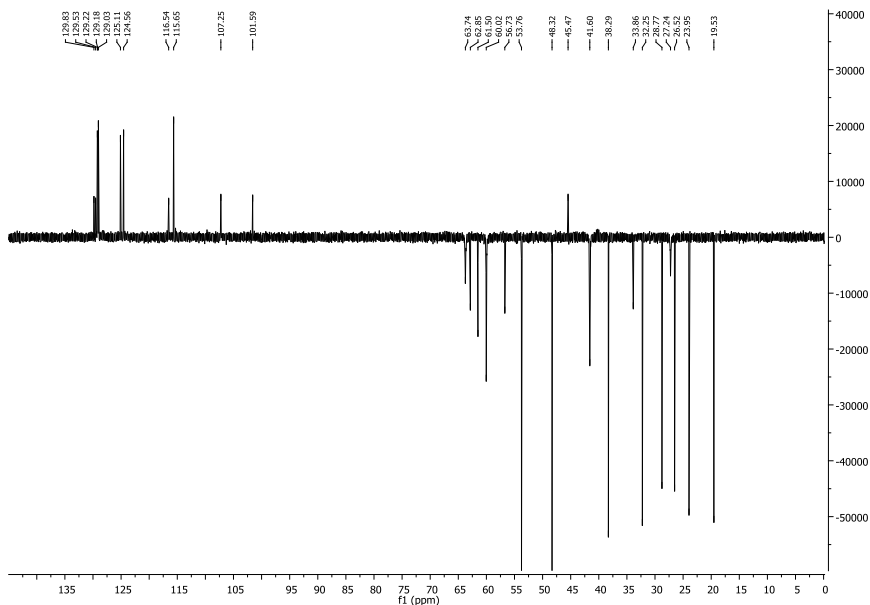


Figure SI-13. DEPT spectra of the addition product of 2-mercaptoethanol to **6** in DMSO-D<sub>6</sub>.

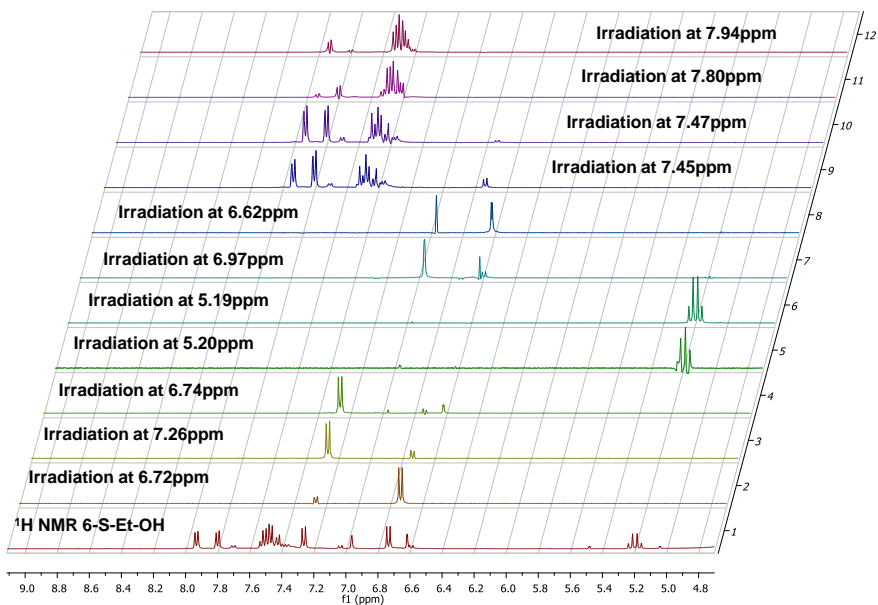


Figure SI-14. sel-TOCSY spectra of the addition product of 2-mercaptoethanol to **6** in DMSO-D<sub>6</sub>.

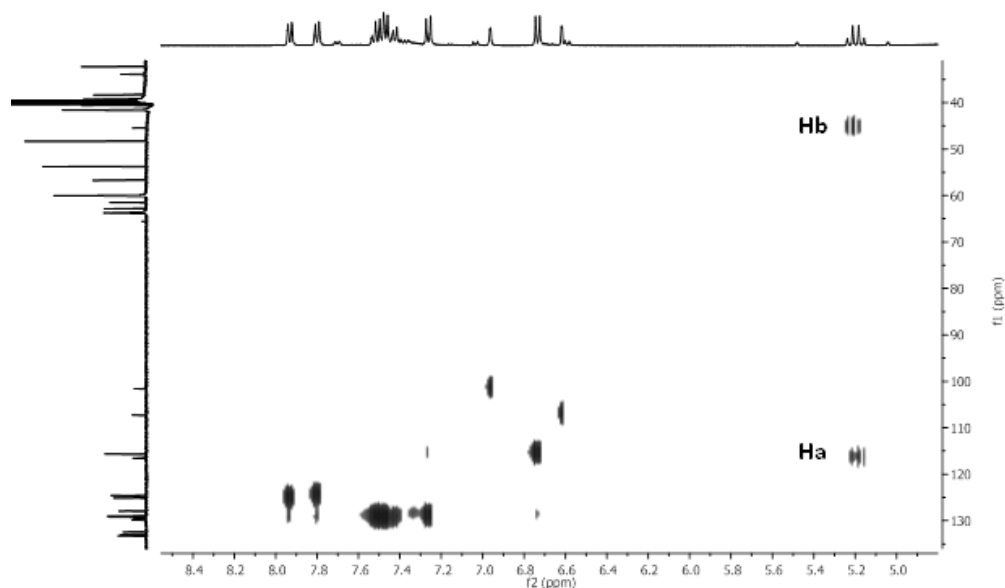


Figure SI-15. HSQC spectra of the addition product of 2-mercaptoethanol to 6 in DMSO-D6.

HSCQ experiment resulted the most remarkable of all the NMR measurements carried out to elucidate the chromo-fluorogenic mechanism and to identify the final product of the reaction involving quinone 6 and 2-mercaptoethanol.

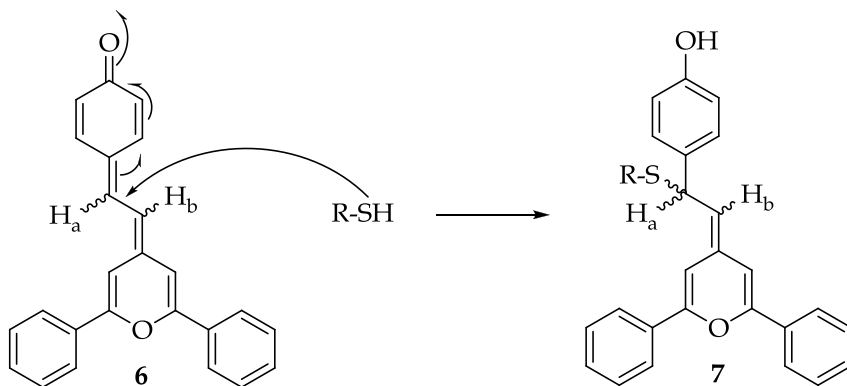


Figure SI-16. Mechanism of the 1,6-conjugated addition of thiol-containing biomolecules to chemosdosimeter 6.

HSQC spectra (figure SI-15) of the reaction product clearly indicated the existence of a correlation between H<sub>b</sub> proton (see figure SI-15 and figure SI-16) and a benzylic carbon (at ca. 45 ppm) and also between H<sub>a</sub> proton and an olefinic carbon (at ca. 116 ppm). These correlations clearly pointed to a thiol 1,6-conjugated addition that yielded product **7** (see also figure SI-16). Moreover, we were able to isolate the final product of the reaction between **6** and GSH and results of HRMS measurement supported the formation of derivative **7**.

### *Determination of GSH in plasma*

GSH was determined in artificial human plasma by a standard addition method. The artificial plasma was prepared according to a well established protocol. Then the plasma was doped with conventional quantity of biothiols (Cys: 178.4 μM; Hcy: 5.9 μM and GSH: 6.3 μM). Then, 20 μl of the obtained plasma were added to 2.7 mL of chemodosimeter **6** ( $2.5 \times 10^{-4}$  M) in water-CTAB (20 mM). A standard addition method was carried out by measuring the emission of the solution of chemodosimeter **6** in the presence of increasing concentrations of GSH ( $2.5 \cdot 10^{-6}$  to  $1.75 \cdot 10^{-5}$  M range). The determined GSH concentration in artificial plasma was 5.92 μM, with a calculated recovery of 94%, demonstrating that Hcy and Cys do not interfere in the measurement.

### *X-ray crystallographic study*

Diffraction data for a blue crystal (dimensions of about 0.50 x 0.42 x 0.30 mm) of **5**(NO<sub>3</sub>) have been collected at ambient temperature by means of an Enraf-Nonius CAD4 four circle diffractometer equipped with a punctual detector (scintillation counter). **5**(BF<sub>4</sub>) forms only small single crystals and

diffraction data for a blue crystal (dimensions of about 0.15 x 0.12 x 0.08 mm) have been collected at ambient temperature by means of a Bruker-Axs CCD-based diffractometer. Both diffractometers work with graphite-monochromatized MoK $\alpha$  X-radiation ( $\lambda = 0.71073 \text{ \AA}$ ). Crystal data for the two molecular complexes are shown in Table SI-1.

Data reductions (including intensity integration, background, Lorentz and polarization corrections) for intensities collected with the conventional diffractometer were performed with the WinGX package; <sup>4</sup> absorption correction was not applied to the data. Frames collected by the CCD-based system were processed with the SAINT software <sup>5</sup> and intensities were corrected for Lorentz and polarization effects; absorption effects were empirically evaluated by the SADABS software <sup>6</sup> and absorption correction was applied to the data (min./max. transmission factors were 0.806/0.992).

Both crystal structures were solved by direct methods (SIR 97) <sup>7</sup> and refined by full-matrix least-square procedures on  $F^2$  using all reflections (SHELXL 97). <sup>8</sup> Anisotropic displacement parameters were refined for all non-hydrogen atoms.

**Table SI-1.** Crystal data for investigated crystals.

	5(NO <sub>3</sub> )	5(BF <sub>4</sub> )
<i>Formula</i>	C <sub>25</sub> H <sub>19</sub> O <sub>5</sub> N	C <sub>25</sub> H <sub>19</sub> O <sub>2</sub> F <sub>4</sub> B
<i>M</i>	413.41	438.21
<i>Crystal system</i>	triclinic	triclinic
<i>Space group</i>	<i>P</i> -1 (no. 2)	<i>P</i> -1 (no. 2)
<i>a</i> [Å]	8.846(2)	9.458(5)
<i>b</i> [Å]	10.208(3)	10.250(5)
<i>c</i> [Å]	12.644(3)	11.558(5)
<i>a</i> [°]	69.56(2)	83.424(5)
$\beta$ [°]	84.07(2)	76.519(5)
$\gamma$ [°]	73.221(19)	77.504(5)
<i>V</i> [Å <sup>3</sup> ]	1024.3(4)	1061.4(9)
<i>Z</i>	2	2

## Supporting Information

Temperature (K)	293	293
$\rho_{\text{calcd}}$ [ $\text{g cm}^{-3}$ ]	1.340	1.371
$\mu$ Mo $K_{\alpha}$ [ $\text{mm}^{-1}$ ]	0.094	0.109
Scan type	$\Omega$ scans	$\Omega$ scans
$\theta$ range [ $^{\circ}$ ]	2 – 25	2 – 25
Measured reflections	3795	11021
Unique reflections	3606	3779
$R_{\text{int}}$	0.0295	0.0319
Strong data [ $I_0 > 2\sigma(I_0)$ ]	2253	2242
Refined parameters	280	319
$R1$ , $wR2$ (strong data)	0.0849, 0.1377	0.0594, 0.0982
$R1$ , $wR2$ (all data)	0.1573, 0.1930	0.1577, 0.1941
GOF	1.130	1.021
Max/min residuals [ $e\text{\AA}^{-3}$ ]	0.387 / -0.315	0.224 / -0.216

Hydrogen atoms were placed at calculated positions with the appropriate AFIX instructions and refined using a riding model. CCDC 922786 and 922787 contain the supplementary crystallographic data for this paper. These data can be obtained free of charge via [www.ccdc.cam.ac.uk/conts/retrieving.html](http://www.ccdc.cam.ac.uk/conts/retrieving.html) (or from the Cambridge Crystallographic Data Centre, 12 Union Road, Cambridge CB21EZ, UK; fax: (+44) 1223-336-033; or e-mail: [deposit@ccdc.cam.ac.uk](mailto:deposit@ccdc.cam.ac.uk)).

The compound **5**(NO<sub>3</sub>) crystallizes in the triclinic space group *P*-1 and the asymmetric unit is composed by one **5** ion and one NO<sub>3</sub><sup>-</sup> counterion. ORTEP view of **5**(NO<sub>3</sub>) is reported in Figure SI-17. Pyrylium ring is coplanar with the hydroxystyryl group and one phenyl ring: the relative dihedral angles are 3.90° and 0.96°. The remaining phenyl ring forms a dihedral angle respect with the pyrylium group of 22.81°.

The flat aromatic groups favour the creation of face-to-face  $\pi$ -interactions. The  $\pi$ -stacked molecules form column having a zig-zag style show in figure SI-18. The shortest centroid-centroid distances occur

between the pyrylium ring and the phenolic ring of an overlying **5** ion. Longer distances occur between pyrylium ring and the phenyl ring of an underlying **5** ion. The non-coplanar phenyl ring is not involved in supramolecular  $\pi$ -interactions.

The hydroxyl group acts as H-donor towards the nitrate counterion. The bifurcated O-H $\cdots$ O H-bond involves as H-acceptor two O atoms of the same NO<sub>3</sub> group. The remaining O<sub>nitrate</sub> atom profits of three very weak C-H $\cdots$ O H-bonds having as H-donor species two CH groups of the aromatic rings and a CH of the olefinic C=C group. The H-bond motif originates the supramolecular dimer shown in figure SI-19. Geometrical features of the H-bond are reported in Table SI-2. Tables SI-3, SI-4 and SI-5 showed selected distances and angles for **5**(NO<sub>3</sub>).

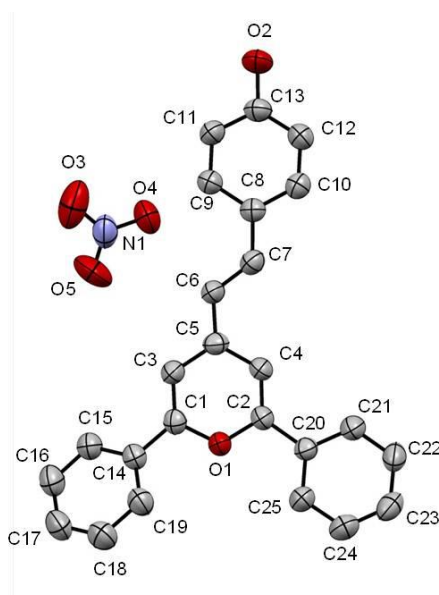


**Figure SI-17.** ORTEP view of the complex **5**(NO<sub>3</sub>) (ellipsoids are drawn at the 50% probability level).

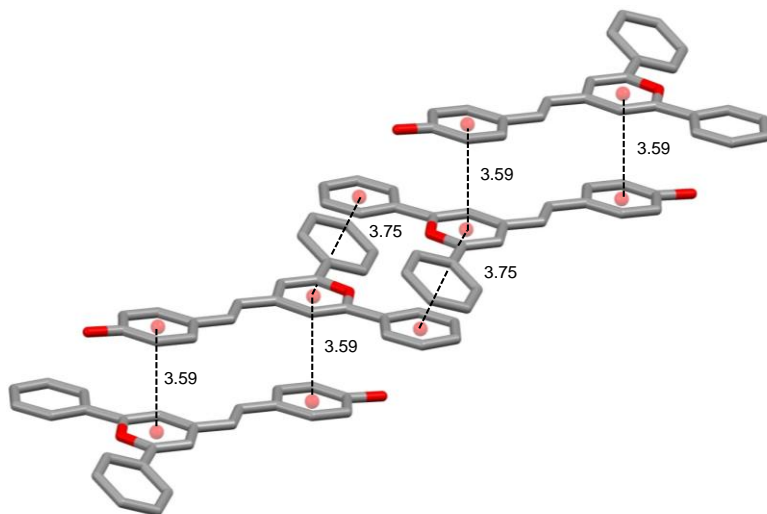


Figure SI-18. A simplified view of the  $\pi$ -stacked  $5(\text{NO}_3)$

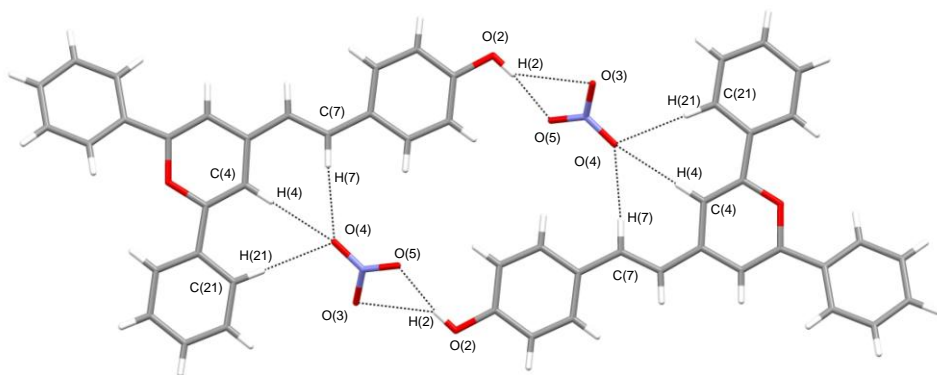


Figure SI-19. A simplified view of the H-bond-dimer  $5(\text{NO}_3)$

Table SI-2. Geometrical features of hydrogen bonds distance in  $5(\text{NO}_3)$

Donor group (D)	$D \cdots A$ (Å)	$H \cdots A$ (Å)	$D-H \cdots A$ (°)	Acceptor atom (A)
O(2)-H(2O)	3.191(1)	2.511(1)	141.12(1)	O(3) <sub>NO3-</sub>
O(2)-H(2O)	2.769(1)	1.986(1)	159.43(1)	O(5) <sub>NO3-</sub>
C(21)-H(21C)	3.777(1)	3.016(1)	158.85(1)	O(4) <sub>NO3-</sub>
C(4)-H(4C)	3.300(1)	2.405(1)	161.46(1)	O(4) <sub>NO3-</sub>
C(7)-H(7C)	3.375(1)	2.479(1)	161.90(1)	O(4) <sub>NO3-</sub>

Table SI-3.  $\pi$ - $\pi$  bonds distance ( $\text{\AA}$ ) for 5( $\text{NO}_3$ )

<i>donor (D)</i>	<i>D...A</i>
C(5)-C(8)	3.564
C(4)-C(8)	3.480
C(4)-C(9)	3.564
C(2)-C(11)	3.568
O(1)-C(13)	3.638
C(1)-C(12)	3.659
C(3)-C(10)	3.627
C(7)-C(7)	3.377
C(7)-C(6)	3.575
C(1)-C(23)	3.397
C(9)-C(9)	3.310
O(1)-C(24)	3.606
O(1)-C(20)	3.676
O(1)-C(25)	3.582
C(2)-C(25)	3.446
O(2)-C(21)	3.766
C(1)-C(22)	3.680
C(2)-C(20)	3.842
C(4)-C(25)	3.822
C(5)-C(24)	3.767
C(3)-C(23)	3.665
C(24)-C(24)	3.367
Centroid O(1)-C(5) – centroid C(8)-C(13)	3.594
Centroid O(1)-C(5) – centroid C(20)-C(25)	3.753
Centroid O(6)-C(7) – centroid C(6)-C(7)	3.575

Table SI-4. Distances bond ( $\text{\AA}$ ) for 5( $\text{NO}_3$ )

C1	C3	1.361(5)
C1	O1	1.362(4)
C1	C14	1.458(5)
C2	C4	1.349(5)
C2	O1	1.354(4)
C2	C20	1.466(5)
C3	C5	1.406(5)
C3	H3	0.9300

Supporting Information

C4	C5	1.413(5)
C4	H4	0.9300
C5	C6	1.429(5)
C6	C7	1.344(5)
C6	H6	0.9300
C7	C8	1.448(5)
C7	H7	0.9300
C8	C9	1.396(5)
C8	C10	1.398(5)
C9	C11	1.376(5)
C9	H9	0.9300
C10	C12	1.372(6)
C10	H10	0.9300
C11	C13	1.392(6)
C11	H11	0.9300
C12	C13	1.375(6)
C12	H12	0.9300
C13	O2	1.357(5)
C14	C19	1.386(6)
C14	C15	1.390(6)
C15	C16	1.377(6)
C15	H15	0.9300
C16	C17	1.374(7)
C16	H16	0.9300
C17	C18	1.363(7)
C17	H17	0.9300
C18	C19	1.384(6)
C18	H18	0.9300
C19	H19	0.9300
C20	C25	1.387(5)
C20	C21	1.392(6)
C21	C22	1.385(6)
C21	H21	0.9300
C22	C23	1.367(6)
C22	H22	0.9300
C23	C24	1.368(6)
C23	H23	0.9300
C24	C25	1.383(6)

C24	H24	0.9300
C25	H25	0.9300
O2	H2O	0.8200
N1	O4	1.208(5)
N1	O5	1.207(6)
N1	O3	1.243(6)

Table SI-5. Angles 5(NO<sub>3</sub>)

C3	C1	O1	119.7(4)
C3	C1	C14	128.2(4)
O1	C1	C14	112.1(3)
C4	C2	O1	120.0(4)
C4	C2	C20	127.4(4)
O1	C2	C20	112.6(3)
C1	C3	C5	121.2(4)
C1	C3	H3	119.4
C5	C3	H3	119.4
C2	C4	C5	121.5(4)
C2	C4	H4	119.2
C5	C4	H4	119.2
C3	C5	C4	116.2(4)
C3	C5	C6	120.6(4)
C4	C5	C6	123.2(4)
C7	C6	C5	124.1(4)
C7	C6	H6	117.9
C5	C6	H6	117.9
C6	C7	C8	127.7(4)
C6	C7	H7	116.1
C8	C7	H7	116.1
C9	C8	C10	117.5(4)
C9	C8	C7	123.3(4)
C10	C8	C7	119.2(4)
C11	C9	C8	121.2(4)
C11	C9	H9	119.4
C8	C9	H9	119.4
C12	C10	C8	121.9(4)
C12	C10	H10	119.1
C8	C10	H10	119.1

Supporting Information

C9	C11	C13	119.7(4)
C9	C11	H11	120.1
C13	C11	H11	120.1
C10	C12	C13	119.6(4)
C10	C12	H12	120.2
C13	C12	H12	120.2
O2	C13	C12	123.3(4)
O2	C13	C11	116.5(4)
C12	C13	C11	120.2(4)
C19	C14	C15	119.0(4)
C19	C14	C1	120.9(4)
C15	C14	C1	120.0(4)
C16	C15	C14	120.1(4)
C16	C15	H15	119.9
C14	C15	H15	119.9
C17	C16	C15	120.1(5)
C17	C16	H16	119.9
C15	C16	H16	119.9
C18	C17	C16	120.4(5)
C18	C17	H17	119.8
C16	C17	H17	119.8
C17	C18	C19	120.2(5)
C17	C18	H18	119.9
C19	C18	H18	119.9
C18	C19	C14	120.1(5)
C18	C19	H19	120.0
C14	C19	H19	120.0
C25	C20	C21	118.9(4)
C25	C20	C2	121.3(4)
C21	C20	C2	119.8(4)
C22	C21	C20	120.0(4)
C22	C21	H21	120.0
C20	C21	H21	120.0
C23	C22	C21	120.5(4)
C23	C22	H22	119.8
C21	C22	H22	119.8
C22	C23	C24	119.9(4)
C22	C23	H23	120.1

C24	C23	H23	120.1
C23	C24	C25	120.8(4)
C23	C24	H24	119.6
C25	C24	H24	119.6
C24	C25	C20	119.9(4)
C24	C25	H25	120.0
C20	C25	H25	120.0
C2	O1	C1	121.4(3)
C13	O2	H2O	109.5
O4	N1	O5	121.5(5)
O4	N1	O3	119.0(5)
O5	N1	O3	119.5(5)

Compound **5**(BF<sub>4</sub>) crystallizes in the triclinic space group *P*-1 and the asymmetric unit is composed by one molecule of **5** ion and one BF<sub>4</sub><sup>-</sup> counterion (see Figure SI-20).

**5** ion shows coplanarity between the pyrylium, the hydroxystyryl group and one phenyl ring: the relative dihedral angle are 4.81° and 3.86°. The remaining phenyl ring forms a dihedral angle of 18.61° with the pyrylium group.

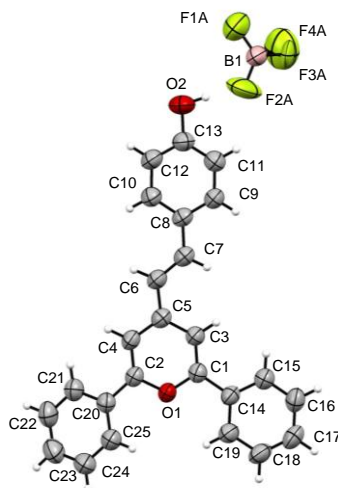


**Figure SI-20.** ORTEP view of the complex **5**(BF<sub>4</sub>) (ellipsoids are drawn at the 50% probability level)

The hydroxyl group acts as H-donor towards the  $\text{BF}_4^-$  counterion and originates a single  $\text{O-H}\cdots\text{F}$  H-bond. Further  $\text{C-H}\cdots\text{F}$  H-bonds can be observed at the solid state: in particular the H-donor C-H groups are both aromatic and olefinic carbons of the ligand moiety. The H-bond motif originates the supramolecular dimer shown in figure SI-21. Geometrical features of the H-bond are reported in Table SI-6. Selected bond distances and angles are shown in Tables SI-7, SI-8 and SI-9.

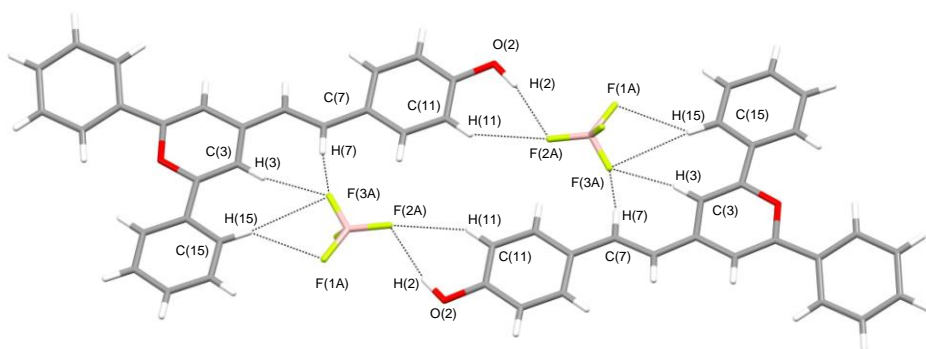


**Figure SI-21.** A simplified view of the H-bond dimer occurring in the crystal of  $5(\text{BF}_4)^-$

Also in this case the flat aromatic groups favor the creation of face-to-face  $\pi$ -interactions originating  $\pi$ -stacked columns of molecules (figure SI-22). The shortest centroid-centroid distance occurs between the pyrylium ring and the phenyl ring of an overlying **5** moiety.

Longer distance occurs between pyrylium ring and the phenolic ring of an underlying **5** ion. The not-coplanar phenyl ring is not involved in supramolecular  $\pi$ -interactions.

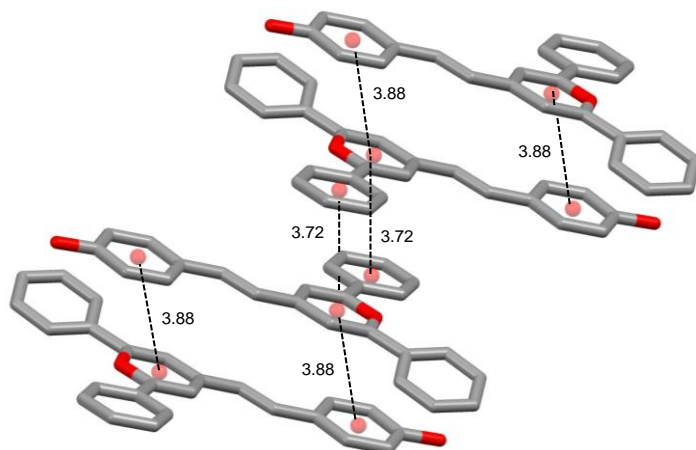


**Figure SI-22.** A simplified view of the  $\pi$ -stacked molecules occurring in the crystal of  $5(\text{BF}_4)$

**Table SI-6.** Geometrical features for hydrogen bonds in  $5(\text{BF}_4)$

Donor group (D)	$D \cdots A$ (Å)	$H \cdots A$ (Å)	$D-H \cdots A$ (°)	acceptor atom(A)
O(2)-H(2O)	2.860(1)	1.971(1)	154.41(1)	F(2A) <sub>BF4</sub>
C(11)-H(11C)	3.238(1)	2.575(1)	128.63(1)	F(2A) <sub>BF4</sub>
C(15)-H(15C)	3.336(1)	2.634(1)	132.73(1)	F(1A) <sub>BF4</sub>
C(15)-H(15C)	3.585(1)	2.663(1)	171.44(1)	F(3A) <sub>BF4</sub>
C(3)-H(3C)	3.406(1)	2.499(1)	164.92(1)	F(3A) <sub>BF4</sub>
C(7)-H(7C)	3.310(1)	2.438(1)	155.92(1)	F(3A) <sub>BF4</sub>

**Table SI-7.**  $\pi$ - $\pi$  bonds distance (Å) for  $5(\text{BF}_4)$

donor (D)	$D \cdots A$
C(1)-C(15)	3.448
O(1)-C(15)	3.716
C(3)-C(15)	3.724
C(3)-C(14)	3.744
C(3)-C(19)	3.668
C(5)-C(18)	3.692
C(5)-C(17)	3.347
C(5)-C(16)	3.650
C(4)-C(16)	3.728
C(2)-C(16)	3.795
Centroid O(1)-C(5) – centroid C(14)-C(19)	3.713

**Table SI-8.** Distances bond (Å) for 5(BF<sub>4</sub>)

C1	O1	1.355(3)
C1	C3	1.360(3)
C1	C14	1.466(3)
C2	O1	1.350(3)
C2	C4	1.360(3)
C2	C20	1.460(3)
C3	C5	1.405(3)
C3	H3	0.9300
C4	C5	1.406(3)
C4	H4	0.9300
C5	C6	1.437(3)
C6	C7	1.343(4)
C6	H6	0.9300
C7	C8	1.442(3)
C7	H7	0.9300
C8	C10	1.389(3)
C8	C9	1.392(4)
C9	C11	1.372(4)
C9	H9	0.9300
C10	C12	1.371(4)
C10	H10	0.9300
C11	C13	1.372(4)
C11	H11	0.9300
C12	C13	1.379(4)
C12	H12	0.9300
C13	O2	1.353(3)
C14	C19	1.387(3)
C14	C15	1.395(3)
C15	C16	1.373(4)
C15	H15	0.9300
C16	C17	1.368(4)
C16	H16	0.9300
C17	C18	1.372(4)
C17	H17	0.9300
C18	C19	1.375(4)
C18	H18	0.9300
C19	H19	0.9300

C20	C25	1.382(4)
C20	C21	1.394(4)
C21	C22	1.373(4)
C21	H21	0.9300
C22	C23	1.370(4)
C22	H22	0.9300
C23	C24	1.368(4)
C23	H23	0.9300
C24	C25	1.380(4)
C24	H24	0.9300
C25	H25	0.9300
O2	H2O	0.949(10)
B1	F3A	1.231(8)
B1	F2A	1.270(8)
B1	F3B	1.300(10)
B1	F1A	1.313(4)
B1	F2B	1.353(8)
B1	F4B	1.404(12)
B1	F4A	1.432(8)
F2A	F4B	1.022(16)
F2A	F2B	1.282(13)
F3A	F3B	0.61(2)
F3A	F4A	1.564(13)
F4A	F2B	1.455(10)

Table SI-9. Angles for 5(BF<sub>4</sub>)

O1	C1	C3	119.7(2)
O1	C1	C14	112.9(2)
C3	C1	C14	127.5(2)
O1	C2	C4	119.8(2)
O1	C2	C20	112.7(2)
C4	C2	C20	127.4(2)
C1	C3	C5	120.9(2)
C1	C3	H3	119.6
C5	C3	H3	119.6
C2	C4	C5	120.8(2)
C2	C4	H4	119.6
C5	C4	H4	119.6

Supporting Information

C3	C5	C4	116.9(2)
C3	C5	C6	123.3(2)
C4	C5	C6	119.8(2)
C7	C6	C5	124.3(2)
C7	C6	H6	117.9
C5	C6	H6	117.9
C6	C7	C8	128.1(2)
C6	C7	H7	116.0
C8	C7	H7	116.0
C10	C8	C9	117.4(2)
C10	C8	C7	123.9(2)
C9	C8	C7	118.8(2)
C11	C9	C8	121.7(2)
C11	C9	H9	119.2
C8	C9	H9	119.2
C12	C10	C8	121.2(3)
C12	C10	H10	119.4
C8	C10	H10	119.4
C9	C11	C13	119.7(3)
C9	C11	H11	120.1
C13	C11	H11	120.1
C10	C12	C13	120.1(3)
C10	C12	H12	119.9
C13	C12	H12	119.9
O2	C13	C11	123.1(3)
O2	C13	C12	117.0(3)
C11	C13	C12	119.9(3)
C19	C14	C15	118.7(2)
C19	C14	C1	121.5(2)
C15	C14	C1	119.9(2)
C16	C15	C14	120.2(3)
C16	C15	H15	119.9
C14	C15	H15	119.9
C17	C16	C15	120.6(3)
C17	C16	H16	119.7
C15	C16	H16	119.7
C16	C17	C18	119.7(3)
C16	C17	H17	120.2

C18	C17	H17	120.2
C17	C18	C19	120.7(3)
C17	C18	H18	119.6
C19	C18	H18	119.6
C18	C19	C14	120.1(3)
C18	C19	H19	120.0
C14	C19	H19	120.0
C25	C20	C21	119.3(2)
C25	C20	C2	121.3(2)
C21	C20	C2	119.3(2)
C22	C21	C20	119.9(3)
C22	C21	H21	120.1
C20	C21	H21	120.1
C23	C22	C21	120.5(3)
C23	C22	H22	119.8
C21	C22	H22	119.8
C24	C23	C22	120.1(3)
C24	C23	H23	120.0
C22	C23	H23	120.0
C23	C24	C25	120.4(3)
C23	C24	H24	119.8
C25	C24	H24	119.8
C24	C25	C20	119.9(3)
C24	C25	H25	120.1
C20	C25	H25	120.1
C2	O1	C1	121.82(19)
C13	O2	H2O	106(2)
F3A	B1	F2A	114.6(7)
F3A	B1	F3B	27.9(9)
F2A	B1	F3B	108.7(9)
F3A	B1	F1A	118.8(5)
F2A	B1	F1A	123.8(6)
F3B	B1	F1A	110.0(7)
F3A	B1	F2B	122.2(8)
F2A	B1	F2B	58.4(6)
F3B	B1	F2B	144.6(8)
F1A	B1	F2B	103.4(6)
F3A	B1	F4B	112.1(9)

## Supporting Information

F2A	B1	F4B	44.6(7)
F3B	B1	F4B	88.6(10)
F1A	B1	F4B	97.9(6)
F2B	B1	F4B	98.0(7)
F3A	B1	F4A	71.5(6)
F2A	B1	F4A	111.5(9)
F3B	B1	F4A	99.0(7)
F1A	B1	F4A	100.7(5)
F2B	B1	F4A	62.9(5)
F4B	B1	F4A	155.9(7)
F4B	F2A	B1	74.6(9)
F4B	F2A	F2B	128.8(15)
B1	F2A	F2B	64.0(6)
F3B	F3A	B1	82.3(13)
F3B	F3A	F4A	141.5(15)
B1	F3A	F4A	60.3(6)
B1	F4A	F2B	55.9(4)
B1	F4A	F3A	48.3(4)
F2B	F4A	F3A	97.0(6)
F2A	F2B	B1	57.5(5)
F2A	F2B	F4A	109.4(8)
B1	F2B	F4A	61.2(5)
F3A	F3B	B1	69.8(15)
F2A	F4B	B1	60.7(9)

## *Supporting Information Bibliography*

- 1 (a) R. Wizinger, P. Ulrich, *Helv. Chim. Acta*, **1956**, 39, 207; (b) D. Markovitsi, C. Jallabert, H. Strzelecka, M. Veber, *J. Chem. Soc., Faraday Trans.*, **1990**, 86, 2819.
- 2 K. L. Hoffman, G. Maas, M. Regitz, *J. Org. Chem.*, **1987**, 52, 3851.
- 3 Gans, A. Sabatini and A. Vacca, *Talanta*, **1996**, 43, 1739;  
<http://www.hyperquad.co.uk/index.htm>
- 4 L.J. Farrugia, *J. Appl. Crystallogr.* **1999**, 32, 837-838.

- 5 Bruker. SAINT Software Reference Manual. Version 6. Bruker AXS Inc., Madison, Wisconsin, USA, **2003**.
- 6 G.M. Sheldrick. SADABS Siemens Area Detector Absorption Correction Program. University of Göttingen, Göttingen, Germany, **1996**.
- 7 A. Altomare, M.C. Burla, M. Camalli, G.L. Cascarano, C. Giacovazzo, A. Guagliardi, A.G.G. Moliterni, G. Polidori, R. Spagna, J. Appl. Crystallogr. **1999**, 32, 115-119
- 8 G.M. Sheldrick, Acta Crystallogr. **2008**, A64,112-122.



***Chapter 5:***  
***Controlled Delivery Systems***



## ***5.1 Introduction***

This chapter of this PhD thesis focuses on the synthesis, characterization and final application of organic-inorganic nanoscopic mesoporous hybrid materials for controlled delivery. In the next sections the synthesis, characterization techniques and main features of silica-based materials will be reported. The main objective of this introductory dissertation is to give the lector a general background of the world of the mesoporous organic-inorganic hybrid materials and their applications.

### 5.1.1 Organic-Inorganic-Hybrid Materials

Organic-inorganic hybrid materials are easily obtained by the covalent anchoring of organic molecular compounds to 2D and 3D solid supports.<sup>32</sup>  
<sup>33</sup> The first consequence of this support-directed functionalization is the achievement of an ordered disposition of the organic molecular units. Therefore the covalently anchored organic molecules can organize in a more or less compact monolayer (depending on the grade of functionalization of the surface) in which the movement of the different compounds is reduced, generating new collective processes that generally define the characteristics of the obtained hybrid material. For example the development of these new organic-inorganic hybrid materials allowed to avoid the typical leaching processes of classic receptors (when the receptors are simply adsorbed on an inorganic support) and consequently increased the possibility of reuse the same solid several times. It's also possible to realize subsequent functionalization to obtain a solid surface characterized by the presence of different organic molecules and thus modulate its properties depending on the nature of the anchored organic derivatives. For all these reasons it can be stated that organic-inorganic hybrid materials are not simply physico-chemical mixtures but they can be broadly defined as hetero-supramolecular or nano-composites with (bio)organic and inorganic components, intimately mixed, where at least one of the component domains has a dimension ranging from a few Å to several nanometers.

---

<sup>32</sup> a) *Coord. Chem. Rev.*, Ed P. A. Gale, **2006**, 250. b) J. F. Callan, A. P. de Silva, D. C. Magri, *Tetrahedron*, **2005**, 61, 8551. c) G. J. Mohr, *Sens. Actuators B*, **2005**, 107, 2.

<sup>33</sup> K. Rurack, R. Martínez-Máñez, *The supramolecular chemistry of organic-inorganic hybrid materials*, **2010**, ed. John Wiley & Sons.

Consequently the properties of hybrid materials are not only the sum of the individual contributions of both phases, but the role of their inner interfaces could be predominant.<sup>34</sup>

### 5.1.2 Mesoporous Materials

According to the international Union of Pure and Applied Chemistry (IUPAC), pore sizes are classified into three main categories, namely *micro*-pores, *meso*-pores and *macro*-pores characterized by pore sizes less than 2 nm, between 2 and 50 nm, and larger than 50 nm respectively (see table 1).<sup>35</sup> Among them, thanks to their large internal surface area, microporous and mesoporous materials are attracting considerable research attention for applications in catalysis,<sup>36</sup> filtration and separation,<sup>37</sup> gas adsorption and storage,<sup>38</sup> enzyme immobilization,<sup>39</sup> biomedical tissue regeneration,<sup>40</sup> drug delivery,<sup>41</sup> and chemical/biochemical sensing.<sup>42</sup> Emblematic microporous materials are crystalline framework solids, such as zeolites,<sup>43</sup>

---

<sup>34</sup> C. Sánchez, *J. Mater. Chem.*, **2005**, 15, 3557.

<sup>35</sup> a) G. Zhao, *J. Mater. Chem.*, **2006**, 623-625; b) D. Schaefer, *MRS Bulletin*, **1994**, 14

<sup>36</sup> D.E. De Vos, M. Dams, B.F. Sels, P.A. Jacobs, *Chem. Rev.*, **2002**, 102, 3615.

<sup>37</sup> X. Liu, Y. Du, Z. Guo, S. Gunasekaran, C. -B. Ching, Y. Chen, S. S. J. Leong, Y. Yang, *Microporous Mesoporous Mater.*, **2009**, 122, 114.

<sup>38</sup> a) M. Kruk, M. Jaroniec, *Chem. Mater.*, 2001, 13, 3169. b) A. Corma, M. Moliner, M. J. Diaz-Cabanas, P. Serna, B. Femenia, J. Primo, H. Garcia, *New J. Chem.*, **2008**, 32, 1338. c) C. Ispas, I. Sokolov, S. Andreescu, *Anal. Bioanal. Chem.*, **2009**, 393, 543.

<sup>39</sup> M. Vallet-Regi, M. Colilla, I. J. Izquierdo-Barba, *Biomed. Nanotechnol.*, **2008**, 4, 1.

<sup>40</sup> I. I. Slowing, B. G. Trewyn, S. Giri, V. S. -Y. Lin, *Adv. Funct. Mater.*, **2007**, 17, 1225.

<sup>41</sup> a) M. Vallet-Regi, F. Balas, D. Arcos, *Angew. Chem., Int. Ed.*, **2007**, 46, 7548. b) K. A. Kilian, T. Bocking, K. Gaus, J. King-Lacroix, M. Gal, J. J. Gooding, *Chem. Commun.*, **2007**, 1936.

<sup>42</sup> a) K. A. Kilian, T. Bocking, K. Gaus, M. Gal, J. J. Gooding, *ACS Nano* **2007**, 1, 355. b) A. Jane, R. Dronov, A. Hodges, N. H. Voelcker, *Trends Biotechnol.* **2009**, 27, 230.

<sup>43</sup> M. E. Davis, C. Saldarriaga, C. Montes, J. Garces, C. Crowder, *Nature*, **1988**, 331, 698.

### 5.1.2 Mesoporous Materials

or particular metallophosphates<sup>44</sup> and cacoxenite which present the largest pore dimensions respectively comprised between 10 and 12 Å for zeolites and 14 Å for cacoxenite.<sup>45</sup>

**Table 1.** IUPAC classification of pore size

<i>Pore deifintion</i>	<i>Pore Diameter (nm)</i>
Macropore	> 50
Mesopores	2-50
Micropores	< 2

Examples of meso-structured materials are the M41S silica based scaffolds firstly synthesized by Mobile company researchers in 1992.<sup>46</sup> In particular they gave birth to a new family of mesoporous silica based materials known as M41S phases. Since that moment those silica mesoporous supports have been extensively used as inorganic scaffolds in the development of nanoscopic hybrid materials. The best-known representatives of this class of materials include the silica solid *MCM-41* (Mobile Crystalline Material with a hexagonal arrangement of the mesopores), *MCM-48* (with a cubic arrangement of mesopores) and *MCM-50* (with a lamellar structure).<sup>47</sup> The reasons of a wide-ranging use of this class of materials lay on their unique characteristics such as homogeneous pore size, ranging from approximately 2 to 10 nm, a high pore volume (in the order of 1 cm<sup>3</sup> g<sup>-1</sup>) and a very high specific surface area between 500 and 1000 m<sup>2</sup> g<sup>-1</sup>. Moreover those M41S materials are featured by high chemical inertness and thermal stability. Finally, but not less important, the

<sup>44</sup> M. Estermann, L. B. McCusker, C. Baerlocher, A. Merrouche, H. Kessler, *Nature*, **1991**, 352, 320.

<sup>45</sup> P. B. Moore, J. Shen, *Nature*, **1983**, 306, 356.

<sup>46</sup> C. T. Kresge, M. E. Leonowicz, W. J. Roth, J. C. Vartuli, J. S. Beck, *Nature*, **1992**, 359, 710

<sup>47</sup> J. S. Beck, J. C. Vartuli, W. J. Roth, M. E. Leonowicz, C. T. Kresge, K. D. Schmitt, C. T. W. Chu, D. H. Olson, E. W. Sheppard, *J. Am. Chem. Soc.*, **1992**, 114, 10834.

material synthetic procedure is quite simple and requires inexpensive and nonhazardous precursors. The peculiarity of presenting all these characteristics makes these materials ideal supports for adsorption processes of relatively small molecules and enables them to be suitable platforms for the preparation of hybrid systems for controlled release studies.

### **5.1.3 Synthesis of Mesoporous Materials**

The need of new high ordered porous systems applicable to petrochemical catalysis and featured by pores of larger dimensions to those found in zeolites gave origin to the mesoporous materials. The first successful method and still most studied was pointed out for silica. To build-up a system that presents a high ordered porous structure with homogeneous pore dimensions two main components are necessary:

- a *template* whose function is to direct the construction of the high ordered (crystalline) porous net
- a *polymeric precursor* which has to self-organize around the template and, upon polymerization, build up the final rigid structure

As reported above, the adjective mesoporous refers to a pore diameter between 2-50 nanometers and does not consider the phase of the final mesoporous ordered net. Therefore the first choice that should be taken is about the dimensions of the pore and the shape of the phase. In the first introductory chapter the possibility of auto-aggregation of some kind of molecule was reported and a particular importance was given to the example of *fuzzy* self-assembled micelles. If one looks at the CTAB phase diagram reported at page 15 (see figure 7) can verify that depending on the

### 5.1.3 Synthesis of Mesoporous Materials

temperature and concentration parameters three different supramicellar phases can be obtained: hexagonal, cubic and lamellar phases. Consequently if a particular phase is required for the synthesis of the final mesoporous material it's easy to use the correct conditions of surfactant concentration and solution temperature to achieve the desired phase and thus the correct "template shape". The second template aspect that can be controlled deals with the dimensions of the final pores. In this case the longer the hydrophobic surfactant cue the bigger the final pore, because the intermediate micelle will present bigger dimensions. This last statement has some limitation because if the surfactant hydrophobic cue is too long a bilayer or a vesicle could be formed and this does not allow obtaining the desired template for the preparation of a mesoporous material. Thus, as usual, a correct balance between the previous two aspects should be considered. Once obtained the desired template the polymeric precursor should be added to the reaction mixture. In the correct conditions of pH and temperature the polymerization reaction will take place around the template giving origin to a *high ordered periodic porous net*, containing huge quantity of surfactant. The final step is the elimination of the surfactant by aerobic calcinations or adequate solvent extraction. Moreover researchers described two different mechanisms, involved on the formation process of these composite materials. In the first one, named as True Liquid-Crystal Templating (TLCT) mechanism, the concentration of the surfactant is very high and, as a consequence, a lyotropic liquid-crystalline phase is formed without requiring the presence of the precursor inorganic framework materials (normally tetraethyl- (TEOS) or tetramethylorthosilica (TMOS)).<sup>48</sup> The other mechanism considers that liquid-crystalline phase is formed even

---

<sup>48</sup> G. S. Attard, J. C. Glyde, C. G. Göltner, *Nature*, **1995**, 378, 366.

at lower concentrations of surfactant molecules, for example, in a cooperative self assembly of the template molecules and the added inorganic species.<sup>49</sup> Using these processes, the original approach has been extended by a number of variations. As an example, the use of tri-block copolymer templates under acidic conditions was employed to prepare the so-called SBA (Santa Barbara Amorphous) silica phases,<sup>50</sup> whereas the use of cationic surfactants, such as hexadecyltrimethylammonium bromide (CTAB) was originally used in the synthesis of the first M41S materials, obtaining the hexagonal (MCM-41), the cubic (MCM-48) and lamellar (MCM-50) forms cited above.

The most famous, widely-studied and best known silica-based mesoporous inorganic scaffold is MCM-41. Its synthesis can be considered a classic example of supramolecular chemistry. In fact the first step is the preparation of the template for the attainment of the final hexagonal mesoporous phase (see figure 21). To obtain this template a water solution of CTAB is prepared. Thus, as reported above, in the correct conditions of temperature, pH and concentration the surfactant firstly self-organizes into micelles and secondly micelles give origin to hexagonal shaped supra-micellar aggregates. Once obtained the required template the polymeric precursor (TEOS) is added to the solution and, at basic pH, it polymerizes around the template giving rise to the final mesoporous scaffold with its pores full of surfactant. This is a critical step, because depending on some reaction parameters, temperature, polymeric precursor concentration and

---

<sup>49</sup> A. Monnier, F. Scheth, Q. Huo, D. Kumar, D. Margolese, R. S. Maxwell, G. Stucky, M. Krishnamurthy, P. Petroff, A. Firouzi, M. Janicke, B. Chmelka, *Science*, **1993**, 261, 1299.

<sup>50</sup> a) D. Zhao, J. Feng, Q. Huo, N. Melosh, G.H. Fredrickson, B.F. Chmelka, G.D. Stucky, *Science*, **1998**, 279, 548. b) D. Zhao, Q. Huo, J. Feng, B.F. Chmelka, G.D. Stucky, *J. Am. Chem. Soc.*, **1998**, 120, 6024.

### 5.1.3 Synthesis of Mesoporous Materials

reaction time, *nano* or *micro*-particles can be specifically obtained. As explained before, removal of surfactant by aerobic high temperature calcination or by extraction with adequate solvents allow us to obtain the final mesoporous inorganic scaffold, which presents cylindrical unidirectional empty channels of approximately 3 nm of diameter (when CTAB is used as surfactant) arranged in a hexagonal distribution. The final solid presented a delicate structural order that is very difficult to obtain following traditional synthetic routes.

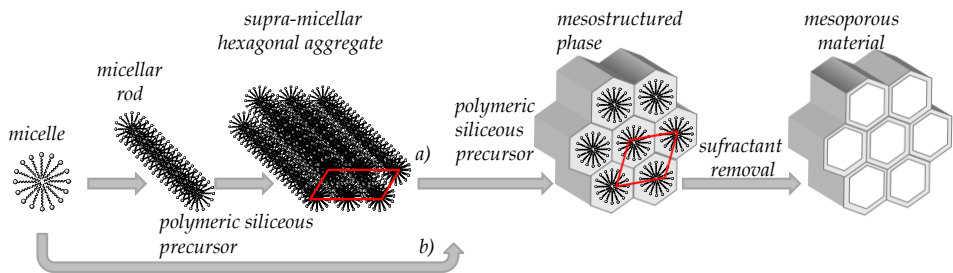


**Figure 21.** Schematic representation of MCM-41 template synthesis: a) true liquid-crystal template mechanism: the liquid crystal phase is intact before the inorganic precursor is added. b) cooperative liquid-crystal mechanism, where addition of the inorganic precursor mediates the ordering of the surfactant micelles.

The principal advantage of this synthetic method is that the high grade of homogeneity of the initial elements is transmitted to the final material, showing a system of pores not only homogeneously in size but also in form and regularity.

### 5.1.4 Functionalization of Mesoporous-Silica-Scaffolds: How to Obtain Organic-Inorganic Hybrid Materials

The further step toward the preparation of organic-inorganic hybrid materials is the functionalization of the inorganic silica-based mesoporous

scaffold. This covalent modification can be easily carried out bearing in mind that the mesoporous silica scaffold presents a high concentration of structural defects in the form of silanol (Si-OH) groups. These silanols can easily react with trialkoxysilane derivatives ((R'O)<sub>3</sub>-Si-R) to give a nucleophilic aliphatic substitution and generate a novel class of organic-inorganic nanocomposites. The features of these hybrid materials can be finely tuned regarding at the chemical nature of the R moiety that can be selected in order to include specific groups with specific reactivity onto the inorganic framework. In addition, these R groups can contain one or more reactive atoms, which can be later chemically modified on the surface of the scaffold. Till now two main procedures for the synthesis of the organic-inorganic mesoporous hybrid materials have been described: <sup>51</sup>

- **co-condensation procedure:** a simultaneous condensation of silica and organosilica precursors is brought about. The first example of direct synthesis or co-condensation functionalization of MCM-41 inorganic scaffold was presented by Stein and coworkers that demonstrated the formation of an organic monolayer of 3-mercaptopropyl groups inside of the pores of MCM-41, as shown in figure 22. <sup>52</sup> In this case, in basic hydrolytic conditions, trialkoxysilane precursors react rapidly with the oligomeric silane (TEOS) to form the final frame structure, in which the organic groups R are bonded to silicon atoms of the inorganic scaffold wall and can therefore interact with chemical species eventually present inside the channels and cavities (Figure 22).

---

<sup>51</sup> Vinu, A.; Hossain, K. Z.; Ariga, K., *Nanosci. Nanotech.*, **2005**, *5*, 347.

<sup>52</sup> Lim, M. H.; Blanford, C. F.; Stein, A., *Chem. Mater.*, **1998**, *10*, 467.

### 5.1.4 Functionalization of MCM matrix

In this case the final extraction of the surfactant can't be performed by aerobic calcination, because this procedure would lead to the oxidative degradation of the organic groups just incorporated. Thus the common procedure to eliminate the surfactant template is a liquid extraction in acidic conditions.



**Figure 22.** Schematic representation of co-condensation synthetic procedure for MCM-41

The co-condensation method usually leads to a homogeneous distribution of the trialkoxysilane derivatives along the material particles and between the surface thereof and the inner surface corresponding to the channels and cavities. Moreover the co-condensation method allows the incorporation of a relatively large amount of functional groups, which generally falls between 2 and 4 mg g<sup>-1</sup>, in the most favorable cases.

- **grafting procedure:** in this case a post-functionalization of the mesoporous silica scaffold is performed. In particular trialkoxysilane derivatives are reacted in the presence of the inorganic scaffold to give the condensation reaction previously reported. This grafting procedure is generally brought about by preparing a suspension of the required quantity of the solid in an anhydrous solvent in the presence of the reactive silane precursor

(figure 23). The presence of the silanol groups on the silica scaffold surface guarantees the formation of a covalent bond between the trialkoxysilane precursors and the solid surface. It's important to underline that the subsequent covalent modification of the inorganic mesoporous scaffold doesn't modify the mesoporous structure of the solid, as demonstrated by X-ray diffraction powder evidences.

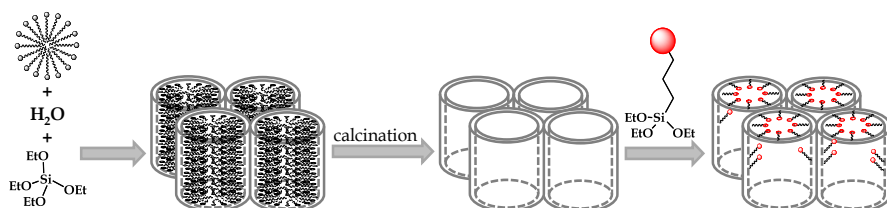


**Figure 23.** Schematic representation of functionalization of MCM-41 skeleton through grafting procedure

Bearing in mind that the distribution of the reactive silanols group in the mesoporous scaffold is on average the same inside and outside of the pores, the distribution of the organic molecules on the solid after the grafting is determined by other factors such as diffusion processes and steric hindrance around the silanols. In this case the external surface of the solid is much more accessible than the inner part of the particle. Thus if the functionalization is carried out before the removal of the surfactant a complete superficial modification is obtained because the interior part of the pores is occupied by the inert template. However if the surfactant is removed before the grafting, due to its steric hindrance the trialkoxysilane organic precursor reacts easier with the silanols on the surface and then with the silanols inside of the pores.

#### 5.1.4 Functionalization of MCM matrix

Moreover functionalization by grafting permits a more rapid and efficient surfactant extraction (calcinations method). Finally this method also permits to firstly load the mesopore with certain molecules and secondly functionalize the surface with another category of organic compound to obtain suitable hybrid materials for controlled delivery processes (see following section). Apart of these reported advantages, the grafting method is somehow preferred because of the existence some practic problems related to the co-condensation synthesis. For example the degree of mesoscopic order of the final materials decreases when concentration of organic silane increases. At this respect, when the organic functionality exceeds 40% mol, disordered materials are obtained. Another aspect is related to the homocondensation reactions. In fact they take place easier between silane groups and, as a consequence, the proportion of terminal organic groups that are incorporated into the pore-wall network is generally lower than would correspond to the starting concentration in the reaction mixture. Also the homogeneous distribution of different organic functionalities in the framework cannot be guaranteed in the co-condensation procedure. Moreover the incorporated organic groups can lead to a reduction in the pore diameter, pore volume, and specific surface areas. In addition only extractive methods can be used to remove the template. Calcination is not suitable, in most cases, in order to avoid the organic functionality destruction during removal of the surfactant.

#### ***5.1.5 Characterization of the Organic-Inorganic-Mesoporous Hybrid materials***

Once obtained the final organic-inorganic mesoporous hybrid material, different characterization techniques must be used in order to verify

various crucial aspects. In particular some different features should be considered: a) the integrity of the mesoporous structure, b) the quantity of organic matter that composes the final material and, in the case of preparation of mesoporous hybrid *nanoparticles*, it's interesting to determine the c) particles average diameter and particle's shape. To verify the achievement and the subsequent preservation, during loading and/or functionalization processes, of the mesoporous network, powder X-ray diffraction (PXRD) and transmission electronic microscopy (TEM) are very useful characterization techniques. As displayed in figure 24 one can clearly determine if a hexagonal or a cubic mesoporous phase has been obtained. Moreover if the same X-ray diffraction pattern is displayed by the final hybrid material, the mesoporous network conservation can be demonstrated.

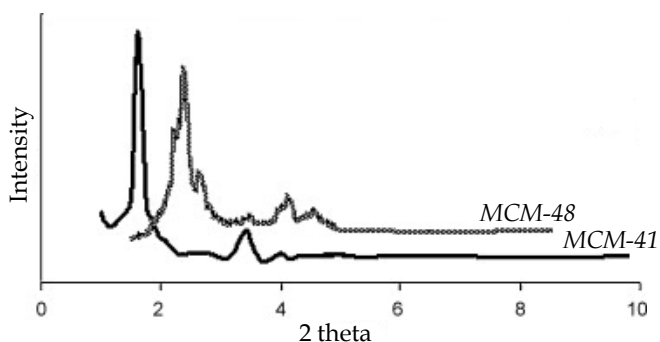


**Figure 24.** X-ray diffraction powder of **MCM-41**, hexagonal phase and **MCM-48**, cubic phase

Apart of PXRD, TEM microscopy is also a useful technique to demonstrate the formation and preservation of a particular phase. In this sense figure 25 reports some examples of mesoporous nanoparticles characterized by different mesophases. As can be noticed different

phases can be distinguished by TEM microscopy, the shape and dimensions of the particles can be evaluated also by this technique.

The organic-inorganic ratio of the final hybrid material can be determined by thermogravimetric (TGA) and/or elemental analysis (EA). In this case the problems can be related to differentiate the amount of two or more different organic molecules in the final material.

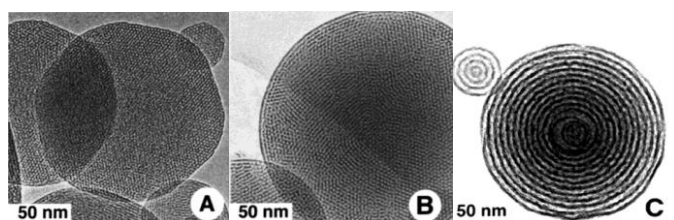


**Figure 25.** TEM micrographs of aerosol-generated particles and an aerosol-deposited thin film. a) Faceted, calcined particles exhibiting 1-D hexagonal mesophase, prepared using CTAB. b) Calcined particles exhibiting cubic mesophase, prepared from the nonionic surfactant Brij-58. c) Calcined particles exhibiting vesicular mesophase, prepared from the ethylene oxide/propylene oxide/ethylene oxide tri-block copolymer P123. Adapted from *Adv. Mater.*, **1999**, *11*, 579-585. © 2007 John Wiley & Sons.

For example when a mesoporous silica based scaffold is firstly loaded with a certain molecule and subsequently functionalized on the surface with a different trialkoxysilane derivative, TGA and EA techniques couldn't be enough to fully characterize the final material. Therefore it can be useful combine these characterization methods with UV-VIS or chromatographic monitorization of the quantity of the loaded compound. The difference between the total organic matter and the loaded cargo gives the amount anchored of the organic groups. Moreover the demonstration of effective loading and grafting procedures can be achieved by nitrogen adsorption desorption measurements. This technique allows determining

the specific surface area of the material. At this respect a comparison between a calcined MCM-41 (very high specific surface area) and a loaded and functionalized MCM-41 scaffold (very low specific surface area) is indicative of a correct pore filling. In summary by considering the resulting data of all these techniques it is possible to state if a hybrid material had conserved its mesoporous network and the amount of loading and/or functionalization.

### **5.1.6 Application of Organic-Inorganic Hybrid Supports: Gated Materials**

Uncapped mesoporous materials have been extensively used as vehicles to store and subsequently deliver organic molecules.<sup>53, 54, 55</sup> This fact is a direct consequence of the presence of a uniform pore system that grants a high load capacity of large amount of chemical species.<sup>56</sup> In this kind of nanoscopic systems the delivery process is regulated by a simple diffusion process, and in general it is no possible or very difficult to control the amount of delivered cargo. In the last years these “germinal” systems based on mesoporous materials, evolved and the concept of **molecular gate** was introduced. Molecular or supramolecular gates can be defined as

---

<sup>53</sup> a) M. Vallet-Regi, A. Rámila, R. P. del Real, J. Pérez-Pariente, *J. Chem. Mater.* **2001**, *13*, 308.

b) B. Muñoz, A. Rámila, J. Pérez-Pariente, I. Díaz, M. Vallet-Regi, *Chem. Mater.* **2003**, *15*, 500.

<sup>54</sup> a) J. M. Rosenholm, E. Peuhu, L. T. Bate-Eya, J. E. Eriksson, C. Sahlgren, M. Linden, *Small*, **2010**, *6*, 1234. b) M. Liong, J. Lu, M. Kovichich, T. Xia, S. G. Ruehm, A. E. Nel, F. Tamanoi, J. I. Zink, *ACS Nano*, **2008**, *2*, 889.

<sup>55</sup> K.K. Cotí, M. E. Belowich, M. Liong, M. W. Ambrogio, Y. A. Lau, H. A. Khatib, J. I. Zink, N. M. Khashab, J. F. Stoddart, *Nanoscale*, **2009**, *1*, 16.

<sup>56</sup> (a) M. Vallet-Regi, A. Rámila, R.P. del Real, J. Pérez-Pariente, *J. Chem. Mater.* **2001**, *13*, 308-311. (b) B. Muñoz, A. Rámila, J. Pérez-Pariente, I. Díaz, M. Vallet-Regi, *Chem. Mater.* **2003**, *15*, 500-503.

### 5.1.6.1 Light-driven Molecular Gates

nanoscopic supramolecular-based devices, attached to certain solid supports, in which mass transport can be triggered by a target external stimulus that can control the state of the gate (closed or open) at will. In particular, depending on the type of the applied stimulus, it's possible to modify the properties of the anchored molecules (i.e. polarity, conformation, size, interaction with other species etc.) which in turn results in a control of the delivery.<sup>57</sup> A schematic representation of a gate-like superstructure is shown in figure 26.

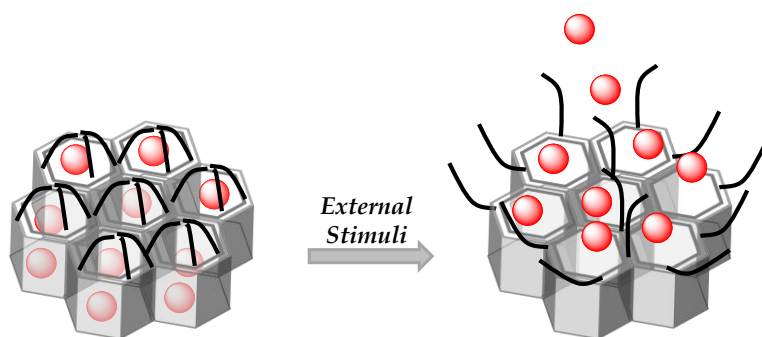


**Figure 26.** Schematic representation of the operation principle of a molecular gate in a mesoporous support.

The scheme shows how the outer surface of a mesoporous support is functionalized with suitable molecules. Upon the application of an external stimulus, the gate opens and allows the release of previously entrapped guests (i.e., dyes, drugs, etc.). A suitable and general protocol to verify the performance of these gated materials is to load the mesoporous framework with a dye and study its delivery through UV and/or fluorescence spectroscopy. Once demonstrated the possibility of load and deliver

<sup>57</sup> (a) Q. Fu, G.V.R. Rao, L.K. Ista, Y. Wu, B.P. Andrzejewski, L.A. Sklar, T.L. Ward, G.P. López, *Adv. Mater.*, **2003**,15, 1262; (b) I.-I. Slowing, J. L. Vivero-Escoto, B. G. Trewyn, V. S.-Y. Lin, *J. Mater. Chem.*, **2010**, 20, 7924; (c) S. Angelos, M. Liong, E. Choi, J.I. Zink, *Chemical Engineering Journal* **2008**, 137, 4

organic dyes in a controlled manner from a mesoporous matrix, it is also possible to load the biocompatible mesoporous hybrid materials with bioactive molecules (such as vitamins, cytotoxic spices, hormones, etc.).<sup>58</sup> The external stimuli, able to induce the controlled release of the entrapped cargo, can be classified in: physical,<sup>59</sup> chemical,<sup>60</sup> or biochemical.<sup>61</sup>

<sup>58</sup> (a) A. B. Descalzo, R. Martínez-Máñez, F. Sancenón, K. Hoffmann, K. Rurack, *Angew. Chem. Int. Ed.*, **2006**, *45*, 5924; (b) S. Saha, K.C.F. Leung, N.T. Nguyen, J.F. Stoddart, J.I. Zink, *Adv. Func. Mater.*, **2007**, *17*, 685; (c) I.I. Slowing, J.L. Vivero-Escoto, C.W. Wu, V.S.-Y. Lin, *Adv. Drug Deliv. Rev.*, **2008**, *60*, 1278; (d) E. Aznar, R. Martínez-Máñez, F. Sancenón, *Expert Opinion*, **2009**, *6*, 643; (e) K.K. Cotí, M.E. Belowich, M. Liong, M.W. Ambrogio, Y.A. Lau, H.A. Khatib, J.I. Zink, N.M. Khashab, J.F. Stoddart, *Nanoscale*, **2009**, *1*, 16.

<sup>59</sup> C. R. Thomas, D. P. Ferris, J.-H. Lee, E. Choi, M. H. Cho, E. S. Kim, J. F. Stoddart, J. -S. Shin, J. Cheon, J. I. Zink, *J. Am. Chem. Soc.*, **2010**, *132*, 10623-10625.

<sup>60</sup> (a) E. Johansson, E. Choi, S. Angelos, M. Liong, J.I. Zink, *Sol-Gel Sci Technol*, **2008**, *46*, 313; (b) S. Angelos, E. Choi, F. Vögtle, L. De Cola, J.I. Zink, *J. Phys. Chem. C*, **2007**, *111*, 6589; (c) D.P. Ferris, Y.-L. Zhao, N.M. Khashab, H.A. Khatib, J.F. Stoddart, J.I. Zink, *J. Am. Chem. Soc.*, **2009**, *131*, 1686; (d) Q. Lin, Q. Huang, C. Li, C. Bao, Z. Liu, F. Li, L. Zhu, *J. Am. Chem. Soc.*, **2010**, *132*, 10645; (e) Q. Lin, Q. Huang, C. Li, C. Bao, Z. Liu, F. Li, L. Zhu, *J. Am. Chem. Soc.*, **2010**, *132*, 10645; (f) H.-M. Lin, W.-K. Wang, P.-A. Hsiung, S.-G. Shyu, *Acta Biomaterialia*, **2010**, *6*, 3256; (g) J. Lai, X. Mu, Y. Xu, X. Wu, C. Wu, C. Li, J. Chen, Y. Zhao, *Chem. Commun.*, **2010**, *46*, 7370; (h) T.D. Nguyen, K.C.-F. Leung, M. Liong, Y. Liu, J.F. Stoddart, J.I. Zink, *Adv. Funct. Mater.* **2007**, *17*, 2101; (i) B.G. Trewyn, I.I. Slowing, S. Giri, H.T. Chen, V.S.-Y. Lin, *Acc. Chem. Res.*, **2007**, *40*, 846; B.G. Trewyn, S. Giri, I.I. Slowing, V.S.-Y. Lin, *Chem. Commun.*, **2007**, 3236; (j) F. Torney, B.G. Trewyn, V.S.-Y. Lin, K. Wang, *Nat. Nanotechnol.* **2007**, *2*, 295; (k) M. Fujiwara, S. Terashima, Y. Endo, K. Shiokawa, H. Ohue, *Chem. Commun.*, **2006**, 4635; (l) T.D. Nguyen, Y. Liu, S. Saha, K.C.-F. Leung, J.F. Stoddart, J.I. Zink, *J. Am. Chem. Soc.* **2007**, *129*, 626. (m) Q. Yang, S. Wang, P. Fan, L. Wang, Y. Di, K. Lin, F.-S. Xiao, *Chem. Mater.*, **2005**, *17*, 5999; (n) T.D. Nguyen, K.C.-F. Leung, M. Liong, C.D. Pentecost, J.F. Stoddart, J.I. Zink, *Org. Lett.* **2006**, *8*, 3363. (o) K.C.-F. Leung, T.D. Nguyen, J.F. Stoddart, J.I. Zink, *Chem. Mater.* **2006**, *18*, 5919; (p) K. C.-F. Leung, C.-P. Chak, C.-M. Lo, W.-Y. Wong, S. Xuan, C. H. K. Cheng, *Chem. Asian J.* **2009**, *4*, 364; (q) C. Park, K. Oh, S.C. Lee, C. Kim, *Angew. Chem. Int. Ed.*, **2007**, *46*, 1455; (r) W. Guo, J. Wang, S.-J. Lee, F. Dong, S. S. Park, C.-S. Ha, *Chem. Eur. J.*, **2010**, *16*, 8641; (s) R. Liu, P. Liao, Z. Zhang, R. J. Hooley, P. Feng, *Chem. Mater.* **2010**, *22*, 5797. (t) C. Coll, R. Casasús, E. Aznar, M. D. Marcos, R. Martínez-Máñez, F. Sancenón, J. Soto, P. Amorós, *Chem. Commun.* **2007**, 1957-1959.

<sup>61</sup> (a) A. Schlossbauer, J. Kecht, T. Bein, *Angew. Chem. Int. Ed.*, **2009**, *48*, 3092-3095. (b) C. Park, H. Kim, S. Kim, C. Kim, *J. Am. Chem. Soc.*, **2009**, *131*, 16614-16615. (c) E. Climent, R. Martínez-Máñez, F. Sancenón, M. D. Marcos, J. Soto, A. Maquieira, P. Amorós, *Angew. Chem. Int. Ed.*, **2010**, *49*, 7281- 7283. (d) Y. Klichko, N. -M. Khashab, Y. -W. Yang, S. Angelos, J.F.

### 5.1.6.1 Light-driven Molecular Gates

The controlled release of bioactive molecules is interesting from a pharmaceutical point of view. In particular the use of gated materials may open new possibilities to deliver target substances to specific cells and/or prevent cargo degradation due to the metabolic processes.

In this context, when this project began, there were few examples in which the cargo released were biomolecules or drugs, and even fewer works related with the use of nanoscopic gated materials for release in intracellular media.<sup>62</sup> In the following part of this introduction some selected examples of molecular gates will be reported.

#### **5.1.6.1 Light-Driven Molecular Gates**

The first example of a light driven molecular gate, which was also the first gated material example based on a MCM-41 matrix, was described by Fujiwara and coworkers in 2003.<sup>63</sup> The authors showed how the uptake, storage and release of organic molecules in a mesoporous scaffold could be regulated through the photocontrolled and reversible intermolecular dimerization of coumarin derivatives attached to the pore outlets (see figure 27). In particular the MCM-41 surface was functionalized with coumarin derivatives that can undergo [2+2] electrocyclic photoisomerization of the double bonds to give the more hindered cyclobutane derivatives, upon >310 nm irradiation. Moreover MCM-41 had been previously loaded with cholestane to monitor the efficiency of the

---

Stoddart, J.I. Zink, *Microporous and Mesoporous Materials*, **2010**, 132, 435-441. (e) E. Climent, A. Bernardos, R. Martínez-Máñez, A. Maquieira, M.D. Marcos, N. Pastor-Navarro, R. Puchades, F. Sancenón, J. Soto, P. Amorós, *J. Am. Chem. Soc.*, **2009**, 131, 14075-14080.

<sup>62</sup> a) E. Aznar, R. Martínez-Máñez, F. Sancenón, *Expert Opin. Drug Deliver.*, **2009**, 6, 643. b) J. L. Vivero-Escoto, I. I. Slowing, B. G. Trewyn, V. S.-Y. Lin, *Small*, **2010**, 6, 1952.

<sup>63</sup> (a) Mal, N. K.; Fujiwara, M.; Tanaka, Y. *Nature*, **2003**, 421, 350-353.

system. The authors demonstrated that upon irradiation of the hybrid material at  $>310$  nm wavelength the coumarin photoisomerization was induced closing the pores and preventing cholestane delivery.

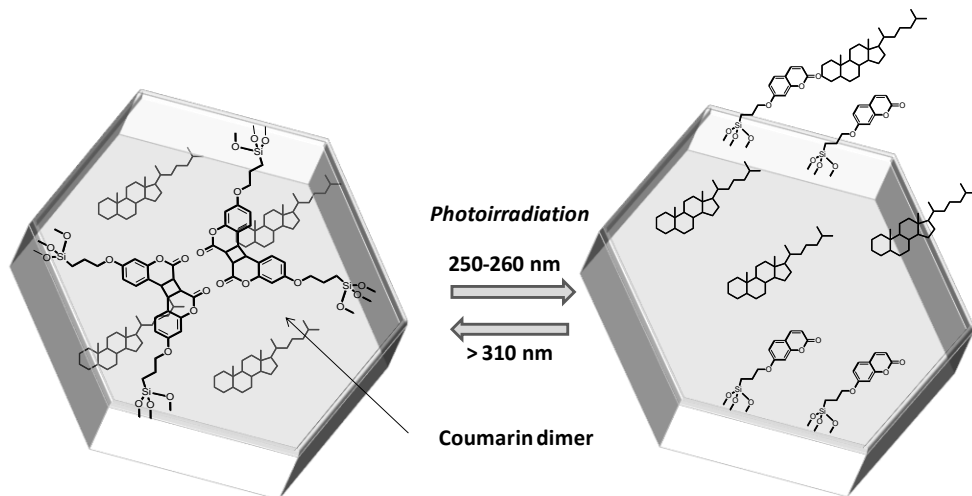


**Figure 27.** Schematic representation of a light-driven molecular gate. Coumarin photoisomerization reaction ( $\lambda > 310$  nm) induced the formation of a cyclobutane dimer that inhibit cargo release. Irradiation with UV light (250-260 nm) induced the photo-opening of cyclobutane ring with the subsequent cargo delivery.

Otherwise the irradiation at 250 nm induced the photochemical rupture of the cyclobutane rings, unblocking the pores and allowing the release of the entrapped cargo. Apart of this first reported example there are several similar works that deal with the photoisomerization paradigm to finely tune mass transport.<sup>64</sup> In this field rotaxanes have proved to be

<sup>64</sup> (a) T. D. Nguyen, K. C.-F. Leung, M. Liong, Y. Liu, J. F. Stoddart, J. I. Zink *Adv. Funct. Mater.* **2007**, *17*, 2101–2110. (b) E. Johansson, E. Choi, S. Angelos, M. Liong, J. I. Zink, *J. Sol-Gel Sci. Technol.* **2008**, *46*, 313–322. (c) J. Lu, E. Choi, F. Tamanoi, J. I. Zink, *Small* **2008**, *4*, 421–426. (d) Y. Zhu, M. Fujiwara, *Angew. Chem., Int. Ed.* **2007**, *46*, 2241–2244. (e) R. Liu, Y. Zhang, P. Y. Feng, *J. Am. Chem. Soc.* **2009**, *131*, 15128 – 15129 (f) D. P. Ferris, Y.-L. Zhao, N. M. Khashab, H. A. Khatib, J. F. Stoddart, J. I. Zink, *J. Am. Chem. Soc.* **2009**, *131*, 1686–1688. (g) S. Angelos, Y.W. Yang, N. M. Khashab, J. F. Stoddart, J. I. Zink, *J. Am. Chem. Soc.* **2009**, *131*, 11344 – 11346.

suitable molecules to design gated materials based on photoisomerization reactions. For example Stoddart's group reported in 2009 the use of functionalized azobenzene derivatives (AB) prepared from 4-(3-triethoxysilylpropylureido)azobenzene (TSUA) and (E)-4-((4(benzylcarbamoyl)phenyl)diazanyl)benzoic acid (BPDB), to give modified MCM-41 nanoparticles (NPs) (see figure 28).<sup>65</sup> Then they evaluated light-operated dye (Rhodamine B, RhB) release from the MCM-41 NPs upon dissociation of the  $\beta$ -CD rings from the BPDB stalks. In fact irradiation of AB at 351 nm caused AB isomerization from the more stable *trans* to the less stable *cis* configuration. Previous investigations had demonstrated a high binding affinity in aqueous solution between  $\beta$ -CD and *trans*-AB derivatives and a low, if any, binding between  $\beta$ -CD and *cis*-AB derivatives.<sup>66</sup>

In the case of MCM-41 carrying AB-containing stalks,  $\beta$ -CD will thread onto the stalks and bind to *trans*-AB units, thus sealing the nanopores and stopping release of the cargo. By contrast, upon irradiation (351 nm), the isomerization of *trans*-to-*cis* AB units leads to the dissociation of  $\beta$ -CD rings from the stalks, thus opening the gates to the nanopores and releasing the cargo. To demonstrate the operation principle of this system, the authors

---

<sup>65</sup> (a) N. Liu, K. Yu, B. Smarsly, D. R. Dunphy, Y.-B. Jiang, C. J. Brinker, *J. Am. Chem. Soc.* **2002**, *124*, 14540–14541. (b) N. Liu, Z. Chen, D. R. Dunphy, Y.-B. Jiang, R. A. Assink, C. J. Brinker, *Angew. Chem., Int. Ed.* **2003**, *42*, 1731–1734. (c) N. Liu, D. R. Dunphy, P. Atanassov, S. D. Bunge, Z. Chen, G. P. López, T. J. Boyle, C. J. Brinker, *Nano Lett.* **2004**, *4*, 551–554

<sup>66</sup> (a) P. Bortolus, S. Monti, *J. Phys. Chem.* **1987**, *91*, 5046–5050. (b) N. Yoshida, A. Seiyama, M. Fujimoto, *J. Phys. Chem.* **1990**, *94*, 4254–4259. (c) A. M. Sanchez, R. H. de Rossi, *J. Org. Chem.* **1996**, *61*, 3446–3454. (d) H. Murakami, A. Kawabuchi, K. Kotoo, M. Kunitake, N. Nakashima, *J. Am. Chem. Soc.* **1997**, *119*, 7605–7606. (e) M. Takei, H. Yui, Y. Hirose, T. Sawada, *J. Phys. Chem.*

also prepared a pyrene-modified  $\beta$ -cyclodextrin (Py- $\beta$ -CD) as capping moieties with the TSUA stalks on the surfaces of MCM-41 NPs.

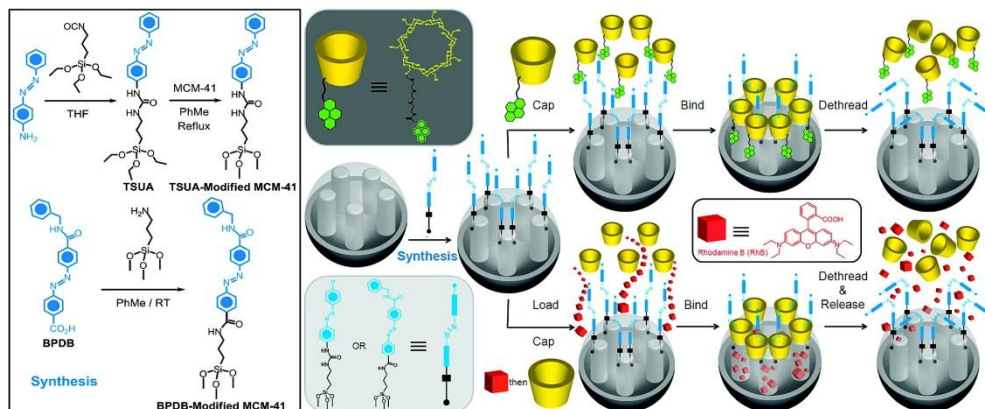


**Figure 28.** Synthesis of TSUA- and BPDB-modified MCM-41. Two approaches to the operation and function of the AB-modified MCM-41 NPs carrying nanovalves. Py- $\beta$ -CD or  $\beta$ -CD threads onto the *trans*-AB stalks to seal the nanopores. Upon irradiation (351 nm), the isomerization of *trans*-to-*cis* AB units leads to the dissociation of Py- $\beta$ -CD or  $\beta$ -CD rings from the stalks, thus opening the gates to the nanopores and releasing the cargo. Adapted with permission from *J. Am. Chem. Soc.* **2009**, *131*, 1686–1688 © 2008 American Chemical Society

Finally the authors demonstrated the uncapping process by the rupture of the complex “Py- $\beta$ -CD-TSUA *trans* double bond” upon irradiation, through monitoring the emission band of Py.

The first example of a two-input (photochemical and chemical) gated hybrid system operative in water was reported by Martínez-Máñez et al.<sup>67</sup> This nanodevice consisted of a MCM-41 silica matrix, loaded with the dye Ru(bipy)<sub>3</sub><sup>2+</sup> and containing spiropyran photochrome units attached to the external surface of the inorganic support (see figure 29). This molecule

<sup>67</sup> E. Aznar, R. Casasús, B. García-Acosta, M. D. Marcos, R. Martínez-Máñez, F. Sancenón, J. Soto, P. Amorós, *Adv. Mater.*, **2007**, *19*, 2228.

### 5.1.6.1 Light-driven Molecular Gates

could be transformed reversibly between two forms, the neutral spirocyclic and the positively charged merocyanine, upon the application of light.

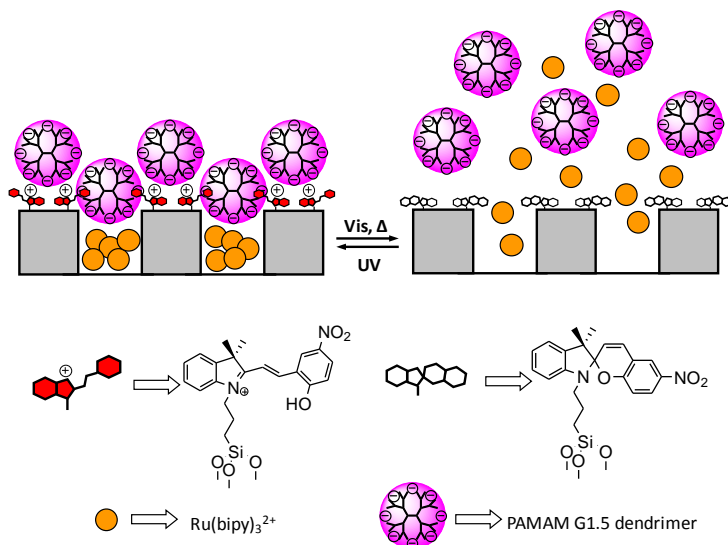


**Figure 29.** Schematic representation of an MCM-41 support functionalized with spirobenzopyran derivatives and capped with PAMAM G1.5 dendrimers. Adapted from *Adv. Mater.*, **2007**, *19*, 2228. © 2007 John Wiley & Sons.

To obtain a gated mesoporous material, negatively charged G1.5 PAMAM dendrimers (G1.5) were used as molecular stoppers, thanks to the coulombic interaction between their negative charges and the positively charged merocyanine. Irradiation with visible light induced the transformation of the merocyanine isomer to its neutral spirocyclic form (which does not present any affinity for the negatively charged dendrimers) allowing the release of the entrapped dye. Furthermore, the functional task of the dendrimers was also switched on/off by simple adjustment of the pH. At acidic pH (pH ca. 2) G1.5 PAMAM dendrimers are protonated and are unable to interact with the charged merocyanine isomer with the subsequent dye release.

A related approach to design a light driven gated material is the use of photocleavable organic molecules as molecular gates. Till now very few examples based on photocleavage reactions had been reported. In particular Lin's group synthesized gold nanoparticle-capped mesoporous silica materials for the release of the hydrophobic anticancer drug *paclitaxel* into cells. The role played by gold nanoparticles was to inhibit cargo uncontrolled delivery from the mesopores through their attachment to the SMP material throughout a photoresponsive linker (a nitroaromatic compound). Irradiation at 365 nm induced the photocleavage of the nitroaromatic-organic linker, with the subsequent removal of the gold nanoparticles from the SMP surface and the final release of the hosted molecules.<sup>68</sup>

In a very similar approach, Kim et al. prepared mesoporous silica particles that contained calcein as guest molecules, *o*-nitrobenzyl ester moieties as a photocleavable linker and  $\beta$ -cyclodextrins ( $\beta$ -CD) as "gatekeepers" (see figure 30).<sup>69</sup>

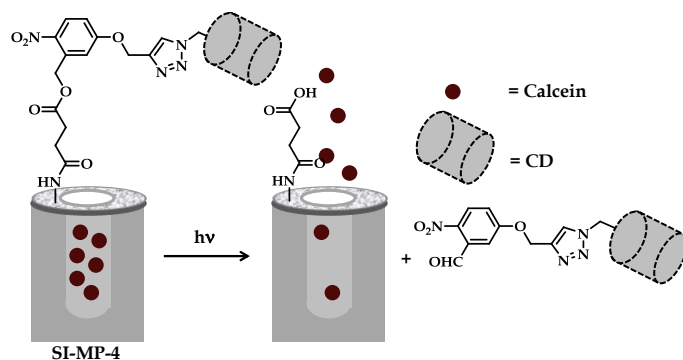


**Figure 30.** Schematic illustration of the controlled delivery protocol. Irradiation at 350 nm induced the photodegradation of the *p*-nitrophenol derivative with the subsequent removal of the CD capping moiety allowing the diffusion of the entrapped cargo.

<sup>68</sup> a) S. Giri, B. G. Trewyn, M. P. Stellmaker, V. S.-Y. Lin, *Angew. Chem., Int. Ed.*, **2005**. (b)

<sup>69</sup> Park, C.; Lee, K.; Kim, C. *Angew. Chem. Int. Ed.* **2009**, *48*, 1275-1278.

Irradiation at 350 nm induced the rupture of *o*-nitrobenzyl ester moiety that detaches the  $\beta$ -cyclodextrins gatekeepers with the subsequent calcein release.

### **5.1.6.2 Redox-Driven Molecular Gates**

Another important and attractive stimulus to regulate the molecular gate opening-closing protocols, are electrons. In particular the functionalization of silica-based nano and micrometric mesoporous materials with redox-active chemical species open the possibility to use electrochemical stimuli to finely tune the molecular gates state (open or closed). This electro-active type of hybrid materials have been proposed to be very suitable for intracellular controlled release processes thanks to the in-cell presence of redox active molecules such as NAD<sup>+</sup>-NADH or lipoic-dihydrolipoic acid.

A large number of examples have been described in the last decade, but they can be summarized into two main fundamental groups: (i) systems based in the reduction and consequent breakage of disulfide bonds (that linked the capping molecule to the mesoporous scaffold) or (ii) systems where the redox-induced movement of certain capping molecules induces the change in the state of the molecular gate (open-closed). One of first examples of electrochemically-driven molecular gates was presented by Lin and coworkers in 2003.<sup>70</sup> That system consisted of a mesoporous silica inorganic scaffold, loaded with bioactive molecules as vancomycin or ATP and functionalized on the outer surface with 2-(propylsulfanyl)ethylene diamine. The pores were later blocked by the

---

<sup>70</sup> D.R. Radu, C.-Y. Lai, K. Jeftinija, E.W. Rowe, S. Jeftinija, V.S.-Y. Lin, *J. Am. Chem. Soc.* **2004**, *126*, 13216.

addition of cadmium sulfide nanoparticles functionalized with thioglycolic acid which can easily suffer an amidation reaction with the amine group anchored to the solid surface (gate closed). The addition of reductive molecules such as Cleland's reagent, (dithiothritol, DTT) or mercaptoethanol (ME), induced the reduction of the disulfide bridges between the cadmium sulfide nanoparticles and the hybrid materials, leading to the release of the entrapped cargo.

Another example of mesoporous systems capped with bulky species linked to the silica surface by -S-S- bridges was reported in 2008 by Feng and coworkers.<sup>71</sup> In this case the system consisted of poly(*N*-acryloxysuccinimide)-grafted mesoporous silica (named as PNAS-MS), in which the polymers are attached at the pore entrance of the particles. The working principle of the system is illustrated in figure 31.

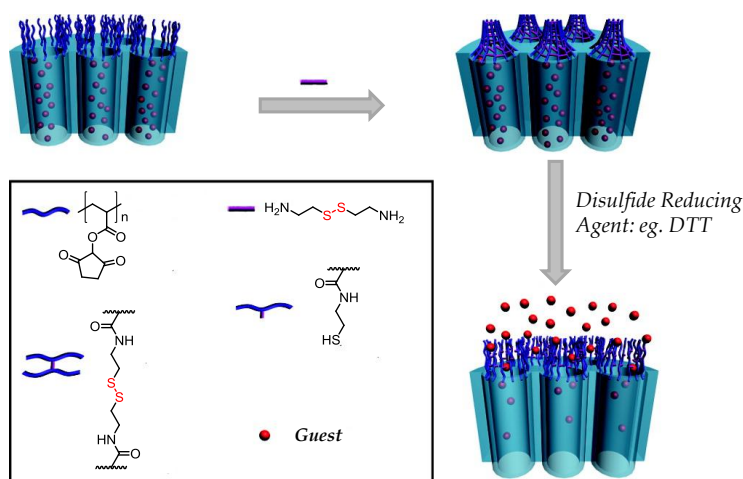


**Figure 31.** Schematic illustration of redox-responsive nanogated ensemble based on polymeric network-capped mesoporous silica. The addition of reducing agent determines the breakage of the disulfides bridges and the consequent controlled delivery. Adapted from *J. Am. Chem. Soc.*, **2008**, *130*, 14418-14419 © 2008 American Chemical Society.

<sup>71</sup> R. Liu, X. Zhao, T. Wu, P. Feng, *J. Am. Chem. Soc.*, **2008**, *130*, 14418.

After loading the porous matrix with dye molecules, the openings of PNAS-MS were blocked by the addition of cystamine, a disulfide-based bifunctional primary amine, which allowed polymer chains to be cross-linked through the reaction between cystamine and *N*-oxysuccinimide groups along the polymer chain. The polymeric network formed around the pore opening can be reopened by the cleavage of the disulfide bond of cystamine upon the addition of disulfide reducing agents such as DTT, with the subsequent cargo release.

A very recent example of disulfide rupture controlled delivery system was reported by Yang et al.<sup>72</sup> In this case MSNs were end-capped with collagen, making this one the first example of mesoporous material capped with an endogenous extracellular matrix component. In particular collagen was immobilized on the exterior surface of the MSNs by disulfide bonds easily reducible with DTT. The material was finally functionalized by grafting of Lactobionic acid as targeting moiety. These nanoparticles are selectively internalized in a human liver hepatocellular carcinoma cells.

The other fundamental redox approach to modulate the open-closed state of the molecular gate is based on the stabilization/destabilization of supramolecular complexes via the oxidation/reduction of suitable groups. The supramolecular systems that better fit with this paradigm are rotaxanes and pseudo-rotaxanes. The IUPAC Compendium of Chemical Terminology defines rotaxanes as “*molecules in which a ring encloses another rod-like molecule having end-groups too large to pass through the ring opening, whereas the pseudorotaxanes can be defined as rotaxane-like molecular assembly in which the threading component has ends small enough to permit threading or*

---

<sup>72</sup> Z. Luo, K. Cai, Y. Hu, L. Zhao, P. Liu, L. Duan, W. Yang, *Angew. Chem. Int. Ed.*, **2011**, 640-643.

dethreading of the macrocyclic molecule".<sup>73</sup> One of the first examples of controlled delivery systems based on the use of a pseudo-rodaxane as molecular gate was reported by Stoddart and coworkers.<sup>74</sup> In this case the authors loaded the MCM-41 mesoporous scaffold with an iridium complex dye and functionalized the inorganic silica based surface with a 1,5-dioxynaphtalene derivative (DNPD). Through the addition of cyclobis(paraquat-*p*-phenylene) (CBPQT<sup>4+</sup>) the formation of a pseudorotaxane on the external surface of the solid is induced. (see figure 32).

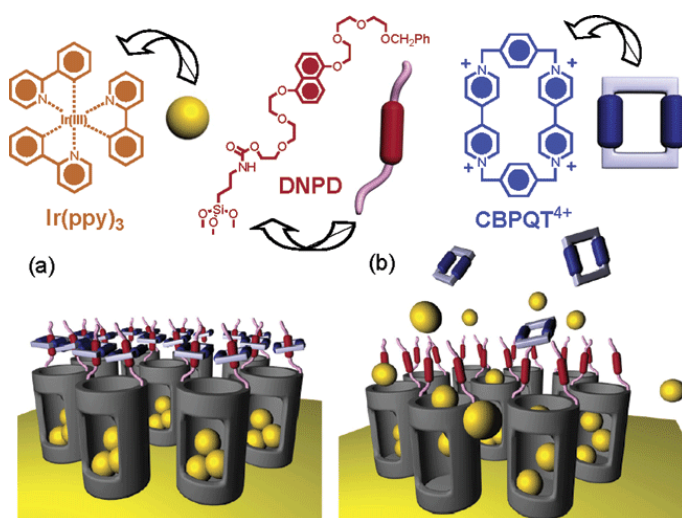


**Figure 32.** Graphical representations of operation of nanovalves. (a) The orifices of the nanopores (diameter 2 nm) are covered with pseudorotaxanes (formed between DNPD and CBPQT<sup>4+</sup>) which trap the luminescent  $\text{Ir(ppy)}_3$  molecules inside the nanopores. (b) Upon their reduction, the CBPQT<sup>2+</sup> bisradical dication is released and so allow the  $\text{Ir(ppy)}_3$  to escape. Adapted from *J. Am. Chem. Soc.*, **2004**, 126, 3370. Copyright © 2004 American Chemical Society.

<sup>73</sup> A. D. McNaught, A. Wilkinson, IUPAC. *Compendium of Chemical Terminology*, 2nd ed. (the "Gold Book"). Blackwell Scientific Publications, Oxford, **1997**. XML on-line corrected version: M. Nic, J. Jirat, B. Kosata; updates compiled by A. D. Jenkins, <http://goldbook.iupac.org>, 2006 created by M. Nic, J. Jirat, B. Kosata; updates compiled by A. D. Jenkins.

<sup>74</sup> R. Hernandez, H.-R Tseng, J.W. Wong, J.F. Stoddart, J.I. Zink, *J. Am. Chem. Soc.*, **2004**, 126, 3370-3371.

### 5.1.6.2 Redox-driven Molecular Gates

This new non-covalent supramolecular ensemble blocks the pores preventing the delivery of the dye. If a reductive agent is added to the mixture (in this case  $\text{NaCNBH}_3$ ) the reduction of DPND starts a spontaneous dethreading of the CBPQT<sup>4+</sup> ring allowing the release of the guest.

The evolution of that gated system is the achievement of a total reversible hybrid material able to be open or closed on command in a reversible manner. This kind of material was synthesized by Stoddart et al. in 2005.<sup>75</sup> In this case the authors firstly synthesized a [2]rotaxane bearing a DNPD and a tetrathiafulvalene moiety as redox center, linked each other through a oligoethylenglycol chain. (see figure 33).

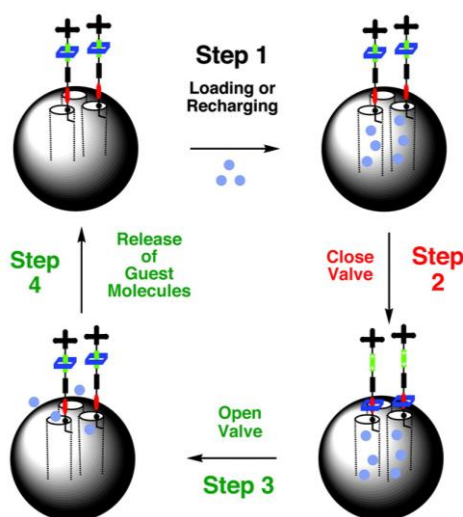


**Figure 33.** Schematic representation of the mechanism for the operation of the reversible nanovalve. Adapted from *Natl. Acad. Sci. USA*, **2005**, *102*, 10029.

The rotaxane was completed by the presence of a rigid spacer and a CBPQT<sup>4+</sup> as movable molecule. The redox-induced movement was

<sup>75</sup> T.D. Nguyen, H.-R. Tseng, P.C. Celeste, A.H. Flood, Y. Liu, J.F. Stoddart, J.I. Zink, *Proc. Natl. Acad. Sci. USA*, **2005**, *102*, 10029-10034.

dependent on the addition of oxidant or reducing species that changed the oxidation state of TTF and, consequently, the preference of CBPQT<sup>4+</sup> for TTF or DNPD groups. With this movement the state of the gate was changed from closed to open at will.

### **5.1.6.3 pH-Driven Molecular Gates**

pH changes is another stimulus that can be employed to regulate opening-closing process in gated materials. In this area, organic molecules that contain protonable functional groups had been used for the design and preparation of pH-driven molecular gate-like scaffoldings. Changes in their steric hindrance induced by variations in their size/shape or attraction/repulsion interactions with other charged species can finely regulate the open-close protocol. Among the most important advantages provided by pH-driven molecular gates there are, the reversibility of the delivery protocol and the possibility to operate in aqueous media (*vide infra*). Furthermore, it is possible to finely control the pH at which the gate-state is open/closed by selecting a suitable pH sensitive molecular unit anchored onto the outer surface of the silica support. Moreover, these systems can be applied to intracellular controlled delivery operations, thanks to the pH difference between the extracellular environment (cytosol, pH 7) and endosomes and lysosomes (pH 5). In this field R. Martínez-Mañez and coworkers developed the first pH driven molecular gate in 2004.<sup>76</sup> This new hybrid material consists of a particular solid support belonging to the MCM-41 family (UVM-7), which was functionalized on the outer surface with poly-aminic trialkoxysilane derivatives and in the

---

<sup>76</sup> R. Casasús, M. D. Marcos, R. Martínez-Mañez, J. V. Ros-Lis, J. Soto, L. A. Villaescusa, P. Amorós, D. Beltrán, C. Guillem, J. Latorre, *J. Am. Chem. Soc.*, **2004**, *126*, 8612-8613.

### 2.1.6.3 pH-Driven Molecular Gates

inner of the pores with thiol groups. To verify the correct pH dependent open-close paradigm squaraine was added to the reaction mixture, because this particular dye is characterized by an intense light blue color that is lost when squaraine reacts with thiols to give a colorless derivative.<sup>77</sup> At acidic pH the repulsions between the protoned aminic groups impeded the dye entrance into the pores and, as a consequence, the solution remains light blue. However if the solution is brought to basic pH the amines are deprotonated and the electrostatic repulsions do not take place. In this situation squaraine can reach the interior part of the pores where are located the thiols, react with them and give a colorless solution.

Some years later the same R&D group developed another pH driven molecular gate. In this case the authors prepared a calcined MCM-41 solid support and loaded the pores with the dye molecule  $\text{Ru}(\text{bipy})_3^{2+}$ .<sup>78</sup> Then the surface was functionalized by the grafting of a polyamine trialkoxysilane derivative. The resulting hybrid material can function as a molecular gate. In fact acidic pH induces the amine protonation and the consequent electrostatic repulsion that determined the pore blocking. Otherwise if the pH was brought to neutral value the poly-amines were in the deprotonated form that granted the cargo free diffusion from the inner of the pores to the solution (figure 34). The open-close protocol of this hybrid system could also be controlled, at a fixed pH, by the presence of different anions that display certain coordination ability with the tethered amines. In fact at pH 6, when the amines are in their protonated form, large

---

<sup>77</sup> J. V. Ros-Lis, B. García-Acosta, D. Jiménez, R. Martínez-Mañez, F. Sancenón, J. Soto, F. Gonzalvo, M. C. Valldecabres, *J. Am. Chem. Soc.*, **2004**, *126*, 4064-4065.

<sup>78</sup> a) R. Casasús, E. Climent, M. D. Marcos, R. Martínez-Mañez, F. Sancenón, J. Soto, P. Amorós, J. Cano, E. Ruiz, *J. Am. Chem. Soc.*, **2008**, *130*, 1903-1917.

anions can block the pores upon coordination, whereas small anions do not. A step forward was the employment of a similar hybrid material for selective chemical recognition processes. In particular the pores of an MCM-41 solid support were loaded with  $\text{Ru}(\text{bipy})_3^{2+}$  dye and then the scaffold surface was functionalized with the same trialkoxysilane polyamine derivative. The designed material was able to differentiate GMP from ATP and ADP.<sup>79</sup>

The above reported examples deal with delivery processes induced by the switch from acidic to neutral pH. Other systems able to selectively deliver the cargo at acidic pH have also been described. For example Xiao et al. reported a molecular gate capable to release vancomycin at acidic pH by anchoring carboxylates on porous SBA-15 silica rods and using the positively charged poly-(dimethyldiallylammonium chloride) (PDDA) as blocking agent.<sup>80</sup>

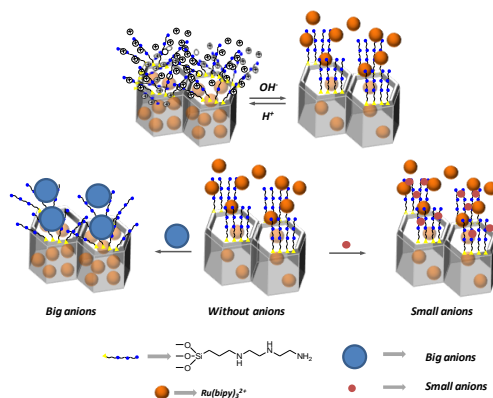


**Figure 34.** Schematic representation of pH driven molecular gate: the acidic pH induces the protonation of amines that repel each other blocking the pores. At basic pH determines the amines are unprotonated allowing the delivery of the dye.

<sup>79</sup> R. Casasús, E. Aznar, M. D. Marcos, R. Martínez-Máñez, F. Sancenón, J. Soto, P. Amorós, *Angew. Chem.Int. Ed.*, **2006**, 45, 6661.

<sup>80</sup> Q. Yang, S. Wang, P. Fan, L. Wang, Y. Di, K. Lin, F. -S. Xiao, *Chem. Mater.* **2005**, 17, 5999-6003

At acidic pH the protonation of carboxylates resulted in the disruption of the coulombic interactions with the positively charged polyelectrolyte PDDA, with the subsequent release of the vancomycin.

Apart from carboxylates and amines also rotaxanes have been used as pH triggerable molecular gates. The first example of a hybrid material functionalized with a pH tunable rotaxane was reported by Stoddart and Zink in 2006.<sup>81</sup> In this case a [2]pseudorotaxane was synthesized via encirclement of dialkylammonium cations (grafted in the outer surface of a mesoporous material that was previously loaded with coumarin 460) with the macrocyclic polyether dibenzo[24]crown-8 (DB24C8), through hydrogen-bonding interactions (see figure 35). The formation of the 1:1 complex between the ammonium cation and the macrocycle leads to pore closure, whereas addition of a base induced the dethreading of the [2]pseudorotaxane due to the deprotonation of the dialkylammonium groups, releasing the coumarin 460 from the pores to the solution. In further studies, the same authors found that addition of other cationic species (fluorodialkylammonium salts and metal ions) were able to activate the delivery of the probe molecules by competitive binding with the macrocycle, inducing a shift of the equilibrium between the ring and the stalk.<sup>82</sup>

Another supramolecular system, that attracted great attention for the development of molecular gates based in inclusion complexes, are cyclodextrins (CD) as blocking agents. Using CDs Kim's group have

---

<sup>81</sup> T.D. Nguyen, K.C.-F. Leung, M. Liang, C.D. Pentecost, J.F. Stoddart, J.I. Zink, *Org. Lett.* **2006**, *8*, 3363-3366.

<sup>82</sup> K. C. -F. Leung, T. D. Nguyen, J. F. Stoddart, J. I. Zink, *Chem. Mater.* **2006**, *18*, 5919.

reported a pH-responsive pseudorotaxane-based gated material.<sup>83</sup> In this work they loaded silica mesoporous support with calcein and anchored polyethyleniminic (PEI) stalks on the outer surface.

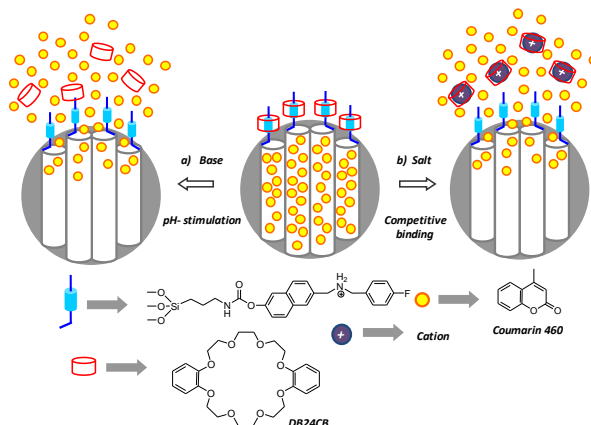


**Figure 35.** Graphical representation of the operating supramolecular nanovalves from DB24C8/dialkylammonium tethered MCM-41 porous silica particles.

Then, the pores were closed by addition of  $\alpha$ - and  $\gamma$ -cyclodextrins at pH 11.0 due to the formation of inclusion complexes with the PEI polymer (of 1:1 PEI: $\alpha$ -CD and 2:1 PEI: $\gamma$ -CD stoichiometries). The new gated system prevented the release of calcein at pH 11.0 whereas when pH was fixed at 5.5, calcein release was observed due to amine protonation and subsequent dethreading of the polypseudorotaxanes.

Very recently, a stimulated release of size-selected cargos in succession from mesoporous silica nanoparticles containing the large Hoechst 33342 and the smaller *p*-coumaric acid dyes was reported. This system was able to release both dyes by the application of two different stimuli, first, lowering the pH, and then by adding a reducing agent.<sup>84</sup> In this case a different

<sup>83</sup> C. Park, K. Oh, S.C. Lee, C. Kim, *Angew. Chem. Int. Ed.* **2007**, *46*, 1455-1457.

<sup>84</sup> C. Wang, Z. Li, D. Cao, Y. -L. Zhao, J. W. Gaines, O. A. Bozdemir, M. W. Ambrogio, M. Frasconi, Y. Y. Botros, J. I. Zink, J. F. Stoddart, *Angew. Chem. Int. Ed.*, **2012**, *51*, 5460-5465.

### 2.1.6.3 pH-Driven Molecular Gates

approach was followed, in fact the  $\beta$ -CD rings were directly attached onto MCM-41 surface through a linker that encloses disulfide units. The  $\beta$ -CD cavities was then plugged with methyl orange (MO), able to form reversible inclusion complexes in response to changes in pH. In this gated material, the small molecules of *p*-coumaric acid were released after protonation of MO (due to the displacement of MO from the  $\beta$ -CD rings), and the large ones Hoechst 33342 were released after cleavage of the disulfide bonds upon addition of mercaptoethanol (ME). Therefore,  $\beta$ -CD rings not only acted as gatekeepers for the larger molecules but also allowed small molecules diffusion to the solution when pH was decreased and MO was moved out of their cavities. Figure 36 shows a schematic representation of the dual-cargo release process.

The above described examples show the potential applicability of pH as external stimuli for cargo release. pH is one of the most studied stimuli for the development of gate-like materials thanks to their easy measurement and modification.

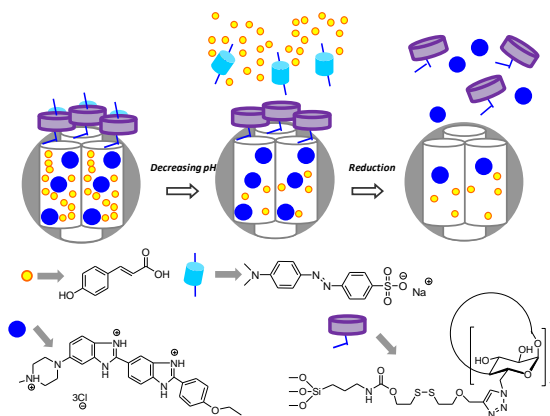


**Figure 36.** Schematic representation of the dual-cargo release process. The dual cargos can be released one step at a time by, first of all, lowering the pH and then adding mercaptoethanol.

#### 5.1.6.4 Temperature Driven Molecular Gates

As reported above there are many examples of gated hybrid materials. However, very few of them are triggered by temperature.

The first system was reported by G. P. Lopez et al. In particular this nano-device was prepared using modified SMP functionalized with the well-known temperature sensitive polymer *N*-isopropylacrylamide (PNIPAAm). This polymer exhibits a hydrophilic-hydrophobic transition at a “lower critical solution temperature” (LCST) of about 32 °C in water. At temperatures below the LCST, the polymer is in the coil conformation (hydrated), while above the LCST it is in the globule or collapsed state (dehydrated). Temperature triggered control of molecular transport through the porous network of the hybrid particles was demonstrated by measuring release of fluorescein. The fluorescein in the silica/PNIPAAm particles was released slowly at room temperature (below the LCST of PNIPAAm) and faster at 40 °C (above the LCST). This is likely due to the PNIPAAm chain being hydrated and expanded at room temperature. At 40 °C, the PNIPAAm is dehydrated and collapsed so that the entrapped fluorescein can readily diffuse through the porous network and be released from the microparticles.<sup>85</sup>

Another important example of temperature triggerable gated material was reported by Aznar and coworkers. In particular the authors prepared a silica based mesoporous nanoscopic hybrid material, loaded with safranin-O and functionalized on the surface with octadecyltrimethoxysilane.<sup>86</sup> These alkyl chains are not able to close the

---

<sup>85</sup> Q. Fu, G. V. R. Rao, T. L. Ward, Y. Lu, G. P. López, *Langmuir*, **2007**, 23, 170-174.

<sup>86</sup> E. Aznar, L. Mondragón, J. V. Ros-Lis, F. Sancenón, M. D. Marcos, R. Martínez-Mañez, J. Soto, E. Pérez-Payá, P. Amorós, *Angew. Chem. Int. Ed.*, **2011**, 50, 11172-11175.

### 5.1.6.4 Temperature-Driven Molecular Gates

pores but are suitable to interact with paraffins via London forces setting up a hydrophobic layer that could block the pores, depending on the magnitude of the alkyl chains, inhibiting guest release. An increase of the temperature above paraffin melting point results in the paraffin melting and the subsequent release of the entrapped guest (see figure 37).

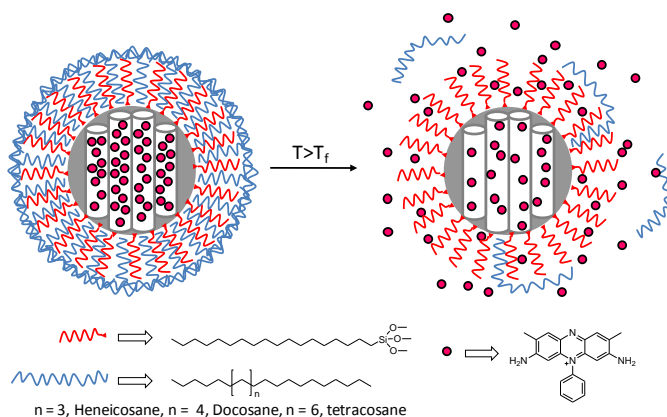


**Figure 37.** Schematic representation of the gated material functionalized with octadecyltrimethoxysilane and capped with paraffin. The delivery of the entrapped guest (safranin-O) is triggered when temperature rises above paraffin melting point.

A similar approach was followed by Bein and co-workers when they described a temperature-driven molecular gate based on the use of double-strand DNA.<sup>87</sup> The authors grafted biotin-labeled DNA double strands on the pore outlets of colloidal mesoporous silica nanoparticles through a click chemistry reaction and then loaded the material with fluorescein. Finally, the pores were closed by adding the protein avidin through the formation of the strong biotin-avidin complex. The controlled delivery of the cargo was induced by heating up to the specific melting temperature of the double stranded DNA sequence, that determined the opening of the pores.

<sup>87</sup> A. Schlossbauer, S. Warncke, P. M. E. Gramlich, J. Kecht, A. Manetto, T. Carell, T. Bein, *Angew. Chem. Int. Ed.*, **2010**, 49, 4734-4737.

### 5.1.6.5 Biochemical Triggers

This section will focus on nanoscopic mesoporous silica nanoparticles (MSNs) functionalized with bioactive triggerable molecules. The great attention that attracted these hybrid systems rose from the possibility of using tailor-made biomolecules that may provide fine selectivity in the design of advanced gate-opening devices.

The first example of gated mesoporous system that responds to an enzyme was described by Stoddart et al. and consisted in a mesoporous support with a [2]rotaxane capped with an ester-linked adamantyl stopper.<sup>88</sup> Upon addition of porcine liver esterase the bulky adamantyl stopper was released allowing cargo delivery. One year later Martínez-Máñez and co-workers demonstrated that the attachment of a lactose derivative as gatekeeper on the surface of nanoscopic silica mesoporous supports provided a suitable method for the design of mesoporous systems, that were able to deliver entrapped guests by a bio-controlled uncapping using  $\beta$ -D-galactosidase, due to the enzymatic hydrolysis of the glycosidic bond in the anchored lactose.<sup>89</sup> Some years later, in order to improve the efficiency of this system, the authors developed nanoscopic MCM-41 silica supports loaded with a dye and functionalized, on the pore outlets, with different commercially available hydrolyzed starch derivatives (see figure 38). The obtained nanoscopic hybrid materials were able to deliver anticancer drug doxorubicin into intracellular media of HeLa and LLC-PK1 cells.

---

<sup>88</sup> K. Patel, S. Angelos, W.R. Dichtel, A. Coskun, Y.-W. Yang, J.I. Zink, J.F. Stoddart, *J. Am. Chem. Soc.*, **2008**, *130*, 2382-2383.

<sup>89</sup> A. Bernardos, E. Aznar, M. D. Marcos, R. Martínez-Máñez, F. Sancenón, J. Soto, J. M. Barat, P. Amorós, *Angew. Chem. Int. Ed.*, **2009**, *48*, 5884-5887.

### 5.1.6.5 Biochemical Triggers

Heise et al. loaded silica nanoparticles with fluorescein-conjugated dextran molecules and grafted, onto the external surface, a specific peptide sequence containing terminal bulky fluorenylmethoxycarbonyl (Fmoc) fragments.<sup>90</sup> The final material was able to release their cargo only upon addition of thermolysin to the aqueous suspensions of the hybrid nanoparticles. Addition of this enzyme induced the cleavage of the peptide sequence that removed the bulky Fmoc groups and, as a consequence, delivery of the dye was observed.

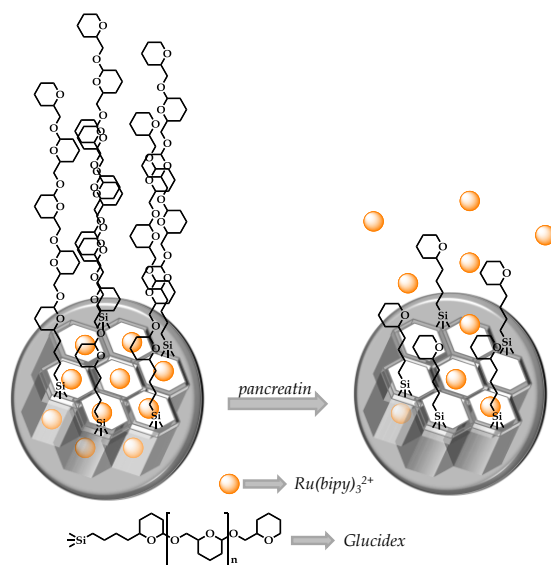


**Figure 38.** Schematic representation of the gated material capped with hydrolyzed starch derivatives (Glucidex 47, Glucidex 39 and Glucidex 29) and their opening in the presence of pancreatin.

Martínez-Máñez et al. prepared a MCM-41 support loaded with the dye  $\text{Ru}(\text{bipy})_3^{2+}$  and containing onto their surface peptide sequences anchored by click chemistry. Aqueous solutions of this material are unable to release the entrapped dye, whereas addition of targeted proteolytic enzymes

<sup>90</sup> P. D. Thornton, A. Heise, *J. Am. Chem. Soc.*, **2010**, *132*, 2024-2028.

induced the enzymatic hydrolysis of the peptide sequences with the subsequent diffusion of the ruthenium complex.<sup>91</sup>

## **5.2 Objectives**

As reported above, our aim, in this second part of the PhD thesis, was the design and synthesis of new systems for the controlled release of molecules with possible future application in nanomedicine. When we set up the project for this PhD thesis there were very few examples of enzyme triggerable nanoscopic mesoporous hybrid systems for controlled delivery processes. For this reason it was in our aim to synthesize a different trialkoxysilane derivatives capable to block the mesopores and able to suffer enzymatic hydrolysis.

As reported above another important stimulus which can be used to induce controlled delivery is light. However, when this work started, there were a certain lack of mesoporous systems capped with photocleavable molecules for controlled delivery. Thus we decided to contribute to this field synthesizing the second example of a gated material able to release its cargo upon the photodegradation of the molecular gate.

Specifically our aims were:

- Design, synthesis, characterization and application of a new nanoscopic organic-inorganic hybrid systems able to release target molecules in the presence of esterase enzyme.

---

<sup>91</sup> C. Coll, L. Mondragón, R. Martínez-Mañez, F. Sancenón, M. D. Marcos, J. Soto, P. Amorós, E. Pérez-Payá, *Angew. Chem. Int. Ed.*, **2011**, 50, 2138-2140.

## 5.2 Objectives

- Design, synthesis, characterization and application of a dual enzyme-triggerable system for controlled release induced by the treatment with different enzymes, specifically urase and amidase.
- Design, synthesis, characterization and application of an organic-inorganic nanoscopic hybrid system for the selective controlled release into targeted senescent cells.
- Design, synthesis and characterization of a new phototriggerable molecular gate able to control the diffusion processes from the inner to the outer of mesoporous silica nanoparticles channels, upon irradiation at a specific wavelength.

The following sections will detail the synthetic procedures, the characterization, main features and the *in vitro* controlled delivery studies of the organic-inorganic hybrid materials obtained. The application of these systems for the controlled delivery in cells will also be reported.

***Chapter 6:***

***Design of enzyme-mediated controlled release systems based on silica mesoporous supports capped with ester-glycol groups***



***Design of enzyme-mediated controlled release systems based on silica mesoporous supports capped with ester-glycol groups***

Alessandro Agostini,<sup>[a]</sup> Laura Mondragón,<sup>[a]</sup> Lluís Pascual,<sup>[a]</sup> Elena Aznar,<sup>[a]</sup> Carmen Coll,<sup>[a]</sup> Ramón Martínez-Mañez,<sup>\*,[a]</sup> Félix Sancenón,<sup>[a]</sup> Juan Soto,<sup>[a]</sup> M. Dolores Marcos,<sup>[a]</sup> Pedro Amorós,<sup>[c]</sup> Ana M. Costero,<sup>\*, [b]</sup> Margarita Parra<sup>[b]</sup> and Salvador Gil<sup>[b]</sup>

<sup>[a]</sup>*Centro de Reconocimiento Molecular y Desarrollo Tecnológico (IDM), Unidad Mixta Universidad Politécnica de Valencia-Universidad de Valencia. Departamento de Química, Universidad Politécnica de Valencia, Camino de Vera s/n, 46022, Valencia, Spain.*

*CIBER de Bioingeniería, Biomateriales y Nanotecnología (CIBER-BNN).*

<sup>[b]</sup>*Centro de Reconocimiento Molecular y Desarrollo Tecnológico (IDM), Unidad Mixta Universidad Politécnica de Valencia-Universidad de Valencia, Spain. Departamento de Química Orgánica, Facultad de Ciencias Químicas, Universitat de Valencia, 46100 Burjassot, Valencia, Spain.*

<sup>[c]</sup>*Institut de Ciència del Materials (ICMUV), Universitat de València. P.O. Box 22085, E-46071 València, Spain.*

***Received: March 25, 2012,***

***Revised: September 13, 2013***

***Published online: September 21, 2012***

*Langmuir*, 2012, 28, 14766–14776

## **6.1 Abstract**

An ethylene glycol capped hybrid material for the controlled release of molecules in the presence of esterase enzyme has been prepared. The final organic-inorganic hybrid solid **S1** was synthesized by a two step procedure. In the first step the pores of an inorganic MCM-41 support (in the form of nanoparticles) were loaded with [Ru(bipy)<sub>3</sub>]Cl<sub>2</sub> complex and then, in the second step, the outer of the pores were functionalized with ester-glycol moieties than acted as molecular caps. In the absence of an enzyme the release of the complex from aqueous suspensions of **S1** at pH 8.0 is inhibited due to the steric hindrance imposed by the bulky ester-glycol moieties.

Upon the addition of esterase enzyme, delivery of the ruthenium complex was observed due to the enzymatic hydrolysis of the ester bond in the anchored ester-glycol derivative inducing the release of oligo(ethylene glycol) fragments. The hydrolysis of the ester bond results in a size reduction of the appended group therefore allowing the delivery of the entrapped cargo.

The **S1** nanoparticles were not toxic for cells as demonstrated by cell viability assays using HeLa and MCF-7 cell lines and found associated to lysosomes as shown by confocal microscopy. However when **S1** nanoparticles were filled with the cytotoxic drug camptothecin (**S1-CPT**), **S1-CPT**-treated cells undergo cell death as a result of **S1-CPT** cell internalization and subsequent cellular enzyme-mediated hydrolysis and aperture of the molecular gate that induced the release of the camptothecin cargo. These findings point to a possible therapeutical application of these nanoparticles.

## **6.2 Introduction**

The design of nanoscopic hybrid materials containing “molecular gates” able to selectively release an entrapped cargo in the presence of external stimuli has recently attracted great attention.<sup>1</sup> In this area, and as an alternative to polymer materials, mesoporous silica nanoparticles (MSN) have been used due to their unique properties such as large load capacity, biocompatibility and easy functionalization.<sup>2</sup> The incorporation in these supports of gated ensembles has recently been used for the design of on-command delivery nano-devices using diverse physical and chemical target-dependent triggers.<sup>3</sup> For instance, MSN-based supports displaying controlled release have been prepared using changes in pH,<sup>4</sup> redox reactions<sup>5</sup> and light.<sup>6</sup> Additionally, the preparation of nanogated MSN designed to trigger cargo release using bio-molecules has also been recently reported. For instance, antigen-antibody interaction,<sup>7</sup> hybridization of single stranded DNA<sup>8</sup> and enzymes have been used as keys in pore opening protocols. In this field the development of enzyme-responsive biogated MSN is appealing taking into account the possibility of prepare tailor-made sequences that may provide fine selectivity in the design of advanced gate-opening devices. However, despite these interesting features, this is a barely studied field. The first example of gated mesoporous system that responds to an enzyme was described by Stoddart’s group and consisted in a mesoporous support with a [2]rotaxane capped with an ester-linked adamantyl stopper.<sup>9</sup> Upon addition of porcine liver esterase the bulky adamantly stopper was released allowing cargo delivery. Bein and co-workers prepared a mesoporous support capped with the couple avidin-biotin that was able to release fluorescein upon addition of protease trypsin.<sup>10</sup> Our group has reported the use of an MCM-

41 support capped with lactose that was able to release the entrapped cargo upon addition of  $\beta$ -D-galactosidase due to the hydrolysis of the glycosidic bond.<sup>11</sup> Also hydrolyzed starch has been used as molecular cap in the preparation of a hybrid material that was able to deliver its cargo in the presence of pancreatin enzyme.<sup>12</sup> Kim et al. prepared silica nanoparticles functionalized with  $\beta$ -cyclodextrin as gate-keepers that are able to release calcein upon addition of lipase and amylase enzymes.<sup>13</sup> Heise and coworkers used certain peptide sequences as molecular caps that were hydrolyzed with thermolysin enzyme.<sup>14</sup> Very recently, a peptide sequence was grafted, through a click chemistry reaction, in the pores outlets of mesoporous silica nanoparticles.<sup>15</sup> This hybrid system was able to release the entrapped cargo upon addition of a protease enzyme. Finally, Qu and coworkers prepared MCM-41 silica nanoparticles loaded with rhodamine B and capped with a double stranded DNA fragment.<sup>16</sup> Addition of endonucleases induced the rupture of the double strand allowing cargo release.

Moreover, capping systems could be envisioned based on the large number of possibilities to explore that could bring enzyme-mediated reactions. In particular, esterases are a class of enzymes included in the hydrolases family which are able to hydrolyze ester bonds in several substrates. Esterases of different types are extended in the living systems and might be used as effective triggers for controlled release applications. Moreover, from an organic chemistry point of view, the formation of esters is a classical reaction and a number of suitable capping systems can be prepared using ester linkages. In addition, cell internalization of mesoporous silica nanoparticles via endocytosis will allow the access of the material to lysosomal hydrolytic enzymes (such as esterases) which will

activate the release of the payload. Within this context, and bearing in mind our interest in the preparation of gated MSN for delivery applications using biomolecules we report herein the synthesis of oligo(ethylene glycol) capped MSN that are selectively uncapped using an esterase (crude esterase from porcine liver) via rupture of an ester bond.

### **6.3 Experimental Section**

**Methods:** XRD, TG Analysis, elemental analysis, EDX microscopy, N<sub>2</sub> adsorption-desorption and fluorescence techniques were employed to characterize the prepared materials. Powder X-ray measurements were performed on a Philips D8 Advance diffractometer using Cu K<sub>α</sub> radiation. Thermo-gravimetric analysis were carried out on a TGA/SDTA 851e Mettler Toledo balance, using an oxidant atmosphere (air, 80 mL/min) with a heating program consisting on a heating ramp of 10 °C per minute from 393 to 1273 K and an isothermal heating step at this temperature during 30 minutes. TEM images were obtained with a 100 kV Philips CM10 microscope. N<sub>2</sub> adsorption-desorption isotherms were recorded on a Micromeritics ASAP2010 automated sorption analyser. The samples were degassed at 120 °C in vacuum overnight. The specific surface areas were calculated from the adsorption data in the low pressures range using the BET model. Pore size was determined following the BJH method. Fluorescence spectroscopy was carried out on a Felix 32 Analysis Version 1.2 (Build 56) PTI (Photon Technology International). <sup>1</sup>H and <sup>13</sup>C nuclear magnetic resonance (NMR) were acquired with a Varian 300 spectrometer (Sunnyvale, CA, USA). Live cellular internalization studies were performed with a Cytomics FC 500 (Beckman Coulter Inc.) and a confocal Leica microscope handled with a TCS SP2 system, equipped with an

acoustic optical beam splitter (AOBS). Cell viability measurements were carried out with a Wallac 1420 workstation. For the electroporation of cells, a Gene Pulser Xcell™ Eukaryotic System was employed (Bio-rad Laboratories S.A., Spain).

**Reagents:** The chemicals tetraethylorthosilicate (TEOS), *n*-cetyltrimethylammonium bromide (CTAB), sodium hydroxide (NaOH), [Ru(bipy)<sub>3</sub>]Cl<sub>2</sub>, tetraethylenglycol, 3-chloropropanoyl chloride, (3-mercaptopropyl)triethoxysilane, sodium iodide, potassium carbonate and sodium carbonate were purchased from Sigma-Aldrich. Analytical-grade solvents were from Scharlab (Barcelona, Spain). D-MEM with L-glutamine, foetal calf serum (FCS), trypan blue solution (0.4%) cell culture grade, trypsin, wheat germ agglutinin Alexa Fluor 647, and Hoechst 33342 were provided by Gibco-Invitrogen. The cell proliferation reagent WST-1 was obtained from Roche Applied Science. Annexin V-FITC and propidium iodide were purchased from BD Pharmingen. Camptothecin was provided by Sequoia Research Products, Ltd. All reactives were used as received.

**Synthesis of the silica mesoporous nanoparticles support (MCM-41):** The MCM-41 mesoporous nanoparticles were synthesized by the following procedure: *n*-cetyltrimethylammoniumbromide (CTAB, 1.00 g, 2.74 mmol) was first dissolved in 480 mL of deionized water. Then a 3.5 mL of NaOH 2.00 M in deionized water was added to the CTAB solution, followed by adjusting the solution temperature to 80 °C. TEOS (5.00 mL, 2.57 · 10<sup>-2</sup> mol) was then added dropwise to the surfactant solution. The mixture was allowed stirred for 2 h to give a white precipitate. Finally the solid product was centrifuged, washed with deionized water and ethanol, and was dried

at 60 °C (MCM-41 as-synthesized). To prepare the final porous material (MCM-41), the as-synthesized solid was calcined at 550 °C using oxidant atmosphere for 5 h in order to remove the template phase.

**Synthesis of 2-(2-(2-hydroxyethoxy)ethoxy)ethyl 3-chloropropanoate 1:**

Tetraethylenglycol (1.54 g, 7.93 mmol) and Na<sub>2</sub>CO<sub>3</sub> (2 g) were suspended in diethyl ether (25 mL). Then, 3-chloropropanoyl chloride (0.5 g, 3.94 mmol) was added dropwise to the previous suspension. The mixture was stirred at room temperature during 3 hours. Then the crude was filtered in order to eliminate the Na<sub>2</sub>CO<sub>3</sub> and the solvent was eliminated by rotary evaporation. Yield 90.5%. <sup>1</sup>H NMR (300Mhz, CDCl<sub>3</sub>): δ 2.79 (t, 2H, CH<sub>2</sub>-CO), δ 3.5-3.8 (m, 16H, O-CH<sub>2</sub>), δ 4.31 (t, 2H, CH<sub>2</sub>-Cl) ppm. <sup>13</sup>C NMR: δ 37.87, 39.37, 61.60, 62.12, 64.39, 69.44, 70.64, 70.92, 71.03, 73.08, 170.76 ppm.

**Synthesis of the molecular gate 2: 1** (482 mg, 1.69 mmol), NaI (327 mg, 2.2 mmol) and anhydrous CH<sub>3</sub>CN (25 mL) were refluxed during 1 hour. Then, anhydrous K<sub>2</sub>CO<sub>3</sub> (500 mg, excess), and (3-mercaptopropyl)triethoxysilane (350 μl, 1.56 mmol) were added to the same flask and stirred at reflux overnight. The reaction mixture was then filtered, the CH<sub>3</sub>CN was eliminated by rotary evaporation and the residue taken up in CH<sub>2</sub>Cl<sub>2</sub> and filtered once more in order to eliminate the remaining carbonate. Yield: 72.1%. <sup>1</sup>H NMR (300Mhz, CDCl<sub>3</sub>): δ 0.72 (m, 2H, CH<sub>2</sub>-Si), δ 1.17-1.1.23 (m, 9H, CH<sub>3</sub>-CH<sub>2</sub>), δ 1.55-1.73 (m, 2H, CH<sub>2</sub>-CH<sub>2</sub>-CH<sub>2</sub>), 2.41-2.85(m, 6H, 2CH<sub>2</sub>-S; CH<sub>2</sub>-CO), 3.41-3.81(m, 22H, CH<sub>2</sub>-O) ppm. <sup>13</sup>C NMR: δ 10.04, 18.49, 23.32, 26.93, 35.03, 35.25, 58.56, 61.32, 61.70, 63.88, 69.28, 69.96, 70.39, 70.43, 70.64, 70.70, 70.76, 72.71, 72.80, 171.17 ppm.

**Synthesis of solid S1:** With the aim to obtain solid **S1**, MCM-41 calcined (512 mg) was suspended in anhydrous CH<sub>3</sub>CN (25 mL) and then [Ru(bipy)<sub>3</sub>]Cl<sub>2</sub> (302 mg, 0.404 mmol) was added to the suspension. Then 10 ml of CH<sub>3</sub>CN were collected with a Dean-Stark apparatus from reaction mixture, in order to remove the water present in the pores of the solid by azeotropic distillation. Afterwards the mixture was stirred at room temperature during 24 hours. Subsequently compound **2** (1.25 g, 2.58 mmol) was added and the mixture was stirred during 5.5 hours. Then the solid was filtered, washed with distilled water, suspended in water in a flask and stirred at room temperature overnight in order to remove all the [Ru(bipy)<sub>3</sub>]Cl<sub>2</sub> present outside of the pores. Afterwards the solid was filtered and dried at 38 °C overnight.

**Synthesis of solid S1-CPT:** With the aim to obtain solid **S1-CPT**, MCM-41 calcined (84 mg) was suspended in a mixture of anhydrous CH<sub>3</sub>CN (10 mL) and anhydrous methanol (10 mL) and then camptothecin (47 mg, 0.135 mmol) was added to the final suspension. Afterwards the mixture was stirred at room temperature during 24 hours. Subsequently compound **2** (400 mg, 0.905 mmol) was added and the mixture was stirred overnight. Then the solid was filtered, washed with distilled water, methanol, acetone, suspended in methanol in a flask and stirred at room temperature overnight in order to remove all the camptothecin present outside of the pores. Afterwards the solid was filtered and dried at 38 °C overnight.

**Cell Culture Conditions:** The HeLa human cervix adenocarcinoma and the MCF-7 breast cancer cells were purchased from the German Resource Centre for Biological Materials (DSMZ) and were grown in D-MEM

supplemented with 10% FCS. Cells were maintained at 37 °C in an atmosphere of 5% carbon dioxide and 95% air and underwent passage twice a week. Cells were electroporated with the plasmid pEGFP from Clontech containing the mouse gene Lamp1 kindly donated by Jennifer Lippincott (Eunice Kennedy Shriver National Institute of Child Health and Human Development, Bethesda, MD, USA).

**WST-1 Cell Viability Assay:** Cells were cultured in sterile 96-well microtiter plates at a seeding density of  $2.5 \times 10^3$  and  $3 \times 10^3$  cells/well for HeLa and MCF-7, respectively, and they were allowed to settle for 24 h. **S1** in DMSO was added to cells at a final concentration of 200, 100 and 50  $\mu\text{g}/\text{mL}$ . After 23 hours, WST-198 (10  $\mu\text{L}$  of a 5  $\text{mg}/\text{mL}$  solution) was added to each well. Cells were further incubated for 1 h (a total of 24 h of incubation was therefore studied), and absorbance was measured at 595 nm. Two independent experiments containing sixtuplicates were performed. Results were expressed as (mean  $\pm$  SE).

**Live Confocal Microscopy S1 Cellular Internalization:** HeLa and MCF-7 cells were seeded in 24 mm  $\phi$  glass coverslips in six-well plates at a seeding density of  $5 \times 10^4$  cells/well. Once the cells attached to the plate, they were treated with **S1** or **S1-CPT** when indicated at a final concentration of 100  $\mu\text{g}/\text{mL}$  for 24 and 48 hours. Then, cells were stained with 10  $\text{ng}/\text{mL}$  of Hoechst 33342 (except in case of **S1-CPT**, as CPT was detected at the same wavelength than Hoechst 33342) and 5  $\mu\text{g}/\text{mL}$  wheat germ agglutinin (WGA) Alexa Fluor 647 for 30 min in PBS containing 10% FCS or keeping the medium in case of **S1-CPT** treatments. Slides were

visualized under a confocal microscope. Experiment in identical conditions was done twice.

**Nanoparticles subcellular localization studies:** HeLa cells were electroporated employing Gene Pulser Xcell™ Eukaryotic System according to manufacturer's protocol in the presence of LAMP1-GFP plasmid. Then, cells were seeded and after 24 h were treated with **S1** at concentrations of 100 µg/mL for 24 h. Finally, cells were stained with 10 ng/mL of Hoechst 33342 and 5 µg/mL wheat germ agglutinin (WGA) Alexa Fluor 647 for 30 min in PBS containing 10% FCS. Slides were visualized under a confocal microscope.

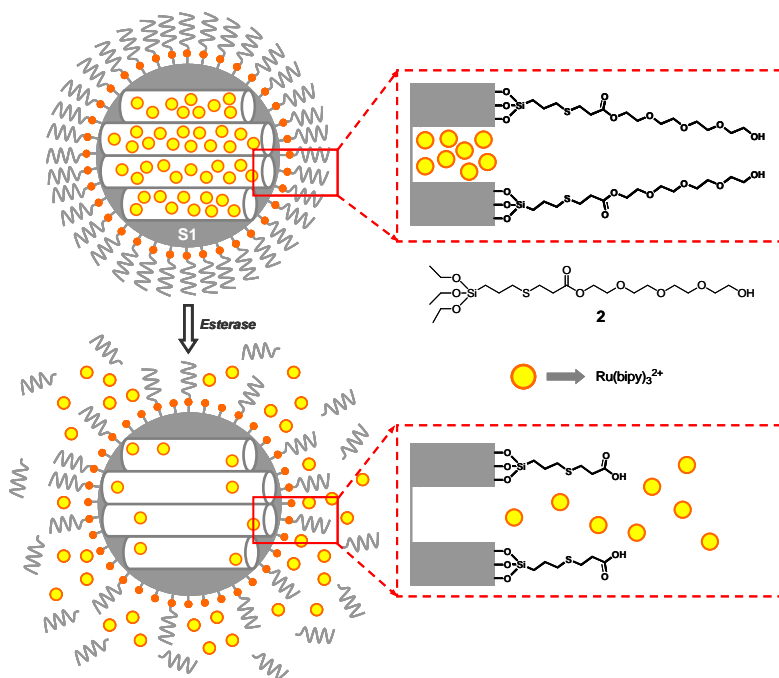
**Cytofluorometry Studies employing S1:** To develop the cytofluorometry studies, cells were seeded at  $2.5 \times 10^4$  or  $4 \times 10^4$  cells/well for HeLa and MCF-7, respectively, in a 24-well plate. After 24 h, cells were treated with **S1-CPT** or MCM-41 at concentrations of 200, 100 and 50 µg/mL for 24 and 48 hours. Finally, cells were stained with propidium iodide and Annexin V-FITC according to manufacturer's protocol in order to quantify dead cells and cells initiating cell death processes. Quantification of PI positive and Ann V positive stainings was performed employing WinMDI program version 2.9. Two independent experiments containing duplicates were performed. Results were expressed as (mean ± SE).

## **6.4 Results and discussion**

### **Design and synthesis of the gated material**

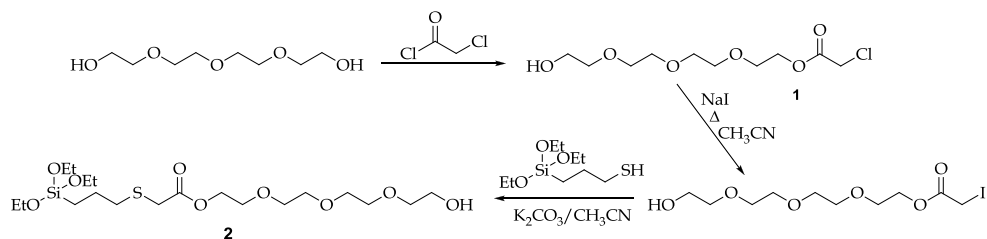
Incorporation of gate-like ensembles on mesoporous scaffolds has been proved to be a suitable approach for the development of nanoscopic hybrid

materials for mass transport control.<sup>17</sup> Most of the reported examples used molecular and supramolecular interactions for the fine tuning of mass delivery. In spite of this fact there are several examples of gated materials controlled by the presence of certain bio-molecules. Following these examples in the application of bio-molecules as triggers for controlled release purposes we centred our attention in the use of enzymes as selective 'biological-keys'. We selected nanoparticles of the MCM-41 family as mesoporous scaffold.<sup>18</sup> This support is a suitable inorganic matrix because presented several important characteristics such as homogeneous porosity, high inertness and ease of functionalization.<sup>19</sup> Additionally, MCM-41 nanoparticles contain mesopores in the 2-3 nm range that allows a rapid uptake and release of the selected guests. Scheme 1 shows the proposed paradigm of the enzyme-controlled gated material.



**Scheme 1.** Schematic representation of the controlled release mechanism of S1 in the presence of a specific enzyme (esterase) able to hydrolyze the ester moiety.

In order to prepare the designed material the mesopores of the MCM-41 nanoparticles were loaded with  $[\text{Ru}(\text{bipy})_3]\text{Cl}_2$ . Then, the external surface was functionalized with the ester glycol **2** (see Scheme 2) yielding the final hybrid material **S1**.



**Scheme 2.** Synthesis of precursor **1** and trialcoxysilane derivative **2** used as molecular gate.

These groups have been selected bearing in mind reported examples which describe that oligo- and poly-ethylen glycol coating on silica nanoparticles provide non-toxic, biocompatible and protective covering for *in vivo* applications.<sup>20</sup> The release of the ruthenium complex from **S1** would be inhibited due to the steric hindrance induced by the bulky glycol chain anchored in the pore voids of the MCM-41 nanoparticles. Upon addition of an esterase enzyme the hydrolysis of the ester moiety, present in the structure of **2**, is expected to induce the cleavage of the glycol chain. As a consequence, a clear size reduction in the appended gate would be produced enabling the release of the entrapped ruthenium complex.

The mesoporous silica nanoparticulated material (a calcined MCM41-like solid) was prepared following well-kwon procedures using TEOS as hydrolysable inorganic precursor and the surfactant hexadecyltrimethylammonium bromide (CTAB) as porogen species.<sup>21</sup> The ester containing glycol, **2** derivative, was prepared in two steps from tetraethylene glycol and 3-chloropropanoyl chloride (see scheme 2). At this respect, reaction between tetraethylene glycol and 3-chloropropanoyl

chloride leads to the formation of monoester derivative **1**. In the second step a nucleophilic substitution reaction between **1** and (3-mercaptopropyl)triethoxysilane in the presence of sodium iodide yielded the final glycol ester **2**.

In order to ensure the correct functionality of the final hybrid material we made use of a two step synthetic procedure that has been recently used by other authors and by our group to prepare responsive gated structures containing a certain cargo inside the pores and suitable switchable ensembles on the pore outlets.<sup>22</sup> In this procedure the mesoporous nanoparticles were added to a solution containing a high concentration of [Ru(bipy)<sub>3</sub>]Cl<sub>2</sub> complex in order to achieve an efficient loading of the pores. Then, product **2** was added to the suspension. With this protocol, the final **S1** material should ideally contain the ester glycol **2** anchored on the external surface, whereas the ruthenium complex should be located inside the mesopore channels. This could be possible bearing in mind that the grafting reaction of **2** is carried out when the pores are filled with the ruthenium complex. Also, with this procedure, the grafting of **2** is performed in a suspension which still contains in the solution a high concentration of ruthenium complex. The later inhibited the diffusion of the [Ru(bipy)<sub>3</sub>]Cl<sub>2</sub> from the pores to the solution, therefore hampering the entrance of **2** into the inner of the pores. The final orange solid (**S1**) was isolated by filtration, washed with distilled water and dried at 38 °C for 12 hours.

The same two step synthetic protocol was used for the preparation of a second gated material **S1-CPT**. In this case, we used a higher proportion of camptothecin (1.607 mmol/gr of MCM-41) when compared to the dye amount in sample **S1** (0.789 mmol/gr of MCM-41) and the mesoporous

nanoparticles drug uptake was performed in acetonitrile-ethanol mixtures to favour the drug dissolution. Finally, product **2** was added to the suspension and the final material isolated by filtration, washed with distilled water, methanol and acetone and dried at 38 °C overnight. In this last step, and due to the relatively small size of the camptothecin, a higher proportion of compound **2** was used in order to warrant a properly closing effect of the gate.

Finally, and for comparative purposes, a solid **S2** containing only the [Ru(bipy)<sub>3</sub>]Cl<sub>2</sub> complex in the inner of the pores, but lacking the gate ensemble, was also prepared.

### **Materials Characterization**

Solids **S1**, **S1-CPT** and **S2** were characterized using standard procedures. Figure 1 shows powder X-ray patterns of the nanoparticulated MCM-41 support as synthesized, MCM-41 calcined and **S1**.

The PXRD of siliceous nanoparticulated MCM-41 as-synthesized (curve a) shows four low-angle reflections typical of a hexagonal array that can be indexed as (100), (110), (200), and (210) Bragg peaks. A significant displacement of the (100) peak in the XRD powder of the nanoparticulated MCM-41 calcined sample was clearly appreciated in the curve b, corresponding to a cell contraction of ca. 4 Å.

This displacement and the broadening of the (110) and (200) peaks are most likely related to further condensation of silanol groups during the calcination step. Curve c corresponds to the **S1** XRD pattern. In this case, a slight intensity decrease and a further broadening of the (110) and (200) reflections were observed, surely due to a loss of contrast due to the filling of the pore voids with the ruthenium (II) dye.

Nevertheless, the value and intensity of the (100) peak in this pattern strongly evidences that the loading process with the dye and the further functionalization with **2** have not damaged the mesoporous 3D MCM-41 scaffolding.

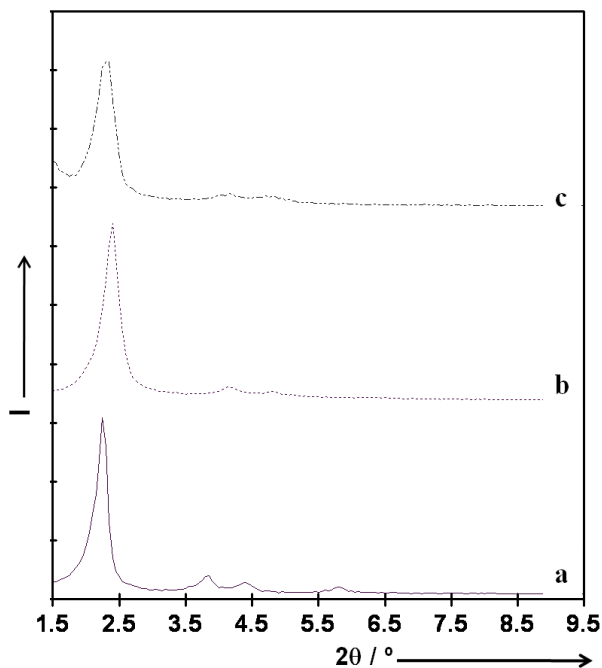


**Figure 1.** X-ray pattern of (a) MCM-41 as synthesized, (b) MCM-41 calcined and (c) **S1** hybrid material.

The same features were obtained for solid **S1-CPT** (data not shown). The preservation of the mesoporous structure in the final functionalized solids **S1** and **S1-CPT** was also confirmed by means of TEM. Figure 2 shows the morphology of the MSN materials. As it can be seen, MCM-41 scaffolding has been prepared as spherical particles with diameters of ca. 100 nm and the loaded and functionalised derivatives **S1** and **S1-CPT** keep the initial morphology of the MCM-41 matrix. The figure also shows the typical channels of the MCM-41 matrix both as alternate black and white stripes or as pseudo hexagonal array of pore voids. These channels are

visualised not only in the calcined material but also in **S1** and **S1-CPT** functionalised derivatives.

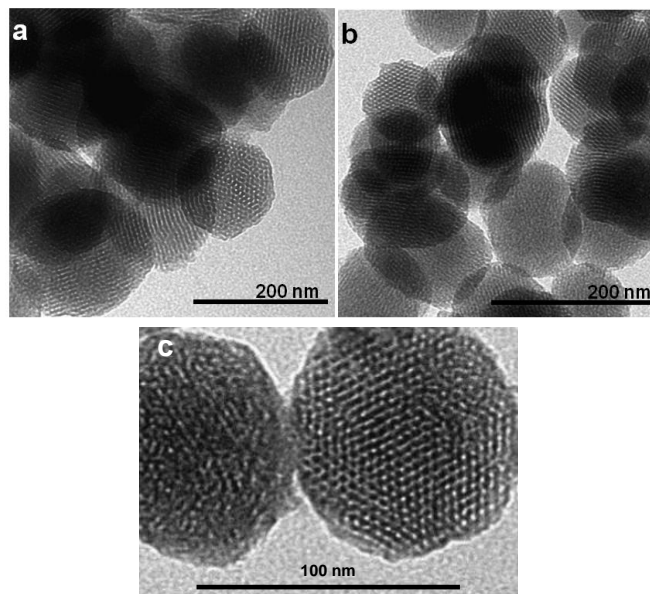


**Figure 2.** (a) TEM image of the calcined MCM-41 showing the typical hexagonal porosity of the MCM-41 matrix. (b) TEM image of solid **S1**. (c) TEM image of solid **S1-CPT**.

The  $N_2$  adsorption-desorption isotherms of the nanoparticulated MCM-41 calcined material shows an adsorption step at intermediate  $P/P_0$  value (0.1-0.3) typical of this family of mesoporous solids (see Figure 3). This step can be related to the nitrogen condensation inside the mesopores by capillarity. The absence of a hysteresis loop in this interval and the narrow BJH pore distribution suggest the existence of uniform cylindrical mesopores with pore volume of  $1.17 \text{ cm}^3 \text{ g}^{-1}$  calculated by using the BJH model on the adsorption branch of the isotherm. The application of the BET model resulted in a value for the total specific surface of  $966 \text{ m}^2 \text{ g}^{-1}$  and a mesopore volume of  $0.78 \text{ cm}^3 \text{ g}^{-1}$ . From the XRD, porosimetry and TEM studies, the  $a_0$  cell parameter (4.43 nm), the pore diameter (2.67 nm) and a

value for the wall thickness (1.76 nm) were calculated. In addition to this adsorption step associated to the micelle generated mesopores, a second feature appears in the isotherm at a high relative pressure ( $P/P_0 > 0.6$ ). This adsorption correspond to the filling of the large voids among the particles and present a volume of  $0.39 \text{ cm}^3 \text{ g}^{-1}$  (calculated by using the BJH model) and then must be considered as a textural-like porosity created during the sample preparation process. In this case, the curves show a characteristic H1 hysteresis loop and a wide pore size distribution.

The  $\text{N}_2$  adsorption-desorption isotherm of **S1** is typical of mesoporous systems with partially filled mesopores (see curve b in Figure 3), and a moderate decrease in the  $\text{N}_2$  volume adsorbed and surface area ( $756 \text{ m}^2 \text{ g}^{-1}$ ) was observed respect to the calcined MCM-41 matrix.

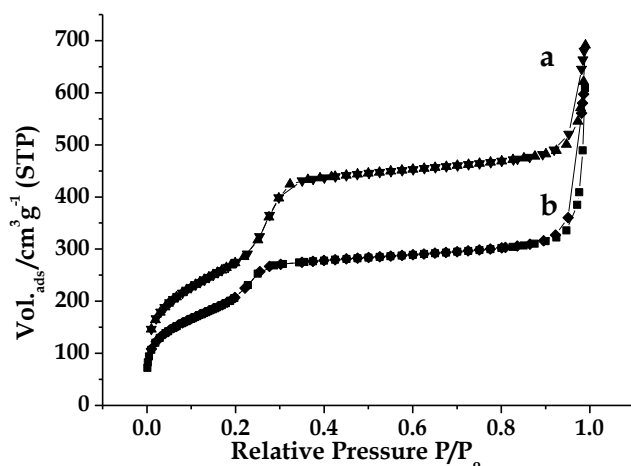


**Figure 3.** adsorption-desorption isotherms for (a) MCM-41 calcined mesoporous material and (b) **S1** material.

The same features were observed for solid **S1-CPT** namely a moderate decrease in the  $\text{N}_2$  volume adsorbed indicative of mesoporous systems with partially filled mesopores (data not shown) and a decrease in the surface area ( $711 \text{ m}^2 \text{ g}^{-1}$ ).

BET specific surface values, pore volumes, and pore sizes calculated from the N<sub>2</sub> adsorption-desorption isotherms for MCM-41, **S1** and **S1-CPT** are listed in Table 1. It can be seen that **S1** and **S1-CPT** solids show similar specific surface, pore volume and pore size values what is indicative of similar pore blocking for N<sub>2</sub> adsorption due to the cooperative effect of guest molecules and functional groups in both active materials. In both solids, the remaining porosity must be associated to a certain leaching of guest molecules (dye or cytotoxic) during the construction of the gate-like scaffold and the subsequent washing step.

The content of organic matter in the final hybrid solids **S1** and **S1-CPT** were determined by elemental and thermogravimetric analysis. Values are detailed in Table 2. The amount of compound **2** anchored on sample **S1** is significantly lower than the measured for sample **S1-CPT**.

**Table 1.** BET specific surface values, pore volumes and pore sizes calculated from the N<sub>2</sub> adsorption-desorption isotherms for selected materials.

Sample	$S_{BET}$ ( $m^2g^{-1}$ )	Pore BJH ( $P/P_0 < 0,6$ ) <sup>a</sup> (nm)	Pore BJH ( $P/P_0 > 0,6$ ) <sup>b</sup> (nm)	Total pore volume <sup>c</sup> ( $cm^3g^{-1}$ )	Pore volume ( $P/P_0 < 0,6$ ) <sup>d</sup> ( $cm^3g^{-1}$ )	Pore volume ( $P/P_0 > 0,6$ ) <sup>e</sup> ( $cm^3g^{-1}$ )
MCM-41	966	2.67	45.4	1.17	0.78	0.39
<b>S1</b>	705	2.30	45.2	0.85	0.45	0.30
<b>S1-CPT</b>	711	2.39	44.6	0.87	0.51	0.36

<sup>a</sup> Estimated pore size calculated from BJH model in the isotherm adsorption branch, for  $P/P_0 < 0,5$ , that can be associated to the surfactant generated mesopores

<sup>b</sup> Estimated pore size calculated from BJH model in the isotherm adsorption branch, for  $P/P_0 > 0,5$ , that can be associated to the textural porosity

<sup>c</sup> Total pore volume, calculated by BJH model.

<sup>d</sup> Pore volume for  $P/P_0 < 0,5$ , that can be associated to the surfactant generated mesopores

<sup>e</sup> Pore volume for  $P/P_0 > 0,5$ , that can be associated to the textural porosity

This result is in good accordance with the experimental conditions used as the proportion of compound **2** added to prepare solid **S1** is *ca.* half

the amount of that used in the case of the **S1-CPT** synthesis. Then, an average density of 1.6 molecules of compound **2** per nm<sup>2</sup> can be estimated for sample **S1** taking into account that only the external surface, 65 m<sup>2</sup>/g, is available for anchoring (this last value corresponds to the external BET area of the as-synthesized MCM-41 nanoparticles).

This proportion of compound **2** requires a density of silanol groups of *ca.* 4.8 Si-OH/nm<sup>2</sup> (if it is assumed that all functional silane groups are connected to the silica surface through their three ethoxy moieties). This density of silanol groups fits very well with the expected value for active porous silica (4-6 Si-OH/nm<sup>2</sup>). In the case of sample **S1-CPT**, a higher compound **2** density can be estimated (3.4 molecules/nm<sup>2</sup>). In this last case, functionalization with compound **2** probably occurs not only at the external surface, but also affects the mesopores entrance domain.

Finally, the resulting amount of guest species included inside the mesopores is significantly higher in the case of solid **S1-CPT**. Several factors such as the used experimental conditions (higher proportion of camptothecin than dye), the lower size of the drug (probably leading to a more efficient packing), and the different interaction with the support could account for this values.

**Table 2.** Content of **2**, dye and camptothecin in the prepared solids **S1** and **S1-CPT** in mg/g SiO<sub>2</sub> ( $\alpha$ ).

<i>Solid</i>	$\alpha_2$	$\alpha_{dye}$	$\alpha_{CPT}$
<b>S1</b>	258.7	14.7	-
<b>S1-CPT</b>	305	-	17

The length of the trialkoxysilane derivative **2** is about 2.55 nm (by quantum chemical calculations at semiempirical level using HyperChem

software) value that matches well the diameter of the pores of solid **S1** (2.67 nm). From this point of view, a tight pore capping could be expected. However, this pore closure should be understood as a cooperative process involving several oligoethylene glycol molecules. In particular, bearing in mind the spacing value (3.69 nm), the pore diameter in **S1** and the content of **2**, and assuming the existence of a hexagonal cell unit it can be determined that there are ca. 16 molecules of derivative **2** for each pore. This is a high value that also pointed to an important pore closure. The similar situation could be expected for solid **S1-CPT**.

### **Delivery studies**

In a first step the controlled delivery of the ruthenium complex from solid **S1** in the presence and in the absence of esterase enzyme was studied. In a typical delivery experiment, 5 mg of solid **S1** were suspended in 10 mL of water at pH 8.0. Then 2.5 mL of an aqueous solution containing esterase ( $C_{\text{enzyme}} = 0.3 \text{ mg/mL}$ , pH 8) was added and the final suspension was stirred. Uncapping and subsequent delivery of the dye to the aqueous solution was easily detected via monitorization of the spin allowed d- $\pi$  metal-to-ligand charge transfer (MLCT) transition band of the  $[\text{Ru}(\text{bipy})_3]\text{Cl}_2$  complex centred at 451 nm or through the emission band centred at 619 nm ( $\lambda_{\text{ex}} = 451 \text{ nm}$ ).<sup>23</sup> As a control experiment dye release was also determined using suspensions of **S1** under similar conditions but in absence of esterase. The difference in dye delivery in both experiments is displayed in Figure 4. As could be seen in the absence of esterase a very low release of the ruthenium complex was observed. However, in the presence of esterase enzyme a massive release of the ruthenium complex was found.

As suggested above, this enzyme-induced delivery is assigned to the enzymatic hydrolysis of the ester bond in the anchored derivative **2** that induces a release of the oligo(ethylene glycol) fragment. The breaking of the ester bond results in a reduction of the size of the appended group therefore allowing the delivery of the entrapped cargo.

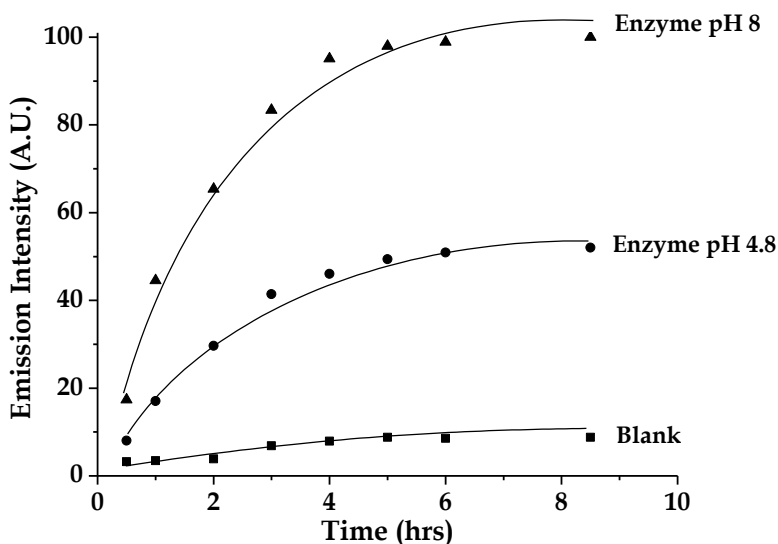


**Figure 4.** Kinetics of the release of  $[\text{Ru}(\text{bipy})_3]\text{Cl}_2$  dye from solid **S1** in the absence (■) and in the presence of esterase enzyme in water at pH 8.0 (▲) and at pH 4.8 (●) respectively at 25 °C.

In order to complete the delivery studies some additional control experiments were carried out. Additionally, in order to further demonstrate that esterase is responsible of the release protocol two more experiments were carried out. In one of them solid **S1** was incubated in the presence of other enzymes such as amidase and urease. In a second experiment the enzyme was denaturated by heating enzyme solutions (pH 8) at 60 °C for 60 minutes before addition of **S1**. In both cases no release of the dye was observed pointing again to the selective enzymatic hydrolysis of the ester bond as the mechanism responsible for the opening of the mesopores.

In spite of the significant reduction of the oligo(ethylene glycol) chain upon the ester hydrolysis induced by esterase the delivery of the [Ru(bipy)<sub>3</sub>]Cl<sub>2</sub> dye is rather slow and a constant cargo delivery through at least 8 hours is observed. The control of the delivery trough time is an additional feature that could be of interest in order to avoid delivery peaks.<sup>24</sup> The low delivery rate may be ascribed to the location of the ester linkages deep inside the thread close to the surface of the inorganic support that hampers a fast hydrolysis in the presence of the enzyme. This observation additionally suggests that it might be possible to modulate the release kinetics via the location of ester linkages in different parts of the molecular threads.

Moreover esterase induced delivery studies at pH 4.8 were performed in order to demonstrate the ability of the enzyme to hydrolyse the ester moiety at lysosomal pH. As can be noted in figure 4 cargo delivery was also observed at this pH. The different delivery rate observed at pH 4.8 (when compared to pH 8) should be ascribed to the use of a pH that was not optimal for the highest activity of the used esterase (i.e. pH 8).

### **Cellular internalization and delivery studies**

Once the chemical characterization and the mechanism of the gate opening process of **S1** was determined, the hybrid material was used in cellular uptake experiments in order to confirm a possible therapeutical application of these nanoparticles as drug-carriers. In this case, experiments employing two different tumorigenic cell lines, HeLa and MCF-7, were carried out. As a first approach, cell viability studies were performed in order to discard any toxic effect associated to nanoparticles or the nature of the molecular gate. Briefly, cells were treated with **S1** for 24 hours before

the addition of WST-1 reagent. Cells metabolically active are able to reduce this yellow reagent into a reduced orange form. Absorbance measurements at 450 nm and subsequent normalization of the measures at 595 nm proved the innocuous effect of **S1** on cell at concentrations tested, as could be seen in Figure 5C.

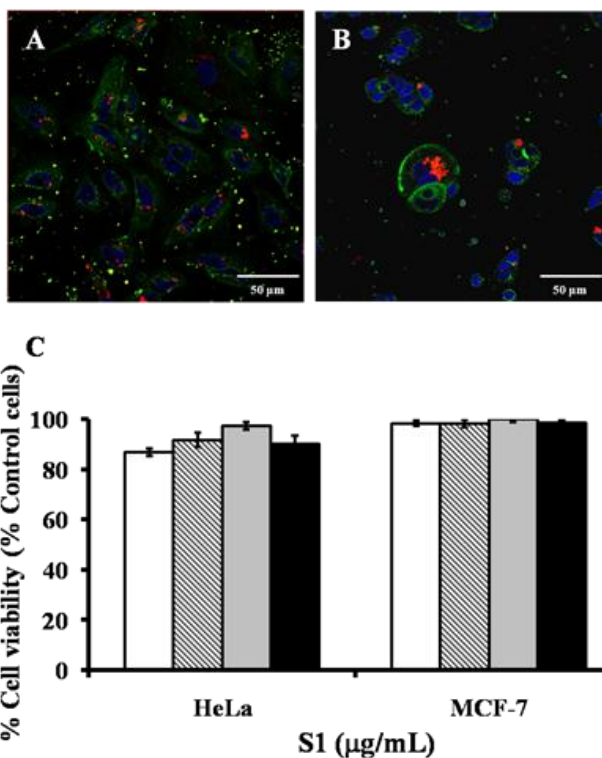


**Figure 5.** **S1** cellular internalization and WST-1 cell viability assay. HeLa and MCF-7 cells were treated with **S1** at concentrations of 25, 50, 100 and 200 µg/mL for 24 h. Then, confocal microscopy studies of **S1** cellular uptake in HeLa (A) and MCF-7 (B) at concentrations of 100 µg/mL were performed by means of [Ru(bipy)<sub>3</sub>]<sub>2</sub>-**S1** associated fluorescence (red) in the presence of the DNA marker Hoechst 33342 (blue) and the plasma membrane marker WGA Alexa Fluor 647 (green). For cell viability studies, (C) HeLa and MCF-7 cells were incubated for 24 h with **S1** at the concentrations stated before and cell viability was quantified employing WST-1 reagent (white, striped, grey and black, respectively).

Complementary to cell viability assays, confocal microscopy internalization studies were developed taking profit of [Ru(bipy)<sub>3</sub>]<sub>2</sub>-**S1**

associated fluorescence (see also Figure 5A and B). These studies confirmed the cellular uptake of the compound due to the appearance of vesicular  $[\text{Ru}(\text{bipy})_3]\text{Cl}_2$  associated fluorescence, probably due to lysosomal localization of nanoparticles. With the aim to confirm that the mechanism of internalization and aperture of the molecular gate of nanoparticles is endocytosis and subsequent esterase degradation once in the lysosomes, HeLa cells were electroporated with the lysosomal marker gene Lamp1 fused to the green fluorescent protein (LAMP1-GFP).

This protein is localized in the membrane of the lysosomal vesicles, when fused to GFP a dotted pattern in the cytoplasm of the cell is observed corresponding to the lysosomes. Once electroporated, cells were treated with 100  $\mu\text{g}/\text{mL}$  of **S1** for 24 h, prior analysis of the fluorescence associated to the  $[\text{Ru}(\text{bipy})_3]\text{Cl}_2$ -**S1** dye and LAMP1-GFP.

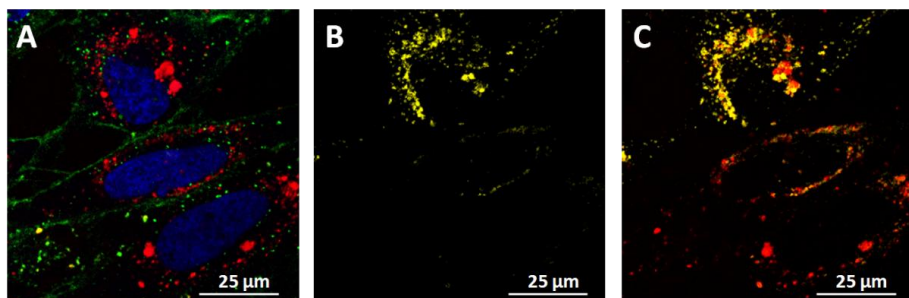


**Figure 6.** Study of the internalization and subcellular localization of **S1** nanoparticles. HeLa cells were electroporated with LAMP1-GFP and 24 h later treated with **S1** 100  $\mu\text{g}/\text{mL}$ . Finally, 24 h later cells were stained as in Figure 5 and (A)  $[\text{Ru}(\text{bipy})_3]\text{Cl}_2$ -**S1** associated fluorescence (red) and (B) LAMP1-GFP (yellow) were followed. (C) When nanoparticles and LAMP1-GFP signal was merged a significant percentage of **S1** colocalized with the lysosomal marker LAMP1.

As a result, a significant number of cells showed a dotted  $[\text{Ru}(\text{bipy})_3]\text{Cl}_2$ -**S1** pattern colocalizing with LAMP1-GFP associated vesicles

confirming endocytosis as the internalization mechanism followed by nanoparticles (Figure 6).

Once demonstrated the biocompatibility of the solid **S1**, and as a possible therapeutical application, a new nanoparticled material loaded with camptothecin (CPT) was synthesized (**S1-CPT**). CPT is a quinoline alkaloid that exerts its cytotoxic activity by inhibiting DNA polymerase I thus disrupting DNA replication processes and causing cell death, but has low solubility which restricts its application in patients.<sup>25</sup> In order to test the effect of **S1-CPT** material, HeLa and MCF-7 cells were selected and treated, as described before, with this new nanoparticles for 24 hours.

In order to determine the effect of the nanoparticles, confocal microscopy and flow cytometry studies were performed. In Figure 7A-D, the effect of MCM-41 and **S1-CPT** nanoparticles are depicted. When observed under the confocal microscope, cells treated with **S1-CPT** presented a cell death processes associated phenotype (detached cells from the plate, plasma membrane blebbing, cellular corpses, among others). A cytoplasmic localization of CPT signal (blue colour in Figure 7D) was observed demonstrating the release of the cargo molecule inside the cell. By contrast, no significant cell death or initiation of cell death processes were observed in MCM-41 treated cells at concentrations.

In case of flow cytometry studies, quantification of dead cells and cells undergoing cell death due to the aperture of the molecular gate was evaluated by means of propidium iodide (PI) and Annexin V (Ann V) stainings, respectively. A significant reduction in cell viability was observed 24 hours after the addition of S1-CPT (Figure 7E, F) reaching 28% of dead cells and 40% of cells undergoing cell death after treating the cells with a dosis of 100 µg/mL of S1-CPT.

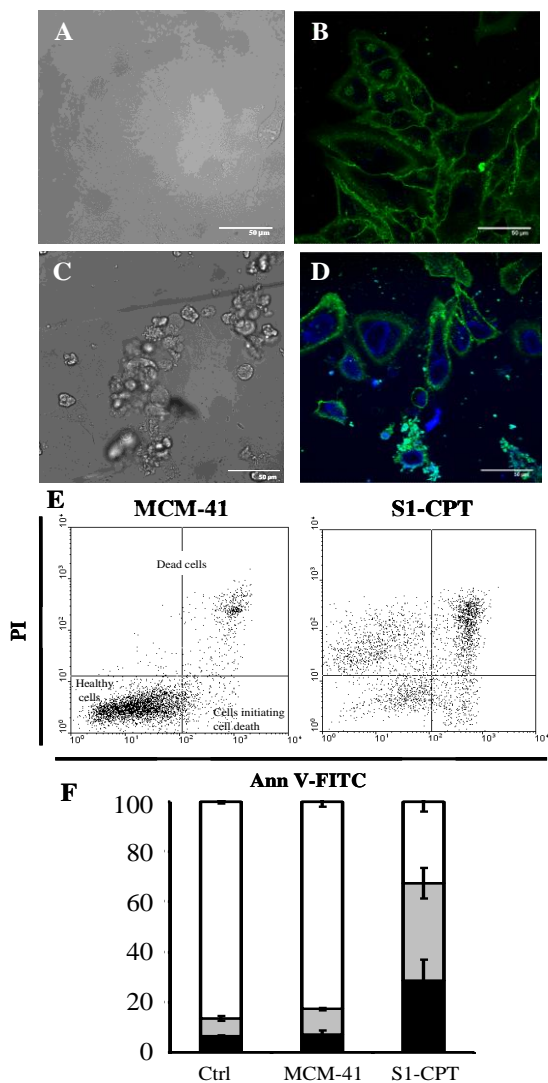


**Figure 7.** S1-CPT cell internalization induces cell death. HeLa cells were treated with control MCM-41 (A, B) or S1-CPT (C, D) at 200  $\mu\text{g}/\text{mL}$  and cells were further incubated for 24 h. MCM-41-treated cells presented normal morphology and remained attached to the plate (A) in confocal microscopy analysis (B) in which plasma membrane was stained with WGA Alexa Fluor 647 (green). In contrast, S1-CPT treated cells presented a phenotype associated to cell death (C) and an in cell diffuse pattern of CPT-associated fluorescence (blue) due to CPT release and subsequent cell death induction. Quantification of cell viability and cell death (E, F) was performed by flow cytometry by means of PI and Ann V stainings, respectively. Percentage of dead cells (black), cells undergoing cell death (grey) and healthy cells (white) are depicted after 24 hours of treatment. Two independent experiments were performed and data are reported as (mean  $\pm$  SE).

These results confirmed the possibility to employ S1 as drug-carrier of CPT in the treatment of different diseases such as cancer.

## 6.5 Conclusions

In summary, we have reported here the synthesis and controlled release studies of a nanoscopic gated material composed by a silica mesoporous scaffolding functionalized with oligo(ethylene glycol) chains anchored to the silica surface via an ester linkage (**S1**). The presence of an esterase enzyme provokes the hydrolysis of the ester located in the molecular threads, inducing dye release. The study demonstrates that it is possible to use relatively simple molecules containing enzyme-hydrolyzable groups for the design of capped materials that can be opened at will. The possibility of include in the thread different ester linkages or different enzyme-mediated hydrolyzable groups makes the design of enzyme-responsive promising materials for advanced drug delivery and regenerative medicine applications. Based on the fact that enzyme-substrate pairs offer a vaste range of different combinations, a proof-of-concept of the possible application of this nanodevice as drug-carrier was performed proving the ability of the **S1-CPT** solid to be internalized by cells through endocytosis and release its cargo, once in the lysosomes, thanks to the presence of lysosomal enzymes, such as esterases.

## 6.6 Bibliography

- 1 Descalzo, A. B.; Martínez-Máñez, R.; Sancenón, F.; Hoffmann, K.; Rurack, K. The supramolecular chemistry of organic-inorganic hybrid materials. *Angew. Chem. Int. Ed.* **2006**, *45*, 5924-5948.
- 2 (a) Beck, J. S.; Vartuli, J. C.; Roth, W. J.; Leonowicz, M. E.; Kresge, C. T.; Schmitt, K. D.; Chu, C. T. -W.; Olson, D. H.; Sheppard, E. W.; McCullen, S. B.; Hoggins,

- J. B.; Schlenker, J. L. A new family of mesoporous molecular sieves prepared with liquid crystal templates. *J. Am. Chem. Soc.* **1992**, *114*, 10834-10843. (b) Wright, A. P.; Davis, M. E. Design and preparation of organic-inorganic hybrid catalysts. *Chem. Rev.* **2002**, *102*, 3589-3614. (c) Kickelbick, G. Hybrid inorganic-organic mesoporous materials. *Angew. Chem. Int. Ed.* **2004**, *43*, 3102-3104.
- 3 (a) Aznar, E.; Martínez-Máñez, R.; Sancenón, F. Controlled release using mesoporous materials containing gate-like scaffoldings. *Expert Opin. Drug Deliv.* **2009**, *6*, 643-655. (b) Zhou, Y.; Guo, W.; Cheng, J.; Liu, Y.; Li, J.; Jiang, L. High-temperature gating of solid state nanopores with thermo-responsive macromolecular nanoactuators in ionic liquids. *Adv. Mater.* **2012**, *24*, 962-967. (c) Bringas, E.; Köysüren, Ö.; Quach, D. V.; Mahmoudi, M.; Aznar, E.; Roehling, J. D.; Marcos, M. D.; Martínez-Máñez, R.; Stroeve, P. Triggered release in lipid bilayer-capped mesoporous silica nanoparticles containing SPION using an alternating magnetic field. *Chem. Commun.* **2012**, *48*, 5647-5649. (d) Baeza, A.; Guisasaola, E.; Ruiz-Hernández, E.; Vallet-Regí, M. Magnetically triggered multidrug release by hybrid mesoporous silica nanoparticles. *Chem. Mater.* **2012**, *24*, 517-524.
- 4 (a) Casasús, R.; Marcos, M. D.; Martínez-Máñez, R.; Ros-Lis, J. V.; Soto, J.; Villaescusa, L. A.; Amorós, P.; Beltrán, D.; Guillem, C.; Latorre, J. Toward the development of ionically controlled nanoscopic molecular gates. *J. Am. Chem. Soc.* **2004**, *126*, 8612-8613. (b) Casasús, R.; Climent, E.; Marcos, M. D.; Martínez-Máñez, R.; Sancenón, F.; Soto, J.; Amorós, P.; Cano, J.; Ruiz, E. Dual aperture control on pH- anion-driven supramolecular nanoscopic hybrid gate-like ensembles. *J. Am. Chem. Soc.* **2008**, *130*, 1903-1917. (c) Aznar, E.; Marcos, M. D.; Martínez-Máñez, R.; Sancenón, F.; Soto, J.; Amorós, P.; Guillem, C. pH and photo-switched release of guest molecules from mesoporous silica supports. *J. Am. Chem. Soc.* **2009**, *131*, 6833-6843. (d) Angelos, S.; Yang, Y. -W.; Khashab, N. M.; Stoddart, J. F.; Zink, J. I. Dual-controlled nanoparticles exhibiting AND logic. *J. Am. Chem. Soc.* **2009**, *131*, 11344-11346. (e) Angelos, S.; Yang, Y. -W.; Patel, K.; Stoddart, J. F.; Zink, J. I. pH-responsive supramolecular nanovalves based on cucurbit[6]uril pseudorotaxanes. *Angew. Chem. Int. Ed.* **2008**, *47*, 2222-2226. (f) Angelos, S.; Khashab, N. M.; Yang, Y. -W.; Trabolsi, A.; Khatib, H. A.; Stoddart, J. F.; Zink, J. I. pH clock-operated mechanized nanoparticles. *J. Am. Chem. Soc.* **2009**, *131*, 12912-12914. (g) Du, L.; Liao, S.; Khatib, H. A.; Stoddart, J. F.; Zink, J. I. Controlled-access hollow mechanized silica nanocontainers. *J. Am. Chem. Soc.* **2009**, *131*, 15136-15142. (h) Yang, Q.; Wang, S.; Fan, P.; Wang, L.; Di, Y.; Lin, K.; Xiao, F. -S. pH-responsive carrier system based on carboxylic acid

modified mesoporous silica and polyelectrolyte for drug delivery. *Chem. Mater.* **2005**, *17*, 5999-6003. (i) Park, C.; Oh, K.; Lee, S. C.; Kim, C. Controlled release of guest molecules from mesoporous silica particles based on a pH-responsive polypseudorotaxane motif. *Angew. Chem. Int. Ed.* **2007**, *46*, 1455-1457. (j) Zhao, Y. -L.; Li, Z.; Kabehie, S.; Botros, Y. Y.; Stoddart, J. F.; Zink, J. I. pH-operated nanopistons on the surfaces of mesoporous silica nanoparticles. *J. Am. Chem. Soc.* **2010**, *132*, 13016-13025. (k) Schlossbauer, A.; Dohmen, C.; Schaffert, D.; Wagner, E.; Bein, T. pH-responsive release of acetal-linked melittin from SBA-15 mesoporous silica. *Angew. Chem. Int. Ed.* **2011**, *50*, 6828-6830. (l) Gan, Q.; Lu, X.; Yuan, Y.; Qian, J.; Zhou, H.; Lu, X.; Shi, J.; Liu, C. A magnetic, reversible pH-responsive nanogated ensemble based on Fe<sub>3</sub>O<sub>4</sub> nanoparticles-capped mesoporous silica. *Biomaterials* **2011**, *32*, 1932-1942. (m) Guo, W.; Wang, J.; Lee, S. -J.; Dong, F.; Park, S. S.; Ha, C. -S. A general pH-responsive supramolecular nanovalve based on mesoporous organosilica hollow nanospheres. *Chem. Eur. J.* **2010**, *16*, 8641-8646. (n) Liu, R.; Zhang, Y.; Zhao, X.; Agarwal, A.; Mueller, L. J.; Feng, P. pH-responsive nanogated ensemble based on gold-capped mesoporous silica through an acid-labile acetal linker. *J. Am. Chem. Soc.* **2010**, *132*, 1500-1501. (o) Meng, H.; Xue, M.; Xia, T.; Zhao, Y. -L.; Tamanoi, F.; Stoddart, J. F.; Zink, J. I.; Nel, A. E. Autonomous in vitro anticancer drug release from mesoporous silica nanoparticles by pH-sensitive nanovalves. *J. Am. Chem. Soc.* **2010**, *132*, 12690-12697. (p) Muhammad, F.; Guo, M.; Qi, W.; Sun, F.; Wang, A.; Guo, Y.; Zhu, G. pH-triggered controlled drug release from mesoporous silica nanoparticles via intracellular dissolution of ZnO nanolids. *J. Am. Chem. Soc.* **2011**, *133*, 8778-8781. (q) Xue, M.; Zhong, X.; Shaposhnik, Z.; Qu, Y.; Tamanoi, F.; Duan, X.; Zink, J. I. pH-operated mechanized porous silicon nanoparticles. *J. Am. Chem. Soc.* **2011**, *133*, 8798-8801. (r) Cauda, V.; Argyo, C.; Schlossbauer, A.; Bein, T. Controlling the delivery kinetics from colloidal mesoporous silica nanoparticles with pH-sensitive gates. *J. Mater. Chem.* **2010**, *20*, 4305-4311. (s) Chen, S. -H.; Liao, W. -N.; Chen, L. -M.; Lee, C. -H. pH-controllable release using functionalized mesoporous silica nanoparticles as an oral drug delivery system. *J. Mater. Chem.* **2011**, *21*, 7130-7137. (t) Choi, Y. L.; Lee, J. H.; Jaworski, J.; Jung, J. H. Mesoporous silica nanoparticles functionalized with a thymidine derivative for controlled release. *J. Mater. Chem.* **2012**, *22*, 9455-9457. (u) Chen, F.; Zhu, Y. Chitosan enclosed mesoporous silica nanoparticles as drug nanocarriers: sensitive response to the narrow pH range. *Micropor. Mesopor. Mater.* **2012**, *150*, 83-89. (v) Jin, D.; Lee, J. H.; Seo, M. L.; Jaworski, J.; Jung, J. H. Controlled drug delivery from mesoporous silica using a pH-response release system. *New. J. Chem.* **2012**, *36*, 1616-1620.

- 5 (a) Trewyn, B. G.; Slowing, I. I.; Giri, S.; Chen, H. T.; Lin, V. S. -Y. Synthesis and functionalization of a mesoporous silica nanoparticle based on the sol-gel process and applications in controlled release. *Acc. Chem. Res.* **2007**, *40*, 846-853. (b) Trewyn, B. G.; Giri, S.; Slowing, I. I.; Lin, V. S. -Y. Mesoporous silica nanoparticle based controlled release, drug delivery and biosensor systems. *Chem. Commun.* **2007**, 3236-3245. (c) Torney, F.; Trewyn, B. G.; Lin, V. S. -Y.; Wang, K. Mesoporous silica nanoparticles deliver DNA and chemical into plants. *Nat. Nanotechnol.* **2007**, *2*, 295-300. (d) Radu, D. R.; Lai, C. -Y.; Jeftinija, K.; Rowe, E. W.; Jeftinija, S.; Lin, V. S. -Y. A polyamidoamine dendrimer-capped silica nanosphere-based gene transfection reagent. *J. Am. Chem. Soc.* **2004**, *126*, 13216-13217. (e) Giri, S.; Trewyn, B. G.; Stellmaker, M. P.; Lin, V. S. -Y. Stimuli-responsive controlled-release delivery system based on mesoporous silica nanorods capped with magnetic nanoparticles. *Angew. Chem. Int. Ed.* **2005**, *44*, 5038-5044. (f) Fujiwara, M.; Terashima, S.; Endo, Y.; Shiokawa, K.; Ohue, H. Switching catalytic reaction conducted in pore void of mesoporous material by redox gate control. *Chem. Commun.* **2006**, 4635-4637. (g) Liu, R.; Zhao, X.; Wu, T.; Feng, P. Tunable redox-responsive hybrid nanogated ensembles. *J. Am. Chem. Soc.* **2008**, *130*, 14418-14419. (h) Nguyen, T. D.; Liu, Y.; Saha, S.; Leung, K. F. -C.; Stoddart, J. F.; Zink, J. I. Design and optimization of molecular nanovalves based on redox-switchable bistable rotaxanes. *J. Am. Chem. Soc.* **2007**, *129*, 626-634. (i) Kim, H.; Kim, S.; Park, C.; Lee, H.; Park, H. J.; Kim, C. Glutathione-induced intracellular release of guests from mesoporous silica nanocontainers with cyclodextrin gatekeepers. *Adv. Mater.* **2010**, *22*, 4280-4283. (j) Luo, Z.; Cai, K.; Hu, Y.; Zhao, L.; Liu, P.; Duan, L.; Yang, W. Mesoporous silica nanoparticles end-capped with collagen: redox-responsive nanoreservoirs for targeted drug delivery. *Angew. Chem. Int. Ed.* **2011**, *50*, 640-643. (k) Ambrogio, M. W.; Pecorelli, T. A.; Patel, K.; Khashab, N. M.; Trabolsi, A.; Khatib, H. A.; Botros, Y. Y.; Zink, J. I.; Stoddart, J. F. Snap-top nanocarriers. *Org. Lett.*, **2010**, *12*, 3304-3307. (l) Wang, C.; Li, Z.; Cao, D.; Zhao, Y. -L.; Gaines, J. W.; Bozdemir, O. A.; Ambrogio, M. W.; Frasconi, M.; Botros, Y. Y.; Zink, J. I.; Stoddart, J. F. Stimulated release of size-selected cargos in succession from mesoporous silica nanoparticles. *Angew. Chem. Int. Ed.* **2012**, *51*, 5460-5465.
- 6 (a) Mal, N. K.; Fujiwara, M.; Tanaka, Y. Photocontrolled reversible release of guest molecules from coumarin-modified mesoporous silica. *Nature* **2003**, *421*, 350-353. (b) Mal, N. K.; Fujiwara, M.; Tanaka, Y.; Taguchi, T.; Matsukata, M. Photo-switched storage and release of guest molecules in the pore void of coumarin-modified MCM-41. *Chem. Mater.* **2003**, *15*, 3385-3394. (c) Zhu, Y.; Fujiwara, M. Installing dynamic molecular photomechanics in mesopores: A

- multifunctional controlled-release nanosystem. *Angew. Chem. Int. Ed.* **2007**, *46*, 2241-2244. (d) Liu, N.; Chen, Z.; Dunphy, D. R.; Jiang, Y. B.; Assink, R. A.; Brinker, C. J. Photoresponsive nanocomposite formed by self-assembly of an azobenzene-modified silane. *Angew. Chem. Int. Ed.* **2003**, *42*, 1731-1734. (e) Aznar, E.; Casasús, R.; García-Acosta, B.; Marcos, M. D.; Martínez-Máñez, R.; Sancenón, F.; Soto, J.; Amorós, P. Photochemical and chemical two-channel control of functional nanogated hybrid architectures. *Adv. Mater.* **2007**, *19*, 2228-2231. (f) Park, C.; Lee, K.; Kim, C. Photoresponsive cyclodextrin-covered nanocontainers and their sol-gel transition induced by molecular recognition. *Angew. Chem. Int. Ed.* **2009**, *48*, 1275-1278. (g) Ferris, D. P.; Zhao, Y. -L.; Khashab, N. M.; Khatib, H. A.; Stoddart, J. F.; Zink, J. I. Light-operated mechanized nanoparticles. *J. Am. Chem. Soc.* **2009**, *131*, 1686-1688. (h) Lin, Q.; Huang, Q.; Li, C.; Bao, C.; Liu, Z.; Li, F.; Zhu, L. Anticancer drug release from a mesoporous silica nanophotocage regulated by either a one- or two-photon process. *J. Am. Chem. Soc.* **2010**, *132*, 10645-10647. (i) Nguyen, T. D.; Leung, K. C. -F.; Liong, M.; Liu, Y.; Stoddart, J. F.; Zink, J. I. Versatile supramolecular nanovalves reconfigured for light activation. *Adv. Func. Mater.* **2007**, *17*, 2101-2110. (j) Lai, J.; Mu, X.; Xu, Y.; Wu, X.; Wu, C.; Li, C.; Chen, J.; Zhao, Y. Light-responsive nanogated ensemble based on polymer grafted mesoporous silica hybrid nanoparticles. *Chem. Commun.* **2010**, *46*, 7370-7372. (k) Knežević, N. Ž.; Trewyn, B. G.; Lin, V. S. -Y. Functionalized mesoporous silica nanoparticle-based visible light responsive controlled release delivery system. *Chem. Commun.* **2011**, *47*, 2817-2819. (l) Knežević, N. Ž.; Trewyn, B. G.; Lin, V. S. -Y. Light and pH-responsive release of doxorubicin from a mesoporous silica-based nanocarrier. *Chem. Eur. J.*, **2011**, *17*, 3338-3342. (m) Sun, Y. -L.; Yang, B. -J.; Zhang, S. X. -A.; Yang, Y. -W. Cucurbit[7]uril pseudorotaxane-based photoresponsive supramolecular nanovalve. *Chem. Eur. J.* **2012**, *18*, 9212-9216. (n) Chang, Y. -T.; Liao, P. -Y.; Sheu, H. -S.; Tseng, Y. -J.; Cheng, F. -Y.; Yeh, C. -S. Near-infrared light-responsive intracellular drug and siRNA release using Au nanoensembles with oligonucleotide-capped silica shell. *Adv. Mater.* **2012**, *24*, 3309-3314. (o) Yan, H.; Teh, C.; Sreejith, S.; Zhu, L.; Kwok, A.; Fang, W.; Ma, X.; Nguyen, K. T.; Korzh, V.; Zhao, Y. Functional mesoporous silica nanoparticles for photothermal-controlled drug delivery in vivo. *Angew. Chem. Int. Ed.* **2012**, *51*, 8373-8377. (p) Croissant, J.; Zink, J. I. Nanovalve-controlled cargo release activated by plasmonic heating. *J. Am. Chem. Soc.* **2012**, *134*, 7628-7631.
- 7 Climent, E.; Bernardos, A.; Martínez-Máñez, R.; Maquieira, A.; Marcos, M. D.; Pastor-Navarro, N.; Puchades, R.; Sancenón, F.; Soto, J.; Amorós, P. Controlled

- delivery systems using antibody-capped mesoporous nanocontainers. *J. Am. Chem. Soc.* **2009**, *131*, 14075-14080.
- 8 Climent, E.; Martínez-Máñez, R.; Sancenón, F.; Marcos, M. D.; Soto, J.; Maquieira, A.; Amorós, P. Controlled delivery using oligonucleotide-capped mesoporous silica nanoparticles. *Angew. Chem. Int. Ed.* **2010**, *49*, 7281-7283.
- 9 Patel, K.; Angelos, S.; Dichtel, W. R.; Coskun, A.; Yang, Y. -W.; Zink, J. I.; Stoddart, J. F. Enzyme-responsive snap-top covered silica nanocontainers. *J. Am. Chem. Soc.* **2008**, *130*, 2382-2383.
- 10 Schlossbauer, A.; Kecht, J.; Bein, T. Biotin-avidin as a protease-responsive cap system for controlled guest release from colloidal mesoporous silica. *Angew. Chem. Int. Ed.* **2009**, *48*, 3092-3095.
- 11 Bernardos, A.; Aznar, E.; Marcos, M. D.; Martínez-Máñez, R.; Sancenón, F.; Soto, J.; Barat, J. M.; Amorós, P. Enzyme-responsive controlled release using mesoporous silica supports capped with lactose. *Angew. Chem. Int. Ed.* **2009**, *48*, 5884-5887.
- 12 (a) Bernardos, A.; Mondragón, L.; Aznar, E.; Marcos, M. D.; Martínez-Máñez, R.; Sancenón, F.; Soto, J.; Barat, J. M.; Pérez-Payá, E.; Guillem, C.; Amorós, P. Enzyme-responsive intracellular controlled release using nanometric silica mesoporous supports capped with saccharides. *ACS Nano* **2010**, *11*, 6353-6368.  
(b) Agostini, A.; Mondragón, L.; Coll, C.; Aznar, E.; Marcos, M.D.; Martínez-Máñez, R.; Sancenón, F.; Soto, J.; Pérez-Payá, E.; Amorós, P. Dual enzyme-triggered controlled release on capped nanometric silica mesoporous supports. *Chem. Open* **2012**, *1*, 17-20.
- 13 Park, C.; Kim, H.; Kim, S.; Kim, C. Enzyme responsible nanocontainers with cyclodextrin gatekeepers and synergistic effects in release of guests. *J. Am. Chem. Soc.* **2009**, *131*, 16614-16616.
- 14 Thornton, P. D.; Heise, A. Highly specific dual enzyme-mediated payload release from peptide-coated silica particles. *J. Am. Chem. Soc.* **2010**, *132*, 2024-2028.
- 15 Coll, C.; Mondragón, L.; Martínez-Máñez, R.; Sancenón, F.; Marcos, M. D.; Soto, J.; Amorós, P.; Pérez-Payá, E. Enzyme-mediated controlled release systems by anchoring peptide sequences on mesoporous silica supports. *Angew. Chem. Int. Ed.* **2011**, *50*, 2138-2140.

- 16 Chen, C.; Geng, J.; Pu, F.; Yang, X.; Ren, J.; Qu, X. Polyvalent nucleic acid/mesoporous silica nanoparticle conjugates: Dual stimuli-responsive vehicles for intracellular drug delivery. *Angew. Chem. Int. Ed.* **2011**, *50*, 882-886.
- 17 (a) Kim, K. T.; Meeuwissen, S. A.; Nolte, R. J. M.; van Hest, J. C. M. Smart nanocontainers and nanoreactors. *Nanoscale* **2010**, *2*, 844-858. (b) Nguyen, T. D.; Leung, K. C. -F.; Liong, M.; Liu, Y.; Stoddart, J. F.; Zink, J. I. Versatile supramolecular nanovalves reconfigured for light activation. *Adv. Func. Mater.* **2007**, *17*, 2101-2110. (c) Angelos, S.; Johansson, E.; Stoddart, J. F.; Zink, J. I. Mesoporous silica supports for functional materials and molecular machines. *Adv. Func. Mater.* **2007**, *17*, 2261-2271.
- 18 (a) Rosenholm, J. M.; Sahlgren, C.; Lindén, M. Towards multifunctional, targeted drug delivery systems using mesoporous silica nanoparticles-opportunities & challenges. *Nanoscale* **2010**, *2*, 1870-1883. (b) Slowing, I. I.; Vivero-Escoto, J. L.; Wu, C. -W.; Lin, V. S. -Y. Mesoporous silica nanoparticles as controlled release drug delivery and gene transfection carriers. *Adv. Drug Deliver. Rev.* **2008**, *60*, 1278-1288.
- 19 (a) Cotí, K. K.; Belowich, M. E.; Liong, M.; Ambrogio, M. W.; Lau, Y. A.; Khatib, H. A.; Zink, J. I.; Khashab, N. M.; Stoddart, J. F. Mechanised nanoparticles for drug delivery. *Nanoscale*, **2009**, *1*, 16-39. (b) Vallet-Regí, M.; Ramila, A.; del Real, R. P.; Pérez-Pariente, J. A new property of MCM-41: Drug delivery system. *Chem. Mater.* **2001**, *13*, 308-311.
- 20 (a) Fox, M. E.; Szoka, F. C.; Fréchet, J. M. J. Soluble polymer carriers for the treatment of cancer: The importance of molecular architecture. *Acc. Chem. Res.* **2009**, *42*, 1141-1151. (b) Lee, S. -M.; Park, H.; Yoo, K. -H. Synergistic cancer therapeutic effects of locally delivered drug and heat using multifunctional nanoparticles. *Adv. Mater.* **2010**, *22*, 4049-4053. (c) Park, J. -H.; von Maltzahn, G.; Ruoslathi, E.; Bathia, S. M.; Sailor, M. J. Micellar hybrid nanoparticles for simultaneous magnetofluorescent imaging and drug delivery. *Angew. Chem. Int. Ed.* **2008**, *47*, 7284-7288. (d) Knop, K.; Hooogenboom, R.; Fischer, D.; Schubert, U. S. Poly(ethylene glycol) in drug delivery: Pros and cons as well as potential alternatives. *Angew. Chem. Int. Ed.* **2010**, *49*, 6288-6308.
- 21 Cabrera, S.; El Haskouri, J.; Guillem, C.; Latorre, J.; Beltrán, A.; Beltrán, D.; Marcos, M. D.; Amorós, P. Generalised syntheses of ordered mesoporous oxides: The atrane route. *Solid State Sci.* **2000**, *2*, 405-420.

- 22 (a) Coll, C.; Casasús, R.; Aznar, E.; Marcos, M. D.; Martínez-Máñez, R.; Sancenón, F.; Soto, J.; Amorós, P. Nanoscopic hybrid systems with a polarity-controlled gate-like scaffolding for the colorimetric signalling of long-chain carboxylates. *Chem. Commun.* **2007**, 1957-1959. (b) Bernardos, A.; Aznar, E.; Coll, C.; Martínez-Máñez, R.; Barat, J. M.; Marcos, M. D.; Sancenón, F.; Benito, A.; Soto, J. Controlled release of vitamin B<sub>2</sub> using mesoporous materials functionalized with amine-bearing gate-like scaffoldings. *J. Control, Release* **2008**, *131*, 181-189. (c) Candel, I.; Bernardos, A.; Climent, E.; Marcos, M. D.; Martínez-Máñez, R.; Sancenón, F.; Soto, J.; Costero, A. M.; Gil, S.; Parra, M. Selective opening of nanoscopic capped mesoporous inorganic materials with nerve agent simulants; an application to design chromo-fluorogenic probes. *Chem. Commun.* **2011**, *47*, 8313-8315.
- 23 (a) Felix, F.; Ferguson, J.; Guedel, H. U.; Ludi, A. The electronic spectrum of tris(2,2'.bipyridine)ruthenium(2+). *J. Am. Chem. Soc.* **1980**, *102*, 4096-4102. (b) Lytle, F. E.; Hercules, D. M. Luminescence of tris(2,2'.bipyridine)ruthenium(II) dichloride. *J. Am. Chem. Soc.* **1969**, *91*, 253-257.
- 24 Vallet-Regí, M.; Balas, F.; Arcos, D. Mesoporous materials for drug delivery. *Angew. Chem. Int. Ed.* **2007**, *46*, 7548-7558.
- 25 (a) Pommier, Y. DNA topoisomerase I inhibitors: Chemistry, biology and interfacial inhibition. *Chem. Rev.* **2009**, *109*, 2894-2902. (b) Li, Q. -Y.; Zu, Y. -G.; Shi, R. -Z.; Yao, L. -P. Review camptothecin: Current perspectives. *Curr. Med. Chem.* **2006**, *13*, 2021-2039.

**Chapter 7:**  
***Dual enzyme-triggered controlled release on  
capped nanometric silica mesoporous supports***



# ***Dual enzyme-triggered controlled release on capped nanometric silica mesoporous supports***

Alessandro Agostini,<sup>[a]</sup> Laura Mondragón,<sup>[a]</sup> Carmen Coll,<sup>[a]</sup> Elena Aznar,<sup>[a]</sup> Enrique Pérez-Payá,<sup>[b]</sup> M. Dolores Marcos,<sup>[a]</sup> Ramón Martínez-Mañez\*,<sup>[a]</sup> Félix Sancenón,<sup>[a]</sup>  
Juan Soto <sup>[a]</sup> and Pedro Amorós <sup>[c]</sup>

<sup>[a]</sup>*Centro de Reconocimiento Molecular y Desarrollo Tecnológico (IDM),  
Unidad Mixta Universidad Politécnica de Valencia-Universidad de Valencia.*

*Departamento de Química, Universidad Politécnica de Valencia,  
Camino de Vera s/n, 46022, Valencia, Spain.*

*CIBER de Bioingeniería, Biomateriales y Nanotecnología (CIBER-BNN).*

<sup>[b]</sup>*Centro de Investigación Príncipe Felipe, Laboratorio de Péptidos y Proteínas,  
Alda. Autopista al Saler, 16, E-46012, Valencia, Spain.*

<sup>[c]</sup>*Institut de Ciència del Materials (ICMUV), Universitat de València. P.O. Box  
22085, E-46071 València, Spain.*

***Received: October 28, 2011,***

***Published online, February 17, 2012***

*ChemistryOpen*, **2012**, *1*, 17–20

## **7.1 Introduction**

The development of nanoscopic hybrid materials equipped with “molecular gates” showing the ability of releasing target entrapped guests upon the application of an external trigger has attracted great attention and has been extensively explored during the past years.<sup>1</sup> These nano-devices are composed by two subunits, namely, a suitable support and certain capping entities grafted on the surface of the scaffolding.<sup>2</sup> The support is used as suitable reservoir in which certain chemicals could be stored whereas the molecules grafted in the outer surface act as a “gate” and could control the release of the entrapped molecules at will. Both components have been carefully selected and arranged in order to achieve a wide range of required functionalities.

As support, mesoporous silica nano-particles (MSN) have been widely used due to their unique properties such as large load capacity, biocompatibility, high surface area and well-known functionalization procedures.<sup>3</sup> Moreover gated MSN have recently been used for the development of on-command delivery nano-devices using several physical and chemical triggers. For instance, MSN displaying controlled release features using light,<sup>4</sup> redox reactions,<sup>5</sup> and pH changes<sup>6</sup> have been described. In contrast, gated nano-materials able to deliver the cargo triggered by bio-molecules are scarce although some few illustrative examples using antigen-antibody interactions,<sup>7</sup> hybridisation of single stranded oligonucleotides,<sup>8</sup> and enzymes<sup>9–14</sup> have been reported. In particular, the use of enzymes is especially appealing taking into account the possibility to synthesise tailor-made enzyme-specific sequences as molecular caps. However, in spite of these interesting features there are few examples using enzymes in opening protocols. The first enzyme-responsive

gated in a mesoporous support was described by Stoddart and co-workers. In that work, a [2]rotaxane ended with a bulky ester-adamantly stopper that acted as molecular gate was removed by porcine liver esterase treatment.<sup>9</sup> Further hybrid systems involving avidin-biotin,<sup>10</sup> lactose,<sup>11</sup> starch,<sup>12</sup>  $\beta$ -cyclodextrins<sup>13</sup> and peptide sequences<sup>14</sup> as capping groups have been reported. These examples offer a chemically simple approach that will benefit of the vast knowledge on enzyme-substrate pairs for the design of versatile systems for controlled release.

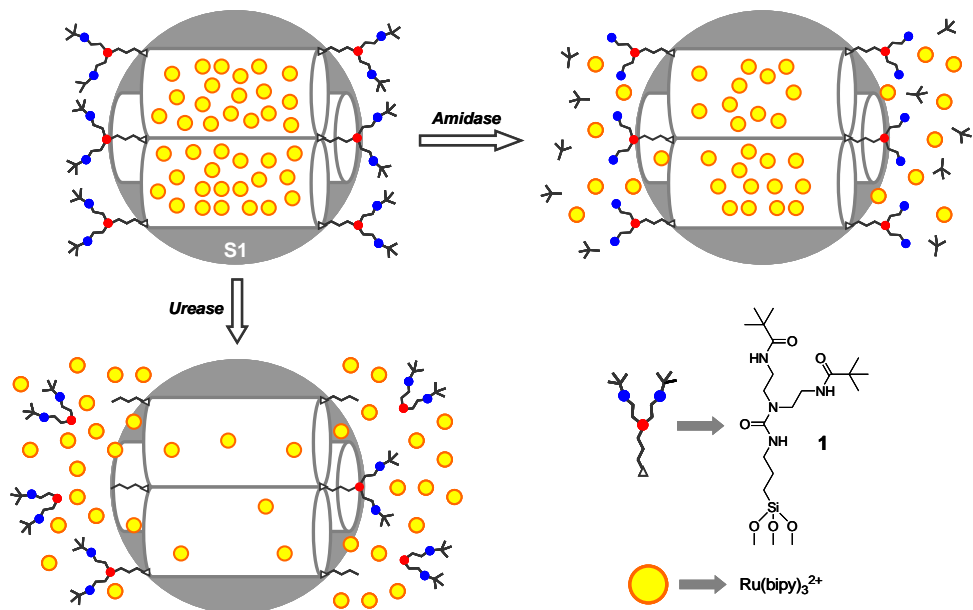
A further step in the field should take into account that the flow of defined biological processes rely on biochemical networks with the participation of multiple enzyme-dependent steps. It would be then useful to define future applications with the development of dual or multiple enzyme-triggered systems using capped mesoporous supports. This would require the design of capping threads containing different enzyme-specific hydrolysable linkers located at defined positions on the external surface of MSN. The whole design will provide highly versatile and specific release nanodevices whose delivery profiles could be controlled and fine-tuned by specific combinations of enzymes.

As a *first-of-its-kind* proof-of-concept, we have prepared a MSN support capped with the molecular entity **1** that contains amide and urea linkages and evaluated it as a multi-enzyme-tuned delivery system.

## **7.2 Results and Discussion**

As inorganic carrier vehicle we selected mesoporous MCM-41 silica nanoparticles of ca. 100 nm of diameter which were prepared following well known procedures using TEOS as hydrolytic inorganic precursor and hexadecyltrimethylammonium bromide (CTAB) as porogen species.<sup>15</sup> The

structure of the nanoparticulated calcined MCM-41 starting material was confirmed by X-Ray diffraction (see Figure 1), TEM and SEM microscopy.



**Scheme 1.** Schematic representation of solid S1 and the enzymatic uncapping mechanism.

The  $N_2$  adsorption-desorption isotherms showed a typical type IV-curve with a specific surface of  $999.6 \text{ m}^2 \text{ g}^{-1}$ , and a pore volume of  $0.79 \text{ cm}^3 \text{ g}^{-1}$ . From the XRD, porosimetry and TEM studies, the  $a_0$  cell parameter (4.44 nm), the pore diameter (2.46 nm) and a value for the wall thickness (1.99 nm) were calculated. For the preparation of **S1**, the calcinated MSN was first loaded with  $[\text{Ru}(\text{bipy})_3]\text{Cl}_2$  that was used as dye for monitoring the enzyme-triggered protocol, and then reacted with the capping molecule **1**. The derivative **1** was synthesised following a two-step procedure from diethylentriamine. In a first step both primary amine moieties of

diethylentriamine were selectively amidated with pivaloyl anhydride at 0 °C.<sup>16</sup> In a second step, the free secondary amine was reacted with (3-isocyanatopropyl)triethoxysilane in the presence of  $K_2CO_3$  yielding the final trialkoxysilane derivative **1** (see Supporting Information for experimental details).

The prepared solid **S1** was characterised using standard techniques. **S1** displays expected features of the MCM-41 phase as it can be observed in the TEM image of Figure 1. This suggests that loading and grafting procedures did not modify the mesoporous structure of the starting material.

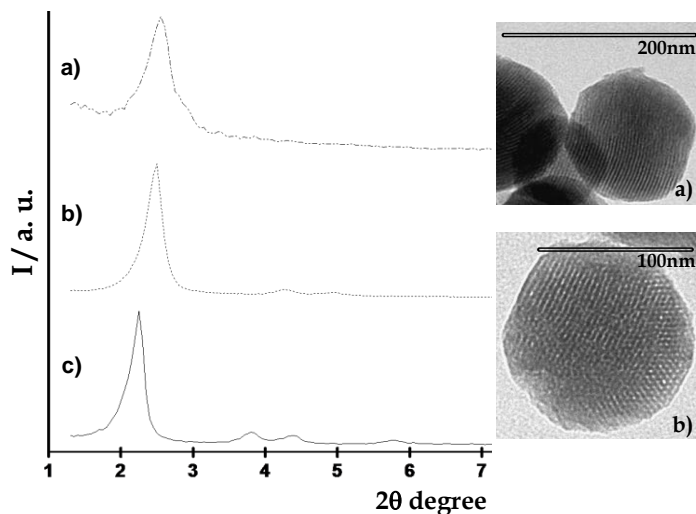


**Figure 1.** Left: powder X-ray patterns of solid **S1** (a), calcined MCM-41 (b) and MCM-41 as synthesized (c). Right: TEM images of solid **S1** (a) and calcined MCM-41 sample (b) showing the typical hexagonal porosity of the MCM-41 mesoporous matrix.

Additionally the  $N_2$  adsorption-desorption isotherm of **S1** was typical of mesoporous systems with filled mesopores, and a significant decrease in the  $N_2$  volume adsorbed and surface area ( $696.5 \text{ m}^2/\text{g}$ ) was observed. The content of ruthenium complex and capping molecule **1** in the final solid **S1**

were determined by thermogravimetric and elemental analysis and amounts to 0.15 and 0.22 mmol / g SiO<sub>2</sub>, respectively.

The presence in the capping molecule **1** of amide and urea moieties allowed the analysis of a multi-enzyme-dependent release of the [Ru(bipy)<sub>3</sub>]<sup>2+</sup> dye from **S1** using amidase and urease enzymes. In a typical experiment, 5 mg of solid **S1** were suspended in 12.5 mL of water at pH 7.5. Then 1 μL of amidase or/and urease was added and the final suspension stirred. As control experiment dye release was also determined using suspensions of **S1** under similar conditions but in absence of enzyme. Uncapping and subsequent delivery of the dye to the aqueous solution was easily detected via monitorisation of the metal-to-ligand charge transfer transition band of the [Ru(bipy)<sub>3</sub>]<sup>2+</sup> dye at 451 nm or through the emission band at 619 nm ( $\lambda_{\text{ex}} = 451 \text{ nm}$ ).<sup>17</sup> The different delivery profiles for both experiments are shown in Figure 2. In the presence of amidase a relatively quick delivery was found (ca. 20 % of the cargo was released in 2 hours), however only a moderate delivery was observed for long periods of time (only 40 % of the dye was delivered after 15 hours). In contrast the urease-stimulated release was slower (for instance no delivery was observed after 2.5 hours), yet at longer times urease was able to deliver a significant larger amount of the cargo from **S1** (ca. 80% of the dye was delivered after 15 hours) than the amidase. We also observed that a very low payload release was detected in the absence of urease or amidase (see Figure 2).

The different enzyme-dependent delivery rates obtained on solid **S1** were related to the design of gate 1, in particular to the relative position of the hydrolysable groups on the molecule. Solid **S1** treatment with amidase induced the hydrolysis of the amide bonds located far away from the surface with the subsequent release of two bulky trimethylacetate moieties.

In spite of this reduction in the steric crowding around the pore outlets, the organic residual that remain anchored was large enough to hamper, to some extent, the release of the dye.

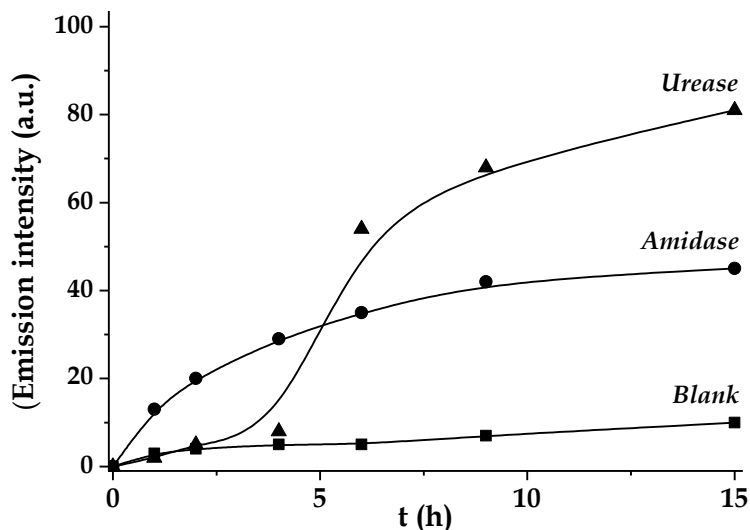


**Figure 2.** Kinetics of the release of  $[\text{Ru}(\text{bipy})_3]^{2+}$  dye from solid **S1** in the presence of amidase and urease.

As a consequence, the degree of cargo release is low but fast. On changing from amidase to urease a completely different response was obtained. Addition of urease induced the hydrolysis of the urea bond located deeper inside the structure of **1** leading to a drastic reduction of the thread size. As consequence, the degree of cargo release is high but quite slow.

Release experiments with **S1** in the presence of both enzymes were also carried out. In this case, a synergic effect was observed; the action of the amidase induced a rapid cargo release, whereas at longer times the combined action of the urease allows a nearly complete cargo delivery (see Supporting Information). Additionally, in order to further demonstrate that the enzymes-treatment is entirely responsible of the cargo release, two

additional experiments were carried out. Solid **S1** was incubated in the presence of non-related enzymes such as esterase and pronase. In a different experiment, prior incubation with solid **S1** the amidase and urease were heat-denaturated at 60°C for 60 minutes. In both experiments no release of the dye was observed.

Once demonstrated the *in vitro* aperture mechanism of **S1**, our next objective was to test the feasibility of using this gated nanodispositive in cells. For this purpose, the HeLa cell line was chosen and treated with **S1** at different doses for 24 hours. Cell viability and cellular uptake of nanoparticles was assessed by WST-1 assay and confocal microscopy (Figure 3).<sup>18</sup>

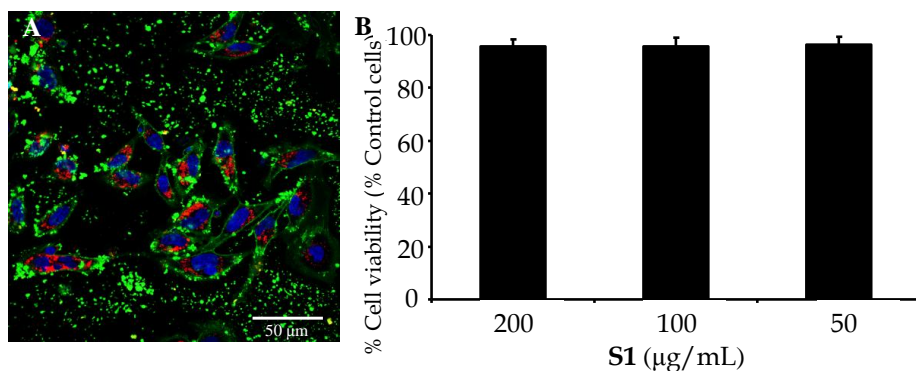


**Figure 3.** Confocal microscopy images corresponding to HeLa cells treated with solid **S1** (100 µg/mL). The cellular uptake of **S1** was followed by [Ru(bipy)<sub>3</sub>]<sup>2+</sup> associated fluorescence (red) in the presence of DNA marker Hoechst 33342 (blue) and the plasma membrane marker WGA Alexa Fluor 647 (green). For cell viability studies, cells were treated with **S1** and after 24 hours of incubation, WST-1 reagent was added and cell viability measured.

The same experiments were also performed using the MCF-7 cell line (see Supporting Information for further details). Confocal images demonstrated the intracellular vesicular localization of **S1** nanoparticles in

red, probably associated to lysosomes. Besides, **S1** solid turned out to be biocompatible at the concentrations tested as no significant reduction in cell viability was observed.

With the aim to demonstrate a possible therapeutical application of these nanodevices as drug-carriers, a new **S1** solid was synthesized containing the chemotherapeutic agent camptothecin (CPT). CPT is a cytotoxic quinoline alkaloid that inhibits DNA polymerase I disrupting DNA replication inducing cell death. HeLa cells were treated as described before in the presence of this new material **S1-CPT**.

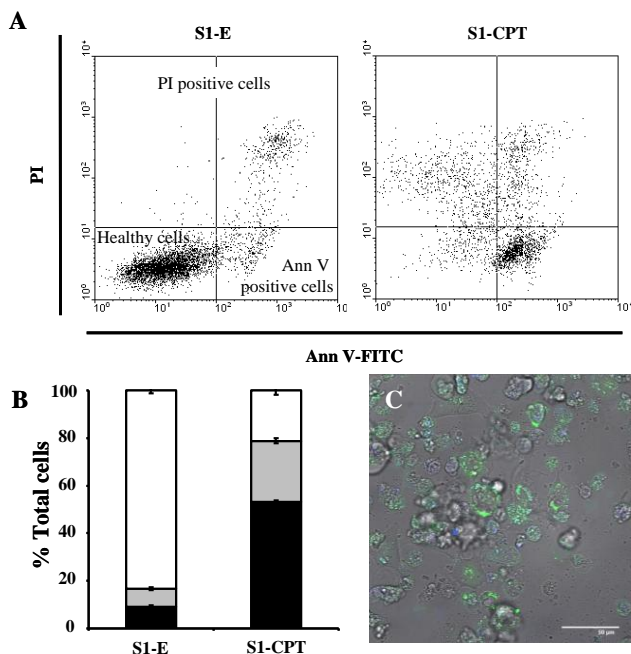


**Figure 4.** **S1-CPT** cell death induction. HeLa cells were treated with 200  $\mu\text{g}/\text{mL}$  of **S1-CPT** or **S1-E** for 24 hours and then flow cytometry studies and quantification of viable cells (white) and dead cells was performed by PI (black) and Ann V (grey) stainings (A,B). Two independent experiments containing duplicates were developed. Statistically significant differences were observed ( $P < 0.05$ , Student t test). Cellular internalization and release of the cargo of **S1-CPT** was followed by confocal microscopy (blue) (C) in the presence of the plasma membrane marker WGA Alexa Fluor 647 (green).

In order to obtain a more detailed analysis of the cell death processes related to the in cell release of CPT from the nanoparticles, the cell viability dye propidium iodide (PI) and the early-stages cell death marker Annexin V (Ann V) were employed (see Supporting Information for further details). Figure 4 portrays the results obtained by confocal microscopy and flow cytometry.

A significant reduction in cell viability was observed 24 hours after the addition of **S1-CPT** by confocal microscopy studies (cells detached from the plate, plasma membrane blebbing, and presence of cellular corpses, among others). These results were confirmed by flow cytometry experiments. Just 24 hours after the addition of 200  $\mu\text{g}/\text{mL}$  of **S1-CPT**, 50% of the cells were dead and 25% had initiated cell death processes. By contrast, no significant reduction in cell viability was observed when cells were treated with **S1-E**, a **S1** solid with no cargo molecule (see Supporting Information for further details).

### **7.3 Conclusions**

In summary, we have reported here the synthesis of new nanoscopic silica mesoporous supports capped with enzyme hydrolysable groups for the design of nanodevices for zero release that are specifically opened in the presence of targeted enzymes. In particular we have designed gated materials capped with bulky organic moieties containing amide and urea linkages that could selectively be hydrolysed in the presence of amidase and urease, respectively. A remarkable different delivery profile was observed depending on the enzyme used. The amidase induced the hydrolysis of two amide bond located far away from the inorganic support allowing an immediate, yet not complete, release of the dye. In contrast, the

urease hydrolysed the urea bond, located deeper inside the capping molecule and closer to the surface of the silica nanoparticle, allowing a near total cargo release but delayed in time. The simultaneous treatment with both enzymes displayed a synergistic effect and a delivery profile showing fast and complete payload release was observed. These results demonstrated that is possible to use relatively simple molecules containing enzyme-hydrolysable groups for the design of versatile capped materials that can be opened at will. The possibility of including, in the capping molecule, different enzyme-hydrolysable groups located in predefined position allow to make a control of the delivery profiles. Based on the fact that enzyme-substrate pairs offer a vast range of different combinations, a proof-of-concept of the possible application of this nanodevice as drug-carrier was performed proving the ability of the **S1-CPT** solid to be internalized by cells and release its cargo. We believe that the design of multi-enzyme-responsive capped materials can have importance in the design of custom-made systems for delivery applications with the aim of controlling the flow of key biological processes in nano- and regenerative-medicine.

## 7.4 Bibliography

- 1 a) S. Saha, K. C. -F, Leung, T. D. Nguyen, J. F. Stoddart, J. I. Zink, *Adv. Func. Mater.* **2007**, *17*, 685-693; b) B. G. Trewyn, I. I. Slowing, S. Giri, H. -T. Chen, V. S. -Y. Lin, *Acc. Chem. Res.* **2007**, *40*, 846-853.
- 2 E. Aznar, R. Martínez-Mañez, F. Sancenón, *Expert Opin. Drug Deliv.* **2009**, *6*, 643-655.
- 3 a) J. S. Beck, J. C. Vartuli, W. J. Roth, M. E. Leonowicz, C. T. Kresge, K. D. Schmitt, C. T. -W. Chu, D. H. Olson, E. W. Sheppard, S. B. McCullen, J. B. Hoggins, J. L. Schlenker, *J. Am. Chem. Soc.* **1992**, *114*, 10834-10843; b) A. P.

- Wright, M. E. Davis, *Chem. Rev.* **2002**, *102*, 3589-3614; c) G. Kickelbick, *Angew. Chem. Int. Ed.* **2004**, *43*, 3102-3104.
- 4 a) N. K. Mal, M. Fujiwara, Y. Tanaka, *Nature* **2003**, *421*, 350-353; b) N. K. Mal, M. Fujiwara, Y. Tanaka, T. Taguchi, M. Matsukata, M. *Chem. Mater.* **2003**, *15*, 3385-3394; c) Y. Zhu, M. Fujiwara, *Angew. Chem. Int. Ed.* **2007**, *46*, 2241-2244; d) N. Liu, Z. Chen, D. R. Dunphy, Y. B. Jiang, R. A. Assink, C. J. Brinker, *Angew. Chem. Int. Ed.* **2003**, *42*, 1731-1734; e) E. Aznar, R. Casasús, B. García-Acosta, M. D. Marcos, R. Martínez-Máñez, F. Sancenón, J. Soto, P. Amorós, *Adv. Mater.* **2007**, *19*, 2228-2231; f) C. Park, K. Lee, C. Kim, C. *Angew. Chem. Int. Ed.* **2009**, *48*, 1275-1278; g) D. P. Ferris, Y. -L. Zhao, N. M. Khashab, H. A. Khatib, J. F. Stoddart, J. I. Zink, *J. Am. Chem. Soc.* **2009**, *131*, 1686-1688; h) Q. Lin, Q. Huang, C. Li, C. Bao, Z. Liu, F. Li, L. Zhu, *J. Am. Chem. Soc.* **2010**, *132*, 10645-10647. i) N. Ž. Knežević, B. G. Trewyn, V. S. -Y. Lin, *Chem. Eur. J.* **2011**, *17*, 3338-3342; j) N. Ž. Knežević, B. G. Trewyn, V. S. -Y. Lin, *Chem. Commun.* **2011**, *47*, 2817-2819.
- 5 a) B. G. Trewyn, S. Giri, I. I. Slowing, V. S. -Y. Lin, *Chem. Commun.* **2007**, 3236-3245; b) F. Torney, B. G. Trewyn, V. S. -Y. Lin, K. Wang, *Nat. Nanotechnol.* **2007**, *2*, 295-300; c) D. R. Radu, C. -Y. Lai, K. Jeftinija, E. W. Rowe, S. Jeftinija, V. S. -Y. Lin, *J. Am. Chem. Soc.* **2004**, *126*, 13216-13217; d) S. Giri, B. G. Trewyn, M. P. Stellmaker, V. S. -Y. Lin, *Angew. Chem. Int. Ed.* **2005**, *44*, 5038-5044; e) M. Fujiwara, S. Terashima, Y. Endo, K. Shiokawa, H. Ohue, *Chem. Commun.* **2006**, 4635-4637; f) R. Liu, X. Zhao, T. Wu, P. Feng, *J. Am. Chem. Soc.* **2008**, *130*, 14418-14419; g) T. D. Nguyen, Y. Liu, S. Saha, K. F. -C. Leung, J. F. Stoddart, J. I. Zink, *J. Am. Chem. Soc.* **2007**, *129*, 626-634.
- 6 a) R. Casasús, M. D. Marcos, R. Martínez-Máñez, J. V. Ros-Lis, J. Soto, L. A. Villaescusa, P. Amorós, D. Beltrán, C. Guillem, J. Latorre, *J. Am. Chem. Soc.* **2004**, *126*, 8612-8613; b) R. Casasús, E. Climent, M. D. Marcos, R. Martínez-Máñez, F. Sancenón, J. Soto, P. Amorós, J. Cano, E. Ruiz, *J. Am. Chem. Soc.* **2008**, *130*, 1903-1917; c) E. Aznar, M. D. Marcos, R. Martínez-Máñez, F. Sancenón, J. Soto, P. Amorós, C. Guillem, *J. Am. Chem. Soc.* **2009**, *131*, 6833-6843; d) S. Angelos, Y. -W. Yang, N. M. Khashab, J. F. Stoddart, J. I. Zink, *J. Am. Chem. Soc.* **2009**, *131*, 11344-11346; e) S. Angelos, Y. -W. Yang, K. Patel, J. F. Stoddart, J. I. Zink, *Angew. Chem. Int. Ed.* **2008**, *47*, 2222-2226; f) S. Angelos, N. M. Khashab, Y. -W. Yang, A. Trabolsi, H. A. Khatib, J. F. Stoddart, J. I. Zink, *J. Am. Chem. Soc.* **2009**, *131*, 12912-12914; g) L. Du, S. Liao, H. A. Khatib, J. F. Stoddart, J. I. Zink, *J. Am. Chem. Soc.* **2009**, *131*, 15136-15142; h) Q. Yang, S. Wang, P. Fan, L. Wang, Y. Di, K. Lin, F. -S. Xiao, *Chem. Mater.* **2005**, *17*, 5999-6003; i) C. Park, K. Oh, S. C. Lee,

- C. Kim, *Angew. Chem. Int. Ed.* **2007**, *46*, 1455-1457; j) L. Chen, J. Di, C. Cao, Y. Zhao, Y. Ma, J. Luo, Y. Wen, W. Song, Y. Song, L. Jiang, *Chem. Commun.* **2011**, *47*, 2850-2852.
- 7 E. Climent, A. Bernardos, R. Martínez-Máñez, A. Maquieira, M. D. Marcos, N. Pastor-Navarro, R. Puchades, F. Sancenón, J. Soto, P. Amorós, *J. Am. Chem. Soc.* **2009**, *131*, 14075-14080.
- 8 E. Climent, R. Martínez-Máñez, F. Sancenón, M. D. Marcos, J. Soto, A. Maquieira, P. Amorós, *Angew. Chem. Int. Ed.* **2010**, *49*, 7281-7283.
- 9 K. Patel, S. Angelos, W. R. Dichtel, A. Coskun, Y. -W. Yang, J. I. Zink, J. F. Stoddart, *J. Am. Chem. Soc.* **2008**, *130*, 2382-2383.
- 10 A. Schlossbauer, J. Kecht, T. Bein, *Angew. Chem. Int. Ed.* **2009**, *48*, 3092-3095.
- 11 A. Bernardos, E. Aznar, M. D. Marcos, R. Martínez-Máñez, F. Sancenón, J. Soto, J. M. Barat, P. Amorós, *Angew. Chem. Int. Ed.* **2009**, *48*, 5884-5887.
- 12 A. Bernardos, L. Mondragón, E. Aznar, M. D. Marcos, R. Martínez-Máñez, F. Sancenón, J. Soto, J. M. Barat, E. Pérez-Payá, C. Guillem, P. Amorós, *ACS Nano* **2010**, *11*, 6353-6368.
- 13 C. Park, H. Kim, S. Kim, C. Kim, *J. Am. Chem. Soc.* **2009**, *131*, 16614-16615.
- 14 a) P. D. Thornton, A. Heise, *J. Am. Chem. Soc.* **2010**, *132*, 2024-2028; b) C. Coll, L. Mondragón, R. Martínez-Máñez, F. Sancenón, M. D. Marcos, J. Soto, P. Amorós, E. Pérez-Payá, *Angew. Chem. Int. Ed.* **2011**, *50*, 2138-2140.
- 15 S. Cabrera, J. El Haskouri, C. Guillem, J. Latorre, A. Beltrán, D. Beltrán, M. D. Marcos, P. Amorós, *Solid State Sci.* **2000**, *2*, 405-420.
- 16 J. M. Goldcamp; D. T. Rosa; N. A. Landers; Mandel, S.M. Bauer. J. A. Krause; M. J. Baldwin, *Synthesis*, **2000**, 2033-2038.
- 17 a) F. Felix, J. Freguson, H. U. Guedel, A. Ludi, *J. Am. Chem. Soc.*, **1980**, *102*, 4096-4102; b) F. E. Lytle, D. M. Hercules, *J. Am. Chem. Soc.*, **1969**, *91*, 253-257.

- 18 A. Bernardos, L. Mondragón, E. Aznar, M. D. Marcos, R. Martínez-Máñez, F. Sancenón, J. Soto, J. M. Barat, E. Pérez-Payá, C. Guillem, P. Amorós, *ACS Nano*, **2010**, *4*, 6353-6368.

# ***Dual enzyme-triggered controlled release on capped nanometric silica mesoporous supports***

Alessandro Agostini,<sup>[a]</sup> Laura Mondragón,<sup>[a]</sup> Carmen Coll,<sup>[a]</sup> Elena Aznar,<sup>[a]</sup> Enrique Pérez-Payá,<sup>[b]</sup> M. Dolores Marcos,<sup>[a]</sup> Ramón Martínez-Mañez\*,<sup>[a]</sup> Félix Sancenón,<sup>[a]</sup>  
Juan Soto <sup>[a]</sup> and Pedro Amorós <sup>[c]</sup>

<sup>[a]</sup>*Centro de Reconocimiento Molecular y Desarrollo Tecnológico (IDM),  
Unidad Mixta Universidad Politécnica de Valencia-Universidad de Valencia.*

*Departamento de Química, Universidad Politécnica de Valencia,  
Camino de Vera s/n, 46022, Valencia, Spain.*

*CIBER de Bioingeniería, Biomateriales y Nanotecnología (CIBER-BNN).*

<sup>[b]</sup>*Centro de Investigación Príncipe Felipe, Laboratorio de Péptidos y Proteínas,  
Alda. Autopista al Saler, 16, E-46012, Valencia, Spain.*

<sup>[c]</sup>*Institut de Ciència del Materials (ICMUV), Universitat de València. P.O. Box  
22085, E-46071 València, Spain.*

***Supporting Information***

### ***Chemicals***

All of the reactants employed were purchased from Sigma-Aldrich Química S. A. (Madrid, Spain) and used without further purification. For cell biology studies, D-MEM with L-glutamine, fetal calf serum (FCS), trypan blue solution (0.4%) cell culture grade, trypsin, wheat germ agglutinin Alexa Fluor 647, and Hoechst 33342 were provided by Gibco-Invitrogen. The cell proliferation reagent WST-1 was obtained from Roche Applied Science. Camptothecin was provided by Sequoia Research Products, Ltd. Annexin V and propidium iodide were provided by BD Pharmingen.

### ***General Techniques***

Powder X-ray diffraction, TG Analysis, elemental analysis, EDX microscopy, N<sub>2</sub> adsorption-desorption techniques were employed to characterize the prepared materials. Powder X-ray measurements were performed on a Philips D8 Advance diffractometer using Cu K<sub>α</sub> radiation. Thermo-gravimetric analysis were carried out on a TGA/SDTA 851e Mettler Toledo balance, using an oxidant atmosphere (air, 80 mL/min) with a heating program consisting on a heating ramp of 10 °C per minute from 393 to 1273 K and an isothermal heating step at this temperature during 30 minutes. TEM images were obtained with a 100 kV Philips CM10 microscope. N<sub>2</sub> adsorption-desorption isotherms were recorded on a Micromeritics ASAP2010 automated sorption analyser. The samples were degassed at 120 °C in vacuum overnight. The specific surface areas were calculated from the adsorption data in the low pressures range using the BET model. Pore size was determined following the BJH method. Fluorescence spectroscopy was carried out on a Felix 32 Analysis Version

1.2 (Build 56) PTI (Photon Technology International.  $^1\text{H}$  and  $^{13}\text{C}$  nuclear magnetic resonance (NMR) were acquired with Varian 300 spectrometer (Sunnyvale, CA, USA). Live cellular internalization studies were performed with a Cytomics FC 500 (Beckman Coulter Inc.) and a confocal Leica microscope handled with a TCS SP2 system, equipped with an acoustic optical beam splitter (AOBS). Cell viability measurements were carried out with a Wallac 1420 workstation.

### ***Synthesis of the silica mesoporous nanoparticles support (MCM)***

The MCM-41 mesoporous nanoparticles were synthesized by the following procedure: *n*-cetyltrimethylammoniumbromide (CTAB, 1.00 g, 2.74 mmol) was first dissolved in 480 mL of deionized water. Then 3.5 mL of NaOH 2.00 M in deionized water was added to the CTAB solution, followed by adjusting the solution temperature to 80°C. TEOS (5.00 mL,  $2.57 \cdot 10^{-2}$  mol) was then added dropwise to the surfactant solution. The mixture was stirred during 2 h to give a white precipitate. Finally the solid product was centrifuged, washed with deionized water and ethanol, and dried at 60°C (MCM-41 as-synthesized). To prepare the final porous material (MCM-41), the as-synthesized solid was calcined at 550 °C using an oxidant atmosphere for 5 h in order to remove the template phase

### ***Synthesis of product I***

A solution of pivaloyl anhydride (1.81 g, 9.72 mmol) in  $\text{CHCl}_3$  (30 ml) was added dropwise to a chloroform solution (30 mL) of diethylentriamine (0.50 g, 4.8 mmol) at 0°C during 30 minutes. After this, the reaction mixture was stirred for another 60 minutes and then filtered. The filtrate was extracted with sat.  $\text{Na}_2\text{CO}_3$  (2 x 20 ml). The  $\text{CHCl}_3$  layer was then dried ( $\text{Na}_2\text{SO}_4$ ),

filtered and the solvent removed by rotary evaporation. The resulting white solid (**I**, 0.85 g, 64 % yield) was washed with *n*-hexane. The <sup>1</sup>H NMR and <sup>13</sup>C NMR data were coincident with the published by Goldcamp et al (see Figure SI-1 and SI-2).<sup>1</sup>

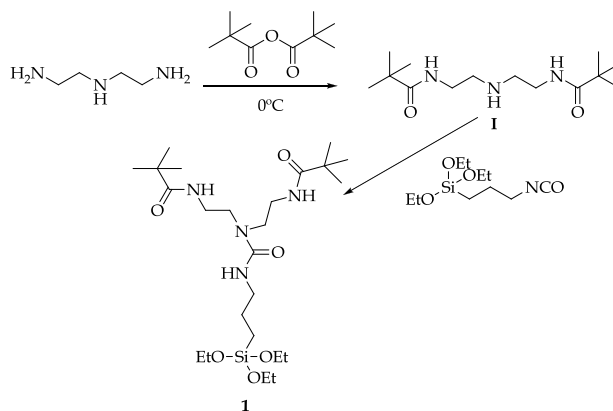


Figure SI-1. Synthesis of compounds **I** and **1**.

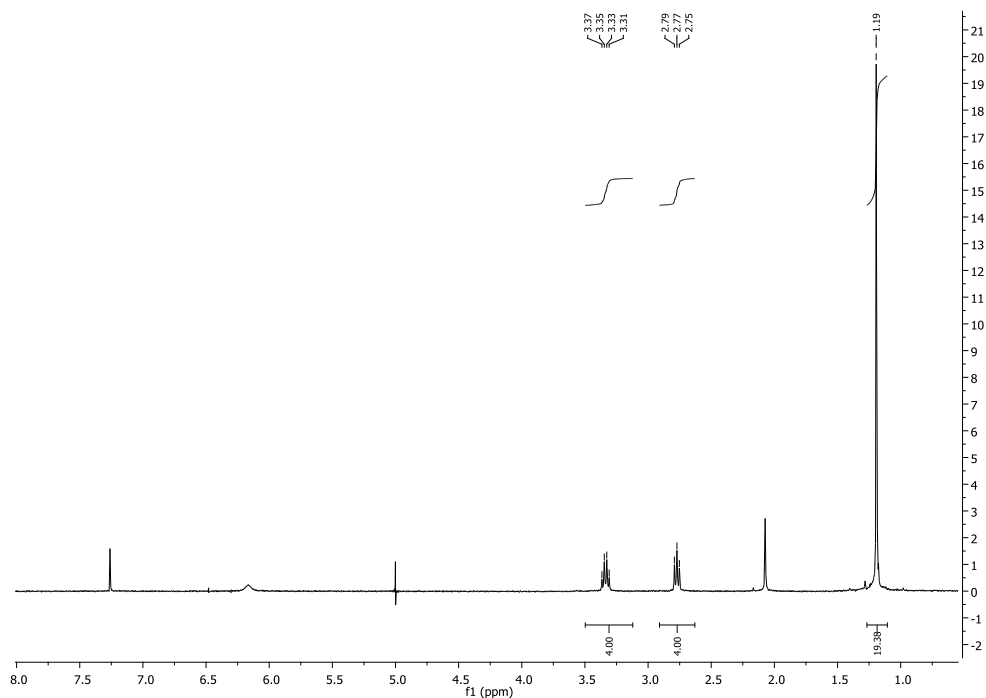


Figure SI-2. <sup>1</sup>H-NMR of compound **I**

*Synthesis of product 1*

**I** (900 mg, 3.31 mmol) was dissolved in chloroform (50 mL) and an excess of anhydrous potassium carbonate was added to the solution. Then 3-(triethoxyethylsilyl)propyl isocyanate (864 mg, 3.50 mmol) was added to the previous mixture in an argon atmosphere. The resultant suspension was stirred at room temperature overnight. The crude reaction was filtered and the solvent removed by rotary evaporation to give the final product (**1**, 1.54 g, 2.98 mmol, 90% yield).

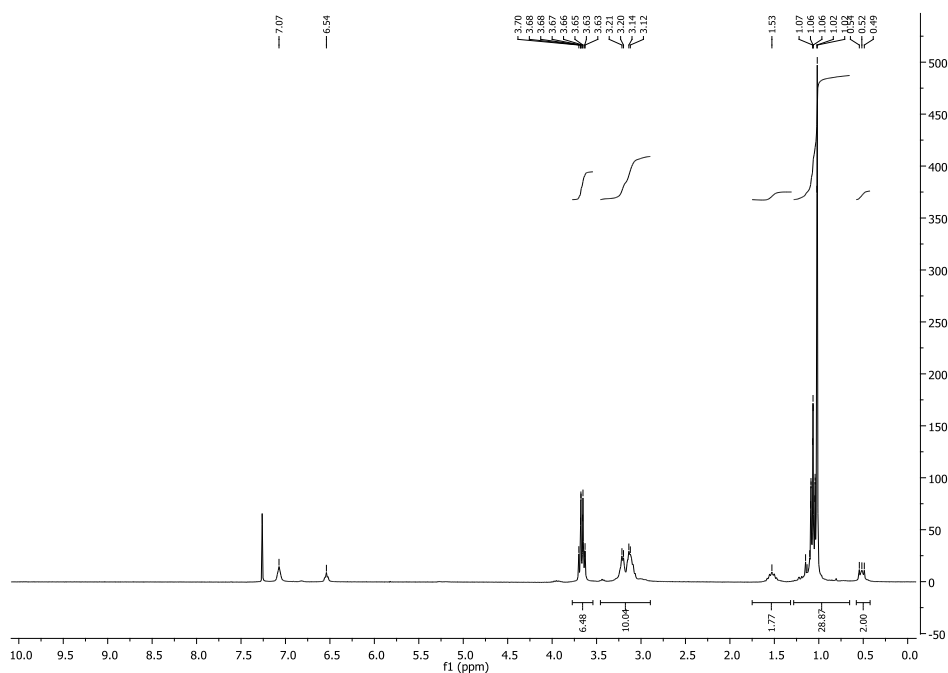


Figure SI-3.  $^1\text{H-NMR}$  of compound **1**

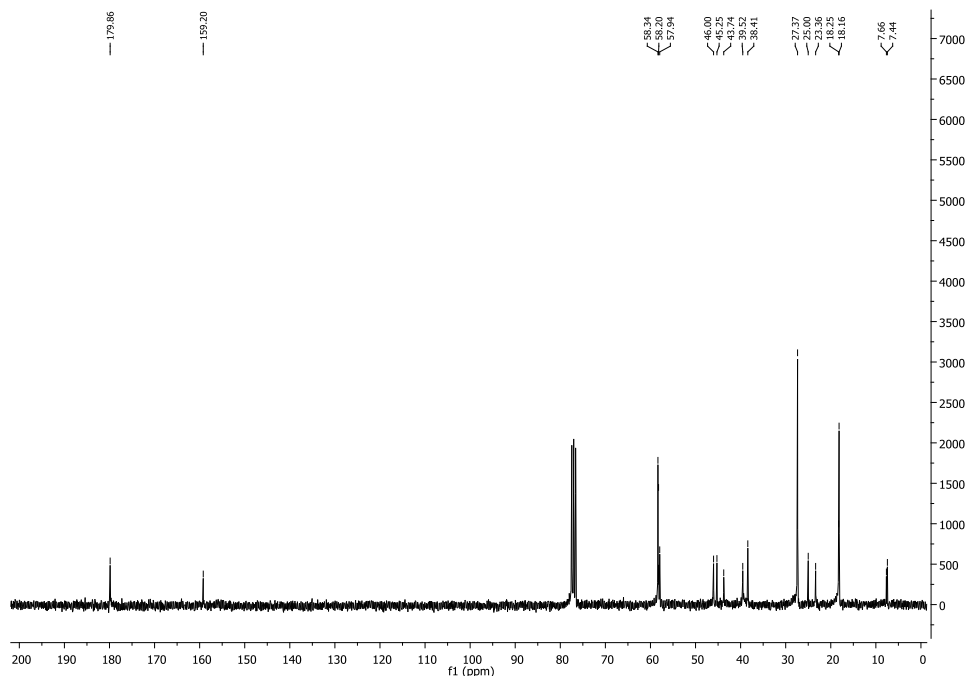


Figure SI-4.  $^{13}\text{C}$ -NMR of compound **1**

### Synthesis of solid **S1**

With the aim to obtain solid **S1**, MCM-41 calcined (512 mg) was suspended in anhydrous  $\text{CH}_3\text{CN}$  (25 mL) and  $[\text{Ru}(\text{Bipy})_3]\text{Cl}_2 \cdot 6\text{H}_2\text{O}$  (302 mg, 0.404 mmol) was added. Then 10 ml of  $\text{CH}_3\text{CN}$  were distilled, with a dean-stark from reaction mixture, in order to remove the water present in the pores of the solid. Afterwards the mixture was stirred at room temperature during 24 hours. Subsequently, product **1** (1.33 g, 2.56 mmol) was added and the mixture was stirred overnight. Then the solid was filtered and washed on the filter paper with distilled water and acetone. Finally, in order to remove all the  $[\text{Ru}(\text{Bipy})_3]\text{Cl}_2 \cdot 6\text{H}_2\text{O}$  present outside of the pores, the solid was suspended in water and stirred at room temperature during 24 hours. Afterwards the solid was filtered and dried at  $38^\circ\text{C}$  overnight.

### *Synthesis of solid S1-E*

With the aim to obtain solid **S1-E**, MCM-41 calcined (208 mg) was suspended in anhydrous CH<sub>3</sub>CN (15 mL). Then 10 ml of CH<sub>3</sub>CN were distilled, with a dean-stark from reaction mixture, in order to remove the water present in the pores of the solid. Subsequently, product **1** (0.45 g, 0.87 mmol) was added and the mixture was stirred overnight. Then the solid was filtered and washed on the filter paper with distilled water and acetone and dried at 38°C overnight.

### *Synthesis of solid S1-CPT*

With the aim to obtain solid **S1-CPT**, MCM-41 calcined (600 mg) was suspended in anhydrous CH<sub>3</sub>CN (25 mL) and camptothecin (540 mg, 1.5 mmol) was added. Then 10 ml of CH<sub>3</sub>CN were distilled, with a dean-stark from reaction mixture, in order to remove the water present in the pores of the solid. Afterwards the mixture was stirred at room temperature during 24 hours. Subsequently, product **1** (1.24 g, 2.4 mmol) was added and the mixture was stirred overnight. Then the solid was filtered and washed on the filter paper with distilled water and acetone. Finally, in order to remove all the camptothecin present outside of the pores, the solid was suspended in water and stirred at room temperature during 24 hours. Afterwards the solid was filtered and dried at 38°C overnight.

### *Materials Characterization*

Solid **S1** was characterized using standard procedures. Figure SI-5 shows powder X-ray patterns of the nanoparticulated MCM-41 support and the **S1** functionalised material. The PXRD of siliceous nanoparticulated MCM-41 as-synthesized (curve a) shows four low-angle reflections typical

of a hexagonal array that can be indexed as (100), (110), (200), and (210) Bragg peaks. A significant displacement of the (100) peak in the XRD powder of the nanoparticulated MCM-41 calcined sample is clearly appreciated in the curve b, corresponding to an approximate cell contraction of 4 Å. This displacement and the broadening of the (110) and (200) peaks are related to further condensation of silanol groups during the calcination step. Finally, curve c corresponds to the **S1** PXRD pattern. In this case, a slight intensity decrease and the disappearance of the (110) and (200) reflections is observed, most likely related to a loss of contrast due to the filling of the pore voids with the ruthenium (II) dye. Nevertheless, the value and intensity of the (100) peak in this pattern strongly evidences that the loading process with the dye and the further functionalization with **1** have not damaged the mesoporous 3D MCM-41 scaffolding.

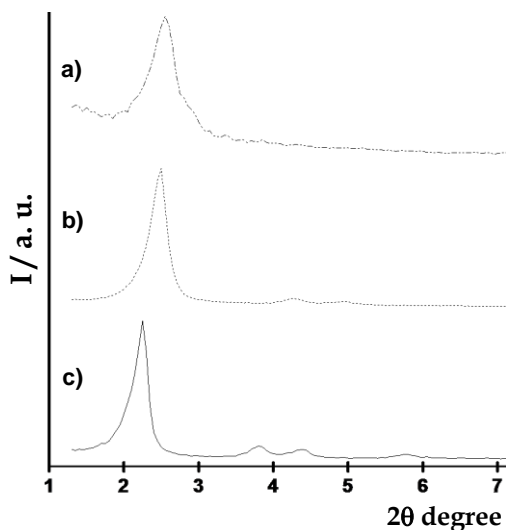


**Figure SI-5.** Powder X ray pattern of: a) solid **S1**; b) calcined MCM-41 and c) MCM-41 as synthesized.

The presence in the final functionalized solid (**S1**) of the mesoporous structure is also confirmed from the TEM analysis, in which the typical

channels of the MCM-41 matrix are visualized as alternate black and white stripes (see Figure S1-6 for solid **S1**). The figure also shows that the prepared **S1** are obtained as spherical particles (shape confirmed by SEM image, see figure SI-7) with diameters of ca. 100 nm. PXRD, TEM and SEM measurements indicated that the loading and grafting procedures did not modify the mesoporous structure of the starting material.

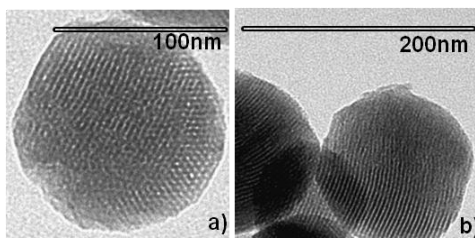


**Figure SI-6.** TEM image of a) the MCM-41 solid support and b) solid **S1**, showing the typical hexagonal porosity of the MCM-41 matrix.

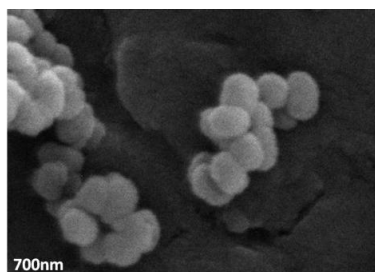


**Figure SI-7.** SEM image of the solid **S1** showing the typical spherical shape of the nanoparticles.

The  $N_2$  adsorption-desorption isotherms of the nanoparticulated MCM-41 calcined material shows an adsorption step at intermediate  $P/P_0$  value (0.1-0.4) typical of this solids (see Figure SI-8). This step can be related to the nitrogen condensation inside the mesopores by capillarity. The absence of a hysteresis loop in this interval and the narrow BJH pore distribution suggest the existence of uniform cylindrical mesopores with pore volume of  $1.18 \text{ cm}^3 \text{ g}^{-1}$  calculated by using the BJH model on the

adsorption branch of the isotherm. The application of the BET model resulted in a value for the total specific surface of 999.6 m<sup>2</sup>/g and a pore volume of 0.79 cm<sup>3</sup> g<sup>-1</sup>. From the XRD, porosimetry and TEM studies, the  $a_0$  cell parameter (4.44 nm), the pore diameter (2.46 nm) and a value for the wall thickness (1.99 nm) were calculated. In addition to this adsorption step associated to the micelle generated mesopores, a second feature appears in the isotherm at a high relative pressure ( $P/P_0 > 0.6$ ). This adsorption correspond to the filling of the large voids among the particles and present a volume of 0.30 cm<sup>3</sup> g<sup>-1</sup> (calculated by using the BJH model) and then must be considered as a textural-like porosity. In this case, the curves show a characteristic H1 hysteresis loop and a wide pore size distribution.

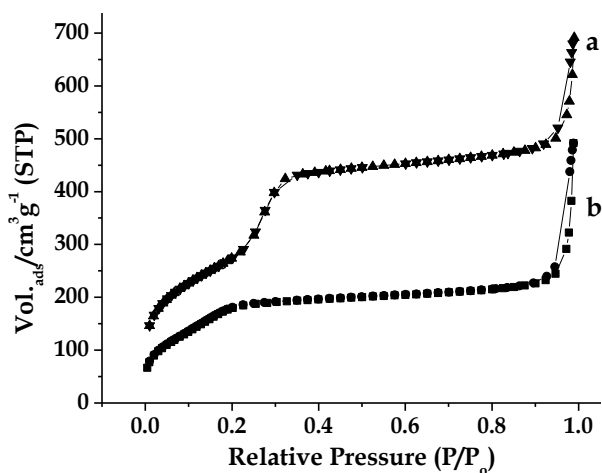


**Figure SI-8.** Nitrogen adsorption-desorption isotherms for a) MCM-41 mesoporous material and b) **S1** material.

The N<sub>2</sub> adsorption-desorption isotherm of **S1** is typical of mesoporous systems with filled mesopores (see Figure SI-8), and a significant decrease in the N<sub>2</sub> volume adsorbed and surface area (696.5 m<sup>2</sup>/g) is observed. Additionally, a certain textural porosity is preserved. BET specific surface

values, pore volumes, and pore sizes calculated from the N<sub>2</sub> adsorption-desorption isotherms for MCM-41 and **S1** are listed in Table 1.

**Table 1.** BET specific surface values, pore volumes and pore sizes calculated from the N<sub>2</sub> adsorption-desorption isotherms for selected materials

<i>Solid</i>	$S_{BET}$ ( $m^2 g^{-1}$ )	<i>Pore Volume</i> <sup>a</sup> ( $cm^3 g^{-1}$ )	<i>Pore size</i> <sup>a</sup> ( <i>nm</i> )
<b>MCM-41</b>	999.6	0.79	2.46
<b>S1</b>	696.5	0.41	2.14

<sup>a</sup> Volume (V) and diameter (D) of mesopore.

The content of product **1**, ruthenium (II) dye and camptothecin in solids **S1**, **S1-E** and **S1-CPT** was determined by thermogravimetric analysis. Values of contents are detailed in Table 2.

**Table 2.** Content of product **1**, complex Ru(bipy)<sub>3</sub><sup>2+</sup> and camptothecin in the prepared solids **S1**, **S1-E** and **S1-CPT** in mmol/g SiO<sub>2</sub>.

<i>Solid</i>	<b>1</b>	<i>Ru(bipy)<sub>3</sub><sup>2+</sup></i>	<i>Camptothecin</i>
<b>S1</b>	0.15	0.22	-
<b>S1-E</b>	0.13	-	-
<b>S1-CPT</b>	0.61	-	0.43

### *Delivery studies of solid S1*

A typical experiment was carried out in batch and four different suspensions were prepared: (a) 5 mg of **S1** and 12.5 ml of water at pH = 7.5 (blank); (b) 5 mg of **S1**, 12.5 ml of water at pH = 7.5 and 20 µl of urease from *Canavalia ensiformis*; (c) 5 mg of **S1**, 12.5 ml of water at pH = 7.5 and 1 µl of amidase from *Pseudomonas aeruginosa*; (d) 5 mg of **S1**, 12.5 ml of water at

pH = 7.5 and 1  $\mu\text{L}$  of amidase from *Pseudomonas aeruginosa* and urease from *Canavalia ensiformis*. The results obtained are showed in Figure SI-9.

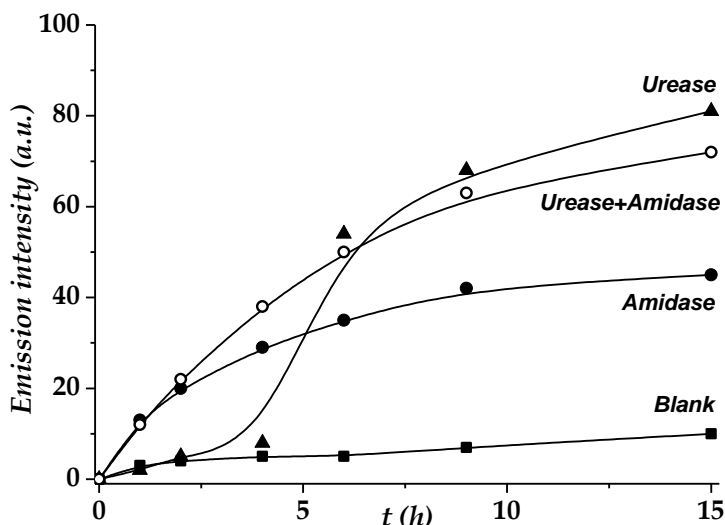


**Figure SI-9.** Kinetics of the release of  $[\text{Ru}(\text{bipy})_3]^{2+}$  dye from solid **S1** in the presence of amidase and urease enzymes.

### *Cell Culture Conditions*

The HeLa human cervix adenocarcinoma and the MCF-7 breast cancer cells were purchased from the German Resource Centre for Biological Materials (DSMZ) and were grown in D-MEM supplemented with 10% of FCS. Cells were maintained at 37 °C in an atmosphere of 5% carbon dioxide and 95% air and underwent passage twice a week.

### *WST-1 Cell Viability Assay*

Cells were cultured in sterile 96-well microtiter plates at a seeding density of 2500 and 3000 cells/well for HeLa and MCF-7, respectively, and they were allowed to settle for 24 h. **S1** in DMSO was added to cells at a final concentration of 200, 100 and 50  $\mu\text{g}/\text{mL}$ . After 23 hours, WST-198 (7  $\mu\text{L}$  of a 5 mg/mL solution) was added to each well. Cells were further

incubated for 1 h (a total of 24 hours of incubation was therefore studied), and absorbance was measured at 450 nm. The results obtained are depicted in Figure SI-10. No cell toxicity associated to nanoparticles was observed in HeLa or MCF-7 cells.

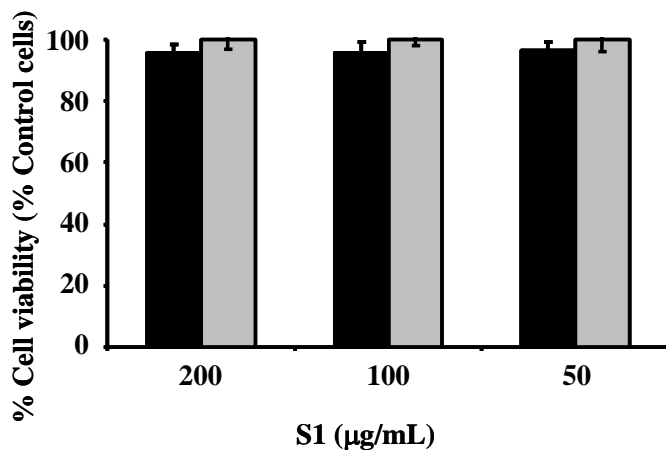


**Figure SI-10.** HeLa (black) and MCF-7 (grey) cells were incubated for 24 hours with **S1** at concentrations of 200, 100 and 50 µg/mL and cell viability was quantified employing WST-1 reagent. Two independent experiments with quadruplicates were performed. Data are expressed as (mean ± SE).

### *Live Confocal Microscopy S1 Cellular Internalization*

HeLa and MCF-7 cells were seeded in 24 mm  $\phi$  glass coverslips in six-well plates at a seeding density of 100000 or 50000 cells/well for 24 hours or 48 hours incubation assays, respectively. After 24 hours, cells were treated when indicated with **S1**, **S1-CPT** or **S1-E** at concentrations of 200 and 100 µg/mL. Then, cells were incubated for 24 or 48 hours prior confocal microscopy studies. For this purpose, cells were stained when indicated with 10 ng/mL of Hoechst 33342 and 5 mg/mL wheat germ agglutinin (WGA) Alexa Fluor 647 for 30 minutes in PBS containing 10% FCS or keeping the medium in case of **S1-CPT** and **S1-E** treatments. Slides were visualized under a confocal microscope.

The internalization of **S1** nanoparticles can be observed in Figure SI-11 by means of  $[\text{Ru}(\text{bipy})_3]^{2+}$ -associated fluorescence (red). A cytoplasmic vesicular signal can be observed in both cell lines proving the internalization of the nanoparticles.

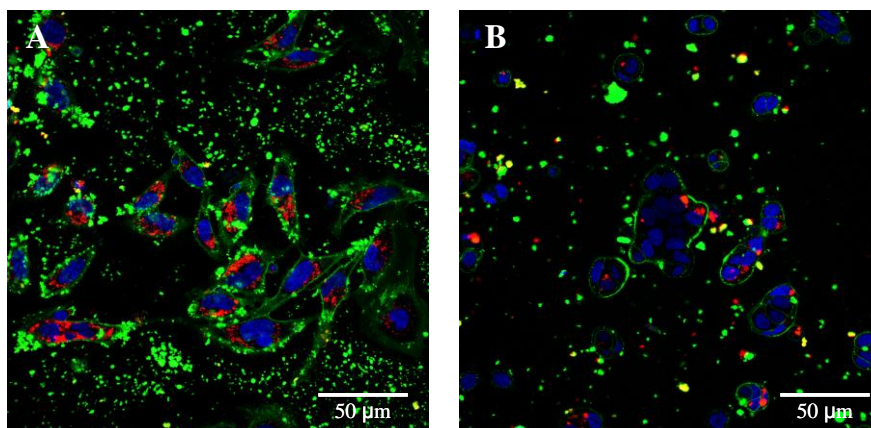


**Figure SI-11.** **S1** cellular internalization. HeLa (A) and MCF-7 (B) cells were treated with **S1** at concentration of 100  $\mu\text{g}/\text{mL}$  for 24 hours. Then, confocal microscopy studies of **S1** cellular uptake were performed by means of  $[\text{Ru}(\text{bipy})_3]^{2+}$ -**S1** associated fluorescence (red) in the presence of the DNA marker Hoechst 33342 (blue) and the plasma membrane marker WGA Alexa Fluor 647 (green). Two independent experiments were performed obtaining similar results.

### *Cytofluorometry Studies Employing S1*

To develop the cytofluorometry studies, HeLa and MCF-7 cells were seeded at 12500 or 25000 cells/well in a 24-well in case of HeLa or 20000 or 40000 cells/well in case of MCF-7 for 24 and 48 hours incubation assays, respectively. plate. After 24 hours, cells were treated with **S1-CPT** or **S1-E** at concentrations of 200 and 100  $\mu\text{g}/\text{mL}$ . Cells were incubated for 24 or 48 hours prior staining them with PI and Ann V according to manufacturer's protocol (BD Pharmingen). Quantification of PI positive and Ann V

positive stainings was performed employing WinMDI program version 2.9 (see Figure SI-12).

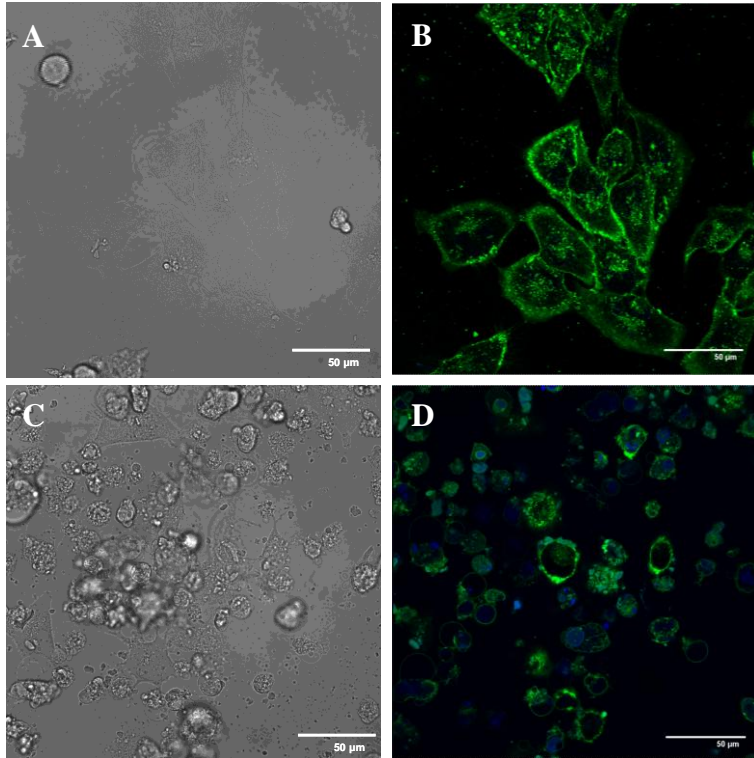


**Figure SI-12.** HeLa cells were treated with 200 µg/mL of **S1-E** (A, B) or **S1-CPT** (C, D) for 24 hours. Then, cellular internalization and release of the cargo of **S1-CPT** was followed by confocal microscopy (blue) in the presence of the plasma membrane marker WGA Alexa Fluor 647 (green). Experiment was performed twice with similar results.



***Chapter 8:  
Targeted cargo delivery in senescent cells using  
capped nanometric silica mesoporous supports***



# ***Targeted cargo delivery in senescent cells using capped nanometric silica mesoporous supports***

Alessandro Agostini,<sup>[a]</sup> Laura Mondragón,<sup>[a]</sup> Andrea Bernardos,<sup>[a]</sup>  
Ramón Martínez-Mañez,<sup>\*[a]</sup> M. Dolores Marcos,<sup>[a]</sup> Félix Sancenón,<sup>[a]</sup>  
Juan Soto,<sup>[a]</sup> Ana Costero,<sup>[a]</sup> Cristina Manguan-García,<sup>[a]</sup> Rosario  
Perona,<sup>\*[a]</sup> Marta Moreno-Torres,<sup>[a]</sup> Rafael Aparicio-Sanchis,<sup>[a]</sup> José  
Ramón Murguía<sup>\*[a]</sup>

<sup>[a]</sup>*Centro de Reconocimiento Molecular y Desarrollo Tecnológico (IDM), Unidad Mixta Universidad Politécnica de Valencia-Universidad de Valencia. Departamento de Química, Universidad Politécnica de Valencia, Camino de Vera s/n, 46022, Valencia, Spain.*

*CIBER de Bioingeniería, Biomateriales y Nanotecnología (CIBER-BNN).*

<sup>[b]</sup>*Centro de Reconocimiento Molecular y Desarrollo Tecnológico (IDM), Unidad Mixta Universidad Politécnica de Valencia-Universidad de Valencia, Spain. Departamento de Química Orgánica, Facultad de Ciencias Químicas, Universitat de Valencia, 46100 Burjassot, Valencia, Spain.*

<sup>[c]</sup>*Instituto de Investigaciones Biomédicas CSIC/UAM, IDIPaz, Madrid, Spain. CIBER de Enfermedades Raras (CIBERER).*

<sup>[d]</sup>*Instituto Universitario Mixto de Biología Molecular y Celular de Plantas, Camino de Vera s/n, E-46071, Valencia, Spain.*

***Received: June 14, 2012***

***Revised: July 31, 2012***

***Published online, September 20, 2012***

*Angew. Chem. Int. Ed.*, **2012**, *51*, 10556 –10560

## **8.1 Introduction**

Normal somatic cells invariably enter a state of irreversibly arrested growth and altered function after a finite number of divisions, called cellular senescence. Senescent cells display a radically altered phenotype that is thought to impair tissue function and predispose tissues to disease development and/or progression. Despite the fact that the immune system destroys many senescent cells, it becomes much less effective at this task during ageing. As a consequence, senescent or “death resistant” cells accumulate in tissues, thus accelerating ageing and contributing to disease development. Senescent cell accumulation alters neighbouring cell behaviour, favours degradation of the extracellular matrix, decreases the pool of mitotic-competent cells, and stimulates cancer.<sup>1</sup> Moreover a number of pathologies are associated with accelerated cellular aging such as Werner adult progeria syndrome, (WS) Hutchinson-Gilford (HGS), and Rothmund-Thompson syndrome (RTS).<sup>2</sup> In WS or RTS telomere erosion is observed in most tissues, even if telomerase is not the main cause of disease.<sup>3,4</sup> Other diseases are more related to tissue-specific accelerated aging such as Dyskeratosis congenita (DC) and idiopathic pulmonary fibrosis (IPF).<sup>5</sup> In these conditions, the replicative capacity of cells is impaired by a defective telomerase activity in the stem cell compartment of high turnover tissues such as skin, pulmonary epithelium and bone marrow. A frequent associated secondary effect in these diseases is the induction of cancer, especially in those that involve shortening of telomeres.<sup>6</sup> To combat this problem, strategies to prevent, replace or remove senescent cells are of fundamental interest both from basic research and application viewpoints. In particular, the design of such therapies would contribute to the treatment of accelerated cellular aging diseases and

may boost the long-term idea that human rejuvenation might be possible. In fact, as a proof-of-concept, two recent demonstrations supported fundamental concept that senescent cells can drive the aging process and that their elimination can be therapeutic. In a first example, inducible removal of p16-positive senescent cells in a genetically-engineered progeroid mouse background arrested virtually all the accelerated aging phenotypes.<sup>7</sup> In a second example, tissue degeneration was reversed by reactivation of telomerase expression in aged telomerase-deficient mice.<sup>8</sup> However these examples were applied to transgenic mice and effective strategies involving the pharmacological reactivation, removal or replacement of senescent cells for treating aging-related conditions in human patients are currently unavailable. A first approach to achieve the goal of remove senescent cell would be related with the development of selective delivery carriers able to release their cargo in these particular cells. However, as far as we know, such targeted release systems have not been described.

Nanotechnology has proved to be an innovative approach to drug-delivery therapies. Drug delivery systems able to release active molecules to certain cells in a controlled manner have recently gained much attention.

Microcapsules polymers<sup>9</sup> dendrimers<sup>10</sup> micelles<sup>11</sup> and nanoparticles<sup>12</sup> have been used as potential drug delivery systems. Alternatively, mesoporous silica nanoparticles (MSN) have been widely used in the past years as reservoirs for drug storage<sup>13</sup> due to their unique mesoporous structure, large specific volume and easy functionalization. Moreover MSN are in general biocompatible and have been reported to undergo cellular uptake via endocytosis. Additionally MSN can be functionalized with molecular/supramolecular ensembles on their external surface to develop

gated-SMS showing “zero delivery” and capable to release of their cargo in response to external stimuli. Using this concept, MSN displaying controlled release using several stimuli have been reported.<sup>14-25</sup>

Given the need to develop new therapeutic ways of preventing the appearance of senescence-related human impairment and disease, we address herein the design of nanoparticles able to display a selective and controlled cargo delivery in senescent cells. The strategy we have followed involves the use of MSN capped with a galactoligosaccharide (GOS) and the specific presence of senescence associated  $\beta$ -galactosidase (SA- $\beta$ -gal) in senescent cells. The existence of SA- $\beta$ -gal in these cells was described in 1995<sup>26</sup> and its presence explained by the overexpression of the endogenous lysosomal  $\beta$ -galactosidase that specifically occurs in senescent cells.<sup>27</sup> The source of SA- $\beta$ -gal activity in senescent cells is encoded by the GLB1 gene<sup>28</sup> and its presence is a surrogate marker for increased lysosome number or activity, which has long been associated with replicative senescence<sup>29,30</sup> and organismal aging.<sup>31,32</sup> We reasoned that if conveniently derivatized with GOS, the gated mesoporous nano-devices would show “zero-release”, yet selectively will release the cargo in cells suffering a senescent process due to a  $\beta$ -galactosidase-mediated hydrolysis of the cap (see Figure 1A).

## **8.2 Results and Discussion**

For this work MCM-41-based MSN as inorganic scaffold were selected.<sup>33</sup> The structure of the mesoporous starting material was confirmed by X-Ray diffraction and TEM (see Figure 1B). For the preparation of the final capped nano-device (**S1**) the calcined MSN were first loaded with Rhodamine-B as model drug and then reacted with the capping oligosaccharide derivative **I**. **I** was prepared starting from a commercially

available galactooligosaccharide polymer (GOS) which was firstly brought to neutral pH and then reacted with 3-aminopropyltriethoxysilane to give the corresponding alkylgluconamine derivative (see Supporting Information for details).<sup>34</sup>

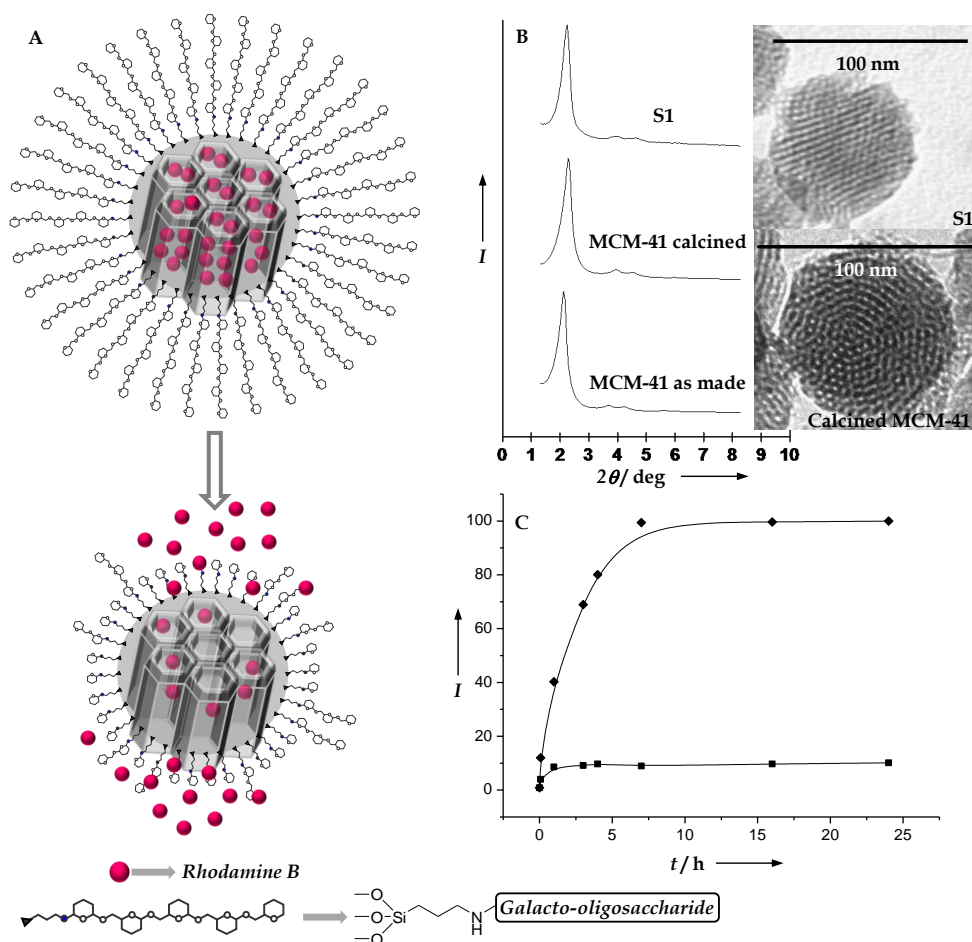


**Figure 1.** Synthesis and characterization of MSN S1 nanoparticles. A) Representation of the gated material S1 capped with an galactooligosaccharide (GOS) and the selective delivery mechanism in the presence of  $\beta$ -gal. B) Power X-ray patterns of MCM-41 as synthesized, calcined MCM-41 and final S1. TEM images of calcined MCM-41 and solid S1 showing the typical porosity of the MCM-41 mesoporous matrix. C) Release profiles of Rhodamine B dye from MSN S1 in the absence (■) and in the presence of  $\beta$ -gal enzyme in water at pH 7.5 at room temperature (◆).

The mesoporous structure of **S1** was confirmed by XRD and TEM studies. The final nanoparticles were roughly spherical having a diameter of ca. 100 nm and an average pore diameter of 2.5 nm (Figure 1B). N<sub>2</sub> adsorption-desorption isotherm of **S1** was typical of mesoporous systems with capped mesopores, and a significant decrease in the N<sub>2</sub> volume adsorbed and surface area (228.4 m<sup>2</sup>/g) was observed when compared with the starting MCM-41-based MSN (999.6 m<sup>2</sup>/g). The maximum delivery of the Rhodamine-B dye from the final material **S1** amounted to 0.14 g/g SiO<sub>2</sub> in weight. Moreover the content of the anchored **I** in **S1** amounted to 0.28 g/ g SiO<sub>2</sub> in weight.

In vitro studies of the delivery of the Rhodamine-B cargo from the MSN **S1** in water in the presence and absence of β-gal were performed (see Figure 1C). Dye release was determined by following the emission of the Rhodamine-B in the solution as a function of time ( $\lambda_{\text{ex}} = 550 \text{ nm}$ ,  $\lambda_{\text{em}} = 580 \text{ nm}$ ). In the absence of the enzyme β-gal a flat baseline was found indicating that the Rhodamine-B cargo remained in the nanoparticles without release. In contrast, in the presence of β-gal delivery of the Rhodamine-B was found as an increase of the dye fluorescence as a function of time. This behaviour was assigned to the galactosidase-induced hydrolysis of the glycosidic bonds in the anchored GOS derivative that results in a reduction of the size of the attached groups finally allowing delivery of the entrapped cargo. In order to confirm this, the supernatant of different aliquots as a function of time of a **S1** and β-gal mixture in water were analysed by MALDI-TOF-MS spectroscopy. At time 0 min no saccharides fragments were observed, whereas in progressive aliquots (increasing hydrolysis time) peaks corresponding to the galactose monomer appeared. In parallel we

confirmed that free galactose increased with time using a Galactose detection Kit (Deltaclon).

Moreover, to further demonstrate that  $\beta$ -gal is responsible of the delivery observed two additional experiments were performed. In one of them solid **S1** was incubated in the presence of protease pepsin, whereas in a second experiment the  $\beta$ -gal enzyme was denaturated by heating. In both experiments no release of the dye was observed from **S1**. As an additional experiment we also studied the delivery of the Rhodamine-B dye from **S1** suspended in cellular media and found no dye delivery in the absence of  $\beta$ -gal.

After demonstrating the effective Rhodamine-B delivery form **S1** in the presence of  $\beta$ -gal *in vitro*, cargo delivery from **S1** in several *in vivo* models was studied. In a first step budding yeast cells were selected due to its genetic tractability and its ease of manipulation. Wild type (WT) and  $\beta$ -gal overexpressing ( $\beta$ -Gal<sup>oe</sup>) yeasts were incubated with MSN **S1** nanoparticles and examined for Rhodamine-B staining by fluorescence microscopy. Staining was only detected in  $\beta$ -Gal<sup>oe</sup> yeast cells with high  $\beta$ -gal activity (see Figure 2A and 2B). Moreover, incubation with MSN **S1** nanoparticles did not affect cell viability throughout the whole experiment (see Supporting Information).

Encouraged by these results we extended our study to the potential applicability of these GOS-capped MSN in human senescent cells. As model cells fibroblasts from X-linked Dyskeratosis Congenita (X-DC) patients were used. X-DC is an inherited rare disease originated by defects in telomere maintenance machinery, resulting in short telomeres in high turnover tissues such as bone marrow and skin. Mutations in *DKC1* gene, encoding a 58kD nucleolar protein that is associated with small nucleolar

RNAs (snoRNAs) in H/ACA snoRNP (small nucleolar ribonucleoprotein) complexes, are responsible for the X-DC.<sup>35</sup>

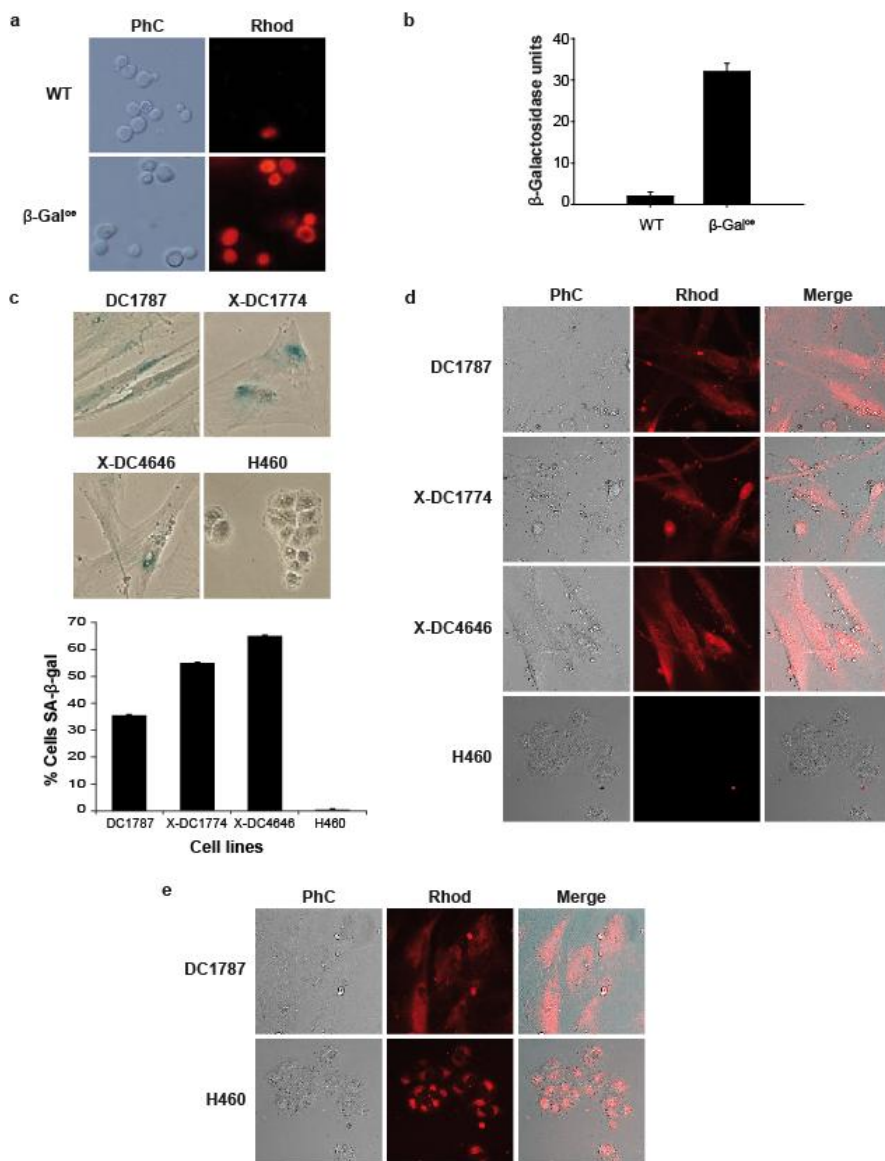


**Figure 2.** Internalization and release of cargo in  $\beta$ -gal overexpressing ( $\beta$ -Gal<sup>oe</sup>) yeast cells and human senescent cells. A) Controlled release of Rhodamine loaded **S1** nanoparticles in wild type (WT) and beta-galactosidase overexpressing ( $\beta$ -Gal<sup>oe</sup>) yeast cells. WT and  $\beta$ -Gal<sup>oe</sup> exponentially growing cultures were incubated with  $\beta$ -gal nanoparticles and examined for Rhodamine staining (Rhod) by fluorescence microscopy. Cells were also visualized using

Nomarski optics (NOM). B) Quantitation of beta-galactosidase activity in WT and  $\beta$ -Gal<sup>oe</sup>. Data represents the mean +/- s.e. of at least three independent experiments each done in duplicate. Three independent  $\beta$ -Gal<sup>oe</sup> strains from the same transformation were assayed with essentially identical results. C) DC1787, X-DC 1774 and X-DC4646 human senescent cells and H460 NSCLC cells were grown in 6 well plates and fixed after four days to assay the acid- $\beta$ -galactosidase activity. The graphic shows the quantitation of the % of blue cells from the total cell population. D) Cells described in C) were seeded onto 1 $\mu$ -slide 8-well ibiTreat microscopy chambers and treated with 50  $\mu$ g/ml MSN **S1** Rhodamine loaded particles. Representative images at 24 hours from Phase contrast (PhC), Rhodamine (Rhod) and combined (Merged) are presented. E) DC1787 and H460 cells were seeded as in D) and treated with silica mesoporous support particles anchored with starch. Images were taken and processed as in D). Representative images at 24 hours from Phase contrast (PhC), Rhodamine (Rhod) and combined (Merged) are presented.

We used the cell lines X-DC1774 and X-DC4646 containing the c.109\_111delCTT and c.385A>T mutations in DKC1 respectively. Aged control human fibroblasts DC1787, and H460 non-small cell lung cancer cells expressing telomerase were also used. X-DC1774, X-DC4646 and aged control fibroblast DC1787, but not H460 cells, expressed SA- $\beta$ -gal (Figure 2C). These cell lines were incubated with Rhodamine-loaded MSN **S1** and monitored by time-lapse microscopy (Figure 2D). The Rhodamine staining released from the particles began at 3 hours and lasted at least until two days. Remarkably, only X-DC1774, X-DC4646 and DC1787 SA- $\beta$ -gal positive cells exhibited fluorescence. No noticeable emission was detected in H460 cells even after 48 hours. Furthermore, cell viability remained unaffected in H460 and DC-1787 cells incubated up to 48 hours with Rhodamine-loaded MSN **S1** (see Supporting Information). Viability results are in good agreement with the observation that in general MSN exhibit good biocompatibility *in vitro*.<sup>36</sup> Moreover, although some reports suggested that, depending on the route of administration *in vivo*, MSN might become toxic,<sup>37</sup> our own data in human cells, are encouraging from the perspective of the potential use of **S1** in *in vivo* models.

The experiments shown above clearly and remarkably show that, despite GOS-capped **S1** nanoparticles are most likely internalized in all cells studied, they only displayed cargo release in  $\beta$ -gal overexpressing cells. Moreover, in order to demonstrate that the lack of Rhodamine staining in H460 cells was not artifactual some additional control experiments were performed. Rhodamine-loaded MSN nanoparticles capped with hydrolyzed starch were also prepared (solid **S2**). MSN of **S2** are similar to **S1** but contain an oligosaccharide that was able to be hydrolyzed by amylase enzyme in lysosomes.<sup>38</sup> When using **S2** in internalization studies under similar conditions to those described above a clear detectable staining was obtained in all cell lines studied (Figure 2E) indicating that the delivery in **S1** was clearly ascribed to a selective cellular  $\beta$ -gal enzyme-mediated opening mechanism.

### **8.3 Conclusions**

In summary, MSN **S1** nanoparticles described here have proved suitable nano-devices to selectively release their cargo in senescent cells with high specificity and lack of detectable toxicity. Nanoparticles **S1** were able to selectively deliver their cargo in SA- $\beta$ -gal positive  $\beta$ -Gal<sup>oe</sup> yeast cells, in aged human fibroblasts DC1787 and in X-DC1774 and X-DC4646 cells from human Dyskeratosis Congenita patients, whereas no cargo release from **S1** was observed in control experiments with H460 non-small cell lung cancer cells and wild type yeast cells. To our knowledge this is the first time that a targeted nanotherapy for senescent cells has been described. These results suggest that by choosing an appropriate cargo (i.e. a telomerase reactivation drug or a cytotoxic drug) prevention and removal/replacement of senescent cells could be possible. Despite the fact

the road from these results to senescent cells removal or rejuvenation therapies remains long and uncertain, we believe that our findings might open up new avenues for developing innovative therapeutic applications to treat or delay age-related diseases.

## 8.4 Acknowledgments

We thank the Spanish Government (projects MAT2009-14564-C04 and FIS PI11-0949) the Generalitat Valencia (project PROMETEO/2009/016) and the Universidad Politécnic de Valencia (UPV PAID-05-09) for support. Fundación Ramón Areces for support. C M-G is supported by CIBERER.

## 8.5 Bibliography

- 1 D. G. Burton, in Cellular senescence, ageing and disease, Age, Dordrecht, Netherlands, **2009**, 31, 1-9.
- 2 C. R. Burtner, B. K. Kennedy, *Nature Rev.* **2010**, 11, 567-578.
- 3 N. Ishikawa, K. Nakamura, N. Izumiyama-Shimomura, J. Aida, A. Ishii, M. Goto, Y. Ishikawa, R. Asaka, M. Matsuura, A. Hatamochi, M. Kuroiwa, K. Takubo, *Aging* **2011**, 3, 417-429.
- 4 A. K. Ghosh, M. L. Rossi, D. K. Singh, C. Dunn, M. Ramamoorthy, D. L. Croteau, Y. Liu, V. A. Bohr, *J. Biol. Chem.* **2012**, 287, 196-209.
- 5 R. T. Calado, N. S. Young, *N. Engl. J. Med.* **2009**, 361, 2353-2365.
- 6 B. P. Alter, N. Giri, S. A. Savage, P. S. Rosenberg, *Blood* **2009**, 113, 6549-6557.
- 7 D. J. Baker, T. Wijshake, T. Tchkonja, N. K. LeBrasseur, B. G. Childs, B. van de Sluis, J. L. Kirkland, J. M. van Deursen, *Nature* **2011**, 479, 232-236.
- 8 M. Jaskelioff, F. L. Muller, J. -H. Paik, E. Thomas, S. Jiang, A. C. Adams, E. Sahin, M. Kost-Alimova, A. Protopopov, J. Cadiñanos, J. W. Horner, E. Maratos-Flier, R. A. DePinho, *Nature* **2011**, 469, 102-106.

- 9 S. Liu, R. Maheshwari, K. L. Kiick, *Macromolecules* **2009**, *42*, 3-13.
- 10 C. C. Lee, J. A. MacKay, J. M. Frechet, F. C. Szoka, *Nature Biotech.* **2005**, *23*, 1517-1526.
- 11 C. W. Pouton, C. J. Porter, *Adv. Drug Deliv. Rev.* **2008**, *60*, 625-637.
- 12 I. Brigger, C. Dubernet, P. Couvreur, *Adv. Drug Deliv. Rev.* **2002**, *54*, 631-651.
- 13 M. Vallet-Regi, F. Balas, D. Arcos, *Angew. Chem. Int. Ed.* **2007**, *46*, 7548-7558; *Angew. Chem.* **2007**, *119*, 7692-7703.
- 14 T. D. Nguyen, K. C. -F. Leung, M. Liong, Y. Liu, J. F. Stoddart, J. I. Zink, *Adv. Func. Mater.* **2007**, *17*, 2101-2110.
- 15 B. G. Trewyn, S. Giri, I. I. Slowing, V. S. -Y. Lin, *Chem. Commun.* **2007**, 3236-3245.
- 16 R. Klajn, J. F. Stoddart, B. A. Grzybowski, *Chem. Soc. Rev.* **2010**, *39*, 2203-2237.
- 17 E. Climent, A. Bernardos, R. Martínez-Máñez, A. Maquieira, M. D. Marcos, N. Pastor-Navarro, R. Puchades, F. Sancenón, J. Soto, P. Amorós, *J. Am. Chem. Soc.* **2009**, *131*, 14075-14080.
- 18 A. Schlossbauer, J. Kecht, T. Bein, *Angew. Chem. Int. Ed.* **2009**, *48*, 3092-3095; *Angew. Chem.* **2009**, *121*, 3138-3141.
- 19 B. G. Trewyn, I. I. Slowing, S. Giri, H. -T. Chen, V. S. -Y. Lin, *Acc. Chem. Res.* **2007**, *40*, 846-853.
- 20 S. Saha, K. C. -F. Leung, T. D. Nguyen, J. F. Stoddart, J. I. Zink, *Adv. Func. Mater.* **2007**, *17*, 685-693.
- 21 Y. -W. Yang, *Med. Chem. Commun.* **2011**, *2*, 1033-1049.
- 22 a) E. Climent, R. Martínez-Máñez, F. Sancenón, M. D. Marcos, J. Soto, A. Maquieira, P. Amorós, *Angew. Chem. Int. Ed.* **2010**, *49*, 7281-7283; *Angew. Chem.* **2010**, *122*, 7439-7441; b) A. Agostini, L. Mondragón, C. Coll, E. Aznar, M.D. Marcos, R. Martínez-Máñez, F. Sancenón, J. Soto, E. Pérez-Payá, P. Amorós, *Chem. Open* **2012**, *1*, 17-20

- 23 K. Ariga, A. Vinu, Y. Yamauchi, Q. Ji, J.P. Hill, *Bull. Chem. Soc. Jpn.* **2012**, *85*, 1-32
- 24 Z. Li, J.C. Barnes, A. Bosoy, J.F. Stoddart, J.I. Zink, *Chem. Soc. Rev.* **2012**, *41*, 2590-2605
- 25 P. Yang, S. Gai, J. Lin, *Chem. Soc. Rev.* **2012**, *41*, 3679-3698.
- 26 G. P. Dimri, X. Lee, G. Basile, M. Acosta, G. Scott, C. Roskelley, E. E. Medrano, M. Linskens, I. Rubelj, O. Pereira-Smith, M. Peacocke, J. Campisi, *Proc. Natl. Acad. Sci. USA* **1995**, *92*, 9363-9367.
- 27 B. Y. Lee, J. A. Han, J. S. Im, A. Morrone, K. Johung, E. C. Goodwin, W. J. Kleijer, D. DiMaio, E. S. Hwang, *Aging Cell* **2006**, *5*, 187-195.
- 28 B. Y. Lee, J. A. Han, J. S. Im, A. Morrone, K. Johung, E. C. Goodwin, W. J. Kleijer, D. DiMaio, E. S. Hwang, *Aging Cell* **2006**, *5*, 187-195.
- 29 M. Knas, A. Zalewska, R. Kretowski, M. Niczyporuk, N. Waszkiewicz, M. Cechowska-Pasko, D. Waszkiel, K. Zwierz, *Folia Histochem. Cytobiol.* *50*, 19353.
- 30 B. Lecka-Czernik, E. J. Moerman, R. J. Shmookler Reis, D. A. Lipschitz, *J. Gerontol. A Biol. Sci. Med. Sci.* **1997**, *52*, B331-B336
- 31 B. W. Gu, J. M. Fan, M. Bessler, P. J. Mason, *Aging Cell* **2011**, *10*, 338-348.
- 32 S. Chigira, K. Sugita, K. Kita, S. Sugaya, Y. Arase, M. Ichinose, H. Shirasawa, N. Suzuki, *J. Gerontol. A Biol. Sci. Med. Sci.* **2003**, *58*, B873-B878.
- 33 S. Cabrera, J. El Haskouri, C. Guillem, J. Latorre, A. Beltrán, D. Beltrán, M. D. Marcos, P. Amorós, *Solid State Sci.* **2000**, *2*, 405-420.
- 34 X. Auvray, C. Petipas, R. Anthore, I. Rico-Lattes, A. Lattes, *Langmuir* **1995**, *11*, 433-439.
- 35 R. Perona, R. Machado-Pinilla, C. Manguan, J. Carrillo, *Clin. Trasl. Oncol.* **2009**, *11*, 711-714.
- 36 F. Tang, L. Li, D. Chen, *Adv. Mater.* **2012**, *24*, 1504-1534
- 37 S. P. Hudson, R. F. Padera, R. Langer, D. S. Kohane, *Biomaterials* **2008**, *29*, 4045-4055

- 38 A. Bernardos, L. Mondragón, E. Aznar, M. D. Marcos, R. Martínez-Máñez, F. Sancenón, J. Soto, J. M. Barat, E. Pérez-Payá, C. Guillem, P. Amorós, *ACS Nano* **2010**, *4*, 6353-6368.

# ***Targeted cargo delivery in senescent cells using capped nanometric silica mesoporous supports***

Alessandro Agostini,<sup>[a]</sup> Laura Mondragón,<sup>[a]</sup> Andrea Bernardos,<sup>[a]</sup>  
Ramón Martínez-Mañez,<sup>\*[a]</sup> M. Dolores Marcos,<sup>[a]</sup> Félix Sancenón,<sup>[a]</sup>  
Juan Soto,<sup>[a]</sup> Ana Costero,<sup>[a]</sup> Cristina Manguan-García,<sup>[a]</sup> Rosario  
Perona,<sup>\*[a]</sup> Marta Moreno-Torres,<sup>[a]</sup> Rafael Aparicio-Sanchis,<sup>[a]</sup> José  
Ramón Murguía<sup>\*[a]</sup>

<sup>[a]</sup>*Centro de Reconocimiento Molecular y Desarrollo Tecnológico (IDM), Unidad Mixta Universidad Politécnica de Valencia-Universidad de Valencia. Departamento de Química, Universidad Politécnica de Valencia, Camino de Vera s/n, 46022, Valencia, Spain.*

*CIBER de Bioingeniería, Biomateriales y Nanotecnología (CIBER-BNN).*

<sup>[b]</sup>*Centro de Reconocimiento Molecular y Desarrollo Tecnológico (IDM), Unidad Mixta Universidad Politécnica de Valencia-Universidad de Valencia, Spain. Departamento de Química Orgánica, Facultad de Ciencias Químicas, Universitat de Valencia, 46100 Burjassot, Valencia, Spain.*

<sup>[c]</sup>*Instituto de Investigaciones Biomédicas CSIC/UAM, IDIPaz, Madrid, Spain. CIBER de Enfermedades Raras (CIBERER).*

<sup>[d]</sup>*Instituto Universitario Mixto de Biología Molecular y Celular de Plantas, Camino de Vera s/n, E-46071, Valencia, Spain.*

## ***Supporting Information***

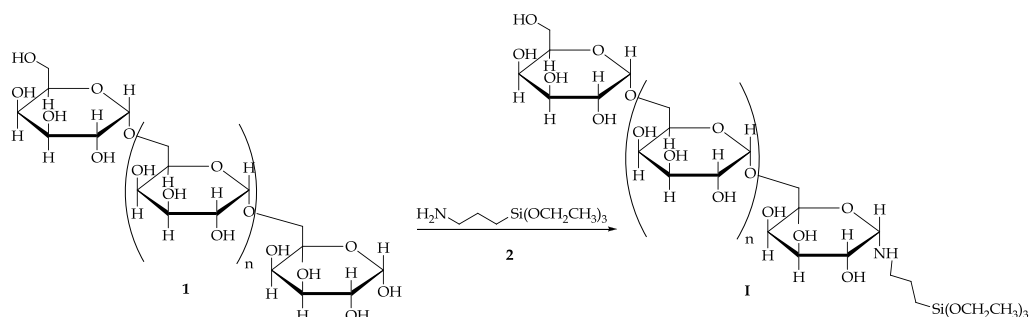
### **Chemicals**

The chemicals tetraethylorthosilicate (TEOS), n-cetyltrimethylammonium bromide (CTAB), sodium hydroxide (NaOH), 3-aminopropyltriethoxysilane, rhodamine-B,  $\beta$ -galactosidase from *Kluyveromyces lactis*, pancreatin from porcine pancreas, and anhydrous ethanol were provided by Aldrich. The hydrolyzed galactooligosaccharide PROMOVITA (GOS) (GOS contains at least 60% of galactooligosaccharides; 33% disaccharides, 39% trisaccharides, 18% tetrasaccharides, 7% pentasaccharides and 3% of higher saccharides) was provided by Zeus Química. All the products were used as received.

The used galactooligosaccharide is in fact a mixture composed of dimeric (33%) trimeric (39%) tetrameric (18%) and mayor length oligomeric (20%) units.

### **General Techniques**

XRD, TGA, EDX microscopy, N<sub>2</sub> adsorption-desorption, fluorescence spectroscopy and NMR techniques were employed to characterize the synthesized materials. X-ray measurements were performed on a Philips D8 Advance diffractometer using CuK $\alpha$  radiation. Thermogravimetric analysis were carried out on a TGA/SDTA 851e Mettler Toledo balance, using an oxidant atmosphere (air, 80 mL/min) with a heating program consisting on a heating ramp of 10 °C per minute from 393 to 1273 K and an isothermal heating step at this temperature during 30 minutes. Fluorescence spectroscopy was carried out on a Felix 32 Analysis Version 1.2 (Build 56) PTI (Photon Technology International). <sup>1</sup>H and <sup>13</sup>C nuclear magnetic resonance (NMR) spectra were acquired with a Varian 300 spectrometer (Sunnyvale, CA, USA).

**Synthesis of the galactooligosaccharide derivative (I):****Scheme SI-1.** Synthetic route for I.

The galactooligosaccharide (**1**) was provided as syrup with a pH 3.8. This syrup was diluted in water and the pH was increased with  $\text{NaHCO}_3$  up to 7. Then, the solution was lyophilized giving a white solid. Afterwards, 5 g of this solid were dissolved in anhydrous ethanol (total volume 100 mL) and a solution of 3-aminopropyltriethoxysilane (**2**, 5.85 mL, 25 mmol) was added. The reaction mixture was stirred for 24 h at room temperature. The solvent was evaporated under reduced pressure to give a white solid (see Scheme SI-1).

$^1\text{H}$  NMR (300 MHz,  $\text{D}_2\text{O}$ ): 0.42 (t, 2H,  $-\text{CH}_2\text{-Si-}$ ), 1.02 (t, 9 H,  $\text{CH}_3\text{-CH}_2\text{-O-Si-}$ ), 1.53 (m, 2H,  $-\text{CH}_2\text{-CH}_2\text{-Si-}$ ), 2.74 (t, 2H,  $\text{NH-CH}_2\text{-CH}_2\text{-CH}_2\text{-Si-}$ ), 3.20-3.77 (m, nH, galactose oligomer,  $\text{CH}_3\text{-CH}_2\text{-O-Si-}$ ), 5.13 (d, 1 H,  $-\text{O-CH-O-}$ ) ppm.

$^{13}\text{C}$  NMR (300 MHz,  $\text{D}_2\text{O}$ ): 9.62 ( $-\text{CH}_2\text{-Si-}$ ), 16.65 ( $\text{CH}_3\text{-CH}_2\text{-O-Si-}$ ), 21.74 ( $-\text{CH}_2\text{-CH}_2\text{-Si-}$ ), 41.96 ( $-\text{NH-CH}_2\text{-CH}_2\text{-CH}_2\text{-Si-}$ ), 57.25 ( $\text{CH}_3\text{-CH}_2\text{-O-Si-}$ ), 61.84 ( $\text{HO-CH}_2\text{-CH-}$ ), 72.67-78.11 ( $\text{HO-CH-}$ ), 89.57 ( $-\text{O-CH-CH}$ ), 94.84 ( $-\text{O-CH-NH-}$ ), 100.25 ( $-\text{O-CH-O-}$ ) ppm.

### ***Synthesis of Mesoporous MCM-41 Nanoparticles***

The MCM-41 mesoporous nanoparticles were synthesized using the following procedure: n-cetyltrimethylammoniumbromide (CTAB, 2.00 g, 5.48 mmol) was first dissolved in 960 mL of deionized water. NaOH (aq) (2.00 M, 7.00 mL) was added to the CTAB solution, followed by adjusting the solution temperature to 95 °C. TEOS (10.00 mL,  $5.14 \cdot 10^{-2}$  mol) was then added dropwise to the surfactant solution. The mixture was allowed to stir for 2.5 h to give a white precipitate. The solid product was centrifuged and washed with deionized water till neutral pH and dried at 60 °C for 12 h (MCM-41 as-synthesized). To prepare the final porous material (MCM-41), the as-synthesized solid was calcined at 550 °C using an oxidant atmosphere for 5 h in order to remove the template phase.

### ***Synthesis of S1***

In a typical synthesis, 50 mg of templated-free MCM-41 and the dye Rhodamine-B (19 mg, 0.04 mmol) were suspended in 10 mL of ethanol in a round-bottomed flask under inert atmosphere. The mixture was stirred for 24 h at room temperature with the aim of achieving the maximum loading in the pores of the MCM-41 scaffolding. Then, an excess of **I** (100 mg in 10 mL of ethanol) were added and the final mixture was stirred for 5.5 h at room temperature. Finally, the solids MSN-S1 were filtered off and washed with water.

### ***Synthesis of S2***

Nanoparticles **S2** were prepared following literature procedures, using a MSN as support, Rhodamine B as cargo and hydrolyzed starch (Glucidex® 47) as capping system. <sup>1</sup>

### *Materials characterization*

Figure 1 (see manuscript) shows powder X-ray diffraction (XRD) patterns of the solids MCM-41 as-synthesized, MCM-41 calcined and **S1**. XRD of siliceous MCM-41 as-synthesized shows four low-angle reflections typical of the hexagonal ordered array that can be indexed as (100), (110), (200), and (210) Bragg peaks. A significant shift of the (100) reflection and a broadening of the (110) and (200) peaks in the XRD powder of the MCM-41 calcined sample is clearly seen. This corresponds to an approximate cell contraction of ca. 6-8 Å due to condensation of silanols during the calcination step. Despite this clear partial order loss, the observation of the (100) and (200) reflections indicates that certain relative mesopore symmetry is preserved after calcination. The N<sub>2</sub> adsorption-desorption isotherms of the mesoporous nanoparticles showed a typical type IV-curve with a specific surface of 999.6 m<sup>2</sup> g<sup>-1</sup>, and a pore volume of 1.17 cm<sup>3</sup> g<sup>-1</sup> (see Figure SI-1 a). From the XRD, porosimetry and TEM studies, the a<sub>0</sub> hexagonal cell parameter (4.43 nm), the pore diameter (2.45 nm) and the value for the wall thickness (1.98 nm) were calculated. For **S1**, the reflections (110) and (200) are partially lost, most likely related to a reduction of contrast because of pore voids filling with the dye. Moreover, the preservation in the final functionalized solids **S1** of the mesoporous structure is also confirmed from the TEM analysis. The N<sub>2</sub> adsorption-desorption isotherm of **S1** is typical of mesoporous systems with filled mesopores (see Figure SI-1 b), and a significant decrease in the N<sub>2</sub> volume adsorbed, surface area (228.4 m<sup>2</sup>/g) and pore volume (0.16 cm<sup>3</sup> g<sup>-1</sup>) was observed. The most relevant feature is the absence of a sharp step at low-medium relative pressure (0.1 < P/P<sub>0</sub> < 0.4). In fact, this solid shows flat curves in that region when compared (at the same scale) to those of the

MCM-41 parent material, this indicates a significant pore blocking and the subsequent reduction of appreciable mesoporosity. Additionally, the curve shows a N<sub>2</sub> adsorption at high relative pressure similar to the calcined MCM-41, confirming that the textural porosity is preserved.

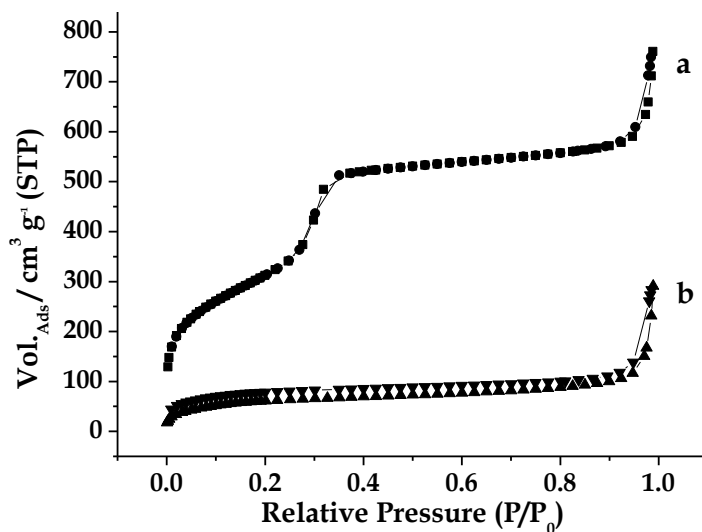


**Figure SI-1.** Nitrogen adsorption-desorption isotherms for (a) MCM-41 mesoporous material and (b) S1.

In order to determine the content of the dye in the mesopores of the final hybrid material, 30 mg of S1 were suspended in 75 ml of water at pH 7.5, in the presence of 7500 ppm of  $\beta$ -galactosidase. The mixture was stirred at room temperature for 72 hours in order to achieve a complete delivery of the dye (Rhodamine B). Afterwards the suspension was centrifugated and the supernatant isolated and dried under reduced pressure. The crude obtained was dissolved in acetone and filtered. The obtained solution was dried and the residue dissolved in 4 ml of methanol. The final content of Rhodamine B was determined through a calibration curve, following the concentration depending increase of the absorption band centred at 550 nm. The content of I in the MSN S1 was calculated from termogravimetric

analysis. Rhodamine-B dye from the final material **S1** amounted 0.14 g/g SiO<sub>2</sub> in weight. Moreover the content of the anchored **I** in **S1** amounted to 0.28g/ g SiO<sub>2</sub> in weight.

### *Cargo Release Studies*

In a typical experiment, 10 mg of **S1** were suspended in 18.75 mL of water at pH 7.5 and then 6.25 mL of enzyme lactozyme ( $\beta$ -galactosidase) solution (0.3 g of enzyme in 10 mL of water at pH 7.5) was added. The delivery of the dye from the pore voids to the aqueous solution was monitorized via the emission band of the dye centred at 580 nm.

To further demonstrate the ability of the  $\beta$ -gal enzyme hydrolyze the capping GOS groups in **S1** MALDI-TOF experiments were performed to characterize the oligomeric fragments produced by the enzymatic hydrolysis. For this purpose the supernatant of different aliquots as a function of time of a **S1** and  $\beta$ -gal mixture in water were analyzed by MALDI-TOF-MS spectroscopy. For each aliquot the silica scaffold was removed by filtration and the resulting solution was treated at 80°C to denaturalize the enzyme which was finally removed it by centrifugation (20 min, 9500 rpm). The supernatant was isolated and analyzed by MALDI-TOF-MS spectroscopy. At 0 min no presence of oligomeric fragments were observed. In progressive aliquots treated in the same matter (increasing hydrolysis time) peaks at 180 (corresponding to the galactose monomer) were found. This signal increased in intensity until 8 h. These evidences are in agreement with a progressive  $\beta$ -gal-induced enzymatic hydrolysis of the galactooligosaccharide chains anchored to the surface.

In parallel, we quantitated the level of free galactose in the same samples using a Galactose detection Kit (Deltaclon). Briefly, 5  $\mu$ l samples

were incubated with galactose oxidase, that oxidizes galactose, which then reacts with a Galactose probe to produce color at 570 nm. As expected, free galactose increased with time.

## *S. Cerevisiae Experiments*

### *Yeast Strains and Culture Conditions*

All yeast strains used in this study have the BY4741 genetic background (MAT $\alpha$  leu2 $\Delta$ 0, his3 $\Delta$ 0, met15 $\Delta$ 0, ura3 $\Delta$ 0). The  $\beta$ -Gal<sup>oe</sup> strain was generated by transforming the WT BY4741 strain with the  $\beta$ -gal p477 (URA3) expression vector.<sup>2</sup> Standard methods for yeast culture and manipulations were used. Minimal medium (SD) contained 2% glucose, 0.67% yeast nitrogen base and the appropriate amino acid supplements to maintain selection of URA3. Yeast cultures were routinely grown at 30°C.

### *Fluorescence Microscopy and Cell Viability Studies*

BY4741 and  $\beta$ -Gal<sup>oe</sup> yeasts were cultured in SD medium overnight at 28 °C in continuous shaking at a density of 10<sup>8</sup> cells/mL. Then, aliquots of 1 mL of this suspension were centrifuged and resuspended in 100  $\mu$ L of SD medium at a pH of 3.7 containing 5 mg/ml of the Rhodamine-loaded **S1** nanoparticles and incubated for 6 h at 40 °C. Intracellular release was monitored by fluorescence microscopy using a NIKON ECLIPSE 600 microscope equipped with a fluorescent NIKON Y-FL lamp;  $\lambda_{\text{ex}}$  = 540 nm,  $\lambda_{\text{em}}$  = 650 nm. After the incubation period, approximately 300 cells were seeded in an YPD plate and incubated for 72 h. Finally, colony formation was quantified. Experiments were repeated twice containing triplicates. Data are expressed as (mean  $\pm$  SE).

## *Human cell experiments*

### Cell culture

Tissue culture reagents were purchased from GIBCO/Invitrogen Corporation /Life Technologies Life Sciences. Dermal fibroblasts from two X-DC patients (X-DC1774 and X-DC4646) and control old passaged fibroblasts (DC1787) were obtained from Coriell Cell Repository. X-DC1774 and X-DC4646 fibroblasts belong to males with c.109\_111delCTT, c.385A>T and c.5C>T *DKC1* mutations, respectively. DC1787 control fibroblasts belong to a carrier female of c.109\_111delCTT *DKC1* mutation. H460 cell were from ATCC and maintained in RMPM supplemented with 10% fetal bovine serum (FBS) and primary human cells were maintained in MEM (Minimum Essential Medium, Gibco) supplemented with 15 % FBS at 37°C and 5% CO<sub>2</sub>. Culture medium was supplemented with gentamicin (56 µg/ml) and L-glutamine (2 mM).

### Senescence analysis

Control and X-DC fibroblasts (1x10<sup>4</sup> cells) were plated onto 6 well plates and fixed after four days to assay the acid-β-galactosidase activity SA-β-gal (Senescence Detection Kit, BioVision, USA). The percentage of senescent cells (blue cells) was calculated in images taken in the bright field microscopy at 100x magnification (Nikon Eclipse TS100 Microscopy, USA).

### In vivo fluorescence microscopy

Nanoparticle cargo release localization was visualized by fluorescence microscopy. For this purpose, cells were grown onto 1µ-slide 8-well ibiTreat microscopy chambers (Ibidi) and treated with the mesoporous silica nanoparticles **S1** or **S2**. Fluorescence was visualized by in vivo microscopy during 48 h in a Microscope Observer Z1. Image acquisition

and processing was as follows: Type, numerical aperture and magnification of the objective lenses: Plan APOCHROMAT de Zeiss 20x, Temperature: 37°C and 5% CO<sub>2</sub>. Camera: Cascade 1k. Acquisition software: Axiovision 4.8. Images were processed using ImageJ and Adobe Photoshop CS were exported to TIFF and mounted using Adobe Photoshop CS.

### Cell viability assays

Viability in the presence of **S1** of H460 (see Figure SI-1) and DC1787 cells (not shown) was determined using a crystal violet based staining method as previously described.<sup>3</sup> Cells were grown in 24-multiwell dishes, treated with different amounts of mesoporous silica nanoparticles and 48 h after treatment, fixed with 1% glutaraldehyde, washed with 1x PBS and remaining cells were stained with 0.1% crystal violet. Colorimetric assay using 595 nm Elisa was used to estimate the number of cells per well. Experiments were repeated three times by quadruplicate.

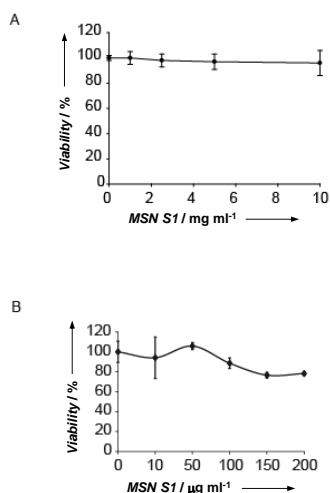


**Figure SI-2.** MSN **S1** nanoparticles are not toxic in yeast and human cells A) Viability of yeast cells incubated with the increasing amounts of MSN **S1** nanoparticles. Incubation conditions are described in materials and methods. B) Viability of H460 cells after 48 hours of treatment with the indicated amounts of MSN **S1** Rhodamine loaded particles.

***Supporting Information Bibliography***

- 1 A. Bernardos, L. Mondragón, E. Aznar, M. D. Marcos, R. Martínez-Máñez, F. Sancenón, J. Soto, J. M. Barat, E. Pérez-Payá, C. Guillem, P. Amorós, *ACS Nano* **2010**, *4*, 6353-6368.
- 2 R. Yang, S. A. Wek, R. C. Wek, *Mol. Cell. Biol.* **2000**, *20*, 2706-2717.
- 3 I. Sánchez-Pérez, J. R. Murguía, R. Perona, *Oncogene* **1998**, *16*, 533-540.



***Chapter 9:***  
***A photoactivated molecular gate***



# ***A photoactivated molecular gate***

Alessandro Agostini,<sup>[a,b]</sup> Félix Sancenón,<sup>[a,b]</sup> Ramón  
Martínez-Máñez,<sup>\*[a,b]</sup> María D. Marcos,<sup>[a,b]</sup> Juan Soto<sup>[a]</sup> and  
Pedro Amorós<sup>[c]</sup>

<sup>[a]</sup>*Centro de Reconocimiento Molecular y Desarrollo Tecnológico (IDM),  
Unidad Mixta Universidad Politécnica de Valencia-Universidad de  
Valencia. Departamento de Química, Universidad Politécnica de Valencia,  
Camino de Vera s/n, 46022, Valencia, Spain.*

<sup>[b]</sup>*CIBER de Bioingeniería, Biomateriales y Nanotecnología (CIBER-BNN).*

<sup>[c]</sup>*Institut de Ciència del Materials (ICMUV), Universitat de València.  
P.O. Box 22085, E-46071 València, Spain.*

***Received: April 3, 2012,***

***Revised: July 16, 2012***

***Published online, August 21, 2012***

*Chem. Eur. J.*, **2012**, *18*, 12218 – 12221

## **9.1 Introduction**

The design and synthesis of mesoporous hybrid capped materials solids, which could be selectively opened upon the application of external stimuli and release an entrapped cargo, have recently caught the interest of the scientific community.<sup>1</sup> In general, these hybrid materials are composed of two main subunits: an inorganic scaffold (with a porous network in which certain chemicals can be stored) and molecular entities grafted on the outer surface which act as molecular gates (that control the delivery of the entrapped cargo).

As inorganic scaffolds, mesoporous silica nanoparticles (MSN) have been widely used because of their unique properties, such as large load capacity, biocompatibility, large surface area and well-known functionalisation procedures.<sup>2</sup> In fact, gated MSN have recently been used as supports for the development of on-command delivery nano-devices using several physical and chemical triggers.<sup>3</sup> In this area, MSN showing controlled release features driven by redox reactions,<sup>4</sup> pH changes<sup>5</sup> and biomolecular interactions<sup>6</sup> have been described.

In this field, light is also a powerful tool for the control of open/closed protocols in mesoporous systems. In particular, by using light-driven gated systems, the release of the cargo can be controlled spatially and temporally by finely tuning the area and the time of the light stimulus. However, there are relatively few examples of photochemically driven molecular gates,<sup>7</sup> some of which are based on reversible photoisomerisation reactions.<sup>8</sup> Recently, we described MSN functionalised with spiropyran photochrome units and capped with PAMAM dendrimers, (G1.5) and MSN capped with gold nanoparticles, which were opened using light as a stimulus.<sup>9</sup> In contrast, only one photo-driven controlled example using a photo-cleavable

gate anchored on the surface of MSN has been reported.<sup>10</sup> In this work, Kim and coworkers prepared an *o*-nitrobenzyl ester derivative bearing a cyclodextrin moiety that was selectively opened by the addition of specific enzymes and by UV irradiation. In particular, the solid was able to release the entrapped cargo (calcein) after UV irradiation at 350 nm due to the photolysis of an *o*-nitrobenzyl ester fragment.

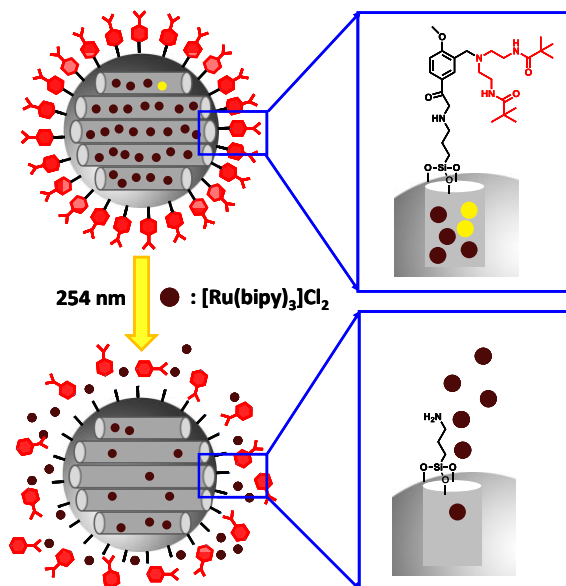
By considering our interest in developing gated materials and the aforementioned ideas, we report herein the synthesis and controlled release studies of a new nanoscopic mesoporous system capped with a photo-cleavable *o*-methoxybenzylamine fragment.

## 9.2 Results and discussion

A schematic representation of the controlled delivery paradigm is shown in Scheme 1. The *o*-methoxybenzylamine group was selected for its well-known photo-cleavage properties, which have been used in a wide range of applications.<sup>11</sup> Based on this methoxybenzylamine fragment, we designed compound **7** which, other than the photo-cleavable group, also contains two bulky *t*-butyl moieties in order to attain an effective pore blockage in the final hybrid material, as well as one trialkoxysilane moiety for anchoring **7** on the external MSN surface. Compound **7** was expected to be bulky enough to preclude the delivery of the entrapped cargo but, at the same time, it was expected to undergo photolysis upon UV irradiation. As a result of photolysis, the steric hindrance of the capping molecule would reduce considerably, thus allowing the release of the entrapped dye.

The synthesis of **7** (see scheme 2) began with the reaction between 4-methoxyacetophenone (**1**) and aqueous formaldehyde in hydrochloric acid, which yielded compound **2**. Then a nucleophilic substitution reaction of **2**

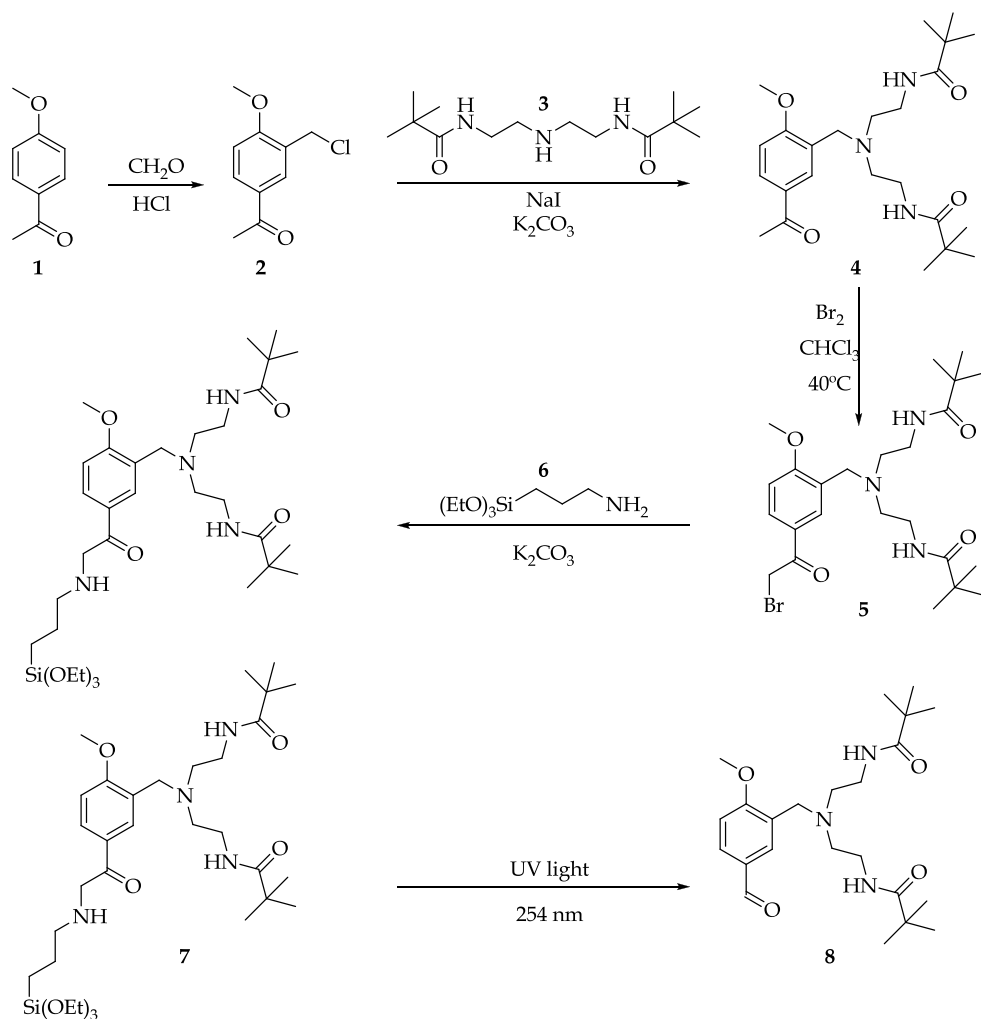
with amine **3** (prepared following a well-known procedure)<sup>12</sup> gave the bulky tertiary amine **4** equipped with two *t*-butylamide moieties. Treatment of tertiary amine **4** with bromine in chloroform gave **5** through an  $\alpha$ -bromination reaction. Finally, trialkoxysilane derivative **7** was prepared by a nucleophilic aliphatic reaction between **5** and (3-aminopropyl)triethoxysilane (**6**) in acetonitrile/ $K_2CO_3$ .



**Scheme 1.** Schematic representation of solid **S1** and the photo-driven uncapping mechanism.

All the synthesised products were characterised using  $^1H$ -NMR,  $^{13}C$ -NMR and HRMS (see Supporting Information). The  $^1H$ -NMR spectrum of trialkoxysilane derivative **7** shows the presence of singlets centred at 1.10 ppm assigned to the methyl groups of both *t*-butyl subunits. The ethoxy moieties appeared as a triplet centred at 1.22 ppm and as a quadruplet centred at 3.85 ppm, whereas the aromatic signals were a pair of doublets

centred at 6.89 and 7.88 ppm and a singlet at 7.90 ppm. Methylene directly linked with the aromatic ring and the tertiary amine nitrogen appeared at 2.51 ppm, whereas the methylene positioned between the aromatic ketone and the secondary amine gave a signal at 3.60 ppm. Finally, the methylene protons linked with amide nitrogen appeared as triplets centred at 3.30 ppm.



**Scheme 2.** Synthesis of trialkoxysilane derivative **7** that acts as a molecular gate and its photolysis reaction.

Prior to anchoring **7** on MSN and in order to test the feasibility of **7** as a photo-cleavable molecule, photolysis studies were carried out. Acetonitrile solutions of **7** were irradiated with a mercury lamp (254 nm) and the photodegradation compounds were studied by gas chromatography coupled with a mass spectrometer. A complete photodegradation of **7** was achieved in three hours, where aldehyde **8** was the major product of this reaction. Product **8** was isolated and characterised by NMR studies (see Scheme 2 and Supporting Information).

After assessing **7** as a suitable photo-cleavable molecule, preparation of the capped materials shown in Scheme 1 was carried out. We selected mesoporous MCM-41 silica nanoparticles of ca. 100 nm in diameter as the inorganic carrier vehicle. This support was prepared by following well-known procedures using TEOS as a hydrolytic inorganic precursor and the surfactant hexadecyltrimethylammonium bromide. After surfactant removal by calcination, MCM-41 nanoparticles were obtained. The structure of the nanoparticulated MCM-41 calcined starting material was confirmed by powder X-Ray diffraction analysis and TEM microscopy (see Figure 1). The N<sub>2</sub> adsorption-desorption isotherms of the prepared nanoparticles showed a typical type IV-curve, with a specific surface of 965.6 m<sup>2</sup> g<sup>-1</sup> and a pore volume of 0.77 cm<sup>3</sup> g<sup>-1</sup>. From the XRD, porosimetry and TEM studies, the a<sub>0</sub> cell parameter (4.34 nm), the pore diameter (2.67 nm) and a wall thickness value (1.67 nm) can be determined. In order to prepare the final capped material, the inorganic support was first loaded with the [Ru(bipy)<sub>3</sub>]Cl<sub>2</sub> fluorophore, which was used as a suitable dye for monitoring the light-triggered protocol. Then, the surface of the solid was functionalised with compound **7** to obtain the final hybrid material **S1**.

Finally, the charged orange solid was filtered, intensively washed with acetonitrile and dried overnight at 36°C.

Figure 1 shows the powder X-ray diffraction patterns of the MSN material as synthesised, the MSN calcined and the final **S1** nanoparticles. **S1** displays the expected features of the MCM-41 phase, indicating that the mesopore in the inorganic scaffolding is preserved throughout the filling process with the ruthenium complex and the anchoring of bulky derivative **7** at the pore outlets. Figure 1a and 1b provides TEM images of the MSN support and of the final hybrid nanoparticles **S1**. Both TEM images show the typical porosity associated with the inorganic support and their spherical form of ca. 100 nm in diameter.

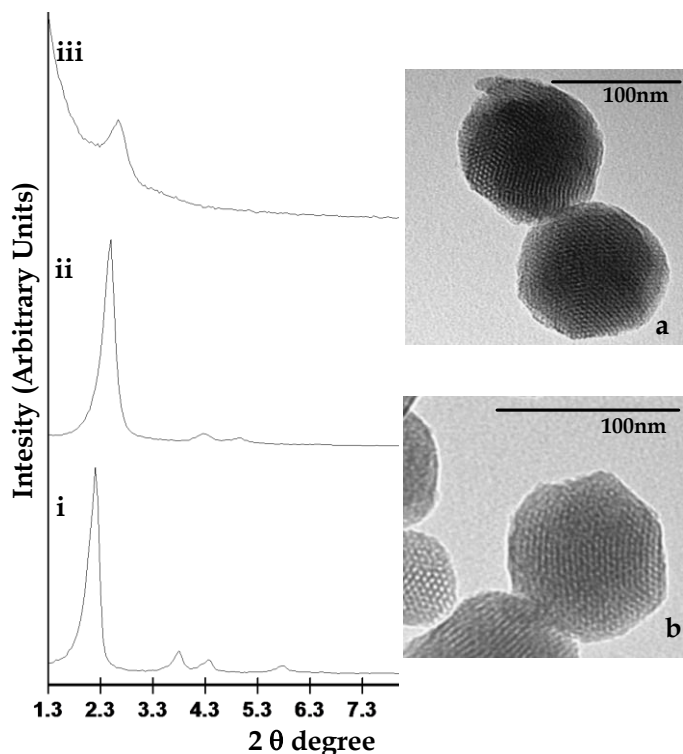


**Figure 1.** Left: Powder-X ray diffractograms showing the MSN patterns as synthesised (i), MSN calcined (ii) and solid **S1** (iii). Right: TEM images of MSN calcined (a) and of final solid **S1** (b).

Additionally, the N<sub>2</sub> adsorption-desorption isotherm of **S1** (see Supporting Information) was typical of mesoporous systems with filled mesopores, and the N<sub>2</sub> volume adsorbed and the surface area (53.6 m<sup>2</sup>g<sup>-1</sup>) significantly decreased when compared with MSN calcined samples. The contents of ruthenium complex and capping molecule **7** in **S1** were determined by thermogravimetric analyses and amounted to 119 mmol / g SiO<sub>2</sub> and 109 mmol / g SiO<sub>2</sub>, respectively.

After synthesising and characterising the capped MSN, the gating properties of **S1** were studied. In a typical experiment, 3 mg of solid **S1** were suspended in anhydrous acetonitrile. Then the sample was stirred and exposed to 254 nm irradiation in a closed photoreactor for a given time. As control experiment, dye release was also determined by using suspensions of **S1** under similar conditions, but in the absence of light (see Supporting Information for details). Photo-triggered molecular gate performance was monitored through the emission band ( $\lambda_{em} = 610$  nm,  $\lambda_{ex} = 451$  nm) of the ruthenium fluorophore delivered to the solution. The dye delivery versus time for both the irradiated and non-irradiated samples is shown in Figure 2.

As explained above, compound **7** was expected to be bulky enough to preclude the release of the entrapped dye in **S1**. In fact, as Figure 2 illustrates, the release of the ruthenium dye in the absence of light was completely inhibited (the gate was closed).

The profile obtained upon UV irradiation clearly differed and a remarkable cargo release was observed due to the photo-cleavage of the methoxybenzylamine fragment. A maximum dye release was noted after ca. 20 minutes of UV irradiation.

Moreover the presence in the solution, upon irradiation, of the aldehyde **8** was also confirmed.

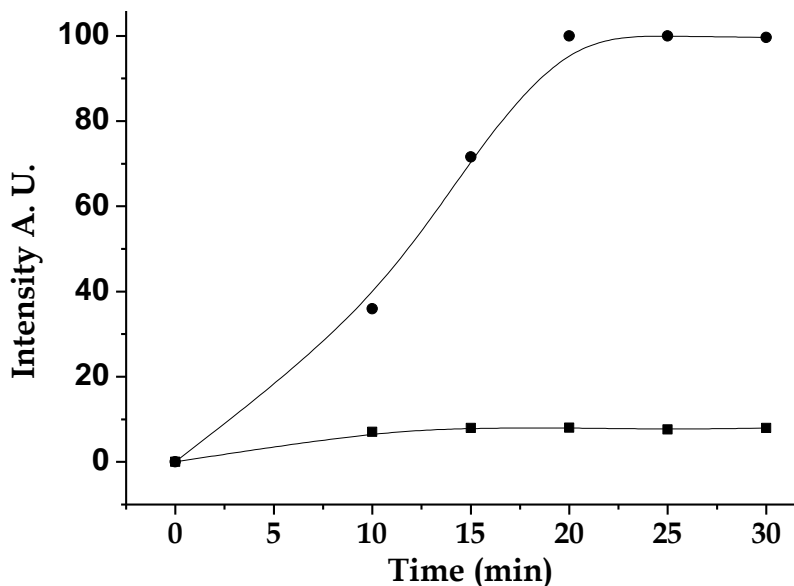


**Figure 2.** Kinetics of the  $[\text{Ru}(\text{bipy})_3]^{2+}$  dye release from solid **S1** in the absence of light (■) and upon irradiation with UV light (●).

### 9.3 Conclusions

To summarise, we report herein the synthesis of a new photo-cleavable organic molecule which, when grafted on the surface of MSN, acts as a molecular gate by allowing the controlled release of an entrapped cargo by simple UV irradiation. The photolysis of the methoxybenzylamine group diminished the steric crowding around the pore outlets, which accounts for the dye delivery and the emission enhancement observed. The design of light-responsive materials is a promising research field that may be of relevance in the development of custom-made materials for advanced delivery applications.

## 9.4 Acknowledgements

The authors thank the Spanish Government (project MAT2009-14564-C04), the Generalitat Valenciana (Project PROMETEO/2009/016) and the CIBER-BBN for their support. AG also thanks the Generalitat Valenciana for his Santiago Grisolia fellowship.

## 9.5 Bibliography

- 1 a) A. B. Descalzo, R. Martínez-Mañez, F. Sancenón, K. Hoffmann, K. Rurack, *Angew. Chem. Int. Ed.* **2006**, *45*, 5924-5948; *Angew. Chem.* **2006**, *118*, 6068-6093; b) A. Cazacu, Y. -M. Legrand, A. Pasc, G. Nasr, A. Van der Lee, E. Mahon, M. Barboiu, *Proc. Natl. Acad. Sci.*, **2009**, *106*, 8117-8122; c) X. Hou, W. Guo, L. Jiang, *Chem. Soc. Rev.*, **2011**, *40*, 2385-2401; d) B. Zhu, J. Li, D. Xu, *Phys. Chem. Chem. Phys.*, **2011**, *13*, 10584-10592.
- 2 a) J. S. Beck, J. C. Vartuli, W. J. Roth, M. E. Leonowicz, C. T. Kresge, K. D. Schmitt, C. T. -W. Chu, D. H. Olson, E. W. Sheppard, S. B. McCullen, J. B. Higgins, J. L. Schlenker, *J. Am. Chem. Soc.* **1992**, *114*, 10834-10843; b) A. P. Wright, M. E. Davis, *Chem. Rev.* **2002**, *102*, 3589-3614; c) G. Kickelbick, *Angew. Chem. Int. Ed.* **2004**, *43*, 3102-3104; *Angew. Chem.* **2004**, *116*, 3164-3166; d) A. Stein, *Adv. Mater.* **2003**, *15*, 763-775.
- 3 E. Aznar, R. Martínez-Mañez, F. Sancenón, *Expert Opin. Drug Deliv.*, **2009**, *6*, 643-655.
- 4 a) B. G. Trewyn, S. Giri, I. I. Slowing, V. S. -Y. Lin, *Chem. Commun.* **2007**, 3236-3245; b) F. Torney, B. G. Trewyn, V. S. -Y. Lin, K. Wang, *Nat. Nanotechnol.* **2007**, *2*, 295-300; c) D. R. Radu, C. -Y. Lai, K. Jeftinija, E. W. Rowe, S. Jeftinija, V. S. -Y. Lin, *J. Am. Chem. Soc.* **2004**, *126*, 13216-13217; d) S. Giri, B. G. Trewyn, M. P. Stellmaker, V. S. -Y. Lin, *Angew. Chem. Int. Ed.* **2005**, *44*, 5038-5044; *Angew. Chem.* **2005**, *117*, 5166-5172; e) M. Fujiwara, S. Terashima, Y. Endo, K. Shiokawa, H. Ohue, *Chem. Commun.* **2006**, 4635-4637; f) R. Liu, X. Zhao, T. Wu, P. Feng, *J. Am. Chem. Soc.* **2008**, *130*, 14418-14419; g) T. D. Nguyen, Y. Liu, S. Saha, K. F. -C. Leung, J. F. Stoddart, J. I. Zink, *J. Am. Chem. Soc.* **2007**, *129*, 626-634.
- 5 a) R. Casasús, M. D. Marcos, R. Martínez-Mañez, J. V. Ros-Lis, J. Soto, L. A. Villaescusa, P. Amorós, D. Beltrán, C. Guillem, J. Latorre, *J. Am. Chem. Soc.* **2004**,

- 126, 8612-8613; b) R. Casasús, E. Climent, M. D. Marcos, R. Martínez-Mañez, F. Sancenón, J. Soto, P. Amorós, J. Cano, E. Ruiz, *J. Am. Chem. Soc.* **2008**, *130*, 1903-1917; c) S. Angelos, Y. -W. Yang, N. M. Khashab, J. F. Stoddart, J. I. Zink, *J. Am. Chem. Soc.* **2009**, *131*, 11344-11346; d) S. Angelos, Y. -W. Yang, K. Patel, J. F. Stoddart, J. I. Zink, *Angew. Chem. Int. Ed.* **2008**, *47*, 2222-2226; *Angew. Chem.* **2008**, *120*, 2254-2258; e) S. Angelos, N. M. Khashab, Y. -W. Yang, A. Trabolsi, H. A. Khatib, J. F. Stoddart, J. I. Zink, *J. Am. Chem. Soc.* **2009**, *131*, 12912-12914; f) L. Du, S. Liao, H. A. Khatib, J. F. Stoddart, J. I. Zink, *J. Am. Chem. Soc.* **2009**, *131*, 15136-15142; g) Q. Yang, S. Wang, P. Fan, L. Wang, Y. Di, K. Lin, F. -S. Xiao, *Chem. Mater.* **2005**, *17*, 5999-6003; h) C. Park, K. Oh, S. C. Lee, C. Kim, *Angew. Chem. Int. Ed.* **2007**, *46*, 1455-1457; *Angew. Chem.* **2007**, *119*, 1477-1479; i) L. Chen, J. Di, C. Cao, Y. Zhao, Y. Ma, J. Luo, Y. Wen, W. Song, Y. Song, L. Jiang, *Chem. Commun.* **2011**, *47*, 2850-2852.
- 6 a) K. Patel, S. Angelos, W. R. Dichtel, A. Coskun, Y. -W. Yang, J. I. Zink, J. F. Stoddart, *J. Am. Chem. Soc.* **2008**, *130*, 2382-2383; b) A. Schlossbauer, J. Kecht, T. Bein, *Angew. Chem. Int. Ed.* **2009**, *48*, 3092-3095; *Angew. Chem.* **2009**, *121*, 3138-3141; c) C. Park, H. Kim, S. Kim, C. Kim, *J. Am. Chem. Soc.* **2009**, *131*, 16614-16615; d) P. D. Thornton, A. Heise, *J. Am. Chem. Soc.* **2010**, *132*, 2024-2028; e) A. Bernardos, E. Aznar, M. D. Marcos, R. Martínez-Mañez, F. Sancenón, J. Soto, J. M. Barat, P. Amorós, *Angew. Chem. Int. Ed.* **2009**, *48*, 5884-5887; *Angew. Chem.* **2009**, *121*, 5998-6001; f) E. Climent, A. Bernardos, R. Martínez-Mañez, A. Maquieira, M. D. Marcos, N. Pastor-Navarro, R. Puchades, F. Sancenón, J. Soto, P. Amorós, *J. Am. Chem. Soc.* **2009**, *131*, 14075-14080; g) A. Bernardos, L. Mondragón, E. Aznar, M. D. Marcos, R. Martínez-Mañez, F. Sancenón, J. Soto, J. M. Barat, E. Pérez-Payá, C. Guillem, P. Amorós, *ACS Nano* **2010**, *11*, 6353-6368; h) E. Climent, R. Martínez-Mañez, F. Sancenón, M. D. Marcos, J. Soto, A. Maquieira, P. Amorós, *Angew. Chem. Int. Ed.* **2010**, *49*, 7281-7283; *Angew. Chem.* **2010**, *122*, 7439-7441; i) C. Coll, L. Mondragón, R. Martínez-Mañez, F. Sancenón, M. D. Marcos, J. Soto, P. Amorós, E. Pérez-Payá, *Angew. Chem. Int. Ed.* **2011**, *50*, 2138-2140; *Angew. Chem.* **2011**, *123*, 2186-2188.
- 7 a) N. Ž. Knežević, B. G. Trewyn, V. S. -Y. Lin, *Chem. Commun.* **2011**, *47*, 2718-2719; b) D. P. Ferris, Y. -L. Zhao, N. M. Khashab, H. A. Khatib, J. F. Stoddart, J. I. Zink, *J. Am. Chem. Soc.* **2009**, *131*, 1686-1688; c) J. L. Vivero-Escoto, I. I. Slowing, C. -W. Wu, V. S. -Y. Lin, *J. Am. Chem. Soc.* **2009**, *131*, 3462-3463.
- 8 a) N. K. Mal, M. Fujiwara, Y. Tanaka, *Nature* **2003**, *421*, 350-353; b) Y. Zhu, M. Fujiwara, *Angew. Chem. Int. Ed.*, **2007**, *46*, 2241-2244; *Angew. Chem.* **2007**, *119*,

- 2291-2294; c) N. K. Mal, M. Fujiwara, Y. Tanaka, T. Taguchi, M. Matsukata, *Chem. Mater.* **2003**, *15*, 3385-3394.
- 9 a) E. Aznar, M. D. Marcos, R. Martínez-Máñez, F. Sancenón, J. Soto, P. Amorós, C. Guillem, *J. Am. Chem. Soc.* **2009**, *131*, 6833-6843; b) E. Aznar, R. Casasús, B. García-acosta, M.D. Marcos, R. Martínez-Máñez, F. Sancenón, J. Soto, P. Amorós, *Adv. Mater.* **2007**, *19*, 2228-2231.
- 10 a) C. Park, H. Kim, S. Kim, and C. Kim, *J. Am. Chem. Soc.* **2009**, *131*, 16614-16615; b) C. Park, K. Lee, C. Kim, *Angew. Chem. Int. Ed.*, **2009**, *48*, 1275-1278; *Angew. Chem.* **2009**, *121*, 1301-1304.
- 11 R. S. Givens, C. H. Park, *Tetrahedron Lett.*, **1996**, *37*, 6259-6262.
- 12 M. J. Goldcamp; D. T. Rosa; N. A. Landers; S. M. Mandel, J. A. Krause-Bauer; M. J. Baldwin, *Synthesis*, **2000**, 2033-2038.

# ***A photoactivated molecular gate***

Alessandro Agostini,<sup>[a,b]</sup> Félix Sancenón,<sup>[a,b]</sup> Ramón  
Martínez-Máñez,<sup>\*[a,b]</sup> María D. Marcos,<sup>[a,b]</sup> Juan Soto<sup>[a]</sup> and  
Pedro Amorós<sup>[c]</sup>

<sup>[a]</sup>*Centro de Reconocimiento Molecular y Desarrollo Tecnológico (IDM),  
Unidad Mixta Universidad Politécnica de Valencia-Universidad de  
Valencia. Departamento de Química, Universidad Politécnica de Valencia,  
Camino de Vera s/n, 46022, Valencia, Spain.*

<sup>[b]</sup>*CIBER de Bioingeniería, Biomateriales y Nanotecnología (CIBER-BNN).*

<sup>[c]</sup>*Institut de Ciència del Materials (ICMUV), Universitat de València.  
P.O. Box 22085, E-46071 València, Spain.*

***Supporting Information***

### **Chemicals**

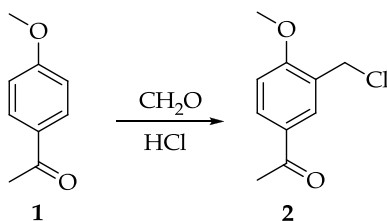
The chemicals tetraethylorthosilicate (TEOS) (98%), *n*-cetyltrimethylammonium bromide (CTAB) ( $\geq 99\%$ ), sodium hydroxide ( $\geq 98\%$ ), tris(2,2'-bipyridyl)dichlororuthenium(II) hexahydrate ( $[\text{Ru}(\text{bipy})_3]\text{Cl}_2 \cdot 6\text{H}_2\text{O}$ ) (100%), 4-methoxybenzophenone, concentrated hydrochloric acid, aqueous formaldehyde (37%), diethylenetriamine, trimethylacetic anhydride, sodium iodide, potassium carbonate, bromine and (3-aminopropyl)triethoxysilane were provided by Sigma-Aldrich. Analytical-grade solvents were acquired from Scharlab (Barcelona, Spain). All the reagents were used as received.

### **General Techniques**

XRD, TG Analysis, and  $\text{N}_2$  adsorption-desorption techniques were employed to characterise the prepared materials. Powder X-ray measurements were performed in a Philips D8 Advance diffractometer using  $\text{Cu K}_\alpha$  radiation. Thermo-gravimetric analyses were carried out on a TGA/SDTA 851e Mettler Toledo balance, using an oxidant atmosphere (air, 80 mL/min) with a heating programme consisting in a heating ramp of  $10^\circ\text{C}$  per minute from 393 to 1273 K and an isothermal heating step at this temperature for 30 minutes. TEM images were obtained with a 100 kV Philips CM10 microscope.  $\text{N}_2$  adsorption-desorption isotherms were recorded on a Micromeritics ASAP2010 automated sorption analyser. Samples were degassed at  $120^\circ\text{C}$  in vacuum overnight. The specific surface areas were calculated from the adsorption data in the low pressures range using the BET model. Pore size was determined following the BJH method. Fluorescence spectroscopy was carried out on a Felix 32 Analysis Version 1.2 (Build 56) PTI (Photon Technology International).  $^1\text{H}$  and  $^{13}\text{C}$  nuclear

magnetic resonance (NMR) were acquired with a Varian 300 spectrometer (Sunnyvale, CA, USA).

### Synthesis of 3-(chloromethyl)-4-methoxybenzophenone 2

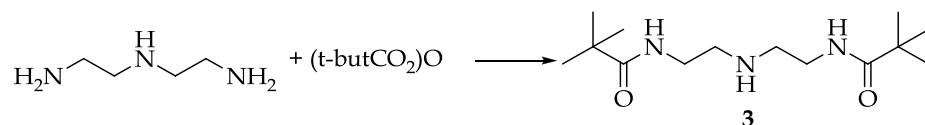


4-methoxybenzophenone (**1**, 705 mg, 6.72 mmol) was suspended in 37% hydrochloric acid (4.81 mL) and then 37% aqueous formaldehyde (0.36 mL, 4.81 mmol) was added. The reaction was allowed to stir overnight. The obtained solid was filtered on a Buchner, dissolved in diethyl ether and dried on sodium sulphate. The subsequent filtration and elimination of the solvent gave the final product **2** (930 mg, 4.69 mmol, 97.4% yield) as a yellow-orange solid.

$^1\text{H-NMR}$  ( $\text{CDCl}_3$ , 400 Mhz):  $\delta$ : 2.49 (s, 3H); 3.88 (s, 3H); 4.59 (s, 2H); 6.86-6.89 (d, 1H,  $J=6.3$  hz); 7.84-7.88 (d, 1H,  $J=6.3$  hz); 7.91 (s, 1H).

$^{13}\text{C-NMR}$ ( $\text{CDCl}_3$ ,100Mhz):  $\delta$ : 26.32, 41.09, 55.93, 110.33, 125.98, 130.21, 131.08, 131.11, 161.13, 196.41.

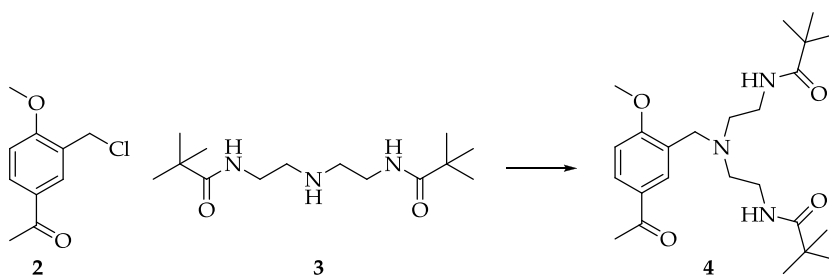
### Synthesis of diamide 3



Diethylenetriamine (0.50 g, 4.81 mmol) was dissolved in  $\text{CHCl}_3$  (30 mL) under stirring at  $0^\circ\text{C}$ . Then, a solution of trimethylacetic anhydride (1.81 g, 9.72 mmol) in  $\text{CHCl}_3$  (30 mL) was added dropwise for 30 minutes. At 1 hour

after the addition, the reaction mixture was filtered. The filtrate was extracted with sat. Na<sub>2</sub>CO<sub>3</sub> (2 x 20 ml). The CHCl<sub>3</sub> layer was then dried (Na<sub>2</sub>SO<sub>4</sub>), filtered, the solvent removed by rotary evaporation and the solid obtained was washed with hexane. Diamide **3** was isolated as a white solid (0.845 g, 3.12 mmol, 64% yield). <sup>1</sup>H-NMR and <sup>13</sup>C-NMR data are coincident with those reported by Goldcamp et al. in a previously published paper. <sup>1</sup>

### Synthesis of product **4**

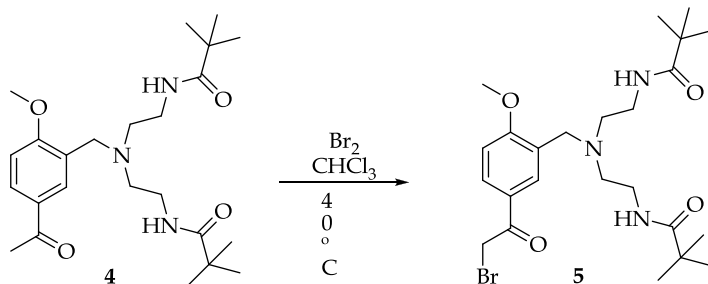


A solution of **2** (73 mg, 0.37 mmol) in anhydrous CH<sub>3</sub>CN (10 ml) was refluxed in the presence of NaI (83 mg, 0.55 mmol) for 1 hour in an argon atmosphere. Afterwards, **3** (100 mg, 0.37 mmol) and K<sub>2</sub>CO<sub>3</sub> (500 mg) were added to the previous suspension, and the final mixture was stirred at reflux for 6 hours. Then, the reaction mixture was filtered to eliminate potassium carbonate, and was evaporated, dissolved in chloroform, filtered again and evaporated to obtain the final product **4** (156 mg, 0.33 mmol, 93% yield), after chromatographic purification.

<sup>1</sup>H-NMR (CDCl<sub>3</sub>, 300 Mhz): δ: 1.04 (s, 18H); 2.50 (s, 3H); 2.53 (m, 4H), 3.2 (m, 4H), 3.53 (s, 2H), 3.77 (s, 3H); 6.86-6.89 (d, 1H, J=6 hz); 7.84-7.88 (d, 1H, J=6 hz), 7.91 (s, 1H).

<sup>13</sup>C-NMR (CDCl<sub>3</sub>, 75 Mhz): δ: 27.32, 28.01, 30.34, 33.56, 38.87, 39.25, 40.01, 51.32, 53.98, 58.64, 100.00, 110.25, 118.97, 119.98, 128.01, 132.54, 134.03, 162.73, 178.02, 178.99, 180.95, 181.56, 190.36.

## Synthesis of product 5

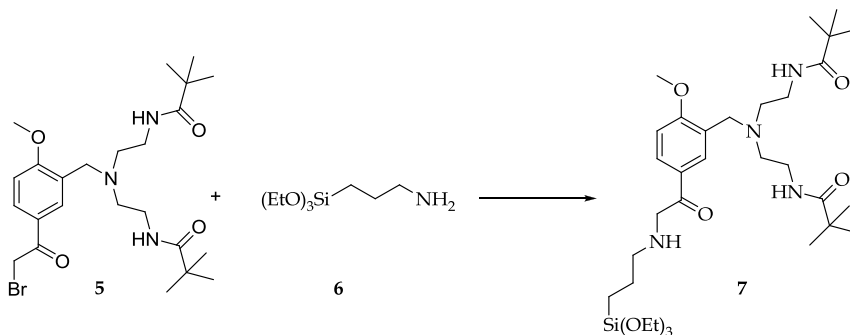


Caution: All the reaction steps must be carried out in the total absence of light. **4** (74 mg, 0.19 mmol) was dissolved in  $\text{CHCl}_3$  (20 mL) and heated to  $40^\circ\text{C}$ . Then,  $\text{Br}_2$  (15  $\mu\text{L}$ , 0.256 mmol) was added and the reaction mixture was stirred at  $40^\circ\text{C}$  until complete decolourisation. Afterwards, diethyl ether (10 mL) was added and the obtained organic phase was extracted twice with saturated  $\text{NaHCO}_3$ , dried with  $\text{Na}_2\text{SO}_4$  and the solvent was finally removed to give product **5** (88 mg, 0.17 mmol, 90% yield), after chromatographic purification.

$^1\text{H-NMR}$  ( $\text{CDCl}_3$ , 300 Mhz):  $\delta$ : 1.04 (s, 18H); 2.53 (m, 4H), 3.2 (m, 4H), 3.53 (s, 2H), 3.77 (s, 3H), 4.5 (s, 2H); 6.86-6.89 (d, 1H,  $J=6$  hz); 7.84-7.88 (d, 1H,  $J=6$  hz), 7.91 (s, 1H).

$^{13}\text{C-NMR}$  ( $\text{CDCl}_3$ , 75 Mhz):  $\delta$ : 27.76, 27.83, 28.76, 29.95, 38.89, 53.16, 54.44, 55.93, 56.24, 100.24, 110.63, 130.54, 130.90, 131.23, 161.94, 179.95, 180.11, 197.08.

## Synthesis of product 7



Caution: All the reaction steps must be carried out in the total absence of light. **5** (123 mg, 0.24 mmol) was dissolved in CH<sub>3</sub>CN (50 mL) and then K<sub>2</sub>CO<sub>3</sub> (500 mg) was added. Afterwards, 3-aminopropyltriethoxysilane (**6**, 7  $\mu$ l, 0.28 mmol) was added and the reaction mixture was stirred at room temperature for 45 minutes. The reaction crude was then filtered and acetonitrile was removed by rotary evaporation. The obtained crude product was dissolved in CHCl<sub>3</sub> (10 ml) filtered and evaporated to obtain product **7** (126 mg, 0.21 mmol, 86% yield) as a pale yellow oil.

<sup>1</sup>H-NMR (CDCl<sub>3</sub>, 300 Mhz):  $\delta$ : 0.58-0.61 (m, 2H) 1.07-1.45 (m, 27H); 1.47-1.53 (m, 2H); 2.51-2.63 (m, 8H); 3.28-3.30 (m, 4H), 3.6 (s, 2H), 3.53 (s, 2H), 3.76-3.86 (m, 9H) 6.86-6.89 (d, 1H, J=6 hz); 7.6-7.8 (d, 1H, J=6 hz), 7.88-7.91 (m, 2H).

<sup>13</sup>C-NMR (CDCl<sub>3</sub>, 75 Mhz):  $\delta$ : -15.32, 9.95, 18.78, 27.29, 28.05, 29.32, 33.51, 36.59, 41.02, 55.63, 60.23, 100.25, 110.59, 118.56, 136.25, 137.85, 152.36, 165.58, 178.91, 198.53.

### *Synthesis of silica mesoporous nanoparticles (MCM-41)*

The MCM-41 mesoporous nanoparticles were synthesised by the following procedure: n-cetyltrimethylammoniumbromide (CTAB, 1.00 g, 2.74 mmol) was first dissolved in deionised water (480 mL). Then NaOH 2.00 M in deionised water (3.5 mL) was added to the CTAB solution, followed by adjusting the solution temperature to 80°C. TEOS (5.00 mL, 2.57  $\times 10^{-2}$  mol) was then added dropwise to the surfactant solution. The mixture was allowed to stir for 2 h to give a white precipitate. Finally, the solid product was centrifuged, washed with deionised water and ethanol, and was dried at 60°C (MCM-41 as-synthesised). To prepare the final porous material (MCM-41), the as-synthesised solid was calcined at 550°C using an oxidant atmosphere for 5 h to remove the template phase.

### *Synthesis of solid S1*

For the purpose of obtaining the final hybrid solid S1, MCM-41 calcined (80 mg) was suspended in anhydrous CH<sub>3</sub>CN (10 mL) and then [Ru(Bipy)<sub>3</sub>]Cl<sub>2</sub>·6H<sub>2</sub>O (80 mg, 0.106 mmol) was added. Afterwards the mixture was stirred at room temperature for 24 hours to achieve maximum pore loading. Subsequently, **7** (150 mg, 0.24 mmol) was added and the mixture was stirred overnight at room temperature in the total absence of light. Then the solid was filtered, washed with distilled water and acetone, suspended in water in a flask, and was stirred at room temperature in the total absence of light for 12 hours. With this procedure, all the [Ru(Bipy)<sub>3</sub>]Cl<sub>2</sub>·6H<sub>2</sub>O present outside the pores was removed. Next, the solid was filtered and dried at 38°C for 12 hours. Caution: The absence of light is compulsory in order to preserve the structural integrity of molecular gate **7**.

### *Materials Characterisation*

Solid **S1** was characterised using standard procedures. Figure SI-1 shows the powder X-ray patterns of the nanoparticulated MCM-41 support and the S1 functionalised material.

The PXRD of siliceous nanoparticulated MCM-41 as-synthesised (curve a) shows four low-angle reflections, which are typical of a hexagonal array that can be indexed as (100), (110), (200), and (210) Bragg peaks.

A significant displacement of the (100) peak in the XRD powder of the nanoparticulated MCM-41 calcined sample can be clearly seen in curve b, corresponding to an approximate cell contraction of 4 Å. This displacement and the broadening of the (110) and (200) peaks are related to a further condensation of the silanol groups during the calcination step. Finally,

curve c corresponds to the **S1** XRD pattern. In this case, a slight drop in intensity and the disappearance of the (110) and (200) reflections are observed, which most likely relate to loss of contrast due to the pore voids filling with the ruthenium (II) dye. Nevertheless, the value and intensity of the (100) peak in this pattern strongly evidences that the loading process with the dye and the further functionalisation with **7** do not damage the mesoporous 3D MCM-41 scaffolding.

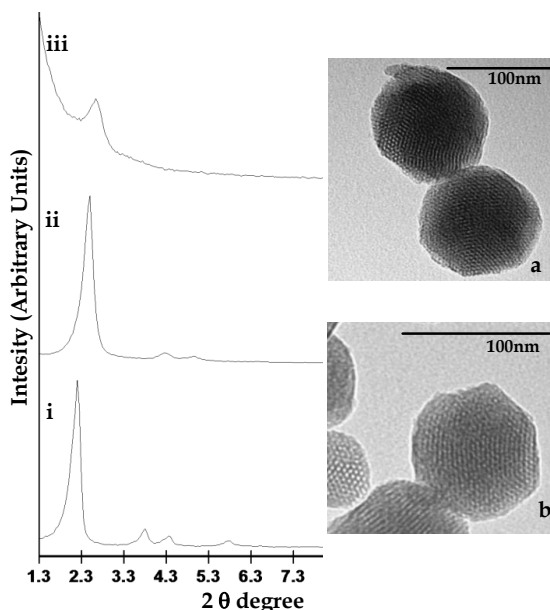


**Figure SI-1.** Left: Powder X ray pattern of MCM-41 as synthesised (i); calcined MCM-41 (ii) and S1 (iii). Right: TEM images of MCM-41 calcined (a) and S1 (b).

The presence in the final functionalised solid (**S1**) of the mesoporous structure is also confirmed by the TEM analysis, in which the typical channels of the MCM-41 matrix are visualised as alternate black and white stripes (see Figure S1-1 for solid **S1**).

The N<sub>2</sub> adsorption-desorption isotherms of the nanoparticulated MCM-41 calcined material show an adsorption step at an intermediate P/P<sub>0</sub> value (0.1-0.3), which is typical of these solids (see Figure SI-2). This step can be

related to nitrogen condensation inside the mesopores by capillarity. The absence of a hysteresis loop in this interval and the narrow BJH pore distribution suggest the existence of uniform cylindrical mesopores with a pore volume of  $0.77 \text{ cm}^3 \text{ g}^{-1}$  calculated by using the BJH model on the adsorption branch of the isotherm. The application of the BET model resulted in a value for the total specific surface of  $965.6 \text{ m}^2/\text{g}$  and in a pore volume of  $0.87 \text{ cm}^3 \text{ g}^{-1}$ .

From the XRD, porosimetry and TEM studies, the  $a_0$  cell parameter (4.34 nm), the pore diameter (2.67 nm) and a wall thickness (1.67 nm) value were calculated. In addition to this adsorption step associated with the micelle-generated mesopores, a second feature appears in the isotherm at a high relative pressure ( $P/P_0 > 0.8$ ). This adsorption corresponds to the filling of the large voids among particles and presents a volume of  $0.37 \text{ cm}^3 \text{ g}^{-1}$  (calculated by using the BJH model) and must then be considered a textural-like porosity.

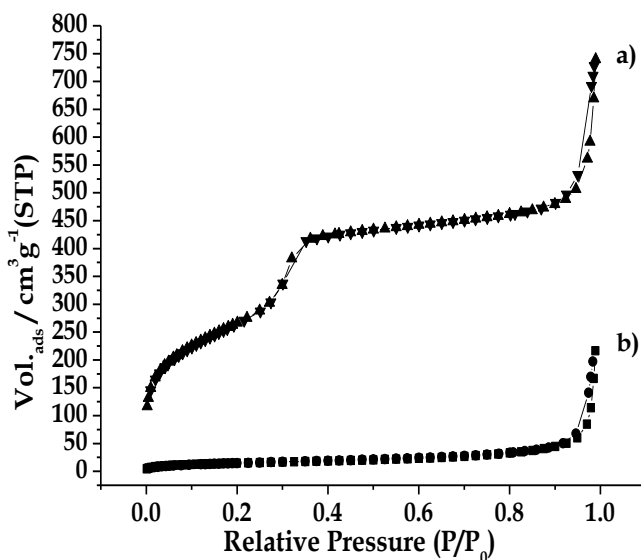


**Figure SI-2.** Nitrogen adsorption-desorption isotherms for: a) MCM-41 mesoporous material and b) S1

In this case, the curves show a characteristic H1 hysteresis loop and a wide pore size distribution.

The N<sub>2</sub> adsorption-desorption isotherm of **S1** is typical of mesoporous systems with filled mesopores (see Figure SI-2), and the N<sub>2</sub> volume adsorbed and surface area (53.62 m<sup>2</sup>/g) significantly decreased. In fact, this solid shows flat curves when compared (on the same scale) to those of the MCM-41 parent material, indicating significant pore blocking and the subsequent absence of appreciable mesoporosity.

Additionally, a certain textural porosity is preserved. The BET-specific surface values, pore volumes, and pore sizes calculated from the N<sub>2</sub> adsorption-desorption isotherms for MCM-41 and **S1** are listed in Table SI-1. The N<sub>2</sub> adsorption-desorption isotherm of this solid is also typical of a mesoporous system with filled mesopores (see Figure SI-2 and Table SI-1); i.e., flat curves when compared to those of the MCM-41 mesoporous material, indicating the absence of mesoporosity.

**Table SI-1.** BET-specific surface values, pore volumes and pore sizes calculated from the N<sub>2</sub> adsorption-desorption isotherms for selected materials.

<i>Solid</i>	$S_{BET}$ (m <sup>2</sup> g <sup>-1</sup> )	<i>Pore Volume</i> <sup>a</sup> (cm <sup>3</sup> g <sup>-1</sup> )	<i>Pore size</i> <sup>a</sup> (nm)
<b>MCM-41</b>	965.6	0.87	2.67
<b>S1</b>	53.6	-	-

The content of product **7** and ruthenium (II) dye in the final **S1** solid were determined by thermogravimetric analyses. Values of content are detailed in Table SI-2.

Table SI-2. Content ( $\alpha$ ) of product 7 and the ruthenium complex in solid S1.

Solid	$\alpha_7$ (mmol/g SiO <sub>2</sub> )	$\alpha_{RuBipy}$ (mmol/g SiO <sub>2</sub> )
S1	0.109	0.119

### Delivery studies of solid S1

A typical delivery experience was carried out in batch and two different suspensions were prepared: (i) 3 mg of S1 and 4 ml of anhydrous acetonitrile degassed with Ar for 15 minutes in dark vials in the absence of light; (ii) 3 mg of S1, 4 ml of anhydrous acetonitrile degassed with Ar for 15 minutes and irradiated in a closed photoreactor with 8 mercury lamps (254 nm) of 8 watts. The ruthenium complex release profiles of both experiences are shown in Figure SI-3.

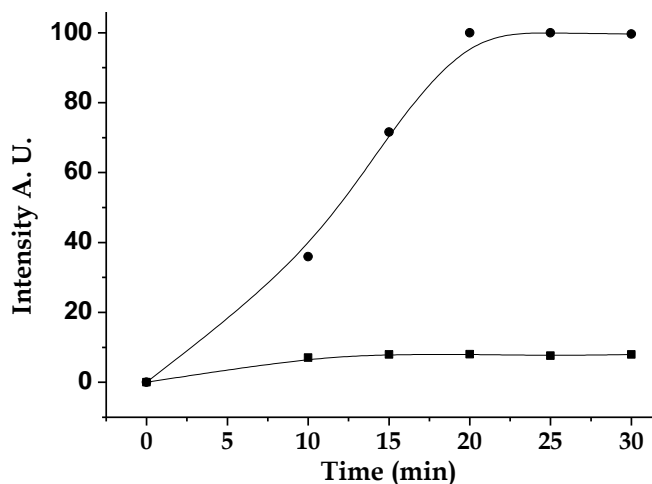
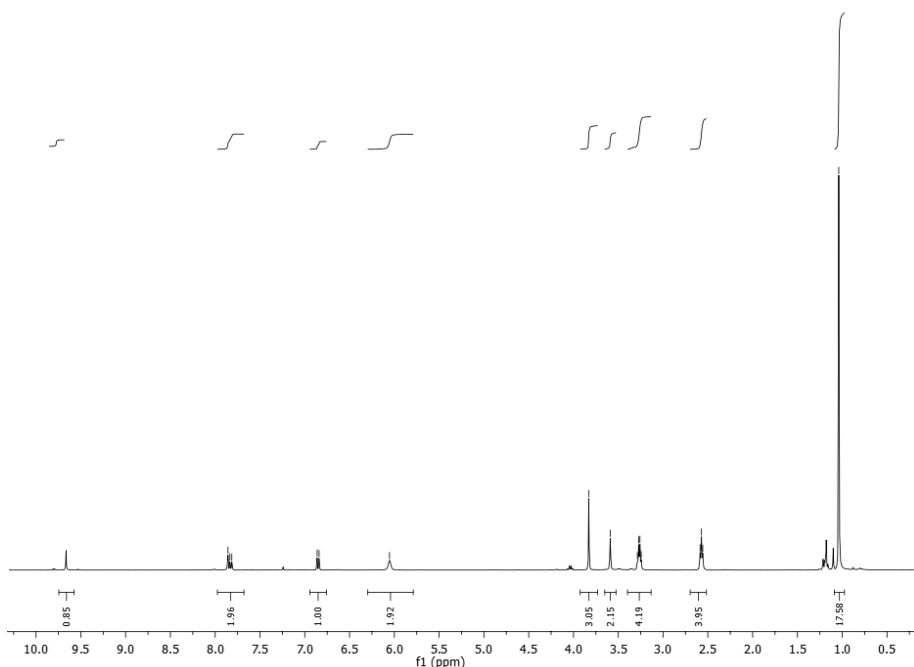


Figure SI-3. Kinetics of the  $[Ru(bipy)_3]^{2+}$  dye release from solid S1 in the absence of light and (■) upon irradiation with UV light of 254 nm (●).

### **Photodegradation of compound 7**

The photo-physical degradation of compound **7** was studied in solution. Quartz test tubes containing 3 mL of an acetonitrile solution of **7** ( $1.0 \times 10^{-4}$  mol dm<sup>-3</sup>) were degassed and then irradiated with a mercury lamp (254 nm). The photodegradation mixture was studied by gas chromatography coupled with a mass spectrometer. A main peak by gas chromatography was observed corresponding to a product of mass 419, which was in agreement with the formation of **8**. Moreover the photodegradation of **7** was repeated 10 times in order to accumulate material for further characterization. The photo-degradation mixture was purified (by column chromatography) and characterized by <sup>1</sup>H and <sup>13</sup>C NMR spectroscopy. Aldehyde **8** was the mainly isolated photoproduct (see Figures SI-4 and SI-5 for its characterization).



**Figure SI-4.** <sup>1</sup>H-NMR spectra of aldehyde **8** in CDCl<sub>3</sub> obtained after photoirradiation of compound **7**.

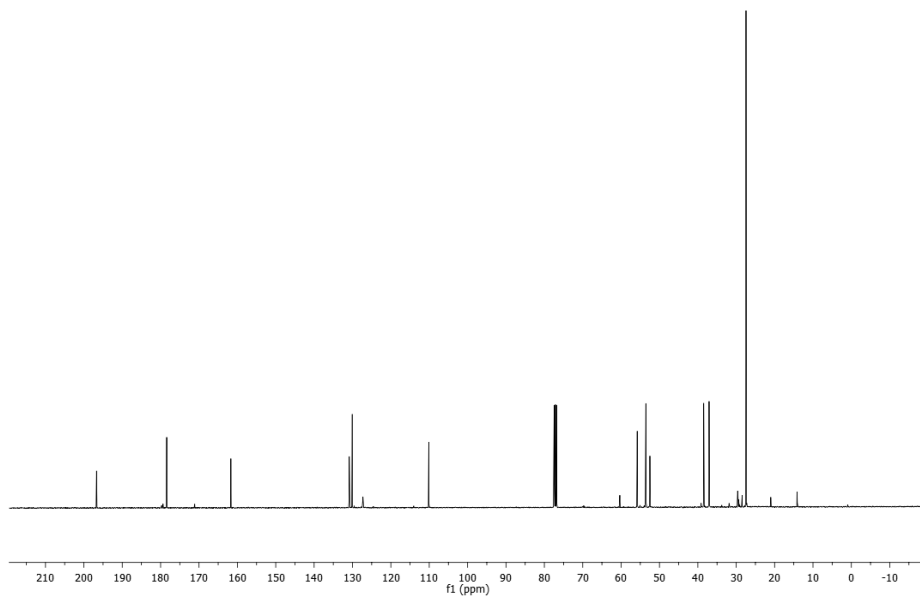


**Figure SI-5.**  $^{13}\text{C}$ -NMR spectra of aldehyde **8** in  $\text{CDCl}_3$  obtained after photoirradiation of compound **7**.

### *Supporting Information Bibliography*

- 1 M. J. Goldcamp; D. T. Rosa; N. A. Landers; S. M. Mandel, J. A. Krause-Bauer; M. J. Baldwin, *Synthesis*, **2000**, 2033-2038.



***Chapter 10:***  
***Conclusions and Future Perspectives***

Molecular chemosensors and systems for controlled delivery of bioactive molecules have been attracting a great attention in the last few years. Thus a lot of new systems for detection of chemical species with biological interest have been developed. Moreover also a variety of nanoscopic mesoporous systems for controlled release processes have been described. The main objective of this PhD thesis was to contribute to the evolution of this field pointing out some new features to solve “real life” problems. In particular we want to apply organic chemistry, in its basic aspects, to develop new chemosensor and new organic-inorganic hybrid materials for the controlled delivery of bioactive molecules into targeted cells.

In the general introduction the main aspects of supramolecular and hetro-supramolecular chemistry were reported. In particular the subjects of molecular recognition chemistry and self-assembly were emphasized, in order to understand the basis on which this thesis lays on.

Following this, in the first chapter, two new, innovative, chemodosimeters for the selective sensing of fluoride anion and glutathione, in aqueous solution, were presented.

- In particular in the case of the chemodosimeter for the sensing of  $F^-$ , the synthesis and characterization of an azo dye functionalized with alkoxy-silyl ethers were reported. Subsequently the chromogenic response to different anions was evaluated and we were able to state that our probe displayed a great selectivity toward fluoride anion, in aqueous solution.

- Following this the synthesis, characterization and sensing properties of a new pyrylium dye were reported. In this case the pyrylium based chemodosimeter was not soluble in pure aqueous solution, thus we prepared a chemosensing ensemble composed by the probe and a surfactant (CTAB). This chemosensing ensemble was able to discriminate between glutathione and all other amino acids, even cysteine, giving a strong chromo-fluorogenic response.

In the second chapter the design, synthesis, characterization and application of four new organic-inorganic nanoscopic hybrid systems for the controlled delivery of bioactive molecules into cells were reported. In particular the driving force of this part of the thesis was the achievement of a system as selective as possible in the controlled delivery into targeted cells.

- The first hybrid material studied can release its cargo through treatment with esterase enzyme. Thus with this hybrid nanoparticles we were able to discriminate between the inner and outer of a cell and release the entrapped molecule only into the intracellular environment. The main drawback of this system is that esterase is ubiquitous in cells, thus we were not able to induce the delivery into a specific cell line.
- In order to obtain more selectivity a photocleavable molecular gate was synthesized and studied. The final aim was the possibility to perform a local irradiation determining the photodegradation of the capping molecule and inducing a selective delivery only into the irradiated cells. The reported hybrid system displayed a good *in vitro* operation but it could't be applied for the intracellular delivery due to the required irradiation wavelength.

- Subsequently we developed a different and innovative molecular gate by which was possible to finely tune the amount of cargo delivered only selecting the appropriate enzyme. In particular this was the first reported dual enzyme triggered molecular gate. In this case the molecular gate was composed by urea and amide bonds. The treatment of the material with amidase or urease enzymes determined the selective hydrolysis of the amide or urea group, located in different position into the molecular gate. Specific hydrolysis of one of the two groups sized the removal of different dimensioned moieties, giving the possibility to tune the intensity of the cargo delivery
- Finally a nanoscopic mesoporous silica based hybrid system able to selectively release its cargo into senescent cells was designed and synthesized. In this case an over-expressed enzyme ( $\beta$ -galactosidase) into senescent cells played the key role. The functionalization of the surface of the mesoporous silica nanoparticles with a galactooligosaccharide allowed us to obtain a system that displayed zero release into normal somatic cells and that delivered its cargo selectively into senescent cells.

In summary with this thesis we explored several ways for the achievement of nanoscopic organic-inorganic hybrid systems for the controlled delivery into targeted cells. A first possible future development is the design of more molecular gates that can selectively respond to enzymes or other macro-biomolecules present just in particular cellular lines.

In particular a selective hydrolysable molecular gate, that respond just to enzymes (or other cellular organelles) present in cancer cells can be

designed, synthesized and anchored to a solid support loaded with an anticancer drug. In this manner the controlled delivery should be achieved just in cancer cells.

Another possibility is design a molecular gate able to selectively drive the nanoparticles to target cells. In this case the structure of the molecular gate has to be compatible with specific cellular membrane receptors that characterize the specific targeted cell.

In this sense polypeptidic sequences are very promising. In fact a custom synthesis can be quite easy achieved and a derivatisation with trialkoxysilane moieties would be possible. Therefore if the chain presents an adequate length would be bulky enough to grant zero uncontrolled release. Finally depending on the peptide sequence the chain is selectively broken by specific not ubiquitous enzymes, furnishing the desired selectivity.

Apart of the selective hydrolysis possibility, polypeptidic chains can also direct the nanoparticles to specific cellular targets. In this case depending on the peptidic sequence a cytoplasmatic or lysosomal internalization can be achieved. Thus being the cytoplasmatic enzymes in most cases different from the lysosomal enzymes is possible to design a polypeptidic molecular gate featured by the presence of selectively hydrolysable sequences by cytoplasmatic or lysosomal enzymes.

Another possibility is to design a photoactive molecular gate able to tune the delivery of the entrapped cargo upon the irradiation with "biocompatible light". This would allow local irradiation and thus a very selective delivery only into the irradiated cells.